جامعة سيدي محمد بن عبد الله بفاس
UNIVERSITÉ SIDI MOHAMED BEN ABDELLAH DE FES

كلية العلوم والتقنيات فاس
FACULTÉ DES SCIENCES ET TECHNIQUES DE FÈS

N° d'ordre : 68/2022

Centre des Etudes Doctorales : Sciences et Techniques et Sciences Médicales.
Formation Doctorale : Sciences de l'ingénieur, Sciences Physiques, Mathématiques et informatique.
Discipline : Sciences de l'ingénieur
Spécialité : Mécanique Énergétique
Laboratoire : Technologies Innovantes

Thèse pour l'obtention de DOCTORAT

Solar Dish Stirling Technology: Multi-criteria optimization and assessments

Préparée par :

Mr. Hamza ALLOUHI

Soutenue le 01 Novembre 2022 à 10h au centre d'Accueil et de Conférences de l'École Supérieure de Technologie de Fès (ESTF) devant le jury :

Nom et Prénom	Grade	Etablissement	Qualité
Abdelmajid SAKA	PES	École Nationales des Sciences Appliquées de FES	Président
Tarik KOUSKSOU	PES	Université de Pau et des Pays de l'Adour	Rapporteur
Miloud RAHMOUNE	PES	École Supérieure de Technologie de Meknès	Rapporteur
Kamar OUAZZANI	PES	École Supérieure de Technologie de Fès	Rapporteur
Rachid SAADANI	PES	École Supérieure de technologie de Meknès	Examinateur
Abdelmajid JAMIL	PES	École Supérieure de Technologie de Fès	Directeur de thèse

Rachid EL MRABET	Directeur Général de Marafik Berkane, Maroc	Invité d'honneur

Acknowledgements

This work is never an individual work, it is the fruit of many experiences, collaborations and meetings.

First of all, I would like to express my sincere and also the deepest thanks to my supervisor **Mr. JAMIL Abdelmajid** from Sidi Mohammed Ben Abdellah University (USMBA-Morocco), for proposing an original research topic that allowed me to progress, learn and enrich both my intellectual and academic skills. I also would like to thank him for giving me this opportunity, for his encouragement and motivation.

I'm highly indebted to **Mr. ALLOUHI Amine** who accompanied me throughout this professional experience with his precious guidance, obviously for his complete availability, for the countless hours spent and for his communicative enthusiasm and benevolence.

Last but not least, I want to address all my recognition to all those who participated directly or indirectly in this adventure, who granting me the time and supporting me during these years. Special thanks to family, colleagues, friends and the rest of people who assisted me attain this incredible challenge.

Abstract

Solar energy is one of the most attractive alternatives to provide clean and sustainable power at competitive costs. Worldwide, the implementation of concentrating solar power (CSP) systems for power generation has escalated considerably. Solar Dish Stirling (SDS) is among the less developed CSP technologies and further research work should be deployed to ensure its global advancement, competitiveness and widespread implementation.

The main objective of the present thesis is to provide several answers related to the potential of solar dish technology as a sustainable power generation mode and to reveal its role in mitigating environmental issues. A thorough and extensive literature review was made to show how this technology has progressed over the past years. The literature review mentioned new and multi-end applications of solar dish concentrator, and outlined general aspects and perspectives for technological development. The state of the art has highlighted the most promising approaches suggested by the scientific community to optimize the energy, exergy and economic performances of the SDS technology.

Power generation remains the most promising application of the SDS system, especially in developing countries with high solar potential. The benefit of implementing such technology for electrification in Moroccan rural region was first emphasized. A comprehensive assessment based on an energy, exergy, economic and environmental analysis (4-E) was developed for this purpose. The particularity of the developed assessment is that it relies on specific sizing of design parameters that were optimized based on a parametric investigations under time-varying meteorological data. This allowed to rank the most relevant Moroccan sites to host projects based on SDS technology. The present thesis dealt also with the improvement of the overall energy and economic performance of SDS power plant from a field layout perspective. In this directive, a multi-objective optimization approach using Elitist Non-Dominated Sorting Genetic Algorithm and multi-criteria decision analysis was introduced to address the best trade-off between energetic and financial performances of a 10 MW SDS power plant operating under climatic data of Ouarzazate and Madrid cities. Two energy and economic conflicting objective functions were considered and guidelines were finally provided to effectively adjust the geometrical key parameters on the SDS field layout. Moreover, a special interest was devoted to the hybridization of the SDS technology with Wind Turbines to supply clean electricity in the residential buildings. In this perspective, a building simulation was performed to design a multi-family residential building while considering the common construction practices for the Moroccan context. The specific feature

of the conducted analysis is to explore the power-to-hydrogen while optimizing the overall integrated Hybrid Renewable Energy System (HRES) under a grid-connection scenario. The Hybrid Renewable Energy optimization was carried out for two Moroccan regions with distinct meteorological variables and most relevant financial and energy metrics were assessed along with sensitivity analyses.

The various studies and investigations carried out in this thesis revealed the potential of SDS integration and opened the perspectives for modern polygeneration applications that can promote living conditions in locations with high solar potential and limit their consumption of energy from conventional sources.

Keywords: Concentrating Solar Power (CSP); Solar Dish Stirling (SDS); Power generation, 4-E analysis; Multi-objective optimization; Hybrid Renewable Energy System (HRES); Residential Building; Hydrogen production.

Résumé

L'énergie solaire est l'une des alternatives les plus prometteuses pour fournir une énergie propre, écologique et durable à des coûts compétitifs. Dans le monde entier, la mise en œuvre des systèmes d'Energie Solaire à Concentration (ESC) pour la production d'électricité s'est considérablement intensifiée. Le Concentrateur Solaire Parabolique à moteur Stirling (CSPS) fait partie des technologies ESC les moins développées et des travaux de recherche supplémentaires devraient être déployés pour assurer son avancement mondial, sa compétitivité ainsi que sa mise en œuvre généralisée.

La présente thèse a pour objectif principal de fournir des éléments de réponse liés au potentiel de la technologie des concentrateurs solaires paraboliques en tant que mode de production d'énergie durable et de révéler son rôle dans la mitigation des problèmes environnementaux. Une étude bibliographique approfondie et extensive a été établie pour fournir une vision globale sur le progrès de cette technologie au cours des dernières années. L'étude bibliographique a également mentionné les nouvelles applications et les divers usages des concentrateurs solaires paraboliques, et a tracé diverses perspectives de développement technologique. L'état de l'art effectué a mis en évidence les approches les plus prometteuses suggérées par la communauté scientifique pour optimiser les performances énergétiques, exergétiques et économiques de la technologie CSPS.

La production d'électricité reste l'application la plus souhaitable du système CSPS, en particulier dans les pays en développement avec un fort potentiel solaire. L'intérêt de la mise en œuvre d'une telle technologie pour l'électrification des régions rurales marocaines a d'abord été souligné. Un bilan global basé sur une analyse énergétique, exergétique, économique et environnementale a été élaboré à cet effet. La particularité de l'évaluation développée est qu'elle repose sur un dimensionnement spécifique des paramètres de conception qui ont été optimisés sur la base d'investigations paramétriques en tenant compte des données météorologiques horaires. Cela a permis de classer et distinguer les sites marocains les plus pertinents pour abriter des projets basés sur la technologie CSPS. La présente thèse a également traité l'amélioration des performances énergétiques et économiques globales des centrales CSPS du point de vue de la disposition et l'aménagement du champ solaire. Dans cette optique, une approche d'optimisation multi-objective en utilisant l'Algorithme Génétique et l'analyse décisionnelle multicritères a été introduite pour mettre en exergue le meilleur compromis entre les performances énergétiques et financières d'une centrale CSPS

de 10 MW fonctionnant sous les conditions climatiques des deux villes Ouarzazate et Madrid. Deux fonctions objectives énergétiques et économiques conflictuelles ont été prises en compte et des lignes directrices ont été finalement fournies pour ajuster effectivement les paramètres géométriques de la disposition du champ solaire CSPS. En outre, un intérêt particulier a été dédié à l'hybridation de la technologie CSPS avec la technologie des éoliennes dans le but de fournir une forme durable et propre de l'électricité aux bâtiments résidentiels. Dans cette perspective, une conception d'une structure d'immeuble multifamilial a été réalisée et simulée dynamiquement en tenant compte des pratiques de construction courantes dans le contexte marocain. La particularité de l'analyse menée est d'explorer davantage le concept 'Power-to-Hydrogen' en optimisant le Système Hybride intégré à sources d'Energies Renouvelables (SHER) sous une configuration connectée au réseau. L'optimisation du Système Hybride intégré à sources d'Energies Renouvelables (SHER) a été réalisée pour deux régions marocaines ayant des données météorologiques distinctes. De plus, les paramètres financiers et énergétiques les plus pertinents ainsi qu'une série d'analyses de sensibilité ont été évalués.

Les différentes études et investigations menées dans cette thèse ont permis de dévoiler le potentiel d'intégration de la technologie CSPS et d'ouvrir les perspectives d'applications modernes de polygénération pouvant favoriser les conditions de vie dans des lieux à fort potentiel solaire et limiter leurs consommation en sources conventionnelles.

Mots clés : Energie Solaire à Concentration (ESC) ; Concentrateur Solaire Parabolique à moteur Stirling (CSPS) ; Production d'électricité ; Analyse 4-E ; Optimisation multi-objective ; Système Hybride intégré à sources d'Energies Renouvelables (SHER) ; Bâtiment résidentiel ; Production d'Hydrogène.

TABLE OF CONTENT

GENERAL INTRODUCTION 20

1. Background 20

2. Structure and scope of the thesis 22

CHAPTER I. Overview on the Solar Dish Technology 25

1. Introduction 25

2. Background: 25

3. Literature review on CSP technologies 29

3.1. Parabolic Through Collector 29

3.2. Solar Tower 30

3.3. Linear Fresnel Reflector: 30

4. Solar Dish Stirling for power generation 31

5. Design improvements of SDS technology 33

5.1. Solar field layout/ Shading Effect 33

5.2. Collector and tracking 34

5.3. Receiver 35

5.4. Stirling Engine 40

5.5. Regenerator 42

6. SDS assessment studies 43

7. Summary 47

CHAPTER II. Novel applications and optimization frameworks of Solar Dish Collectors 48

1. Introduction 48

2. Background 48

3. Solar dish for multi-end use applications 49

4. Novel solar dish applications and concepts 53

4.1. Solar Dish/ microgas turbine solar power generator 53

4.2. Solar dish/Brayton cycle 54

4.3. Solar Dish/Flat Plate collectors 55

4.4. Solar Dish/Photovoltaic cells 55

4.5. Solar Dish/Thermoelectric modules 56

4.6. Solar Dish/PV and TEG 57

5. Solar Dish cogeneration and polygeneration 58
6. Solar Dish Fresh water production 59
7. Solar dish with Phase Change materials 62
8. Optimization of SDS technology 63
9. Summary 68

CHAPTER III. Solar Dish Stirling technology for sustainable power generation in Southern Morocco: 4-E analysis 70

1. Introduction 70
2. Background 71
3. Methods 74
3.1. System description 75
3.2. Examined geographical sites 76
3.3. Thermal model 77
3.4. Mathematical formulation 79
3.5. Performance indexes 82
4. Results and discussion 84
4.1. Weather data 84
4.2. Hourly system energy efficiency 86
4.3. Hourly exergy efficiency 87
4.4. Parametric analysis and optimisation 88
4.5. Economic analysis 93
4.6. Results extrapolation 95
4.7. Environmental impact 96
5. Summary 97

CHAPTER IV. Multi- objective optimization of a SDS field layout using Genetic Algorithm and TOPSIS method 99

1. Introduction 99
2. Background 99
3. Methodology 102
3.1. System description and problem statement 102
3.2. Simulation process and optimization framework 106
3.3. Examined Sites 110

4. Results and discussions 111
4.1. Weather data 111
4.2. Surrogate Model and validation 114
4.3. Multi-objective optimization results 116
4.4. Final optimal solution through decision making method 118
4.5. Sensitivity analyses 122
5. Summary 124
CHAPTER V. Hybrid Renewable Energy System for sustainable residential buildings based Solar Dish Stirling and Wind Turbine with hydrogen production 126
1. Introduction 126
2. Background 126
3. Methodology 132
3.1. Buildings simulation 133
3.1. Examined sites 134
3.2. HRES structure 135
3.3. Assessments metrics and economic model 140
4. Results and discussion 142
4.1. Meteorological data 142
4.2. BEopt simulation results 144
4.3. Electric load Dakhla city 145
4.4. Electric load Ouarzazate city 145
4.5. Hydrogen load 146
4.6. Solar Dish Stirling results from System Advisor Model (SAM) 147
4.7. Wind Turbine power output from Homer Pro 148
4.8. Optimum configuration at Dakhla city 149
4.9. Optimum Configuration at Ouarzazate city 150
4.10. Sensitivity analysis 152
5. Summary 154
GENERAL CONCLUSION AND PERSPECTIVES 156
REFERENCES 160

TABLES LIST

Table 1: Status of total CSP capacity installed (Own computations based on data of Ref. [21]) 21

Table 2: Comparison between the various CSP technologies [32]–[36] 28

Table 3: Published works with main information: power plant capacity, implementation site and overall plant performance 72

Table 4: Design specifications, dimensions, and performance parameters of the SDS system.....76

Table 5: Geographic coordinates of each studied region 77

Table 6: Assumptions and Data ([67], [273]).....83

Table 7: Technical and economic performance of the SDS system, including the optimised parameters 95

Table 8: Comparison of the current study with other works 97

Table 9: Dimensions, characteristics design and performance parameters of the SDS power plant 103

Table 10: Design parameters of the SDS along with their initial values 106

Table 11: Decision variables and their upper and lower limits 109

Table 12: Geographic coordinates of each studied city 111

Table 13: Statistical indices resulting from the introduced surrogate model 114

Table 14: Optimal solutions derived using TOPSIS method for Ouarzazate city 118

Table 15: Optimal solutions derived using TOPSIS method for Madrid city 119

Table 16: Detailed results of the parametrical scenario derived using TOPSIS method showing the optimal decision variables in the case of Ouarzazate city.....124

Table 17 : Detailed results of the parametrical scenario derived using TOPSIS method showing the optimal decision variables in the case of Madrid city. 124

Table 18: Main specification details of the envelope materials [366]:.....134

Table 19: Geographic coordinates of each examined site.....135

Table 20: Cost assumptions and additional technical details 135

Table 21:Optimal design specifications of the Solar Dish Stirling system based on Ref. [110].....137

Table 22: Technical features of the used Bergey Excel (XL10) wind turbine [374]. ..139

Table 23: Optimized HRES design with specific details of all components in Dakhla city 150

Table 24: Optimized HRES design with specific details of all components in Ouarzazate city.....150
Table 25: Sensitivity analysis based on SDS Cost Multiplier reduction in Dakhla city.... 153
Table 26: Sensitivity analysis based on scaled average wind speed variation in Ouarzazate city.....154

FIGURES LIST

Figure 1 : Overview of the available SDS power plant worldwide: (a): Maricopa solar project (USA) [22]; (b): Tooele Army Depot (USA) [23].....22

Figure 2: Solar power plant classification.....26

Figure 3: Sustainable Development Scenario of CSP from 2000 to 2030 [9] 27

Figure 4: Types of CSP technology: (a) Parabolic Through Collector; (b) Solar tower; (c) Linear Fresnel; (d) Solar dish Stirling [28] 28

Figure 5: Solar Dish Stirling Technology with its principal components [25] 32

Figure 6: The studied receiver shapes: (a) Spiral receiver cavity; (b;c) Conical receiver design [99] 37

Figure 7: Stirling engine configurations: (a) α-type; (b) β-type and (c) γ-type [131]....41

Figure 8: Illustrative bloc diagram of SDS improvement pathways 43

Figure 9 : Overview of the integrated SDS system in Tianjin University, China 46

Figure 10: Flow Diagram of the solar distillation setup [162] 49

Figure 11: Schematic diagram of a hybrid solar system based on SDS thermoelectric cooler for power generation and water distillation [164].....50

Figure 12:Schematic illustration of the CHP plant [168] 51

Figure 13: Schematic diagram of the hybrid power generation system [170] 52

Figure 14: Solar Dish-micro Gas Turbine integrated system [181].....54

Figure 15: Schematic of a Brayton cycle based solar dish system [190] 55

Figure 16: Schematic view of the solar dish Thermoelectric Generator [200] 57

Figure 17: Schematic of Solar dish PV-Thermoelectric generator [202] 57

Figure 18: Flow diagram of the combined system [210].....59

Figure 19: Schematic of the solar dish system integrated with a mGT, an organic Rankine cycle, and water desalination process [214].....60

Figure 20: Schematic of the desalination setup [215] 61

Figure 21: Representative view of the overall system [217].....61

Figure 22: Schematic model of the distillation system [218].....62

Figure 23: Process of the thermal-economic optimization approach [225].....63

Figure 24: Optimization algorithm of SDS model [227].....64

Figure 25: Schematic illustration of the adopted optimization approach [232] 66

Figure 26: SDS System with its main devices [25].....75

Figure 27: (a) Energetic chain of the Solar dish Stirling System [67]; **(b)** Diagrams *P-V* and *T-S* of the ideal Stirling Engine cycle.....78
F**igure 28:** Hourly weather data variation during a whole year for the six cities: **(a)**: Beam normal irradiance; **(b)**: Ambient temperature; **(c)**: Wind speed.....86
Figure 29: Hourly variation of the energy efficiency of the SDS system corresponding to a specific day in each season. 87
Figure 30 : Hourly variation of the exergy efficiency of the SDS system corresponding to a specific day in each season. 88
Figure 31: Impact of the variation of the speed of the cooling pump on the annual energy generated.....89
Figure 32: The effect of the change of the receiver aperture diameter on the receiver output energy for the examined sites. 90
Figure 33: Annual Energy versus the receiver aperture diameter. 91
Figure 34: Impact of the variation of the receiver aperture diameter on the receiver losses 92
Figure 35: Effect of the change of the receiver insulation thickness on the annual energy. 93
Figure 36: Levelized Cost of Energy (LCOE) as function of the Cost Multiplier: **(a)** Nominal LCOE; **(b)** Real LCOE.....94
Figure 37: Annual quantity of the mitigated CO_2 emissions per city.....96
Figure 38: Cumulative amount of CO2 avoided for period between 2015 and 2050 under various scenarios [15]. 100
Figure 39: Solar dish Stirling power plant with main field parameters. 103
Figure 40: Schematic view of solar SDS field layout power plant [80]. 105
Figure 41: Schematic illustration of the optimization process. 107
Figure 42: Meteorological Data: **(a)** Direct Normal Irradiation; **(b)** Average Ambient Temperature; **(c)** Wind Velocity. 113
Figure 43 : Dispersion illustration of the proposed surrogate model for the SDS power plant.....115
Figure 44: Two objective Pareto Frontiers for the studied locations. 117
Figure 45: Overall net efficiency and annual power generated using the optimal parameters derived from the optimization approach for Ouarzazate 121

Figure 46: Overall net efficiency and annual power generated using the optimal parameters derived from the optimization approach for Madrid. 122
Figure 47: Two objective Pareto Frontier derived from the optimization process considering the variation of Site Improvement Cost for each site. Final optimal solutions selected by TOPSIS method are marked. 123
Figure 48: World global primary energy consumption by source in 2021 [318] 127
Figure 49: GHG emissions from fuel combustion in selected economies in 2019 [317] 127
Figure 50: Outline of the adopted steps employed for the multi-family building design and HRES assessment 132
Figure 51: Architecture of the simulated building using BEopt software 133
Figure 52: Schematic illustration of the examined HRES 136
Figure 53 : Flow chart diagram illustrating the main steps of the optimization process adopted by Homer Pro software 137
Figure 54: Hourly profile of the Direct Normal Irradiation during a whole year for Dakhla and Ouarzazate 143
Figure 55: Hourly profile of the Ambient Temperature during a complete year for Dakhla and Ouarzazate 144
Figure 56: Hourly profile of the Wind Speed during a whole year for Dakhla and Ouarzazate 144
Figure 57: Hourly variation of the total electric load and break down of the multi-uses consumption of the residential buildings for Dakhla city. 145
Figure 58: Hourly profile of the total electric consumption and break down of the application uses of the residential buildings for Ouarzazate city. 146
Figure 59: Hourly variation of the imposed hydrogen load throughout the year for the examined sites 147
Figure 60: System Power generated of the SDS system using SAM for Dakhla and Ouarzazate 148
Figure 61: Power curve of the Bergey Excel XL 10 Wind Turbine and its related ..... power in Dakhla and Ouarzazate 149
Figure 62: Break down of the total electric generation and total electric consumption for Dakhla according to the optimal configuration 151

Figure 63: Break down illustration of the total energy production and energy utilization for Ouarzazate according to the optimal configuration 152
Figure 64: Sensitivity analysis considering the SDS Cost reduction from 1 to 0.6 in Dakhla 153
Figure 65: Sensitivity analysis considering the variation of the annual average wind speed in Ouarzazate 154

NOMENCLATURE

- *List of abbreviations*

AMTPG Jaya	Adaptive Multi-Team Perturbation Guiding Jaya algorithm
ANN	Artificial Neural Network
ANFIS	Adaptive Neuro-Fuzzy Inference System
BEopt	Building Energy Optimization tool
CFD	Computational Fluid Dynamics
CHOA	Chimp Optimization Algorithm
CHP	Combined Heat and Power system
CSP	Concentrating Solar Power
DG	Diesel Generator
DIR	Directly Illuminated Receiver
DNI	Direct Normal Irradiation
GA	Genetic algorithm
GC	Open Gaz Cycle
GHG	Greenhouse gas emissions
HOMER	Hybrid Optimization of Multiple Energy Resources
HRES	Hybrid Renewable Energy System
ICA	Imperialist Competition Algorithm
INPBE	International Nanofluid Property Benchmark Exercise
LCOE	Levelized Cost of Energy
LCOH	Levelized Cost of Hydrogen
LFR	Linear Fresnel Reflector
LINMAP	Linear Programming technique for Multidimensional Analysis of Preference
MAE	Mean Absolute Error
MENA	Middle East and North Africa region
MLP	Multi-Layer Perceptron
MLR	Multiple non-Linear Regression
MOEA	Multi-Objective Evolutionary Algorithms
MSE	Mean Square Error approach
NSGA-II	Elitist Non-Dominated Sorting Genetic Algorithm II

NZEB	Net Zero Energy Building
ORC	Organic Rankine Cycle
PCM	Phase Change Material
PSO	Particle swarm optimization
PTC	Parabolic Through Collector
PV	Photovoltaic system
RC	Relative Closeness index
RF	Renewable Fraction
RMSE	Root Mean Square Error
RVFL	Random Vector Functional Link network
SAM	System Advisor Model
SC	Steam Rankine Cycle
SDS	Solar Dish Stirling technology
SE	Stirling Engine
SHP	Source Heat Pump system
SSO	Spherical Search Optimization
ST	Solar Tower
TEC	Thermoelectric Cooler
TEG	Thermoelectric Generator
TES	Thermal Energy Storage
TLBO	Teaching-Learning-Based Optimization
TMY	Typical Meteorological Year (Meteorological dataset)
TNPC	Total Net Present Cost
TOPSIS	Technique for Order of Preference by Similarity to Ideal Solution
WT	Wind Turbine

- *List of symbols:*

A_{ap}	Area of the receiver aperture, m²
A_{cav}	Area of the interior cavity, m²
A_{proj}	Projected area of the mirror, m²
A_{SF}	Total solar field area, m²
AE	Annual Energy generated, kWh
AM_{CO_2}	Annual quantity of mitigating CO_2 emissions (tonne/kWh)

$Beale$	Temperature-corrected Beal number
C_0	Project's equity investment
C_n	Annual cost of the project in year n
cf_{grid}	Carbon footprint for the electricity from the grid (gCO_2/kWh)
cf_{SDS}	Carbon footprint for the electricity from the SDS (gCO_2/kWh)
CF	Capacity Factor, %
CRF	Capital Recovery Factor
C_{TAC}	Total Annualized Cost, $
C_{TNPC}	Total Net Present Cost, $
d_{ap}	Aperture diameter, m
d_{cav}	Cavity diameter, m
$d_{CollSep,E-W}$	Separation distance between collectors oriented East-West, m
$d_{CollSep,N-S}$	Separation distance between collectors oriented North-South, m
$d_{nominal}$	Nominal discount rate, %
d_{real}	Real discount rate, %
E_{nonren}	Electricity generated from non-renewable sources, kWh
E_{served}	Electric load Served, kWh
Ex_{in}	Global Exergy input of the SDS, W
f	Engine frequency, 1/s
Gr	Grashof number
$Gr_{s,E-W}$	Ground slope East-West, deg
$Gr_{s,N-S}$	Ground slope North-South, deg
h_{forced}	Coefficient of the forced convection in receiver cavity, W/m²/K
$h_{natural}$	Coefficient of the natural convection, W/m²/K
H_{nonren}	Thermal energy generated from non-renewable energy sources, kWh
H_{served}	Thermal load Served, kWh
$h_{total,convection}$	Global coefficient of convection heat transfer, W/m²/K
I_{DNI}	Direct Normal Insolation, W/m²
$LCOE$	Levelized Cost of Energy, $/kWh
$LCOH$	Levelized Cost of Hydrogen, $/kg
$M_{Hydrogen}$	Total amount of the produced Hydrogen, kg
N	Examination phase in years n
N_{Coll}	Total number of collectors

$N_{Coll,E-W}$	Number of collectors oriented East-West
$N_{Coll,N-S}$	Number of collectors oriented North-South
$Nu_{nat,conv}$	Nusselt number correlation
$P_{controls}$	Controls and tracking power consumption, W
P_{Engine}	Power of the Stirling Engine, W
P_{fan}	Fan power consumption, W
P_{gross}	Total amount of the electrical generated power, W
$P_{in,rec}$	Solar power intercepted by the receiver, W
$P_{in,SE}$	Input power of the SE, W
P_{mean}	Mean pressure engine, Pa
P_{Net}	Net system power, W
$P_{parasitics}$	Parasitic power of tracking and controls, W
P_{pump}	Pump power consumption, W
P_{rated}	Total Capacity of the SE, W
P_{SF}	Total solar field capacity, W
P_{WT}	Power provided by the WT, kW
$P_{WT,STC}$	Wind Turbine power output at standard temperature and pressure, kW
$\dot{q}_{cond}$	Conduction losses at the receiver level, W
$\dot{q}_{conv,tot}$	Total convection heat loss in receiver, W
$\dot{q}_{rad,emit}$	Emitted radiation out of the receiver aperture, W
$\dot{q}_{rad,reflect}$	Reflected radiation out of the aperture, W
RF	Renewable Fraction, %
S_{AVG}	Average shaded area per collector, m²
SIC	Specific Cost of Site Improvement, $
$Sl_{g,H}$	Slot Gap Height, m
$Sl_{g,W}$	Slot Gap Width, m
T_{amb}	Ambient temperature, K
T_C	Compression space temperature, K
T_{cav}	Temperature at the interior walls of the receiver cavity, K
$T_{correct}$	Temperature correction term (from finite-time theory), K
T_H	Space expansion temperature, K
T_s	Apparent temperature of the sun, K

$TCSI$	Total Cost of Site Improvements, $
U_{anem}	Wind speed at the anemometer height, m/s
U_{hub}	Wind speed at the hub height of the WT, m/s
v	Wind speed, m/s
V_{sw}	Swept volume, m^3
z_{hub}	Hub height of the WT, m
z_{anem}	Anemometer height, m

- - *Greek symbols:*

α_{eff}	Effective absorptance of the cavity
α_{cav}	Absorptance of the interior cavity surface
ε	Emissivity of the cavity
η_{Energy}	Energy efficiency
η_{Exergy}	Exergy efficiency
θ	Sun elevation angle, rad
ρ_{ref}	Mirror reflectivity
σ	Stefan-Boltzmann constant, $W/m^2/K^4$
$\varphi_{int,fac}$	Intercept factor
φ_{shade}	Shading factor

GENERAL INTRODUCTION

1. Background

Recently, population growth, elevated rate of urbanization and high energy consumption rates in various anthropogenic activities caused devastating environmental impacts. This challenging situation encouraged scientific community to conduct more researches and investigations to develop sustainable and eco-friendly energy systems [1]–[4]. As it is well-established, energy consumption is massively dominated by coal, natural gas and other conventional resources which accentuates the effects of climate change [5]. In china, the highest amount of greenhouse gases was detected and corresponds to 30% of the global emissions worldwide [6]. Iran is the most emitting country in Middle East followed by Saudi Arabia [6], [7]. South Africa is found to be the largest emitting country in Africa and is responsible of around 50% of the carbon dioxide emissions in the entire continent [8]. The global GHG emissions derived from industrial processes and fuel combustion equalized 36.1 $GtCO_2$ in 2019. In 2020, during the pandemic period, the energy consumption was practically decreased which results in a decline of about 5.8% in the global CO_2 emissions. However, in 2021, the global CO_2 emissions attained the highest annual quantity with a value of 36.3 $GtCO_2$ surpassing slightly the previous peak in 2019 [9]. As a result, many countries continue to deploy great efforts by increasing their energy independence and reducing their total GHG emissions [10]. In this sense, renewable energies were widely recommended as a suitable alternative to limit the conventional energy use and ensure an energy autonomy through clean and sustainable approaches [11]. Among these sustainable alternatives, solar energy is considered as the most important renewable energy source that present several advantages in terms of sustainability and reliability at more accessible costs [12]. Practically, solar energy can be harnessed via two main pathways. The first pathway is the direct conversion of sunlight to electricity by exploring the photovoltaic effect. The second pathway uses thermal energy originating from the sunlight conversion to drive a thermodynamic cycle. Concentrating solar collectors are generally used for this purpose, and the nomination of this process is referred to as Concentrating Solar Power (CSP). Concentrating solar collectors can be also utilised for carbon-free industrial heat generation [13]. The use of CSP systems for power generation can best contribute to achieving sustainability targets in countries with high solar radiation levels [14]. In numbers, the International Energy Agency stated that about 600 MW of CSP newly installed capacity was integrated, corresponding to 20% decline compared

to 2018 and close to the average of the previous ten years. The increase in CSP capacity is expected to come mainly from emerging economies, particularly China, Morocco, and South Africa, where larger plants with more extended hourly storage are predicted to come into service [9]. In the United States, CSP plants could be implemented by 2030 with a total capacity of 118 GW, a capacity that could exceed 1504 GW by 2050. In Europe, the total installed capacity of CSP plants saw a distinctive growth between 0.5 GW in 2006 to 5 GW in 2015 [15]. Among the expected predictions of CSP technology in the coming decades is the transportation of electricity from the MENA region which enjoys a huge area of desert towards the European Union. If only 0.4% of the desert in MENA was exploited by CSP systems, the electricity requirement of the entire European Union could be covered [16]. The use of thermal storage in such power plants is another strength permitting higher performances and flexibility [14], [17].

CSP technologies produce electrical power by concentrating sunrays. This process requires a set of solar concentrators systems, a receiver to collect the thermal heat, a steam turbine, and an electrical generator. Four types of CSP are presently developed: Parabolic Trough Collectors (PTC), Solar Tower (ST), Linear Fresnel Reflector (LFR) and Solar Dish Stirling (SDS) [16]. PTC is the most extensively installed technology with a rate of around 85% of the worldwide capacity of CSPs. ST is the second most developed technology [18],[19] which is gaining remarkable momentum during the few last years. For small-scale applications, LFRs are able to generate electricity at a competitive LCOE [20]. **Table 1** presents an illustration of the contribution of each technology to CSP market progress. It is observed that the SDS technology weakly contributes to the investment status of the CSPs installations worldwide.

Table 1: Status of total CSP capacity installed (Own computations based on data of Ref. [21])

Technology	**Number of projects**				**Capacity (MW)**			
	Operational	Non-currently operational	Under construction	Decommissioned	Operational	Non-currently operational	Under construction	Decommissioned
PTC	75	3	2	2	4706.1	103	650	43.8
LFR	9	3	0	0	241.7	9	0	0
ST	26	2	1	2	1319	8	100	20
SDS	0	2	0	0	0	3	0	0
Total	110	10	3	4	6266.8	123	750	63.8

Maricopa solar project and Tooele Army Depot are the available SDS plants and are located in USA (see **Fig. 1**); both having a nominal capacity of 1.5 MW [21].



(a) **(b)**

Figure 1 : Overview of the available SDS power plant worldwide: (a): Maricopa solar project (USA) [22]; (b): Tooele Army Depot (USA) [23]

SDS technology can ensure a high solar-to-electric conversion efficiency but is still less commercially developed compared to other CSP options. Hence, it is of great importance to conduct more research studies aiming at the assessment and optimization this type of technology in order to make its exploitation more common. This scientific need is more pronounced for countries with high solar energy potential, transitioning energetically to a more sustainable systems such as Morocco. In this context, the current PhD thesis is intended to fill this research gap and develops conceptual methodologies for the multi-criteria assessment and optimization of this CSP technology which has not yet been implemented in any region of MENA.

2. Structure and scope of the thesis

This thesis concerns three dimensions. The first is general, in which the aim is to provide a clear picture of Solar Dish Stirling technology and its potential applications. In this aspect, **CHAPTER I and II** introduce a comprehensive review and systematic summary of state of the art on research and progress of the solar dish technology as a concentrated solar power technology. The efforts mainly include the recent advances, technological challenges, and optimization frameworks in solar dish collector research field. One of the most critical features of this work is discussing novel combinations of solar dish collectors with other power generation devices including PV cells, thermoelectric devices, and thermal collectors. The chapters shed light also into recent thermodynamic cycles that can be powered by solar

dish collector as well as the potential polygeneration applications that can be engineered. Further, the most relevant researches adopting nanofluids and Phase Change Materials in solar dish collectors are reviewed.

In **CHAPTER III**, an energy, exergy, economic and environmental assessment of the Solar Dish Stirling (SDS) technology in thirteen Southern Moroccan sites is performed along with a parametric analysis of various design parameters to optimise this technology under time-varying climatic data. System simulation was conducted on an hourly basis with the help of System Advisor Model software. Annual energy can be maximised by adjusting the receiver aperture diameter, cooling pump speed, and thickness of receiver insulation appropriately.

CHAPTER IV carries out a multi-objective optimization to design the most energy and cost-effective Solar Dish Stirling (SDS) power plant. Meteorological data of two different sites have been considered to simulate the technical and economical performances of 10 MW SDS power plant. Two main energy and economic conflicting objective functions were considered with the ultimate goal to maximize of the annual Capacity Factor (CF) and minimize Total Cost of Site Improvements (TCSI) simultaneously. Several parameters such as the separation distance between collectors, ground slope, slot gap height and width have been parametrically assessed to find out effect on the Capacity Factor and the total cost of site improvement. First, a third-order multiple non-linear surrogate model was constructed. Then, multi-objective optimization using Elitist Non-Dominated Sorting Genetic Algorithm (NSGA-II) has been applied to address the trade-off between the two objective functions. The obtained Pareto Front was identified accordingly and final optimal solution was determined using Technique for Order of Preference by Similarity to Ideal Solution (TOPSIS) decision-making method.

CHAPTER V investigated the potential of Hybrid Renewable Energy System (HRES) based on SDS system and Wind Turbine technology to meet the energy demand in residential sector under a grid-connection scenario with possible generation of clean hydrogen. A design of a multi-family buildings located in two distinct location in Morocco was proposed and building simulation was conducted based on hourly climatic data in order to predict the year-round electrical load of the designed buildings. A techno-economic evaluation based on an extensive optimization process was carried out to prove the viability of the HRES and to select the optimum HRES architecture considering the lowest Net Present Cost (NPC).

Sensitivity analyses are then performed to exhibit the impact of the main functioning features and their effect on the global project viability.

CHAPTER I. Overview on the Solar Dish Technology

1. Introduction

The use of solar powered dish collectors to convert thermal energy into electricity is a promising and renewable alternative that can reduce huge amount of fossil fuel and their related emissions. However, examining the open literature, it is apparent that there is luck of updated and comprehensive details concerning the operating criteria and specifications of this technology which restrict its widespread implementation. In this chapter, a literature review focusing on the different type of CSP systems, the contribution of each technology in the global market were reported. A brief comparison of the solar dish technology with available concentrating solar systems in terms of energetic and economic performances is as well provided. Additionally, an insight into power generation process through solar dish technology as well as the design improvement pathways of the main system components were investigated. Finally, a subsection was dedicated to multi-criteria assessment studies conducted in several locations worldwide.

2. Background:

The world is faced with several constraints to deliver eco-friendly clean energy since the consumption of fossil fuels is gradually depleting, causing harmful impacts on the environment [1],[2]. Around 33.6 Gt of CO_2 emissions are expected to be reached at the end of 2020 as stated by the International Energy Agency [9]. Solar energy is defined as one of the most promising solutions among renewable sources thanks to its user-friendliness and efficiency [25]. Seen the appalling growth of the population, the daily need for electrical energy is increasing. Solar power plants can deliver sufficient electricity. The electricity is generated essentially from photovoltaics technology or solar thermal systems. **Fig. 2** outlines the conversion process of the solar energy to electricity for each technology.

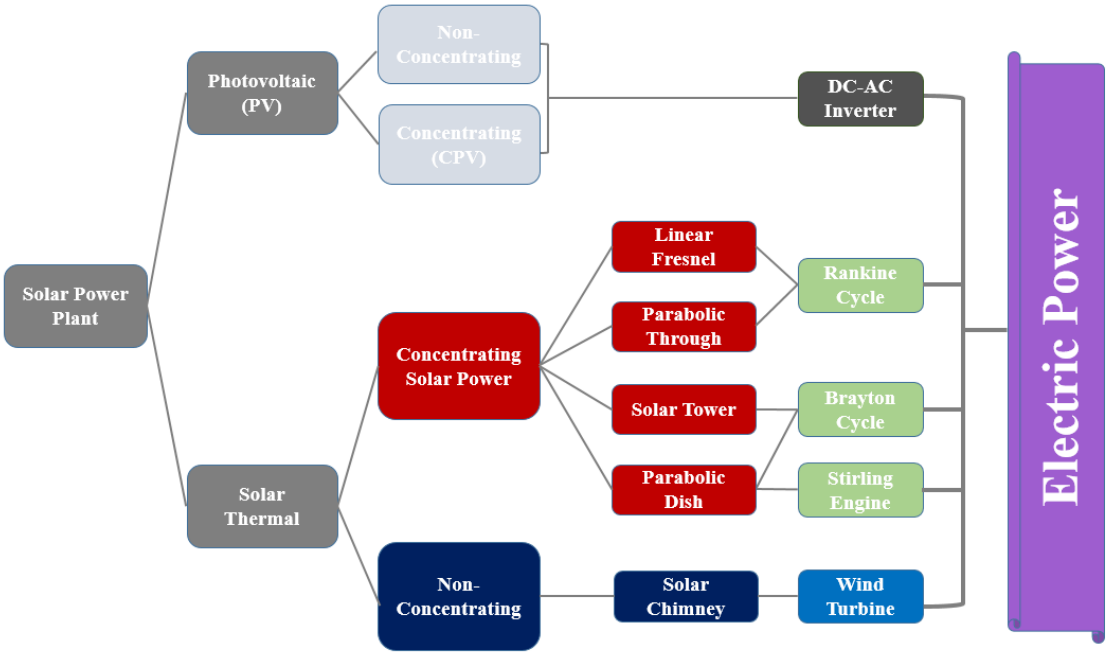


Figure 2: Solar power plant classification

Among the most recognized techniques for producing electrical energy on a large scale, the concentration of solar energy is forecasted to generate an overall electricity contribution of around 7% and 25% in 2030 and 2050, respectively [26]. According to the International Energy Agency, a capacity of about 600 MW has been recently installed, mainly coming from China, South Africa, and Morocco, where massive plants with more interesting hourly storage will get to work [9]. The evolution of the integrated capacity was well marked in Europe; the capacity was around 500 MW in 2006 and reached more than 5000 MW in 2015. The CSP plants in the USA will start up by 2030 with a capacity of around 120 GW and expect an increase of up to 1,500 GW by 2050 [15]. The Sustainable Development Scenario (SDS) established by the IEA predicts the crucial alteration of concentrated solar power generation (CSP), presenting how this type of technology may evolve during the following years to achieve the Sustainable Development Goals (SDGs). **Fig. 3** shows the predicted transformation of CSP from 2000 to 2030 [9].

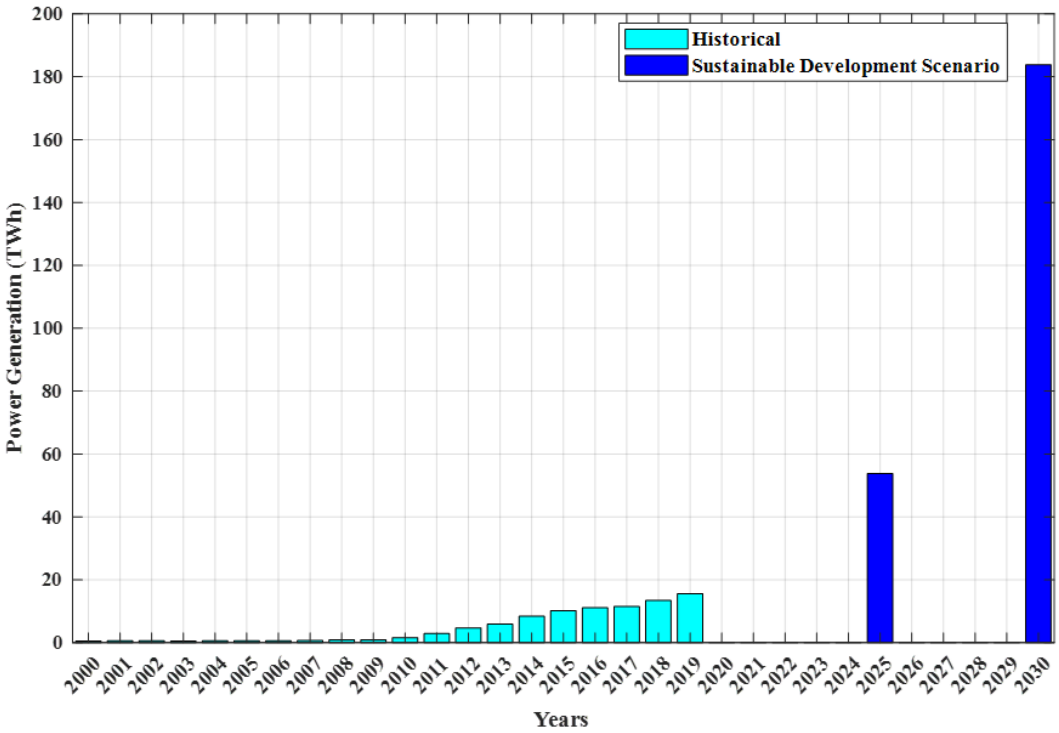
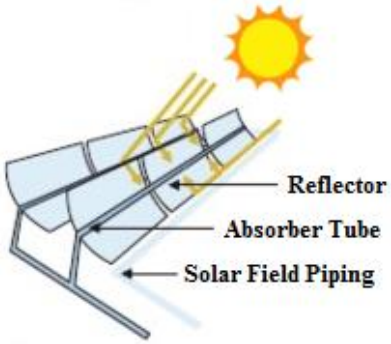
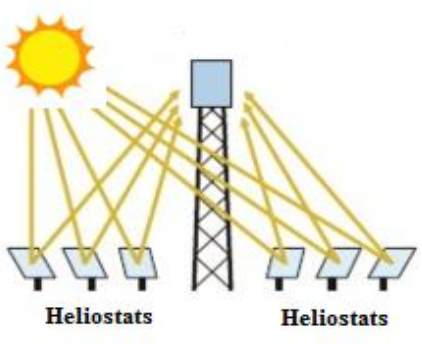


Figure 3: Sustainable Development Scenario of CSP from 2000 to 2030 [9]

Due to their ability to operate at high temperatures and the possibility of introducing heat storage, CSP has been preferred over other renewable energy systems [27]. The concentration of sunray generates electrical energy in CSP plants. The CSP systems are composed of several components: solar concentrators, a receiver, a steam turbine, and an electric generator. CSP systems can be classified into four types, which are Parabolic Trough Collectors (PTC), Solar Tower (ST), Linear Fresnel Reflector (LFR), and Solar Dish Stirling (SDS) [16]. **Fig. 4** illustrates the different types of CSP technologies with the main component of each system. PTCs are the most widely used technology with a rate of around 85% of the installed capacity of CSPs internationally, followed by ST systems [18],[19]. Linear Fresnel Reflectors have been proven to produce energy with competitive LCOE especially in locations that require small-scale systems [20].



(a)



(b)

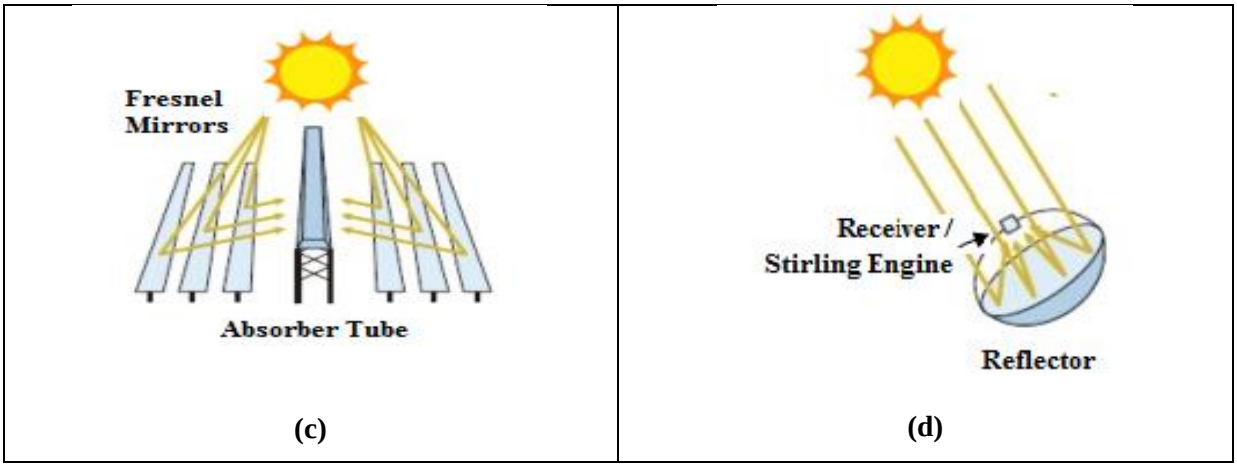


Figure 4: Types of CSP technology: **(a)** Parabolic Through Collector; **(b)** Solar tower; **(c)** Linear Fresnel; **(d)** Solar dish Stirling [28]

Solar dish technology is characterized by a relatively high heat-to-electricity conversion when coupled to Stirling engines (about 30% of the conversion efficiency has been attained as reported in [29], [30]). Additionally, the overall system for electricity generation does not require great amount of water for cooling process since the Stirling engine is air cooled. Since it is modular, solar dish technology is also recommended for standalone uses particularly in rural areas where the energy requirements are limited by the individual utilization. Nevertheless, the SDS system is not able to provide electricity in the absence of solar sunrays since it is not equipped with thermal storage unit [31]. This particularity is considered as the principal disadvantage which limits the large-scale integration and widespread of this technology. A comprehensive comparison between available CSP technologies is furnished in **Table 2**.

Table 2: Comparison between the various CSP technologies [32]–[36]

Feature parameter	Parabolic trough	Linear Fresnel	Solar tower	Parabolic dish
Capacity range (MW)	10–200	10–200	10–200	0.01–0.4
Concentration ratio (-)	70–80	25–100	300–1000	1000–3000
Tracking system (-)	Single axis	Single axis	Two-axis	Two-axis
Operating temperature (°C)	290–390	250–390	250–500	250–700
Power cycle (-)	Steam and organic Rankine	Steam and organic Rankine	Steam Rankine and Brayton	Steam Rankine, Brayton, and Stirling

Feature parameter	Parabolic trough	Linear Fresnel	Solar tower	Parabolic dish
Annual solar/electric efficiency (%)	15%	8–10%	20–35%	25–30%
Capital cost ($/kW)	3972	–	> 4000	12578
Capital cost ($/m^2)	424	234	476	–
Operational and maintenance cost ($/kWh)	0.012–0.02	Low	0.034	0.21
Water consumption (m^3/MWh)	3 (wet cooling) 0.3 (dry cooling)	3 (wet cooling) 0.2 (dry cooling)	2–3 (wet cooling) 0.25 (dry cooling)	0.05–0.1 (for mirror washing only)

In the following, brief discussions of the previous research investigations are furnished.

3. Literature review on CSP technologies

3.1. Parabolic Through Collector

For more than three decades, the solar power plants with parabolic trough collector (PTC) are at the top of the thermally driven solar energy production systems. The PTC is one of the most relevant technologies that generate heat from sunlight and then used the Rankine Cycle to transform it into electricity [37]. The PTC system is made up of large, giant U-shaped mirrors that reflect sun rays onto a receiver. The collector set includes hundreds of troughs arranged in parallel rows. Once the heat from the sun is reflected to the mirror, the curved forms direct most of it into a receiver. The sun tracking system ensures continuously focused radiation on the receiving pipes. The receiver is coloured to reduce the heat losses and achieve maximum absorption of solar irradiation. The receiving tube is filled with a working fluid (water, oil, or molten salt) [38]. Compared to other technological variants of CSP, PTC remains the more mature and reliable technology [39].

Recently, several developments were investigated to assess, optimize, and enhance the performances of PTC technology. Siva Subramanian et al. [40] performed a research work with the principal aim is to convert solar energy into useful work via a PTC considering different absorber surfaces. An appropriate surface was acquired using a form of aluminium sheet. Yang et al. [41] introduced a system consisting of micro-parabolic troughs collectors, evacuated tube collectors, and a mechanism of tracking. The system is competitive and can

achieve an optical and thermal efficiency of 44.1% and 37.5%, respectively. Furthermore, the proposed design could produce the average temperature of thermal solar heat used in industrial production or drive multi-effect absorption chillers. Colmenar-Santos et al. [42] studied the potential of thermal desalination thanks to parabolic and geothermal collectors in the Spanish southeast regions. Applying the theoretical results to the existing desalination plants of the Spanish project “Actions” enables an amortization of 6 years and 510.39 kt/year CO_2, which is kept away from the atmosphere for all these plants. Mendoza Castellanos et al. [43] integrated a thermoelectric-hydraulic system to analyze the performance of PTC/ORC coupling in the production of electrical energy. The obtained results prove that the hydraulic accumulation system ensures a backup of 60 min of continuity when solar irradiation falls by 14%. Several other studies have already been established to improve the performance of PTC systems via geometric and optical optimization [44], using new cavity receivers and enhanced working fluids [45], and assessment of various designs for multi-generation applications [46]–[51].

3.2. Solar Tower

A solar tower (ST), also called a "heliostat" power station, produces heat by channelling the air heated by the sun's rays. The heated air will subsequently drive turbines to produce electricity; ST is made up of several mirrors close to the ground and a receiver positioned in the center at a high position [52]. Binotti et al. [53] elaborated analysis of the different sCO_2 cycles for electricity production in ST power plants and deducted that the best cycle can achieve an annual energy effectiveness of 18.4%. Boukelia et al. [54] have shown that integrating dry cooling systems in solar tower plants can reduce the annual consumption of water by nearly 94.5 %. However, this option can lead to considerable reductions in energy and exergetic yields compared with the classic wet cooling mode.

For an installed capacity of 10 MW based on the solar tower with a Thermal Energy Storage coupled with a Steam Rankine Cycle [55], it was possible to produce electricity at an LCOE of $ 0.0947/kWh, which is lower by 31.82% compared to the plant that uses the Open Gaz Cycle and by 48.8% compared to the plant that uses the Organic Rankine Cycle.

3.3. Linear Fresnel Reflector:

Linear Fresnel collectors (LFRs) are considered as a technological solution to minimize the cost of solar energy concentration, maximize the solar fraction ratio and serve for both power and heat generation for industrial use [56]. LFR installations consist of a series of

reflectors that can rotate through the tracking mechanism, a receiver, a steam turbine, an instrumentation/control process system, and generator [57]. The primary role of reflectors is to concentrate solar radiation in an absorber tube located at the focal point of the Fresnel mirror. A heat transfer fluid circulating in this tube is heated to a high temperature, and through thermal cycles, electrical energy can be supplied.

An extensive operational Linear Fresnel Reflector plant was set up in India in 2014, with an expected electricity production of 280 GWh/year and a capacity of 125 MW. Presently, several plants are under development by Alba Nova in France (12 MW) and by IRESEN in Morocco (1 MW). Four Fresnel reflectors linear plants with a capacity of 50 MW are under construction in China [9]. Research developments are currently focusing on enhancing the energetic and exergetic efficiencies of the LFRs to reach competitiveness against other electricity production options ([58]–[60]). In Saudi Arabia, a techno-economic study concerning the implementation of CSPs with cogeneration gas turbines was established by Mokheimer et al. [61]. It was deduced that the best configuration is obtained with integrating the LFR with the steam side of a 50 MWe gas turbine CHP plant, resulting in a LEC of 5.1 c€/kWh with a reduction potential of 119 ktonnes of annual CO_2 emissions. Moghimi et al. [62] conducted a performance analysis of the LFR technology. The characteristics of a trapezoidal cavity absorber were optimized. The analysis confirmed that a high thermal efficiency could be reached if the system is well optimized. Additionally, the cost of the receiver cavity can be minimized by reducing the side wind load. Sait et al. [63] established a comparison between Linear Fresnel Reflectors and Parabolic Trough Collectors. This comparison led to a similarity of the two combinations in terms of optical performances and flux intensities. It was indicated that the LFR does not require a large capital investment compared to the PTC since the design is more flexible. Additionally, it can generate steam directly without resorting to the usage of thermal oil and heat exchanger [64]. Abbas et al. [40] conducted a study that offered an optimal and innovative design of receiver for LFR, satisfactory returns for the whole day were achieved even with a considerable variation in the intensity of radiation.

4. Solar Dish Stirling for power generation

The solar dish collector can be employed for diverse applications apart from power generation. The most developed application is for power generation using Stirling engines. Solar dish Stirling systems have shown promising results in terms of efficiency conversion; about 30% of the sunray could be harnessed and converted into electricity [65]. The Solar

Dish Stirling technology mainly consists of a set of parabolic mirrors, metallic support, and the Stirling Engine [66]. **Fig. 5** represents a working model of a Solar Dish Stirling with the primary operating devices. Once the energy is absorbed, it would be directly transmitted to the working fluid in the Stirling engine (SE) using a receiver. SE adopts the same principle as most other engines; it converts thermal energy into mechanical power by acting on the pressure of the fluid. When it is cold, the pressure of the working fluid must be increased, and it must likewise be reduced when it is hot. The movement is now linear; it will then be transformed into rotation to produce electricity using an electric generator [67].

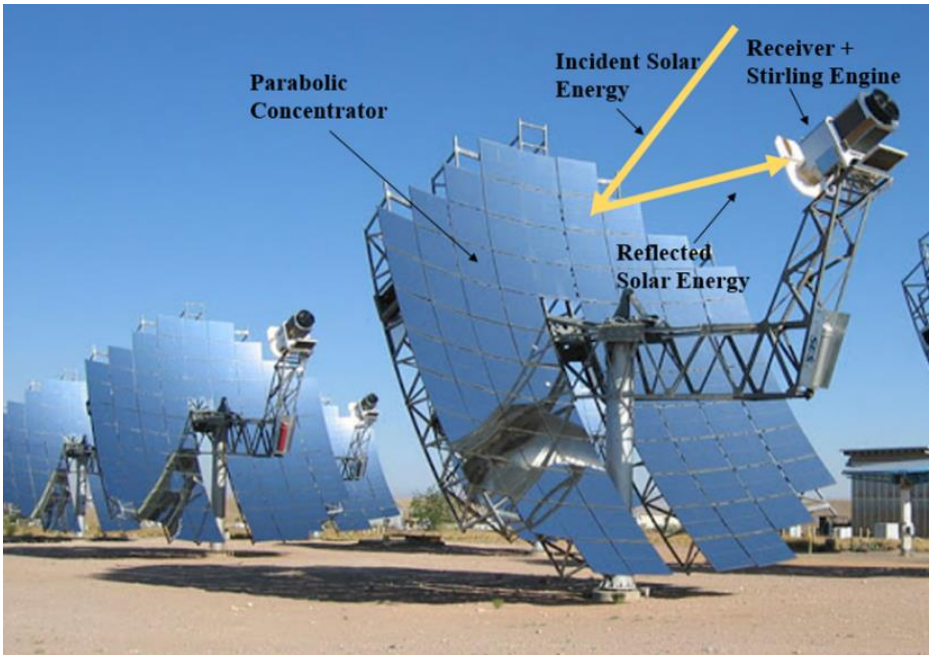


Figure 5: Solar Dish Stirling Technology with its principal components [25]

Compared to other internal combustion engines, the Stirling engine offers high efficiency with low exhaust emissions, hence the interest in stimulating the integration of this kind of technology, eco-friendly, to electricity production [68]. Compared with Photovoltaics systems, SDS systems remain less efficient in terms of cost and power generation but more promising in terms of solar to electricity conversion efficiency [69]. Photovoltaics are also applicable and suitable for small-scale use; even so, SDS technology presents a great potential when their integration is oriented to large-scale applications [70]. It should also be noted that PV technology has a higher impact on the environment than CSP systems [71]. For an SDS system, several parameters such as solar radiation, collector design, and receiver parameters, can strongly influence the losses at the receiver level [72]. For this reason, the design modelling for the different components of the system must be improved with more numerical and experimental studies. Ferreira et al. [73] carried out a comparative study to assess the

performance of an alpha type Stirling engine driven by biomass and solar energy. The use of biomass can lead to more than 87.5% solar energy; also, the temperatures of the solar source receiver and the boiler bed are 501.85 ° C and 1014.85 ° C, respectively. The LCOE of the system driven by biomass and solar source were found to be 0.109 € / kWh and 0.166 € / kWh, respectively.

Different design parameters [74] and technical aspects in solar dish components must be investigated to achieve maximum yields and avoid further losses. Several reviewers' articles have approached this field of study to demonstrate the interest in optimizing those design specifications for more rational use [65], [75]–[77]. Several studies were conducted as part of the dimensioning of the design parameters, optimizing the geometric quantities of the SDS system's components to minimize the various types of losses that can considerably influence the global energy yields [75].

5. Design improvements of SDS technology

5.1. Solar field layout/ Shading Effect

One of the most critical aspects to maximize the energy yields of solar dish concentrators is to configure properly the solar field so as to minimize the different losses caused by field layout and shading effects [78]. Igo et al. [79] deduced that opting for an unstaggered and rectangular field arrangement can strongly contribute in reducing power losses in a solar dish power plant. Xu et al. [80] revealed that rotating and shifting columns in a solar dish field allowed for the most outstanding results. It was also concluded that the regularly spacing should be avoided for optimal operating conditions. Reddy et al. [81] deduced a solar dish field layout configuration that ensures a good agreement between the spacing of collectors and the amount of shading throughout a year. With the proposed configuration, the power generated can exceed 12 GW per year in Tiruchirappalli city, India. Cumpston et al. [82] optimized the solar dish field arrangement and revealed that using rectangular arrangement with adjusted spacing in North-South direction, the thermal power generated can exceed 49 percent of annual thermal energy per unit collector area. Since each location possesses a specific weather profile, solar field disposition is location-dependent and consequently, one can expect a remarkable change in terms of cost and performances. From another side, solar field layout parameters as well as the array shading characteristics can differently affect energy and financial indexes. Hence, multi-objective optimization approaches based on evolutionary optimization algorithm can be employed to detect the best trade-off between the energy and cost criteria.

5.2. Collector and tracking

Several works carried out the influence of the tracking mechanism on the solar dish performances [83]. Spin elevation-tracking mechanism can minimize the concentrator's tracking errors and allow for better optical design performances [84], [85]. The improvement of the collector structure can maximize its optical efficiency. Further outdoor conditions such as soiling can negatively affect this efficiency.

Buscemi et al. [86] analysed through a numerical model the impact of mirror soiling in the desert on the optical efficiency and the net electricity production of the solar dish Stirling collector. The proposed numerical model can assist activities of cyclical cleaning of the collector mirrors for optimal operating conditions. Mendoza Castellanos et al. [87] have developed a mathematical model that allowed defining the opt-geometric parameters and the dimensioning elements of the system and parameterize the control and tracking mechanisms of an SDS. The results reveal that for collectors with diameters between 10 and 20 m, a negligible variation of about 2% in overall efficiency is observed. Zayed et al. [88] modelled an SDS system to characterize overall efficiency and power generation. The proposed model is based on the opt-geometric dimensioning analysis to detect the optimal parameters that guarantee the best energy yields. The results obtained under the meteorological conditions of Tianjin in China show that values of more than 18 kW and 58 kW are reached with concentrator diameters of 10 and 17.5 and efficiency, which varies between 23.7% and 24.25%. Hafez et al. [89] developed a theoretical study to select better SDS components' design parameters that can positively influence the economics and the power output. The results show that to achieve a value of about 97% of the net conversion power, it is necessary to opt for a non-metallic polymeric film as optimal reflector material. Other works were reported to assess the technical and economic impact of the material adopted at the level of the reflective surface. Cavallaro et al. [90] suggested an inexpensive reflective surface based on fine polymer films which could be covered by aluminium or silver. In terms of market availability, a number of manufactures used vacuum membrane for solar dish collector technology [91]. Hijazi et al. [92] established a study in which the main objective is to construct a solar parabolic dish with high system performance and low cost. For this reason, stainless steel sheets have been exploited as reflective area. For a dish diameter of 5 m and 10 m, a rectangular beam of 40 mm* 8mm and 90 mm*8mm, respectively, better results could be obtained. Ferreira et al. [93] conducted a mathematical analysis to carefully detect the geometrical design parameters of solar dish collectors and the receiver variables that allowed for more rational use of the SDS technology. It has been observed that for a dish diameter

value of 6.58 m and a receiver aperture diameter of 0.12 m with a rim angle of approximately 41°, the total cost is at least 4717 €. The results also show the impact of the receiver and dish parameters on the cavity's absorber temperature, contributing to a thermal efficiency of around 64% in the ideal case. Schmitz et al. [94] suggested a novel solar dish system which utilizes facets with elliptical vacuum membrane. The model was experimentally evaluated and it was proved that such facets minimize the cost of manufacturing compared with the other systems. A concentration ratio of about 3140 and radiative power of around 4000 W was obtained using a 60*60 mm surface area. Buscemi et al. [95] optimized the collector aperture size of a SDS system based primarily on the hourly frequency diffusion of the direct normal irradiation (DNI). The proposed approach was numerically modelled and experimentally calibrated using data of the existing SDS in Palermo, Italy. It has been revealed that in locations which enjoy a DNI values between 2000 and 2500 kWh/m²/y, the optimized system can generate an annual energy between 70 and 87 MWh_e, respectively. Basem et al. [96] proposed a novel power generation system based on a solar dish concentrator integrated with a two-axis tracking mechanism. The suggested system is designed and adjusted accordingly to provide water vapor which will then be exploited to generate electricity using Rankine cycle. The overall system efficiency and the global power generated were found to vary from 32% to 42% and 800 W to 1000 W, respectively with a maximum steam temperature value attaining 400.1°C.

The optimization of the various optical and geometrical parameters of the solar dish concentrator is necessary to achieve maximum energy harvesting. This achievement could be more enhanced if tracking device and effective reflective material are introduced simultaneously. Also, mitigation soiling options should be applied because of their high influence on the overall system efficiency. In this regard, passive or low-cost cleaning systems can show promising results. All previous strategies should be technically and financially assessed prior their test and experimentation in real applications.

5.3. Receiver

The optical performance can be improved if the geometry of the heating tubes and the cavity of the receiver are optimized. Liu et al. [97] have developed different designs of receiver heating tubes to achieve more gain in terms of absorbed energy. Mohammadnia et al. [98] studied the integration of a thermoelectric generator (TEG) as an energy harvester in the receiver cavity of a Solar Dish Stirling system to capture more solar radiation and enhance overall system yield. A power of about 14 kW is obtained at solar noon with an improvement

of system performances of about 20% at the start of the day and 30% at the end. Pavlovic et al. [99] conducted a comparison between the spiral design and the conical design for the cavity receivers of a SDS based on an improved thermal model (see **Fig. 6**). The study allowed for fixing many coils for each design and optimize the receiver's location. The results revealed that at 100° C, the thermal and exergy efficiency in the case of the conical design is 5.63% and 6.67% respectively, thus, with a value of 200°C, these values can reach 40.45% and 42.06% respectively. In addition, an increase of 1.38 is observed in optical efficiency. It was as well shown by Tharun et al. [100] based on a comparison investigation between the conical and elliptical cavity receivers that the coefficient of heat losses using elliptical cavity receiver is higher than the conical one. Garrido et al. [101] established a comparative study of four Dish Stirling cavities by experimentally analysing the impact of the form and diameter of the cavity aperture at different operating temperatures. Results analysis proved that the parameters of the receiver cavity must be optimized according to the mechanisms of the system; thus, adopting the inverted conical form of the cavity may present more efficiency to the overall system. Conical shape was also recommended by Daabo et al. [102]. It has been revealed that the highest optical efficiency was obtained using a conical configuration with a value of 72.2% against 68.7% and 65.4% when using the spherical and cylindrical shapes, respectively. Hussain et al. [103] studied the heat losses occurring in the cavity receiver of a solar Stirling engine, and experiments were elaborated to distinguish the promising configuration based on two dimensionless criteria (the aperture ratio AR and the aperture position AP). It was observed that the cylindrical cavity of the receiver with AR and AP equal to 0.5 and 0.53 respectively is very appropriate. Yang et al. [104] proposed a system able to lessen convective heat losses occurring in the cavity receiver. The solution consists of an air curtain control system that can avoid up to 58% of the heat losses, and the results can be slightly enhanced using the counter clockwise circulation mode. Yan et al. [105] proposed a cavity receiver of an SDS that improves the optical efficiency. This design relies on a reflecting cone placed at the bottom of the cavity and a tracking mechanism. The simulation results show that the adoption of the reflective cone allows increasing the optical efficiency by approximately 4.18% for an SDS system of 38kW. Moreover, it turned out that the optical efficiency can be enhanced for reduced values of the receiver window radius. Garrido et al. [106] conducted an experimental study and simulation analysis of four types of receiver cavities for an SDS system. The results showed a great advantage in terms of efficiency when using reverse conical cavity because it reduces the surface exposed to the convection losses. It has also been found that satisfactory results can be obtained for values less than 0.95 of the

interception factor. The radiative losses in the case of an aperture diameter of 190 mm become greater than convection losses when the cavity and receiver temperature are 590°C and 705°C, respectively. A correction must be introduced depending on the irradiation value, so that the thermocouple will be able to regulate peak-operating temperatures.

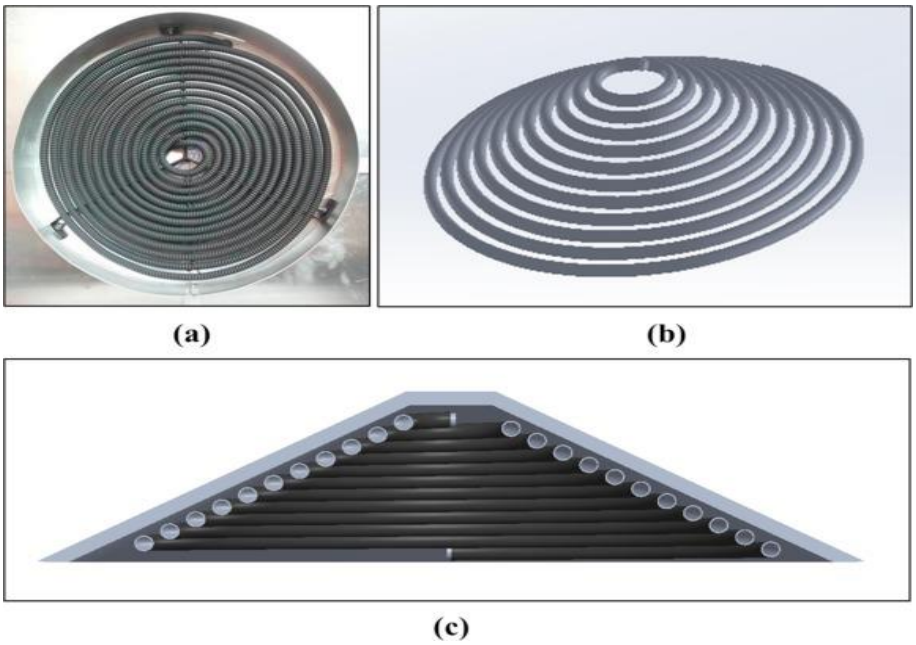


Figure 6: The studied receiver shapes: **(a)** Spiral receiver cavity; **(b;c)** Conical receiver design [99]

The impact of several parameters on the overall efficiency of a Stirling engine technology has been investigated [107]. An increase in engine efficiency of more than 8.8% is observed when the wall temperature of the absorber changes from 700 K to 1000 K. Additionally, increasing the tilt angle from 0° to 60° can improve engine efficiency by 7.7%. For high aperture ratio values, engine power and system efficiency are decreased. The receiver absorptance is a parameter that greatly affects heat loss; therefore, it should have more interest during the study [108]. Zou et al. [109] proposed a design of a cylindrical cavity receiver of a Solar Dish Stirling system. The receiver is open at the front and closed by a bottom at the back, it contains a helical pipe inside and insulation at the outside of the cavity. The study of this design made it possible to obtain an optimum value of 0.35 m for the internal diameter of the cavity and 0.403 m for the length of the cavity. Maximum efficiency of 71.41% has been achieved when using the optimum values. The findings assessment reported in Ref. [110] revealed that the optimum values of the receiver insulation thickness and the receiver aperture diameter which ensure the highest annual energy yields were found 30 mm and 70 mm, respectively. Chandrashekara et al. [111] performed the use of the exfoliated graphite coating on a cavity absorber with sensible heat storage for a Scheffler dish

system. Such coating type can ameliorate the energy performances in desalination and concentrating power process up to 40% and absorbance of solar irradiation of about 97%. Loni et al. [112] established a comparative study of several cavity receiver shapes of solar dish collectors using nanofluids. The results revealed that with the use of the nanofluids, the hemispherical cavity could allow for higher thermal efficiency up to 12.9 % more than cubical and cylindrical cavities. Kumar and Yadav [113] conducted an experimental study of a solar dish concentrator considering different size of reflective material. An anodized sheet of aluminium with various size has been integrated which made receiver diameter values to range between 0.15 m and 0.304 m. It has been shown that a maximum outlet receiver temperature of about 309°C was attained which coincides with a value of 0.15 m of receiver diameter. The findings also revealed that the temperature decreases at the outer surface while increasing the receiver size.

Using nanofluids in solar dish systems as working fluid can have several impacts on the overall energy performance. Loni et al. [114] performed 4 nanofluids types using a cylindrical shape of the cavity receiver to extract the one that provides the best yields. The higher nanoparticles concentration ratio (between 0 and 5%) reveals that the thermal efficiency and the entropy generation decreases while the exergy efficiency increases. Additionally, Cu thermal oil presented more promising results in terms of exergy compared with SiO_2, Al_2O_3, and TiO2 thermal oils. Pavlovic et al. [115] obtained the same conclusions when analysing the suitability of the Cu thermal oil at the level of the exergy yields with a value of 12.29%, which could allow for more favorable results if the corrugated absorber was introduced, in the other hand, the use of the water with nanofluids particles presents encouraging results in terms of thermal efficiency. Loni et al. [116] established practically the same analysis using spiral shape of the cavity. Different results were obtained for an aperture of the solar collector equal to $10.29\,m^2$ and a concentration ratio of about 28.46%; the exergy and thermal efficiencies were calculated and found close to 10% and 35%, respectively. Furthermore, Al_2O_3 shows better energy efficiencies while CuO manifests great interest in terms of exergy. For a cylindrical form of the cavity receiver, Loni et al. [117] suggested the use of MWCNT based thermal oil as a working fluid in a solar dish concentrator system. The experimental results show that the obtained thermal efficiency with MWCNT oil nanofluids was equal to 63.9%, which is higher than that obtained using pure thermal oil. In addition, this solution could increase the cavity's thermal efficiency up to 13.12%. Rajendran et al. [118] investigated the impact of SiC+Water nanofluids on the exergy efficiency and the thermal conductivity of a solar dish receiver. The average exergy efficiency of the water was

calculated 21.08%. This value attained 37.06 %.when using the SiC+Water nanofluids. Pakhare et al. [119] examined the experimental results of a solar dish collector designated to heat water with and without nanofluids. It has been clear that the use of the Al_2O_3 nanoparticles improves the collector efficiency by 10% and the water temperature in the storage system up to 90°C while it did not exceed 85°C before.

International Nanofluid Property Benchmark Exercise (INPBE) is formed to report on the eliminate inconsistencies of the Nanofluid properties including thermal conductivity and viscosity measurements. INPBE provides a balance between true and false information, which is around in the field since a first false claim was made on the benefits of nanofluids some 15 years ago [120]. The exercise's main methodology is to compare the data regarding the nanofluids obtained from various organizations for the same samples. To generalize the results, INPBE methodology intends to choose test nanofluids with a broad range of parameters including aqueous and nongaseous basefluids, metallic and oxidic particles, near-spherical and elongated particles, high and low particle loadings. Although there are some systematic differences in thermal conductivity measurements because of difference in measurement techniques, the thermal conductivity enhancement is somehow consistent at the same temperature measured with the same techniques [121]. In another INPBE study, influence of particle shape and concentration on the viscosity of the same nanofluids were examined and compared. It was observed that the dependency on viscosity was strong for spherical and rod-shaped nanoparticles due to particle agglomeration [122].

From the literature survey, it was revealed that the receiver is among the most critical components in the SDS technology having remarkable influence on the overall system performances. The selection of the cavity shape should be appropriately examined to ensure the highest optical efficiency. In this regard, experimental evaluation, multi-criteria analysis and CFD modelling are substantial to detect the efficient receiver cavity configuration. More studies must be carried out on heat losses at the level of receiver cavity, this factor have a huge influence on the global energy performances. Environmental effects such as wind flow should be covered during the power losses investigation. Convective heat losses problem can be minimized by applying proper coating and coverage [123]. Furthermore, parametric analyses should be performed to select the optimal values of the receiver aperture diameter as well as the insulation thickness for a given operation scenario. Nanofluids were proven to have positive impact on the efficiency of the thermal cavity especially at elevated temperature levels. Nevertheless, cost-effective assessment with exergetic and economic analysis must be performed for comparison with the conventional thermal improvement approaches for more

insightful conclusions. Previous investigations reported that the integration of TEG allowed to capture more solar irradiance and eventually, can significantly contribute to the global efficiency enhancement, but financial constraints and adaptation to large-scale systems remain a major challenge.

5.4. Stirling Engine

At the level of the Stirling Engine, several geometric variables and operating parameters should be well selected to achieve considerable enhancement on engine performances [124], [125]. Multi-objectives optimization approach and different optimization algorithms are used to discern the best combinations of the decision variables, which allowed for greatest yields [126]–[130]. Three types of Stirling Engine exist with specific differences. Abuelyamen and Ben-Mansour [131] conducted a comparative study between the α, β and γ type Stirling engine using air as working fluid (**Fig. 7**). Numerical based-CFD model considering heat radiation within the engine has been established to simulate the energy performances and comparison against experimental measurement was performed to validate the proposed model. It was shown that maximal thermal efficiency and power output were achieved by γ-type engine with a value of about 9.8% and 9.223 W, respectively. Results revealed that lowest energy performances were detected at the level of the α-type Stirling engine with a value of 1.8% of the thermal efficiency. Bataineh et al. [132] performed a finite time thermodynamic study with the model of the irreversible cycle to optimize the Stirling engine characteristics trained by a solar parabolic dish, which the performances were investigated using the non-linearized heat loss analysis. The maximum value of the global efficiency reaches 32% when the absorber temperature is about 850 K, and the concentrating ratio is equal to 1300. Shendage et al. [133] elaborated a numerical analysis of a 1.5 kWe SDS system (Beta configuration) to guess the global efficiency employing the ARUN160 concentrator experimental correlation. It was revealed that the global efficiency reaches a value of 25% when the expansion space temperature varies from 750 K to 1050 K. It was also observed that the variation of the efficiency is negligible for temperatures higher than 750 K. Kumaravelu and Saadon [134] numerically investigated the integration on different shape of fins attachment in a beta-Stirling engine model. It was observed that the power generated by the engine and the amount of the heat transfer were relatively improved and a maximum efficiency of about 19.03% was attained. Bataineh and Maqableh [135] developed a novel thermal model of a beta-Stirling engine configuration with a rhombic drive as a transfer mechanical device. System was thermodynamically assessed and a difference of around 3.26% of the efficiency was detected compared to experimental data furnished by the GPU-3

Stirling engine. Cheng et al. [136] developed an energy approach to anticipate the performances of an alpha-type four cylinder double acting Stirling engine. The proposed Stirling engine can attain a maximum power shaft of 1103 W at a heating temperature and a rotation speed of around 1200 K and 878 rpm, respectively.



Figure 7: Stirling engine configurations: **(a)** α-type; **(b)** β-type and **(c)** γ-type [131]

Furthermore, the Stirling engine could also be integrated with another CSP technology. Zhu et al. [137] proposed a model based on the coupling of a Stirling engine with a Parabolic Trough Collector instead of the dish collector. The system has been realized and studied for cogenerating electricity and heat, a thermal-to-electric efficiency of about 15%, and a 573K. Aksoy et al. [138] have elaborated a study on a micro-energy conversion system based on a beta type Stirling engine, which will receive radiation from a Fresnel lens. The conversion efficiency of around 5.6% has been achieved with a shaft power exceeding 60 W with an aluminium cavity. An energy production system based on Stirling technology and Fresnel lenses has been proposed. A storage system uses Zeolite pellets impregnated with magnesium sulfate to conserve thermal energy and use it in periods when there are no sun rays [139].

Maximal overall efficiency and electric power output can be attained if the Stirling engine parameters are appropriately tailored. In this sense, CFD simulation can be suitable to describe Stirling engine kinematics avoiding efforts and complications encountered in experimental tests. Moreover, valid thermodynamic models should be elaborated in order to evidence the optimal operating and design characteristics such as engine speed, expansion phase angle and temperature ratio. Improvements pathways for maximal power output can be also achieved by the integration of regenerator with high effectiveness index. Improved and economically viable working fluids can play important role in this context.

5.5. Regenerator

Regenerators ensure two objective functions, which are thermal storage and internal exchanger tasks. The integration of this module in the Stirling engine improves its efficiency and guaranties high thermodynamic performance [140], [141]. Various works were performed for the investigation and the optimization of different characteristic design of the regenerator [142], [143]. Ye et al. [144] established a one-dimensional thermodynamic model allowing studying exergy at the regenerator level of a solar Stirling engine by visualizing the impact of the exergy losses of heat transfer and flow friction as well as other parameters such as engine efficiency. The results allowed detecting an optimal value of 35 mm of the length of the regenerator; this value ensures both a high value of the engine efficiency with a reduced value of the exergetic losses. Chahartaghi et al. [145] analyzed the energy and exergy of a beta-Stirling Engine at several operating conditions thermodynamically. It has been revealed that heat and frictional losses could be amplified if the rotational speed is increased. In addition, results showed that a maximum value of exergy efficiency could be obtained at a reduced length value of the regenerator. A longer regenerator length value can positively impact the exergy efficiency when the selected working fluid is hydrogen.

It can be concluded that higher thermal efficiency in Stirling engine was attained with high regenerator effectiveness. Increasing the regenerator effectiveness depend primarily on the minimization of the global heat losses which are due to pressure drops. Flow friction, regenerator matrix porosity and throttling process drastically affect the effectiveness of the regenerator [77]. The main regenerator role is to recover the energy of the working fluid. Hence, imperfect regeneration can occur due to the convective thermal resistance between the regenerator area and the working fluid [73]. In this aspect, performance analysis considering energetic and exergetic assessment is suggested to optimize and select the different parameters and factors of regenerator module.

Fig. 8 illustrates a summarizing chart of the various research development of the SDS technology.

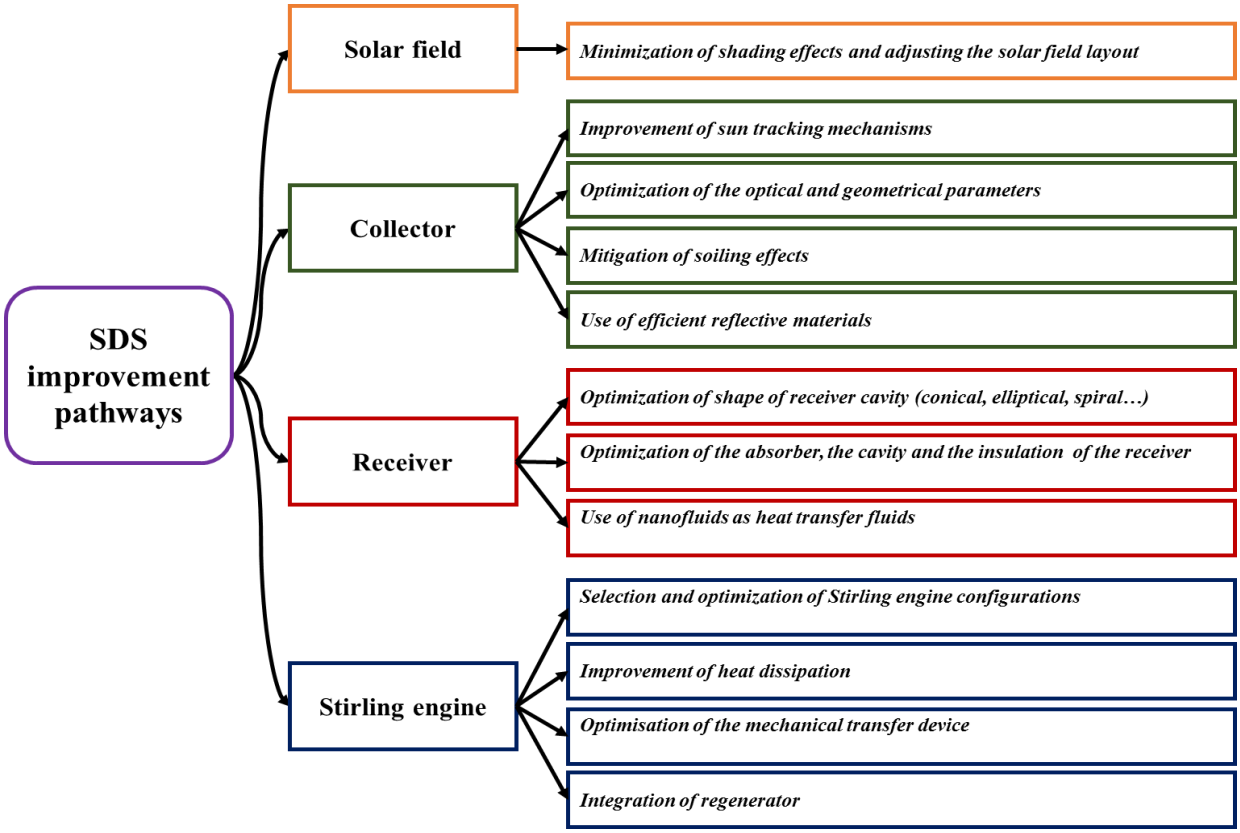


Figure 8: Illustrative bloc diagram of SDS improvement pathways

6. SDS assessment studies

Several investigators developed numerical models and carried out energy, exergy, and economic analyses of solar Dish Stirling technology in various locations worldwide as a sustainable power generation alternative. Lessandro et al. [146] have drawn up a study to select the best geographical location for implementing SDS technology in Brazil. The methodology of the analytic hierarchy and the fuzzy logic was applied in coordination with the geographic information system (GIS). It turned out that the state of Bahia has a high potential for solar energy and therefore presents the best location for SDS implementation compared to the other investigated areas. Lai et al. [141] opted for a modified theoretical model of the SDS to study the system's performance. The results show that for higher components effectivity such as the regenerator and the heat exchangers, the system's overall efficiency can exceed 44%. Farsakoglu et al. [147] developed a 3-D model to deal with the constraints encountered during the design and analysis of SDS system with generator. This work optimized the parameters that can influence the system performance. A small-scale experimental application was developed based on solar dish concentrator with polished aluminium sheets. The obtained global efficiency was ranging between 24% and 36%. A theoretical study was conducted by Babikir et al. [148] estimates the production and the

monthly output of an SDS to cover part of the electrical need in Chad. A value of 21% of the overall system efficiency is obtained when the direct normal irradiation is 906 W/m². Farsakoğlu et al. [149] developed a mathematical model to enhance the performance of the SDS system. The mathematical model predicts a maximal output power of the overall system equal to 250 W with a concentration ratio 94 times better. The proposed system is installed in Kilis city, Turkey, and can generate more than 400 kWh/ year of electricity with an overall efficiency of 17%. Mendoza Castellanos [150] validated the mathematical model of SDS performed by Mendoza et al. [87]. The results pointed out that for values between 520 and 950 W/m² of solar irradiation, the experimental results roughly reveal compatibility with theoretical results. Additionally, the system can reach a value of more than 17% of the efficiency and can produce a power of 1 kW for solar irradiation value of around 725 W/m². In Thailand, a model of SDS has been investigated for power generation to small-scale usage. An engine with a nameplate capacity of 25 kW and a concentrator surface of 131 m² can deliver more than 27 MW per year of electrical energy with an overall system efficiency of about 17% [151]. Moghadam et al. [152] conducted a study on integrating a solar dish Stirling micro-CHP system in a residential building in five locations. It turned out that the choice of the Stirling engine size according to the lower annual demand for electricity is compatible with dry climates. An SDS with constant output capacity or an SDS whose size is chosen according to the maximum annual consumption will be the most suitable combination for hot and humid cities. Vahidi Bidhendi et al. [153] have developed a numerical model validated by experimental measurements with an inaccuracy of about 15% to examine the impact of dynamic parameters of an SDS system. The results show that the minimum value of solar irradiation with which the engine could start is 480 W/m². The annual efficiency reaches a value of 16% in a city in Brazil (Natal); the solar energy converted into electricity is only about 20% of the total value radiated toward the dish. It has also been found that reducing the compression temperature by a value close to 30° C can improve the maximum power by more than 5%. Kadri et al. [25] assessed the performance of the SDS integration in a Tunisian zone within the framework of rural electrification. The model consists of an SDS coupled with a synchronous generator and a storage battery. Experimental tests have validated the simulation results to conclude that the proposed system can guarantee autonomy and stability of electricity production under the meteorological conditions applied for a rural house in the target site. A European project called BIOSTIRLING - 4SKA (B4S) led by B4SKA and fourteen European companies was designed to implement Stirling solar power plants for efficient storage and hybridization on an industrial scale. The perspectives of this project is to

establish a methodology that addresses maintainability, reliability, and cost assessment. The first system was tested in Portugal in 2017, generating a power of 4 kW and avoiding the constraints of Stirling technology and hybridization [154]. Sookramoon et al.[155] experimentally studied a two-stage SDS in Thailand. The results show that the system can provide a conversion efficiency of about 3.71%. With a speed value of 55.6 rpm, the motor was able to generate a power of 0.359 W. In addition, the electrical power delivered can reach 0.27 W with a generator efficiency of about 79%. Yan et al. [156] suggested a design of Solar Dish Stirling (SDS) with a nameplate capacity of 38 kW. An area of 204 m² of a parabolic dish and a focal length of about 9.49 m were adopted with a heat engine known as Flexgen S260. The system was tested for several locations, and a conversion efficiency of 25.3% was obtained at a DNI of 750 W/m². Additionally, a fitting function of a NPO (net power output) was engendered (NPO=0.1003×DNI−36.129**)** to anticipate the annual power generated for DNI values ranging between 460 to 761 W/m². Gholamalizadeh et al. [157] calculated the heat losses at the level of the receiver and the power produced by a pilot dish Stirling system based a mathematical model for remote location in Kerman, Iran. The suggested model was compared with the experimental results of the EuroDish project. It was seen that the greatest amount of the heat losses occurred by convection and radiation with a value of 284W and 2000W, respectively at midday in the middle of July. Power output and receiver efficiency reached approximately 850W of 0.6, respectively.

Before proceeding to the study of the different Concentrating Solar Power technologies, environmental and economic analyses are suitable to reveal the rate of greenhouse gas emissions mitigation and cost- effective feasibility compared to other solar power generation systems. In this regard, various studies have been carried out in this thematic. Affandi et al. [158] investigated the economic and technical feasibility of a 25 kW parabolic dish Stirling system. The investigation considered the annual energy produced, capacity factor, and the LCOE for five regions in Malaysia. It turned out that the average number of operating days of the system is about 70 days, which caused a significant rise in LCOE. Ultimately, the system may be technically feasible but not economically profitable. Zayed et al.[31] presented a model with mathematical based thermodynamic derivation of 25 kW new commercial SDS to predict its performance in the weather of Tianjin, China (**Fig. 9**). The obtained results indicate that the annual electrical energy produced by the system could reach 28.74 MWh with an annual overall efficiency of 19.55% and a LCOE of 0.2565 $/kWh. Allouhi et al. [110] conducted a 4-E analysis of a 25 kW SDS system in thirteen Southern Moroccan locations. Main receiver parameters were properly selected in terms of the annual energy. Maximal

annual energy and overall energetic/ exergetic efficiencies of a 10 MW installed capacity were detected in Ouarzazate city with a value of 23.693 GWh and 24.26 % / 25.98%, respectively. It was also revealed that the proposed power plant can mitigate annually an amount of CO_2 emissions ranging between 7.76 ktonne and 13.85 ktonne depending on the examined site.



Figure 9 : Overview of the integrated SDS system in Tianjin University, China

More comprehensive studies based on energetic, exergetic, economic and environmental (4-E) assessment must be carried out and validated against experimental measurements in order to confirm the benefits and the feasibility of the SDS technology implementation in a specific area. Moreover, it is worth of mention that the global efficiency and the power generated by the SDS are highly dependent on prevailing weather conditions. Accordingly, before proceeding with the implementation of this technology, it is necessary to establish an evaluation of the geographical proposed location in in order to visualize whether its solar potential will allow to make the installation cost profitable in terms of both the power production and the amount of the mitigated greenhouse emissions. Then, the operating parameters of the different components of the SDS system should be carefully selected and optimized in order to maximize the global energetic and exergetic performances. Further, multi-objective optimization is a strong approach to detect the optimal design configuration that can guarantee the best trade-off between the energetic, economic, and environmental

criteria. Such studies can provide helpful guidelines for achieving market requirements and assist policymakers in evolving strategies for future projects.

7. Summary

This chapter reported a literature survey of the different CSP technologies with a focus on solar dish technology. SDS technology for sustainable power generation was assessed as well as the design improvement pathways of the main SDS components. The concluding remarks of this chapter are:

- An investigation must be carried out to reveal if the solar potential of the examined location will allow to make the implementation cost of the SDS technology effective.
- The focus must be given to investigate the effect of the geometric parameters of the solar dish Stirling components and mainly in the receiver.
- Energy, Exergy, Economic and Environmental assessment studies of solar dish-based systems are of great usefulness to describe the competitivity of the examined concepts.

Further investigations and novel approaches must be established in order to select the best design configuration that can ensure a rational exploitation of this technology in terms of energetic, exergetic, economic, and environmental aspects.

CHAPTER II. Novel applications and optimization frameworks of Solar Dish Collectors

1. Introduction

The research and development activity on solar dish collectors has increased remarkably during the past few years. A rational use and implementation of this technology requires optimum adjustment of several operating and design parameters. The objective is to extract the highest energy generation at competitive costs. In this sense, several attempts were carried out to optimize its implementation for various final usages and accordingly facilitate its widespread commercialization. The current chapter addresses the state-of-art of the SDS technology from a multi-aspect dimension and highlights most recent advances, prospects of solar dish collectors, their applications, and their novel designs. Alternatives to ensure energy autonomy based on hybridisation and coupling of solar dish collectors with other renewable systems were involved. Finally, various approaches and methods used to optimize the design parameters with mutual impact on energy and economic performances were assessed.

2. Background

Recently, Concentrating Solar Power (CSP) systems have received a great attention from the research community [16]. However, insufficient experimental data regarding the operating parameters limit its characterization, modelling, design, optimization, and further utilization. Some review articles have been previously published on this topic and mainly focused on the other CSP systems such as PTC, ST and Linear Fresnel technology [17], [36], [64], [159]. Only few review studies on solar dish technology are available dealing principally with the sizing and analysis of the geometrical and optical design features of the operational system components. For instance, review articles reporting energetic and economic performances were presented by Hafez et al. [75] and Singh et al. [65] based on early technical investigations of the various SDS system components such as solar dish concentrator and receiver parameters. Moreover, Zayed et al.[77] and Aboelmaaref et al. [160] have recently reviewed the thermal performances of the SDS technology as well as its eco-environmental potential in different applications such as desalination processes with storage and hybridization options. Kumar and Agrawal [161] investigated the integration of the SDS technology for cogeneration processes in locations where high energy demand is

required. Several Stirling engine parameters and factors were also discussed and evaluated for power output achievements.

3. Solar dish for multi-end use applications

CSP systems have exhibited encouraging returns in desalination processes compared to traditional methods. Solar Dish Stirling is among the most suitable technologies in desalination cycles because of its compatibility with renewable energy sources [160]. Al-Dafaie et al. [162] used the heat rejected by the solar dish Stirling engine to evaporate water which will be involved in the distillation process (see **Fig. 10**). The results proved that the required quantity of water could be achieved with an encouraging investment cost based on actual weather data.

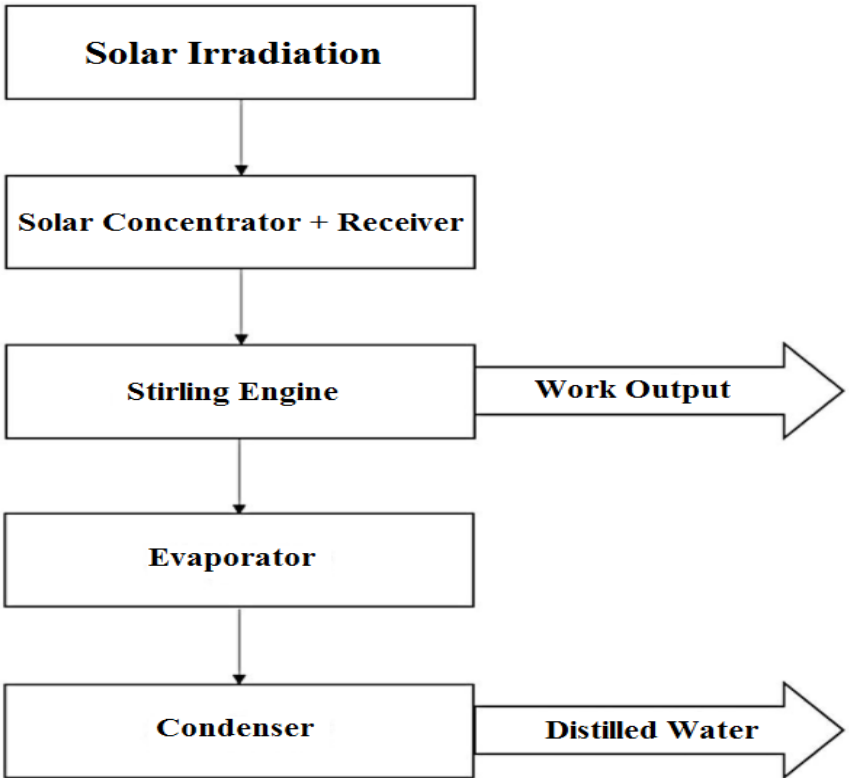


Figure 10: Flow Diagram of the solar distillation setup [162]

Jabari et al. [163] demonstrated the utility of the solar dish Stirling system in zero energy buildings (ZEB). The proposed dish Stirling system was able to satisfy the building's need for electricity and heat. The rejected heat by the engine will be used in the water desalination process. The findings strongly supported the hypotheses already described in terms of feasibility and energy efficiency. Several other studies have been developed in this context, Al-Nimr et al. [164] have also proposed a system based on SDS technology designated to supply both electricity and desalinated water (see **Fig. 11**). The same water

evaporation process has been adopted except that condensation will be done using a thermoelectric cooler powered by a Stirling engine. The integration of the TEC (Thermoelectric Cooler) module, the reuse of the heat rejected by the engine, and the TEC modules have brought a significant improvement on the production rates; more than 40 kg/day of desalinated water has been provided with an efficiency exceeding 64%.

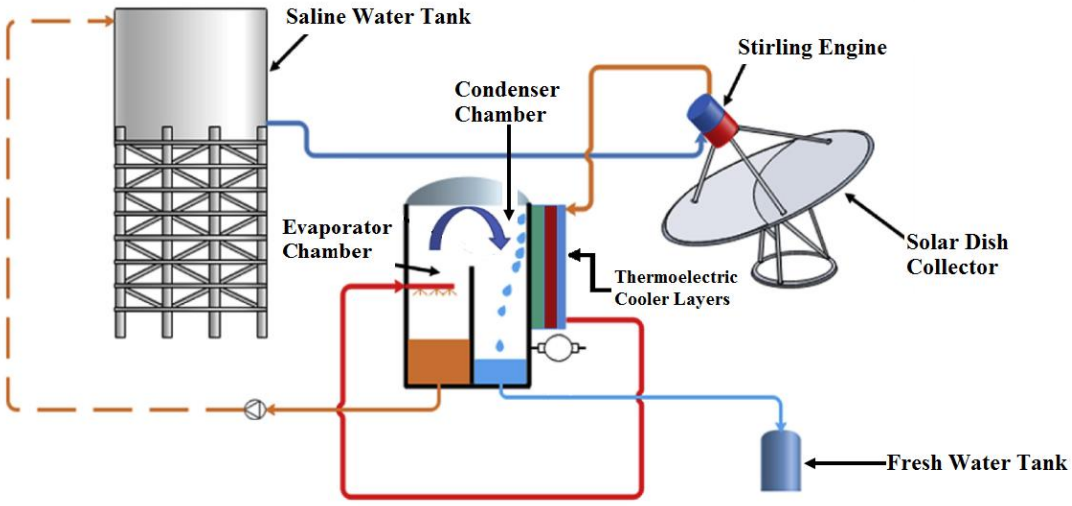


Figure 11: Schematic diagram of a hybrid solar system based on SDS thermoelectric cooler for power generation and water distillation [164]

Açıkkalp et al. [165] proposed a hybrid system that can supply simultaneously electricity, cooling, and heating. The system mainly consists of a solar Stirling engine, a chemical heat pump, and a system of absorption refrigeration. The results show that the proposed system can increase the overall energy efficiency by more than 13% with a maximum power equal to 9.463 kW. Dai et al. [166] proposed a refrigeration system based on SDS technology. The electricity generated by the Stirling engine is transmitted to the refrigerator for the cooling process. The model is based on finite-time thermodynamics and considers the calculation of losses at the level of each system components. The system shows encouraging outcomes that can be used to exploit SDS technology for refrigeration. Recently, Al-Amayreh and Alahmer [167] experimentally investigated the energetic and economic performances of a hybrid system which is composed of solar dish concentrator and PV system in order to supply both heat and light. It was detected that the use of a two-axis tracking device caused a remarkable increase in terms of the thermal efficiency and the average cost by 32.2% and 64.7%, respectively compared to the standard tracking system. An electricity and heat generation plant has been designed to meet the energy system requirements in the engineering department of Palermo. The power station is based on a field of solar dish

Stirling, heat pumps, and a seasonal geothermal storage system. **Fig. 12** shows the overall suggested model which is composed of solar dish collector with seasonal thermal energy storage. Over 96% of the annual thermal needs have been covered, as well as a significant non-consumable amount of electricity can be directed to other uses [168]. Sandoval et al. [169] employed an analysis method based on partitioning solar dish Stirling system performances on solar irradiation, solar dish, and thermal receiver model as well as the model which describes the Stirling engine performance for a city of Natal, Brazil. With the assistance of experimental data exploited at the level of the solar dish and the NS03T Stirling engine, it turned out that the output power and the overall system efficiency can reach over than 1600 W and 26% at 11h during April month, respectively.

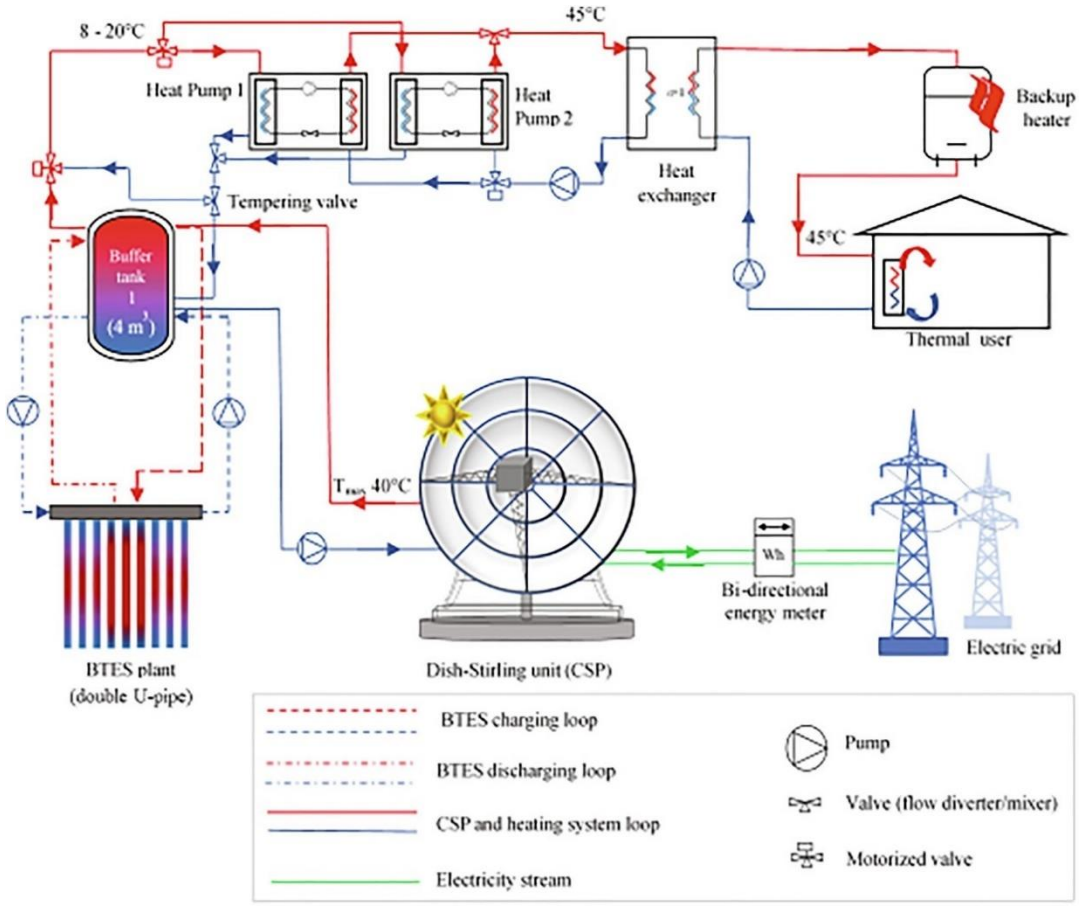


Figure 12:Schematic illustration of the CHP plant [168]

Kadri et al. [170] studied the hybrid system's performance of a grid-connected system which includes both wind turbine and solar Dish Stirling technologies (see **Fig. 13**). Promising results were obtained proving the utility of such hybridization integration. A hybrid-based SDS/wind turbine system was proposed by Shboul et al.[171] for micro-grid power production. The energetic assessment revealed that net power output and the global

efficiency of the Stirling engine were found to be 1500 kWe and 37%, respectively, while the resulting LCOE value ranged from 0.13 to 0.15 $/kWh.

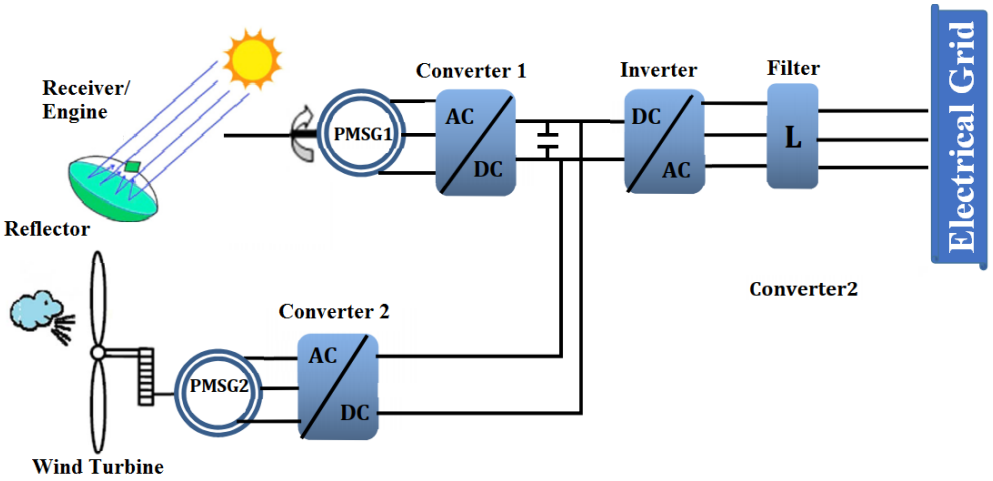


Figure 13: Schematic diagram of the hybrid power generation system [170]

Several coupling configurations have been carried out based on SDS and other power generation systems to ensure stable and clean electricity production while exploiting sunrays as energy source. Rahman et al**.** [172] proposed an interconnected two zones hybrid thermal model based on solar dish Stirling technology and wind power to control power generation automatically. Lai et al. [173] proposed a novel system composed of SDS technology and salinity gradient. The energy produced by the Stirling engine is directed to pressurizing the salt water in order to obtain a concentration gradient that could supply a stable power output with an energy conversion efficiency of around 9%.

Several attempts have been made to integrate SDS into energy generation systems; for example, Tasnin et al. [150] have been able to valorise the integration of this type of technology with geothermal conventional thermal power plants within the creation framework of interconnected electrical systems. Yerbury et al. [174] designed and implemented a micro-generation solar system based on Stirling technology of 150 W. The choice of the adopted materials was carefully taken. The maximum value of the power output was found 88 W when the displacement temperature is 787, 15 K, and the rotational speed is 245 rpm. The mechanical efficiency of the engine can reach a value of 90%. Jabari et al. [175] achieved acceptable use of an industrial heat treatment furnace operating with dish Stirling and wind technology. This configuration was recommended as an alternative to minimize the usage of combustibles and reduce the amount of greenhouse gas emissions. Tavakolpour-Saleh et al. [176] proposed a model of a Stirling converter driven by solar energy to pump water under

several functioning conditions. Jabari et al. [177] proposed a system based on solar Stirling engine along with a diesel engine. The objective of the implementation of this system is to cover the electrical need at peak times in the summer season while ensuring a clean, stable, and autonomous power generation. The results obtained on a microgrid provided a daily reduction of 15.4 $ and minimized the electrical demand of the primary power system. Beltrán-Chacon et al. [178] simulated the performance of an SDS system with an electric induction generator. The proposed model integrates a system with a dead volume of 160 cm^3 to regulate the speed and power according to the variation of the meteorological properties, the mechanical characteristics, and the electrical network parameters. The control system provided an improvement of approximately 18% in electrical energy with a conversion efficiency of around 23.38% at a solar radiation value of 975 W/ m^2.

4. Novel solar dish applications and concepts

4.1. Solar Dish/ microgas turbine solar power generator

The solar dish concentrator can be used as an energy supply source for hybrid microgas turbine. Introducing a 10 kWe hybrid model for small scale application can lead to satisfactory results in the global efficiency when adopting a volumetric receiver with optimal design parameters and material specifications [179]. Thermo-economic analyses and design parameters assessment of a solar dish micro gas-turbine combined-cycle power plant were conducted [180]–[182]. Semprini et al. [183] analyzed a hybrid system's performance consisting of a solar dish collector with a microgas turbine considering Seville city as a reference location. Several design parameters of each component were evaluated while demonstrating the utility of supplementary firing. The results highlighted that the capacity factor attains 29%, with a conversion efficiency ranging between 16.78% and 18.35%. Other studies have developed such combination by adding energy storage by compressed air. Through an energy and exergy analysis, it was revealed that the system could provide 228 kWh and 4 tons of hot water with a power consumption of about 152 kWh [184]. Parabolic dish collectors can also be used as an energy source for microgas turbines in the desalination process. Sánchez et al. [185] conducted a technical and economic analysis of a system that generates both electricity and potable water. With reverse osmosis technology, the system cost varies between 3 and 3.5 €/m^3. It was also revealed that if the process is designated to the production of drinking water only, the solar energy use can exceed 65%.

Fig. 14 represents the schematic view of a combined-cycle system based on the solar dish collector and the microgas turbine.

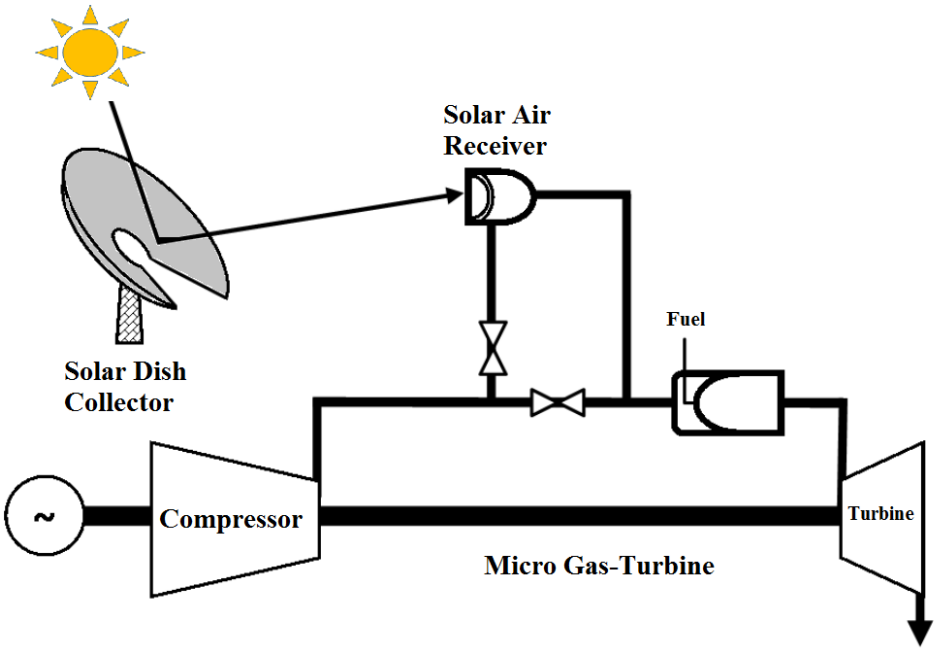


Figure 14: Solar Dish-micro Gas Turbine integrated system [181]

4.2. Solar dish/Brayton cycle

Several works have treated the design parameters analysis of the combined solar Dish Brayton cycle [186], the integration of turbochargers and thermal storage to recuperate the Brayton cycle energy [187], as well as the thermodynamic assessment using multi-objective optimization [188]. Khan et al. [189] adopted a reheated Brayton cycle trained by a solar dish collector for power generation. The simulation considers three types of thermal oil, including nanofluids particles, in order to enhance the heat transfer ratio. With Al_2O_3 oil, high global energy and exergy efficiencies can be reached with a value of 33, 37% and 36.27%, respectively. Li et al. [190] established a solar dish Brayton model using a multi-objective optimization approach considering the performance indicators (power output, the overall efficiency, and thermo-economic performance index). The results revealed that the energy performance indicators of the conventional Brayton cycle are 22.6%, 34.9%, and 18.4%, respectively, which were found to be higher than those obtained by the proposed system. An illustrative view of the system is shown in **Fig. 15**.

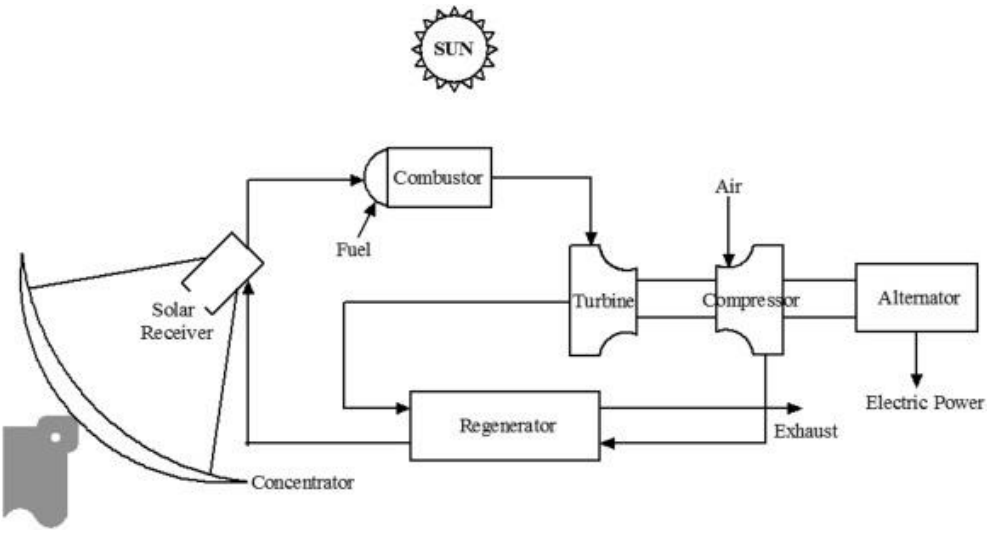


Figure 15: Schematic of a Brayton cycle based solar dish system [190]

4.3. Solar Dish/Flat Plate collectors

Figaj et al. [191] performed dynamic analysis of solar dish coupled with a flat plate collector for small-scale use for heat generation, which afterward will be communicated as an energy source for an absorption-cooling system. The investigation has been experimentally validated and includes economic performances. The results show that the primary energy saving ratio is about 50% with a concentrator efficiency of 0.7, the surface of the concentrator per cooling system capacity is about 1.6 m^2/kW, and the recovery period was predicted to vary between 8 and 23 years.

4.4. Solar Dish/Photovoltaic cells

Due to several advantages and benefits of combining solar dish with photovoltaic cells for power and heat generation [192]-[193], several studies were established to give more comprehensive details helping assess such systems and encourage its implementation, particularly in non-electrified regions [194]. Lv et al. [195] analyzed a solar dish CPV system based on experimental measurements conducted at the level of the focus spot and at the secondary reflector. According to the analysis, the solar irradiation could be focused evenly on the solar cell area and vertically on the concentrator due to the tracking mechanism. The results revealed that the energy efficiency was ranging from 25% to 30% corresponding to Direct Normal Irradiance (DNI) variation.

4.5. Solar Dish/Thermoelectric modules

A system developed by Shanmugam et al. [196] of a thermoelectric generator based on parabolic dish technology is investigated in terms of several characteristics design. The model gives an accuracy of around 10% when comparing with experimental measurements. For promote areas, Eswaramoorthyet al. [197] designed and examined a numerical model of a thermoelectric generator with a capacity of 120 W. The modelled system was driven by a solar dish collector with a surface of 6.3 m² to cover the annual energy need of about 16 kWh for a rural house. This system provides 7% more of the electricity requirement for minimum solar irradiation intensities. Verma et al. [198] carried out constructing a small-scale solar Parabolic Dish (PD) coupled with two types of TEG (TEC1-12706 and SP1848-27145) as a receiver mechanism. An aluminium sheet has been implemented on the PD for more concentration. The efficiency of solar PD reaches 44.16% during May and 52.1% in June. The powers obtained when using TEC1-12706 and SP1848-27145 are 0.665 W and 1.836 W, respectively. The combined overall efficiency of the PD system with the TEC1-12706 module can result in a value of 0.23%, while in the case of SP1848-27145 it is equal to 0.63%. Fan et al.[199] unveiled the potential and benefits of using TEGs in electricity generation process. The model proposed model is mainly based on PD with an opening diameter of 180 cm and a copper receiver plate, where 4 thermoelectric cells have been implemented. For a temperature difference of about 382.15 K, a single TEG can generate 4.9 W with an electrical efficiency up to 2.9%.Shanmugam et al. [200] were able to assess the energy and exergy efficiency of thermoelectric generator based solar dish collector through an experimental analysis. A representative diagram of solar dish thermoelectric generator is shown in **Fig. 16**. The results show that the temperature at the level of the receiver exceeds 400,55K. In addition, the energy and exergy efficiencies vary from 0.94 to 1.68% and 1.01 to 1.81%, respectively. Eswararmoorthy and Shanmugam [201] established a thermodynamic evaluation for the same model. The results reveal that a large amount of energy and exergy losses have been avoided, the overall exergy efficiency of the system is about 2.97%, while the energy efficiency reaches 2.81%.

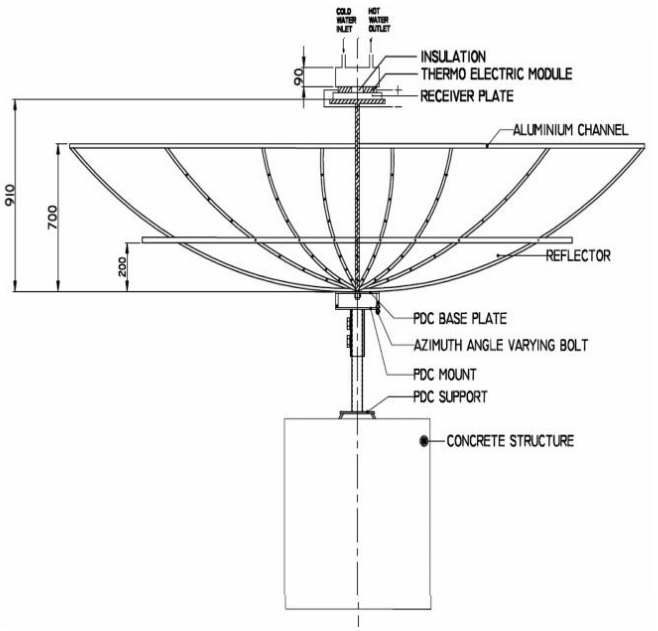


Figure 16: Schematic view of the solar dish Thermoelectric Generator [200]

4.6. Solar Dish/PV and TEG

Bamroongkhan et al. [202] accomplished an experimental investigation of a parabolic dish photovoltaic coupled with a thermoelectric generator and PV cells for power generation. The global efficiency of the proposed model can reach a value of 19.65%. It was also found that the integration of the cooling system can enhance the output power of the PV cell with a percentage of more than 21%, and it can easily get its supply from the output power generated by the overall system. **Fig. 17** illustrates the schematic combination of the proposed system.

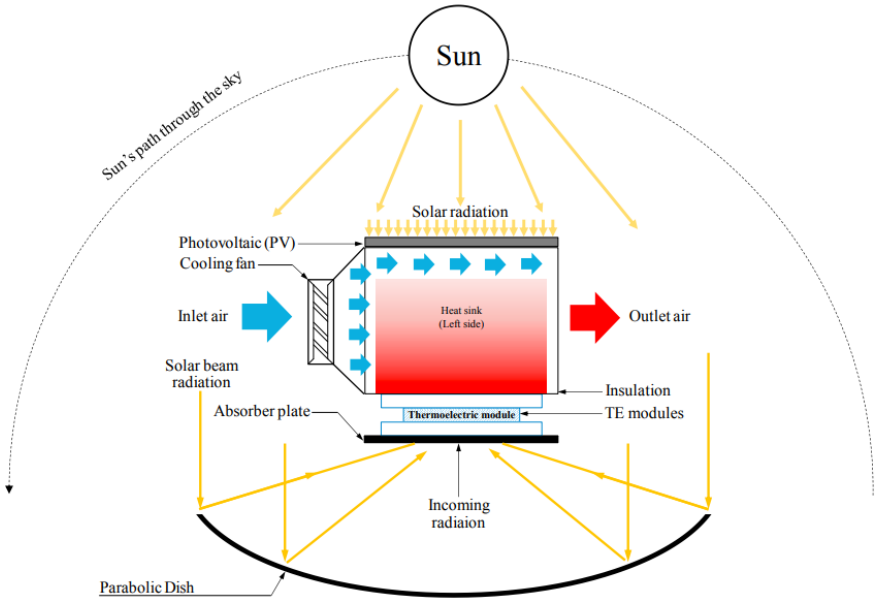


Figure 17: Schematic of Solar dish PV-Thermoelectric generator [202]

5. Solar Dish cogeneration and polygeneration

The parabolic dish collector can be implemented for several quotidian usages [203]. In the cogeneration process, the heat rejected is covered and contributes to improving the system efficiency. In Italy, a development center named HEnergia possesses a solar dish collector with 11.5 kW thermal peak. The system was evaluated during all seasons under different environmental circumstances. In 1326 h of operating, the system provided 5440 kWh and can supply water at temperatures between 40° C and 60°C. In addition, it is possible to adopt these types of technology for heating and cooling in buildings [204]. For small-scale use, Prinsloo et al. [205] proposed a model based on SDS technology for co-generation in rural African villages. This system can serve 3 kW of heat and 1 kW of electricity with a range of 100% renewable energy and can contribute to a significant reduction in fuel use. Solar dish collectors could also generate thermal energy at temperatures up to 1600° C [206]. Accordingly, solar dish technology is considered as one of the most promising solutions to supply electricity and heat for applications that require high temperatures. Gavagnin et al. [207] elaborated the detailed cost investigation of solar dish concentrators combined with Micro gas Turbines (MGT) for cogeneration process. The study considers production, transportation, and implementation costs. It was deduced that the studied system presents more competitivity in terms of financial cost compared to PV systems. It was found that the system cost was ranging between 2500 €/kW_e and 3300 €/kW_e for reduced and high-performance specifications scenario, respectively. Schmitz et al. [208] proposed a model based on six solar dish receivers that contain 36 triple junction CPV cells designated for cogeneration. For PV-operating mode, the suggested system can provide a conversion efficiency to electricity of 28.5%. In contrast, in the polygeneration mode, the efficiency exceeds 26.6% with an output heat temperature of 362,95K, an electric and thermal power of 11.3 kW_e and 21.5 $kW_{th,}$ respectively. Gu et al. [209] designed an innovative cogeneration system based on solar dish Stirling technology. The suggested system includes a control approach that allowed switching between power and heat supply using an adjustable dual receiver. This new configuration showed better system running proportion in three different locations namely Tianjin, Yinchuan, and Lhasa when compared with the standard system. Such cogeneration system is also able to provide power at low LCOE. Moradi et al. [210] investigated a model for multi-generation destined to cover energy needs of a commercial tower in Iran. The proposed model is based on solar dish technology, fuel cell, and a system that generates both heat and cooling, and power (**Fig. 18**). A value of 41.49%, of the fuel cell efficiency, was obtained and validated with experimental measurement. The thermal

efficiency of the global system reached 79.49%, while the electrical efficiency was about 48.73%. The total cost was found 3.470 million dollars, with a recovery time of 4.43 years.

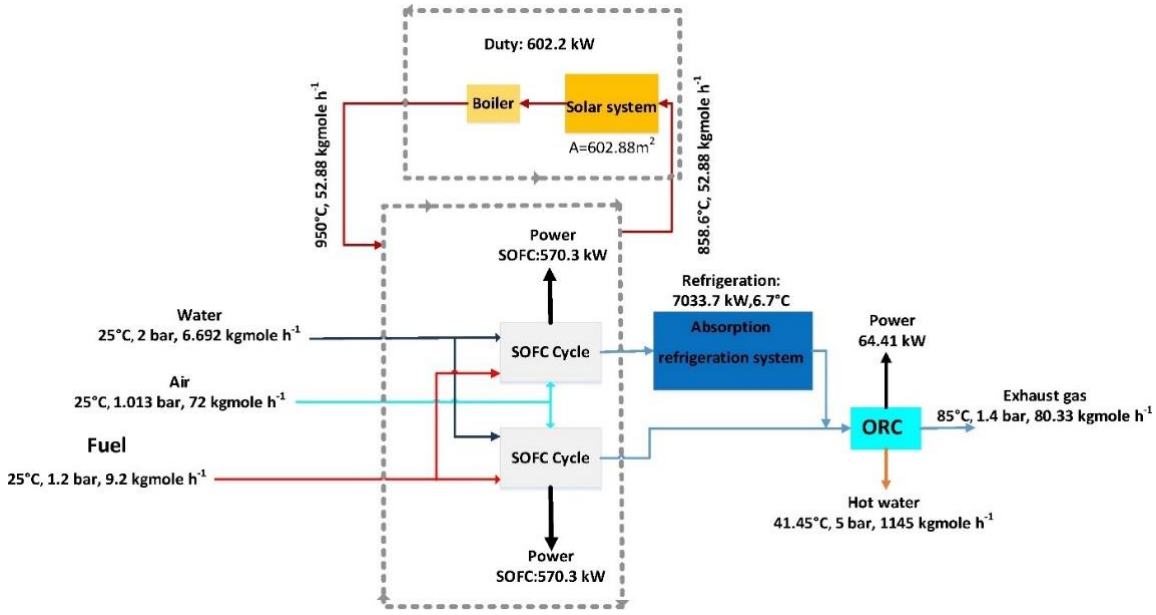


Figure 18: Flow diagram of the combined system [210]

Authors of [211] modelled a hybrid system for polygeneration based on solar dish collectors, oxy-fuel power plant, and an absorption refrigeration cycle. The suggested model can provide 179 MW of power, and 26.27 kg/s of liquid carbon dioxide with a global exergy efficiency of about is 60.74%. The total direct cost is estimated 3.04 cents/kWh with a payback period of 3.3 years.

6. Solar Dish Fresh water production

Parabolic dish concentrator has experienced appreciable ability to supply clean and eco-friendly power for multi-usages. Due to the highly demand of energy and water resources, the implementation of such concentrating solar technologies in desalination process and water treatment was extremely recommended [212]. Prado et al. [213] investigated the performances of a solar desalting system based on dish concentrators. The investigation was validated with experiments and showed that with simplified system of distillation, drinking water requirement for more than two people could be covered. The suggested model unveiled that maximal yield of distilled water was found 4.95 kg/m^2.day. Javidmehr et al. [214] modelled a tri-generation hybrid system for heat, power and desalinated water supply. The system consists of a parabolic dish collector, an mGT, an organic Rankine cycle, a water desalination system, and a way to store energy using compressed air. The global system can

provide 2.5 ton of fresh water during the four hours of discharge mode with a value of about 523 kWh of electrical energy. By optimizing the performance parameters of the system, the round-trip efficiency can vary from 0.652 to 0.735. **Fig. 19** illustrates the schematic design of the CHP system.

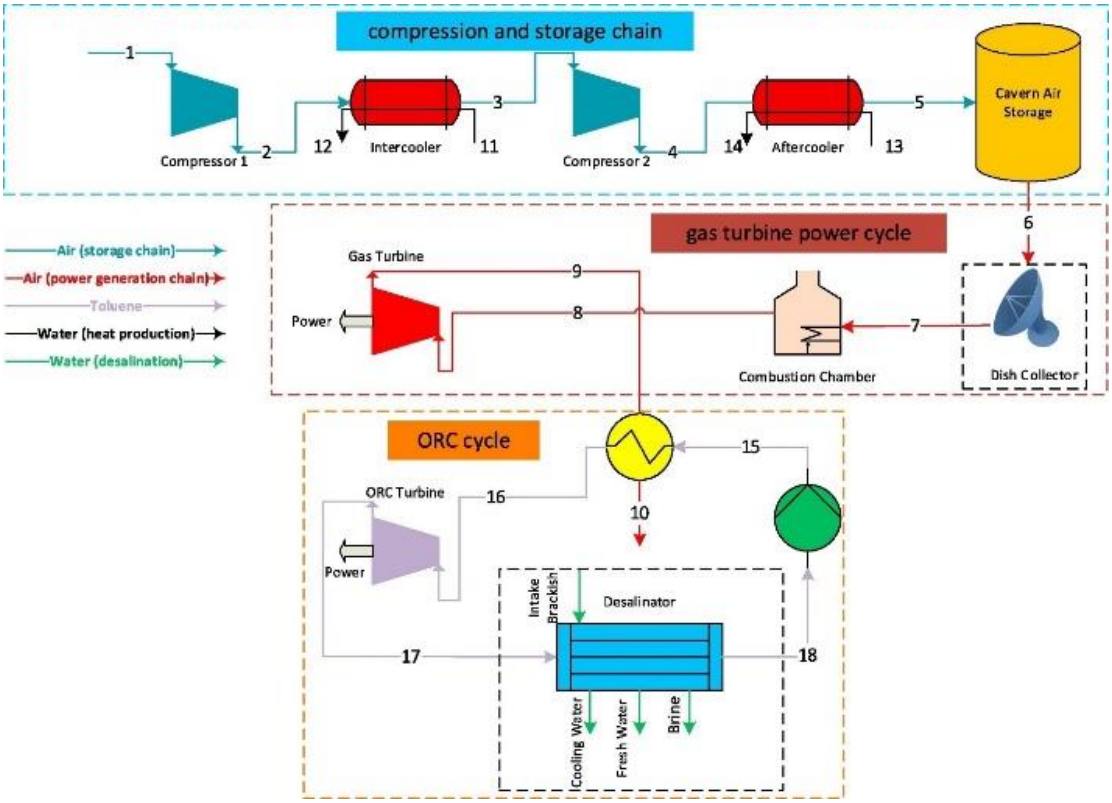


Figure 19: Schematic of the solar dish system integrated with a mGT, an organic Rankine cycle, and water desalination process [214]

Fig. 20 depicted the schematic view of a fresh water production system suggested by Srithar et al. [215]. The system consists of a solar dish concentrator, a triple basin solar still, a photovoltaic panel, and a cover-cooling system. Fins were also integrated to enhance the rate of heat transfer. The experimental results show that the use of a dish concentrator can improve the water temperature in the basin bottom up to 85° C. Additionally, the overall system with appropriate type of fins can provide an amount of 16.94 kg/m2.day of distillate water.

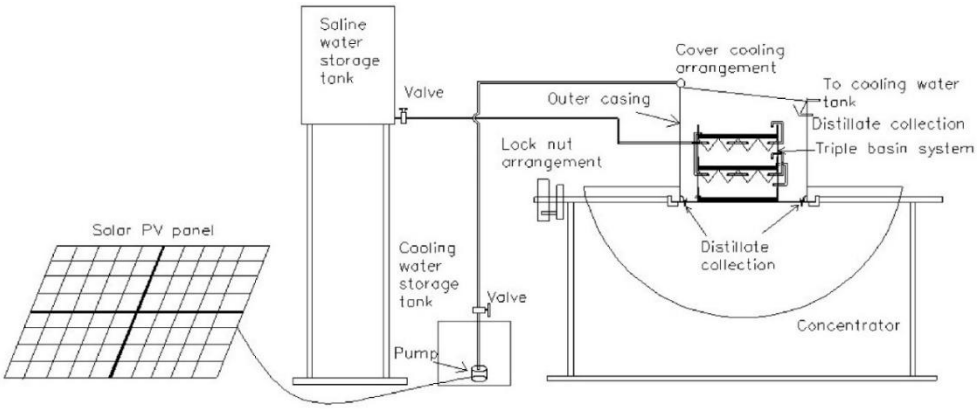


Figure 20: Schematic of the desalination setup [215]

Rafiei et al. [216] proposed a hybrid combined model for solar desalination process based on PVT panels and dish collectors. Three types of receiver cavity (hemispherical, cubical, and cylindrical), various design parameters have been investigated. The results prove that increasing the water and air flow rate while reducing the inlet temperature of the working fluid have remarkable impact on the amount of desalinated water produced. It was also deduced that the use of hemispherical cavity shape can improve the global yield of the system. Bahrami et al. [217] suggested a novel model for desalination process. The suggested model consists mainly on solar still system installed at the focal point of a solar dish concentrator. Theoretical results were validated by experimental measurements and revealed that geometrical parameters have a huge effect on the amount of the distilled water. Additionally, for an aperture diameter of 3 m, 75 kg of distilled water can be obtained at a working period from 8:30 to 17:30. **Fig. 21** outlines the different components of the model.

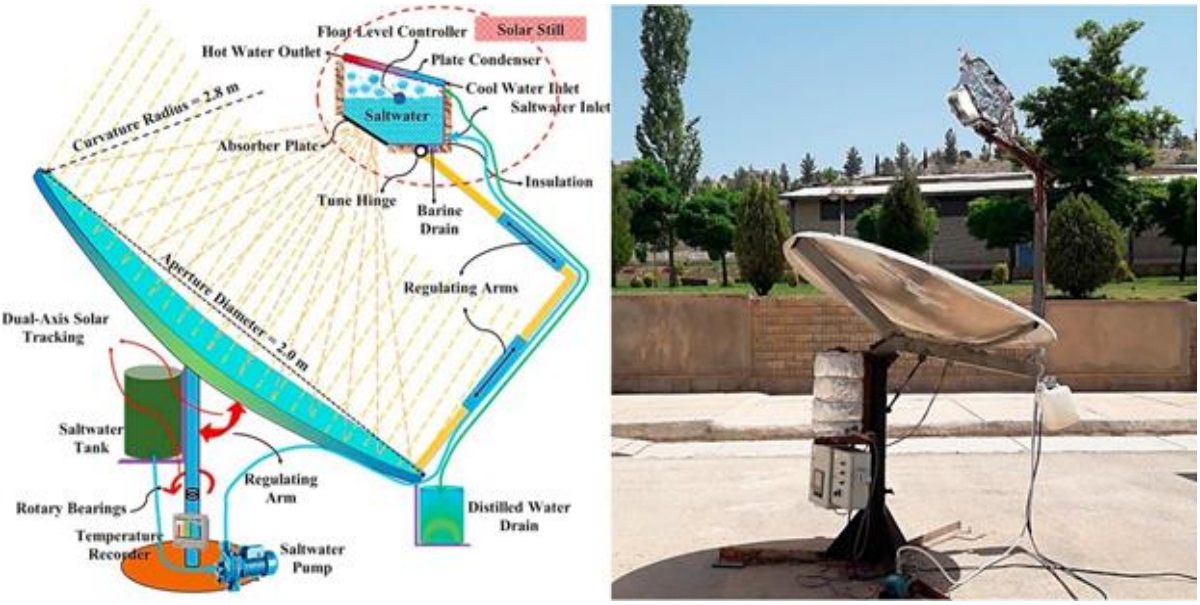


Figure 21: Representative view of the overall system [217]

Kabeel et al. [218] examined the design characteristics of a distillation system based on parabolic dishes integrated with PV modules and solar still, as shown in **Fig. 22**. Experimental results revealed that the daily generation of the fresh water increase for a fixed value of basin water depth of 10 mm. The studied model was able to provide an amount of 13.63 kg/day of the distilled water.

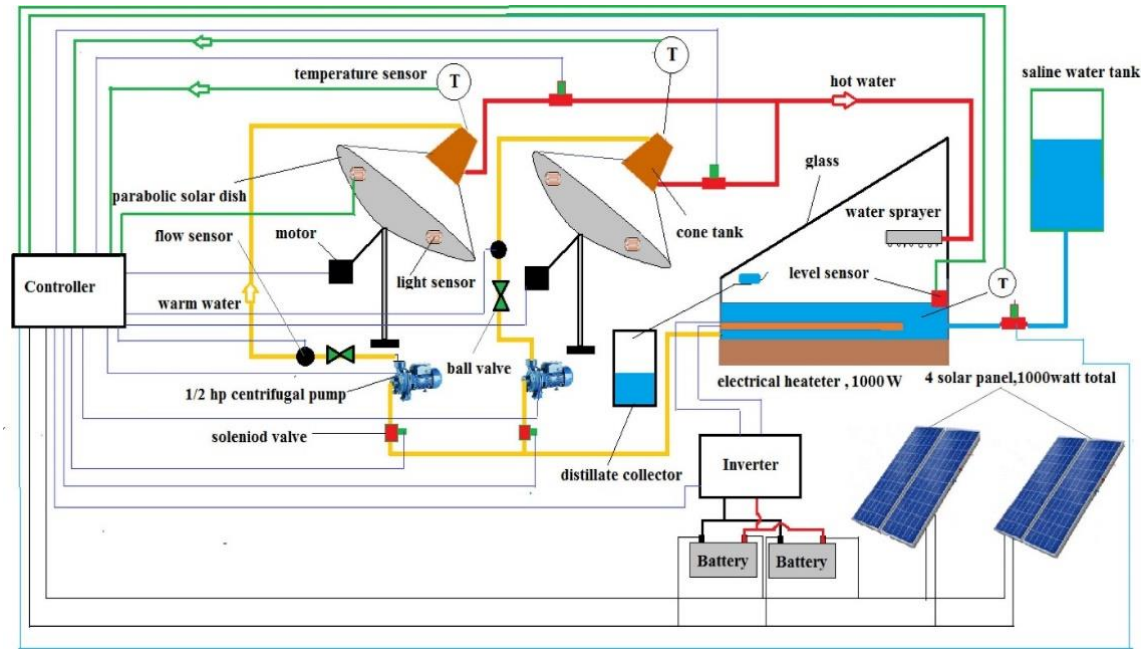


Figure 22: Schematic model of the distillation system [218]

7. Solar dish with Phase Change materials

Many researches have been conducted to assess the integration of Phase change Material in applications that highly require the storage of energy [219]. Several works were performed to evaluate the integration of PCM with solar dish concentrators. For a conventional steam power plant, Mehrpooya et al. [220] proposed a novel system in which solar dish collectors play the role of boiler. The suggested system comprises a tank to store the thermal energy by employing PCM. It has been deduced that the integration of solar dish collector enhances the exergy efficiency up to 41.76%. It was also highlighted that for higher volumes of the PCM tank, the mass flow rate of the heat transfer fluid should be raised. According to Muthu et al. [221], the performance of a parabolic dish Stirling system can be improved by integrating a phase change material as a cooler for the heat sink. Andraka et al. [222] unveiled the necessity of integrating the phase change material in SDS system for thermal storage. It was revealed that the storage by adopting metallic PCM was economically feasible and can exhibit significant improvement in energetic and exergetic efficiencies. The

same research team [223] proposed latent storage based on a solid-liquid phase change (PCM) material suitable for SDS system. The results show that the proposed configuration grants technical and economic feasibility with minimum exergy conduction losses and confirm that such technology could be a leading energy solution in future. Saleh et al. [224] mentioned that the integration of the phase change material in the area under the dish absorber can improve the performances of the solar dish distiller. Compared to the conventional still, the optimized design was able to increase the amount of the distillate from 3580 to 6980 mL/m2.day. In addition, the maximum thermal efficiency was also improved from 30% to 62.4% when compared with the conventional system.

8. Optimization of SDS technology

Looking for the SDS technology's highest energy and economic performance is critical for this technology to be competitive with other power generation modes. Specifically, considerable attention was paid by many researchers to optimize the design and operation parameters of the SDS technology using diverse optimization approaches and methods. Ferreira et al. [225] developed a thermo-economic optimization study for Solar Dish Stirling system (see **Fig. 23**). The adopted optimization approach aimed to ensure the best compromise between two conflicting objective functions namely the global investment cost and the thermal efficiency. The findings presented multiple design prospects for which efficiencies between were ranging between 66% and 76% have been detected for multiple designs.



Figure 23: Process of the thermal-economic optimization approach [225]

Ahmadi et al. [226] established a multi-objective optimization that considers the maximisation of both the output power and the overall thermal efficiency and minimization of the entropy generation rate of a SDS system. Multi-objective evolutionary algorithms (MOEA) based on the NSGA-II algorithm were implemented to address the best trade-off between the objective functions. Several characteristics of the regenerator, heat exchanger and

the operating fluid as well as parameters of the heat sink and heat source were considered as decision variables. Multi-attribute decision-making methods such as the fuzzy Bellman-Zadeh approach, LINMAP, and TOPSIS have been applied to detect a final optimal solution. Carrillo Caballero et al. [227] proposed a model of SDS technology operating with a Directly Illuminated Receiver (DIR) type in Itajubá, Brazil. Multi-objective optimization considering the power output and system efficiency was conducted using the NSGA-II algorithm in the Modefrontier platform. Optimal Pareto front was presented, and a final optimal solution was obtained based on decision-making method (Simple Additive Weighting). The proposed approach disclosed that more than 11 kW of the output power and overall efficiency of about 21% were achieved. **Fig. 24** shows the main steps ensured during the optimization.

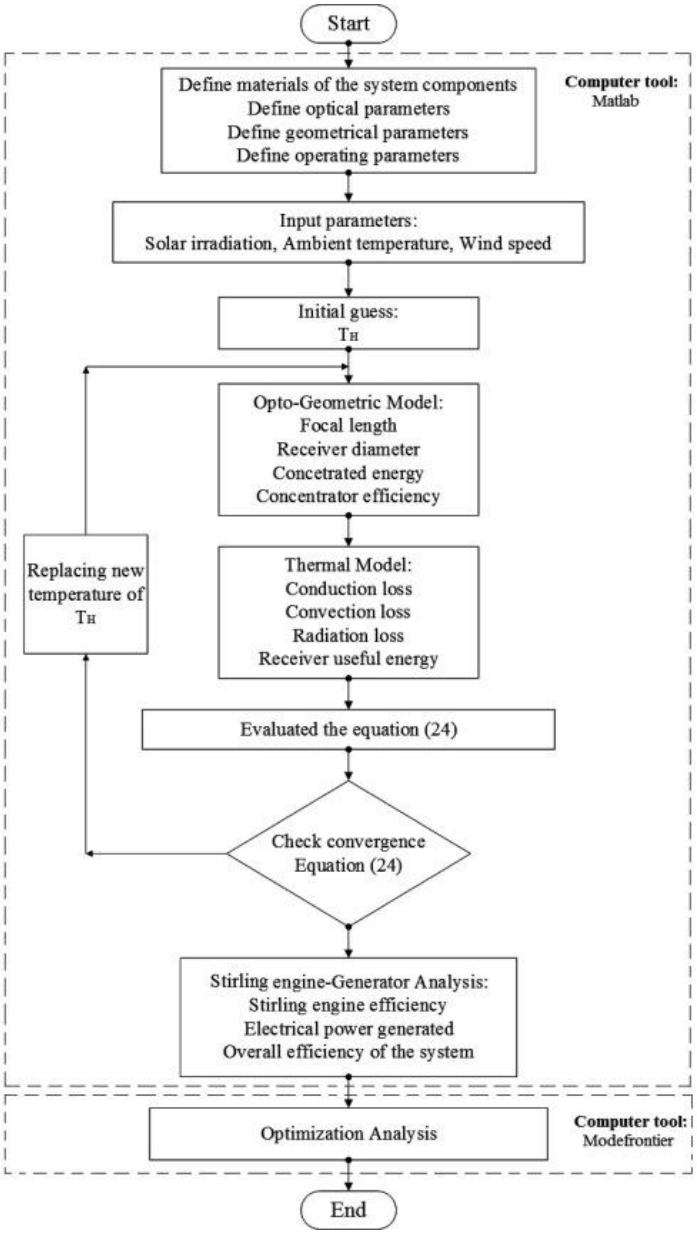


Figure 24: Optimization algorithm of SDS model [227]

Khosravi et al. [228] opted for an artificial intelligence method to simulate the performance of an SDS system. An enormous set of variables such as solar irradiance and concentration factor has been supplied as input parameters to examine several targets such as energy production and system efficiency. It has been revealed that the application of the Adaptive Neuro Fuzzy Inference System (ANFIS) with the Particle Swarm Optimization (PSO) method shows more satisfactory results than other intelligent methods. Ahmadi et al. [229] proposed a multi-objective optimization to detect the ideal configuration of dimensionless power output and thermal efficiency. This optimization is based on thermo-economic analysis and on the NSGA-II algorithm. Final optimal solutions were selected based on decision-making method. The average thermal efficiencies obtained at the level of the dish collector and the Stirling engine device are about 37% and 43%, respectively. A detailed comparative study has been developed by Rao et al. [230], aiming to determine the optimization algorithm that can generate the best solutions for the SDS system operating. The results highlight that the Adaptive Multi-Team Perturbation Guiding Jaya algorithm (AMTPG Jaya) can provide more satisfactory results than other methods such as Fuzzy Bellman-Zadeh, LINMAP, TOPSIS, MOPSO, and MTPG Jaya. Nazemzadegan et al. [231] performed four and three objective optimizations as well as two and single objective optimizations for an SDS. The 4-objective optimization was achieved by particle swarms (MOPSO), considering power, entropy, efficiency, and an economic index. Decision-making methods such as TOPSIS and LINMAP were then introduced. The obtained values when using MOPSO exhibit crucial advantages at the level of the finite time thermodynamic equations of the Stirling engine. Zayed et al. [232] used multiple-objective particle swarm optimization (MOPSO) for an SDS to address the best trade-off between the output power and the overall efficiency. Nine decision parameters, including opto-geometric and other meteorological dimensioning variables, have been included in this optimization. The optimal Pareto frontier was provided, and the final optimal solution was obtained from the LINMAP decision-making method. Maximum power of 23.46 kW and overall efficiency of 30.15% were achieved. Sensitivity assessment reported that when the diameter of the concentrator varies from 2.5 to 15 m, the output power can reach a value between 1.43 to 53.34 kW, respectively. **Fig. 25** describes the different steps used during the optimization approach.

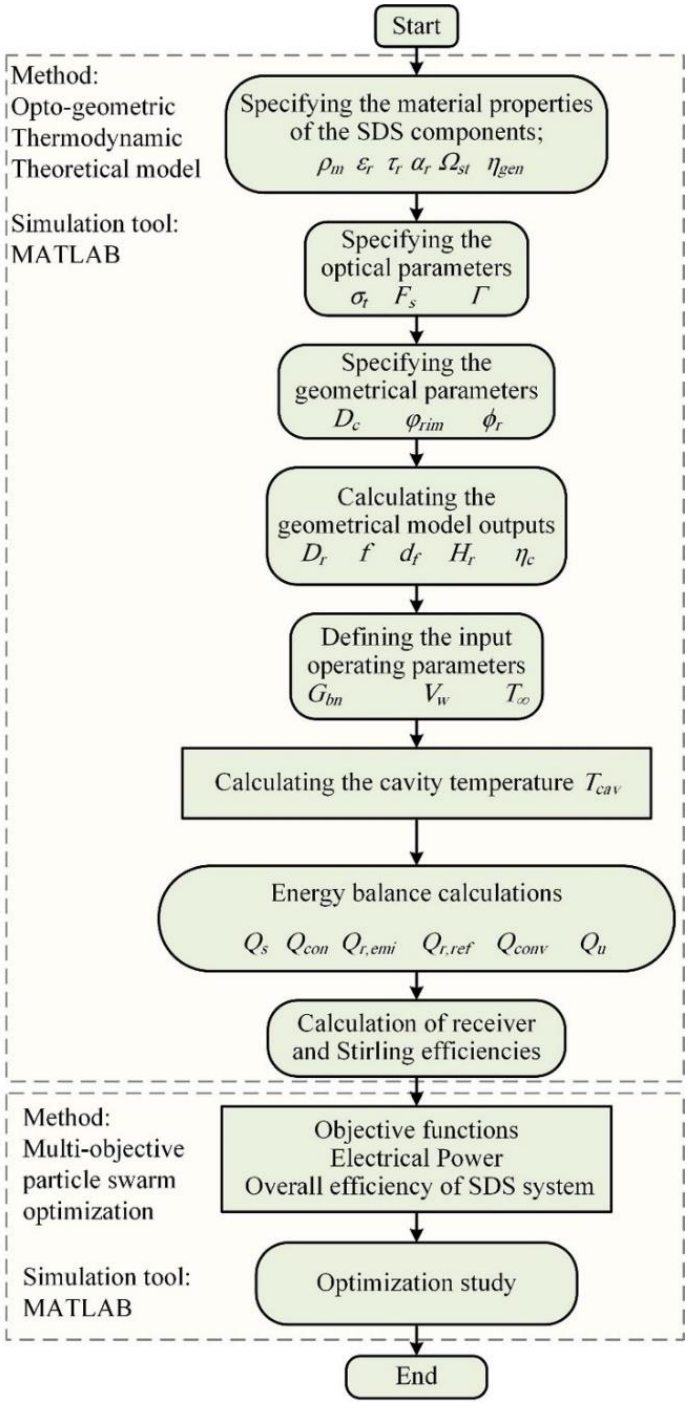


Figure 25: Schematic illustration of the adopted optimization approach [232]

Ferreira et al. [233] proposed a thermo-economical optimization method to evaluate SDS cogeneration micro-systems by maximizing the annual value of the system's operation and considering non-linear economic and thermodynamic constraints. To detect the final optimal solution, the generalized model search optimization algorithm was developed with MATLAB software. Moreover, it was concluded that the system is economically feasible and has a payback period of around 10 years. Sameti et al. [234] used the Neural Network to assess the SDS performances in a smart grid. Afterwards, the ANN approach was followed by

an optimization based on Genetic Algorithm to estimate the power generated by the Stirling engine while exploiting a set of data. When comparing the results with the numerical data, it became evident that ANN-GA combination is effective and can be incorporated into future work. Nazemi et al. [235] developed a model to investigate the performance of a SDS system. All heat loss types could be managed by regulating appropriately the design parameters and characteristics of both receiver and Stirling engine. This analysis was validated by the Eurodish project and Particle Swarm Optimization for two scenarios was performed to detect the best solutions. The second scenario could raise global efficiency from 21.69% to 22.62%. Zayed et al. [236] proposed a hybrid prediction model based on an improved version of the Random Vector Functional Link (RVFL) network combined with the Chimp Optimization Algorithm (CHOA) to forecast the output power generation of a SDS power plant. The suggested model has been compared with other Evolutionary optimization Algorithms such as Particle Swarm Optimization (PSO) and Spherical Search Optimization (SSO) and more promoting results in terms of the instant power yields and the monthly power generated using the RFVL-CHOA combination have been attained with a root mean square value of about 0.00047 and 0.05995, respectively.

Several other optimization methods have been developed to find the best combinations leading to better yields [237], [238]. Kumar et al. [239] optimized the implementation of SDS with a permanent magnet DC generator (PMDC) using the grey wolf optimization approach (GWO). Li et al. [240] have used the Particle Swarm Optimization (PSO) to optimize and regulate properly the control of a SDS coupled to a dual power induction generator (DFIG).

More interest should be accorded to the receiver and the Stirling engine during the analysis and optimization of the SDS system because this is where a large amount of energy and exergy losses are distinguished [241]. Rao et al. [242] used the Teaching-Learning-Based Optimization TLBO approach to detect the better design criteria of a Stirling engine that can affect the power output, the global efficiency, and the heat losses. When comparing with other optimization methods, TLBO can provide more satisfactory results. Hooshang et al. [243] employed an Artificial Neural Network approach based on the Multi-Layer Perceptron optimization to pick up the optimal design values (relative piston stroke, phase angle, and the working frequency) of a ST 500 Stirling engine using experimental data. This study was validated and compared with a thermodynamic analysis algorithm to achieve appreciable results of the global efficiency and the net produced power. Patel et al. [244] established an optimization with multiple objectives for a Stirling engine considering the thermal and exergy efficiency, the power output, and an environmental indicator. The suggested approach is

based on the multi-objective heat transfer search and decision-making method to detect a final single solution from the set of optimal Pareto points. A comparison study of the Particle Swarm Optimization (PSO) and the Imperialist Competitive Algorithm (ICA) with the Mean Square Error approach (MSE) and the correlation coefficient was established by Toghyani et al. [245] to assess the torque and power values resulted from a SE known by (Philips M102C). The PSO approach conducts on better results and leads to good agreement with experimental measurements. Allouhi et al. [246] employed a multi-objective approach to find out the optimal configuration of the solar field layout in two different locations. Genetic algorithm was used to provide Pareto Frontiers and the final optimal solution was derived based on TOPSIS method. The final solution corresponded to the best compromise between capacity factor of the plant and the total cost of site improvements.

Based on was reported earlier, multi-objective optimization offers a potential methodical approach when designing SDS systems with conflicting objective functions such energy performance and cost. Among the most faced problems is to find a global optimal solution and avoid the local optimums. In this regard, some recent intelligent optimization algorithms based on Pareto-dominated techniques exhibited higher performance in terms of solution diversity and convergence compared to conventional approaches. However, the task of finding Pareto fronts becomes more time consuming when dealing with problems that involve more than three objectives. Some more advanced methods were developed to fill this gap and the reader is directed to a recent comprehensive review by Cui et al. [247] for further information on this subject.

9. Summary

Recently, considerable advancement has been made to enhance the performance of solar dish technology to make it more competitive compared to other power generations systems. In this chapter, solar dish technology applications, innovative design for multi-end use applications and the adopted strategies applied in the optimization of this technology were evaluated. The following concluding remarks were highlighted:

- Hybridization of the solar Dish technology allowed for significant energy and economic performances.
- Use of Phase Change Materials and thermoelectric devices still need investigation for various configurations of solar dish technology.
- Novel thermodynamic cycles combined with solar Dish collector showed promising prospects, but the use of the Stirling cycle is still dominant in most research works.

- Solar Dish technology for polygeneration applications such as power generation, water heating and water desalination can be very promising for fresh water-energy supply in sunny regions.

This chapter can provide an updated guideline for the solar dish-technology for designers and engineers working on solar dish technology.

CHAPTER III. Solar Dish Stirling technology for sustainable power generation in Southern Morocco: 4-E analysis

1. Introduction

The precedent literature review highlights that the Solar Dish Stirling (SDS) system exhibits promising development prospects and can supply clean energy for several end-use applications. This technology's technical, optimisation, and financial evaluations in countries with high solar potential are critical to deciding upon the possible implementation in future projects. This can assist policymakers in selecting appropriate sites to achieve the highest energy performance at competitive costs.

Morocco enjoys a huge solar radiation potential, especially in southern regions. Further, the country is currently transitioning towards a more sustainable power system for which CSP is believed to play a fundamental role. Hence, it would be of great interest to carry out a detailed energy, exergy, economic, and environmental (4-E) analysis of the SDS system, as a clean electricity generation alternative in Moroccan rural areas. In this direction, the aim of this chapter is threefold:

- Conduct a detailed energy assessment about the potential of Dish Stirling technology in the Southern regions of Morocco in terms of electricity generation in rural and isolated areas.
- Each implementation site optimises key design and operation parameters to reach the highest energy performance.
- Evaluate energetically, exergetically, economically, and environmentally the Dish Stirling technology and estimate the Levelized cost of electricity under various scenarios.

This comprehensive 4-analysis combined with individual technical optimisation specific to each implantation site was not carried out before, while it can provide a more valuable assessment and ranking of the most promising zones desirable to the SDS technology. This is practically relevant for Morocco, which has no previous experience in implementing this type of CSP technology. Overall approach conducted in this study can be

also a reference for other countries in the African continents for effective integration of such systems.

2. Background

Solar energy plays a fundamental role in the present global energy transition. The power delivered from the sun is clean, abundant, and is becoming progressively competitive against conventional fossil fuels, which are responsible for a tremendous amount of greenhouse gas emissions. Numerous studies have shown that innovations must be developed to produce and store solar energy more effectively [248]. CSP systems have exhibited several advantages in supplying eco-friendly power that can best contribute to cover a great amount of the global energy requirements [14]. The CSP plant consists of different elements such as solar concentrators, a receiver, a steam turbine, and an electric generator. The state of the art of CSP involves 4 technologies which are: Parabolic Trough Collectors (PTC), Solar Dish Stirling (SDS), Solar Tower (ST), and Linear Fresnel Reflector (LFR) [16]. The latest and mature technology is the PTC followed by the solar tower, which is applicable for large scale and can be connected to the high-voltage grid [19]. The success of these concentrating power systems fundamentally depends on the effectiveness, thermal, and optical performances of the used equipment [12]. Solar dish Stirling technology offers a promising alternative to generate clean and sustainable electricity, especially for remote and unelectrified areas. It is also a modular and scalable technology that can serve energy requirements at various levels. In this regard, solar dish Stirling for power generation was assessed by many authors in several countries. **Table 3** summarises related published works for which plant capacity, implementation site, and overall plant performance are given.

Despite all the merits of the SDS technology, it remains less economically effective when compared with other power generation systems. In fact, Awan et al. [69] compared the SDS technology with PV technology based on energetic and economic investigation, considering a total rated capacity of 1 MW for both technologies. The comparative study was applied for Tabuk city in Saudi Arabia, and the results revealed that PV technology offers 6.9% better in terms of capacity factor. The PV technology resulted in a LCOE value of 3.39 ¢/kWh against 11.74 ¢/kWh for the SDS technology. This main barrier has prompted scholars to optimize the efficiency of the SDS technology further and enlarge the spectrum of its potential end-use applications. Current research pathways covered design optimisation of the various system components (dish collector parameters, receiver cavity geometry, Stirling engine and parasitics characteristics...) [65], [123], [251], proposal of new system designs based on the cogeneration and polygeneration concepts [98], [168], [209], [210], [252], use of

artificial intelligence for the performance forecasting [228], [232], application of PCM-based storage and nanofluids [222], [253], [254], generation of clean hydrogen utilising the electricity from SDS [255] and the utilisation in combination with other solar applications such as solar ponds and water desalination [164]. Several parameters such as tilt and azimuth angle as well as the wind velocity can impact the frequency and the amplitude of solar dish concentrators. Through a CFD developed model, Jiaqiang et al. [256] carried out a harmonic response analysis of a large solar dish collector considering the vibration induced by the wind load. The results revealed that the height angle could slightly influence the system frequency. It was also found that the sinusoidal wind load can be allowed for maximal vibration of the dish collector, and subsequently, clear variation of amplitude and rotation angle were observed. Zuo et al. [257] developed a catastrophic analysis to assess the solar dish concentrator stability based on the lift-drag ratio. The value of this ratio allowed detecting the critical stability state of the dish.

Table 3: Published works with main information: power plant capacity, implementation site and overall plant performance

Authors and References	**Plant size**	**Region (city, country)**	**Overall conclusions**
Siva Reddy et al. [258]	50 MW	Jodhpur, India	A 50 MW using 2000 units of parabolic dish Stirling engine solar power plant with a unit power of 25 kW was built. Annual enhancement in energetic efficiency varied from 15.57% to 27.09% and exergetic efficiency varied from 16.83% to 29.18%, respectively.
Abdelhady [259]	50 MW	Benban, Egypt	Annual energy output of about 105 GWh per year has been reached. The LCOE and the avoided GHG emissions are about 13.38

			¢/kWh and 45 million tons per year, respectively.
Reinalter et al. [260]	10.85 kW	Almeria, Spain	A novel SDS system was built. Total system efficiency of 22.5% was reported.
Yan et al. [156]	38.8 kW	Hunan, China	Overall efficiency of 25.3% was reported.
Mancini et al. [261]	24.9 kW	California, USA	System peak efficiency of 28%, and electrical power of 24.9 kW was achieved.
Zayed el al. [31]	25 kW	Tianjin, China	A net annual efficiency of 19.55% with 28.748 MWh energy produced were reported at a levelized cost of energy of about 0.2565$/kWh
Coventry and Andraka [76]	1.5 MW	Arizona, USA	The plant used 60 SDS glass mirrors plated with silver. Total rated peak efficiency was estimated at 29.6%.
Gholamalizadeh and Chung [241]	1 kW	Kerman City, Iran	Maximum total energy and exergy efficiencies of 12.2% and 13.2% were reported.
Mendoza et al. [150]	1 kW	Itajubá, Brazil	Mathematical model reported in Ref. [87] was validated based on experimental measurements. The mathematical model reported an electric power of 1 kW and an overall efficiency of 17.6 % when

			the solar irradiation is around 725 W/m^2. For solar irradiation range between 520 W/m² and 950 W/m², the experimental tests' electric power and overall efficiency attained 1.098 kW and 17.98%, respectively.
Sproul et al. [262]	8 kW	Sandia's National Solar Thermal Test Facility, Albuquerque, USA	Peak efficiency of 22.5% was achieved.
Nazemi and Boroushaki [235]	10 kW	Tehran, Iran	Mathematical model was analysed and validated with Euro dish results. An increase in the total efficiency of the system of 22.62% was achieved

3. Methods

In this study, a single SDS system with a nominal power of 25 kW was analysed and optimised using SAM (System Advisor Model) simulation software in several areas in Morocco. SAM includes a performance and financial model designed to facilitate the decision-making process related to the renewable energy industry. This software performs dynamic simulations of the electricity production of an electrical system, providing a set of 8760 hourly values that represent the system's electricity generation over an entire year scenario [263]. During this study, a TMY3 formatted meteorological dataset (TMY: Typical Meteorological Year) generated by METEONORM software is used when modelling renewable energy systems in SAM. In the first step, the dish Stirling system optimises several parametric studies concerning the receiver aperture diameter, receiver insulation thickness, and the cooling pump speed. In the second step, the configuration of the solar field was extended to a total capacity of 10 MW, and a techno-economic study was carried out based on

optimisation results of the leading design and operation parameters to identify potential sites for implementing this technology in Southern Moroccan areas.

3.1. System description

The SDS comprises a set of parabolic mirrors, metallic support, and double-axis sun-tracking mechanism [66]. The energy absorbed is transmitted to the working fluid in the Stirling engine (SE) by means of a receiver. The SE ensures the conversion of the thermal energy into mechanical power by increasing the working fluid pressure when it is cold and decreasing it when it is hot. The obtained linear movement is mechanically transformed into rotation. An electric generator employs the rotary motion to generate electricity [67]. **Fig. 26** shows a working model of the Dish Stirling Engine with the principal components. The collected heat by the receiver is absorbed partially by a heat transfer fluid (commonly hydrogen or helium). The Stirling engine transforms the available thermal energy to mechanical energy, which powers an electric generator ([31],[67]). Technical details and specific design characteristics for the explored SDS system are presented in **Table 4**.

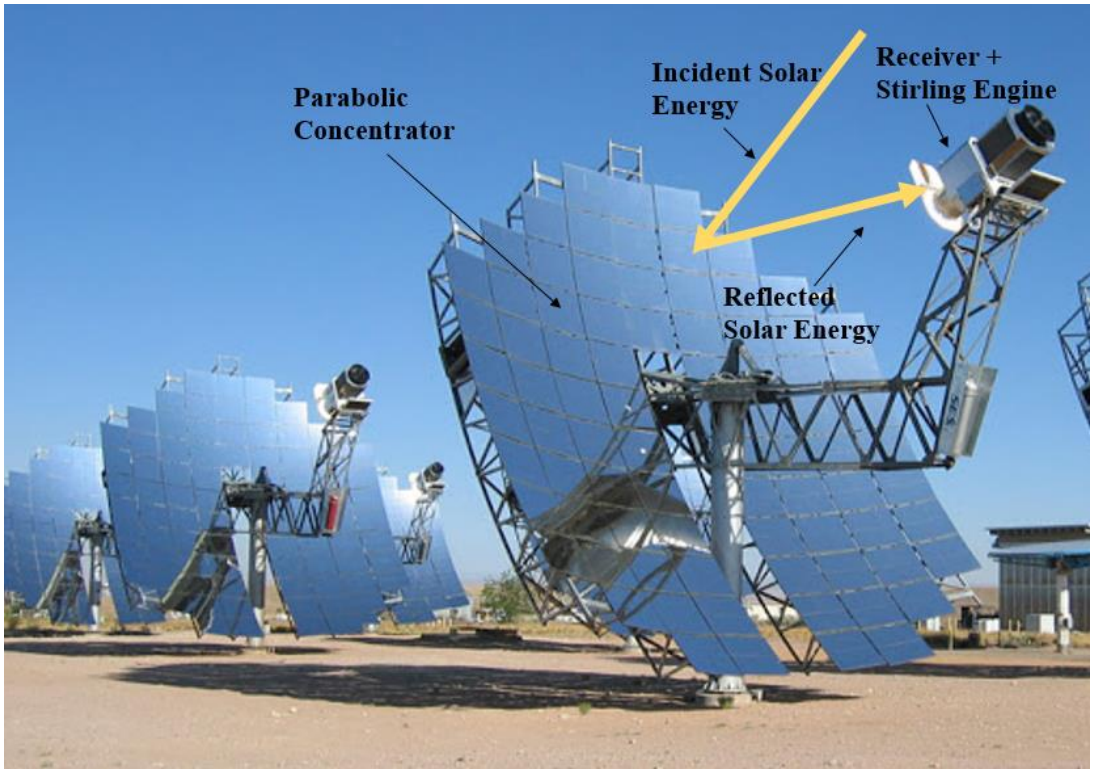


Figure 26: SDS System with its main devices [25].

Table 4: Design specifications, dimensions, and performance parameters of the SDS system

Solar Field	
Wind Stow Speed (m/s)	16
Total Capacity (kW)	25
Collector	
Total area of the mirror (m^2)	91
Reflectance	0.94
Cut-in irradiation (W/m^2)	200
Receiver	
Receiver aperture diameter (m)	0.184
Insulation thickness (m)	0.075
Thermal Conductivity (W/m.K)	0.06
Absorptance coefficient of the absorber	0.9
Absorber surface (m^2)	0.6
Stirling Engine (SE)	
Single Unit Nominal Capacity (kW)	25
Heater Head Set Temperature (K)	993
Functioning Speed (rpm)	1800
Displaced Volume (m^3)	0.00038
Beale Constant	0.04247
Beale 1^{st} order parameter	1.682×10^{-5}
Beale 2^{nd} order parameter	-5.105×10^{-10}
Beale 3^{rd} order parameter	7.073×10^{-15}
Beale 4^{th} order parameter	-3.586×10^{-20}
Pressure constant coefficient	0.658769
Pressure 1^{st} order Coefficient	0.00023496
Parasitics	
Control system (W)	150
Reference cooling pump speed (rpm)	1800
Speed range of the cooling fan (rpm)	400-650

3.2. Examined geographical sites

This work aims to study the potential use of Dish Stirling Solar technology to produce electricity in remote and rural Moroccan areas. The southern region of Morocco enjoys a

substantial solar energy potential and is at the same time looking to integrate massively solar energy projects in the future. **Table 5** represents the geographical information of these regions, highlighting a total of 13 cities.

Table 5: Geographic coordinates of each studied region

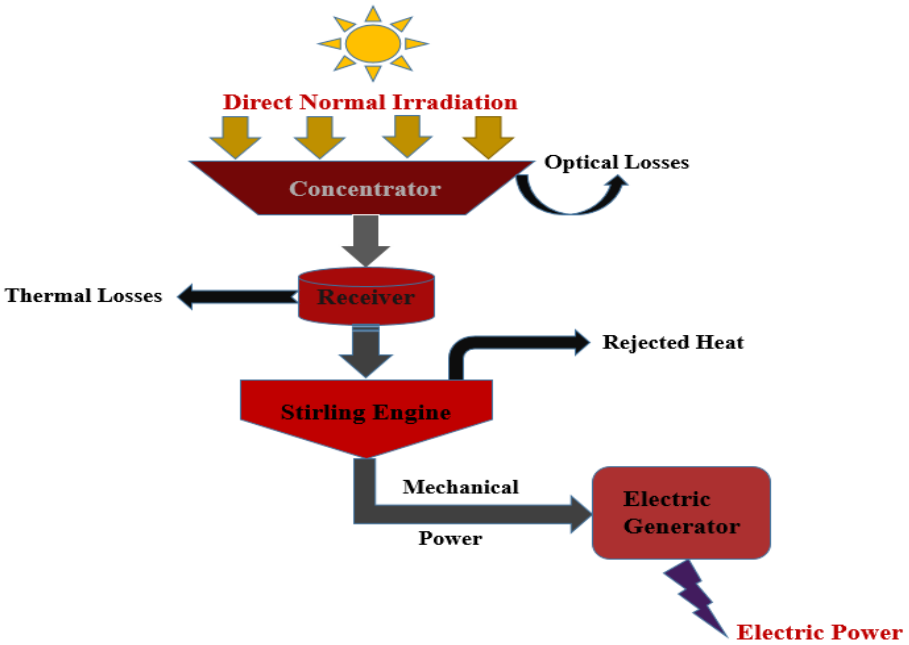
Region	**City**	**Latitude (°N)**	**Longitude (°W)**	**Altitude (m)**
Marrakech-_Safi	Marrakech Safi	31° 37′ 46″ 32° 17′	7° 58′ 52″ 9° 14′	466 45
Draa-Tafilalet	Errachidia Ouarzazate Midelt	31° 55′ 55″ 30° 55′ 23″ 32° 41′	4° 25′ 28″ 6° 54′ 15″ 4° 44′	1045 1140 1515
Souss-Massa	Agadir Taroudant	30° 25′ 30° 28′ 45″	9° 36′ 8° 52′ 34″	23 238
Guelmim-Oued Noun	Guelmim Tan-Tan	28° 59′ 17″ 28° 25′ 46″	10° 03′ 27″ 11° 05′ 53″	294 67
Laayoune-Sakia El Hamra	Laayoune Essamara	27° 09′ 13″ 26° 44′ 22″	13° 12′ 12″ 11° 40′ 13″	68 191
Dakhla-Oued Ed-Dahab	Dakhla Aousserd	23° 43′ 00″ 21° 55′	15° 57′ 00″ 15° 01′	5 318

3.3. Thermal model

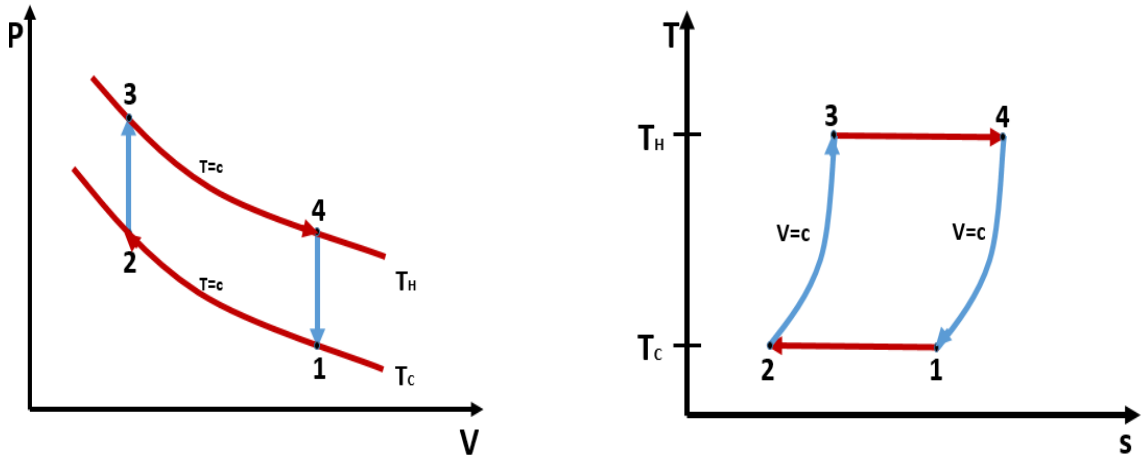
In a Solar Dish Stirling system, three forms of energy can be distinguished and subject to different conversion categories: solar energy (Direct Normal Irradiation), thermal energy, and electrical energy. When the concentrator surface receives solar radiation, it is focused on the receiver at a very high concentration ratio. Three essential types of losses are observed: 1: Optical losses at the level of concentrator; 2: Thermal Losses in the receiver; 3: Rejected heat by the Stirling engine and which can be explained as the thermal and mechanical losses [67]. **Fig. 27 (a)** illustrates a general thermal analysis model of the Solar Dish Stirling system. In the Stirling engine, the thermodynamic cycle consists of four processes [264], as shown in **Fig. 27 (b)** :

- Isothermal compression process (1-2): The working fluid pressure increases, and its volume decreases while its temperature remains constant T_C. The heat of the working fluid is rejected to an external sink.

- Isochoric heat addition process heating (2-3): The working fluid passes through the regenerator and captures heat in this phase. The temperature and pressure of the working fluid will increase while the volume remains constant.
- Isothermal expansion process (3-4): The working fluid is heated from the external source during this transformation. The volume of the working fluid increases, and its pressure decreases at a constant temperature T_H.
- Constant volume cooling process (4–1): The regenerator will receive heat from the working fluid; the pressure and temperature during this process will decrease at a constant volume.



(a)



(b)

Figure 27: (a) Energetic chain of the Solar dish Stirling System [67]; **(b)** Diagrams *P-V* and *T-S* of the ideal Stirling Engine cycle.

3.4. Mathematical formulation

The mathematical description listed below is based on previous work by Fraser et al. [264]. The system advisor Model also uses this formulation for the energy analysis for Solar Dish Stirling, and for this reason, a brief description is given.

- **Collector**

The concentrator redirects sun's rays to the receiver, where it is focused on the absorber. The solar energy captured by the receiver ($P_{in,rec}$) is written as follows:

$$P_{in,rec} = I_{DNI} \cdot A_{proj} \cdot \rho_{ref} \cdot \varphi_{int,fac} \cdot \varphi_{shade} \quad \textbf{(1)}$$

with (I_{DNI}) is the direct normal irradiation, (A_{proj}) is the projected area of the mirror, ($\varphi_{int,fac}$) and (ρ_{ref}) are the terms describing the intercept factor and mirror reflectivity, (φ_{shade}) is the shading factor. The intercept factor describes the fraction of the energy reflected from the solar dish collector and which enters the receiver aperture. The mirror reflectivity is the parameter responsible for losses at the level of the collector. It represents the ratio between the energy reflected and the total incident energy.

The shading coefficient φ_{shade} was extracted from Osborn theory [265] and can be expressed in terms of the projected area of the mirror (A_{proj}) and the average value of the shaded area per dish (S_{AVG}):

$$\varphi_{shade} = \frac{A_{proj} - S_{AVG}}{A_{proj}} \quad \textbf{(2)}$$

- **Receiver**

The thermal power entering the SE is obtained according to the power captured by the receiver ($P_{in,rec}$) and the different types of thermal losses in the receiver, it can be defined as follows:

$$P_{in,SE} = P_{in,rec} - \dot{q}_{rad,reflect} - \left(\dot{q}_{cond} + \dot{q}_{conv,tot} + \dot{q}_{rad,emit}\right)_{losses} \quad \textbf{(3)}$$

$\dot{q}_{rad,reflect}$ and $\dot{q}_{rad,emit}$ describe the reflected and emitted radiation at the receiver aperture outlet, respectively. Whereas $\dot{q}_{conv,tot}$ represents the heat loss rate due to the convection heat transfer. It should be noted that the conduction losses ($\dot{q}_{cond}$) through the receiver are negligible. In order to calculate the different types of thermal losses at the level of the receiver, it is necessary to determine the coefficient of both natural and forced convection ($h_{natural}$, h_{forced}). The coefficient of the natural convection ($h_{natural}$) employed for the cavity is defined from the free convection Nusselt correlation number developed by Stine and McDonald based on experimental data [266] (see Eqs. (4-5)). The correlation was carried out

in order to determine the convection losses occurring at the receiver cavity, considering that the characteristic length is equal to the diameter of the interior cavity:

$$Nu_{nat,conv} = 0.088 \cdot Gr^{1/3} \cdot (T_{cav}/T_{amb})^{0.18} \cdot (cos\theta)^{2.47} \cdot \left(d_{ap}/d_{cav}\right)^{S} \quad \textbf{(4)}$$

$$S = -0.982 \cdot \left(d_{ap}/d_{cav}\right) + 1.12 \quad \textbf{(5)}$$

with Gr is the Grashof number, T_{cav} describes the average temperature in the interior walls of the cavity, T_{amb} is the ambient temperature, θ designates the angle of the sun elevation, d_{ap} and d_{cav} are the aperture diameter and the cavity diameter, respectively.

The forced convection correlation used to determine the forced heat transfer coefficient for the cavity was defined according to Ma et al. [267], is given in the following equation:

$$h_{forced} = 0.1967 \cdot v^{1.849} \quad \textbf{(6)}$$

with v is the wind speed.

The coefficient of the total convection heat transfer can be obtained by summing the two terms of natural convection ($h_{natural}$) and forced convection (h_{forced}) coefficient [267]:

$$h_{total,convection} = h_{natural} + h_{forced} \quad \textbf{(7)}$$

The total amount of the receiver losses caused by convection can be defined as:

$$\dot{q}_{conv,tot} = h_{total,convection} \cdot A_{cav} \cdot (T_{cav} - T_{amb}) \quad \textbf{(8)}$$

where A_{cav} refers to the area of the interior cavity.

The amount of the emitted radiation from the receiver ($\dot{q}_{rad,emit}$) is illustrated based on Stefan Boltzmann's law as shown in the following equation:

$$\dot{q}_{rad,emit} = \varepsilon \cdot A_{ap} \cdot \sigma \cdot (T_{cav}^4 - T_{amb}^4) \quad \textbf{(9)}$$

where ε designates the emissivity, σ is the constant of Stefan Boltzmann and A_{ap} is the area of the receiver aperture.

The quantity of solar radiation reflected from the receiver ($\dot{q}_{rad,reflect}$) is expressed as a function of the effective absorptance of the cavity (α_{eff}) and the solar power entering at the receiver ($P_{in,rec}$) as highlighted by Duffie and Beckman [268]:

$$\dot{q}_{rad,reflect} = \left(1 - \alpha_{eff}\right) \cdot P_{in,rec} \quad \textbf{(10)}$$

The effective absorptance (α_{eff}) can be expressed as a function of α_{cav} (absorptance of the interior cavity surface) and the total surface area of the interior cavity [268]:

$$\alpha_{eff} = \frac{\alpha_{cav}}{\alpha_{cav}+(1-\alpha_{cav})\cdot(A_{ap}/A_{cav})} \quad \textbf{(11)}$$

- **Stirling Engine**

The Stirling Engine (SE) is located in the terminal process for power generation. In order to calculate the net electricity generated (P_{Net}), the gross output power (P_{gross}) should be found first. The mathematical model of the SE is formed according to the Beale curve fit equation and the correction temperature parameter ($T_{correct}$) [264]. The model calculates the gross output considering the Beale curve fit equation, the mean pressure engine, the swept volume, the engine frequency, and $T_{correct}$ based on the finite time theory given by McMahan et al. [269]:

$$Beale\#_{corrected} = P_{gross}/[P_{mean} \cdot V_{sw} \cdot f \cdot T_{correct}] \quad \textbf{(12)}$$

The parameter $T_{correct}$ covers the term of both expansion (T_E) and compression space (T_C) temperatures:

$$T_{correct} = (1 - (T_H/T_C)^{0.5}) \quad \textbf{(13)}$$

The heater head's operating temperature can be considered the temperature of the expansion space (T_H), while the temperature of the compression space (T_C) can be extracted from the ambient temperature provided by the weather data file.

A single day of data for a specific Stirling engine is sufficient to characterise the $T_{correct}$ given in the equation (13) and engender a curve fit using the input power entering at the Stirling engine derived from the receiver and collector models given in Eq. (3). The following equation gives the gross output power provided by the SE:

$$P_{gross} = Beale_{curve} \cdot [P_{mean} \cdot V_{sw} \cdot f \cdot T_{correct}] \quad \textbf{(14)}$$

with $Beale_{curve}$ is the Beale coefficient for the current operating conditions.

- **Parasitic Power Model**

The parasitic losses ($P_{parasitics}$) include the controls and tracking, fan and pump power consumptions denoted respectively as $P_{controls}$, P_{fan} and P_{pump}. The net electricity generated (P_{Net}) is simply deduced by subtracting the estimated parasitic losses from the gross available power:

$$P_{Net} = P_{gross} - \left(P_{controls} + P_{fan} + P_{pump}\right) \quad \textbf{(15)}$$

It is interesting to stress that the fan and pump power consumption are estimated according to the performance equation of the dimensionless pump and the fan laws [270].

3.5. Performance indexes

- **Hourly energy efficiency of the global system**

The energy efficiency generated by the entire SDS system η_{net} can be expressed in terms of the net electrical power generated, the dish concentrator aperture area and the direct normal irradiation:

$$\eta_{Energy} = \frac{P_{net}}{A_{proj} \cdot I_{DNI}} \quad \textbf{(16)}$$

- **Hourly exergy efficiency of the global system**

The exergy input of the solar dish Stirling system can be expressed as bellow [271]:

$$Ex_{in} = I_{DNI} \cdot A_{proj} \cdot \left(1 - \frac{4}{3}\frac{T_{amb}}{T_s} + \frac{1}{3}\left(\frac{T_{amb}}{T_s}\right)^4\right) \quad \textbf{(17)}$$

T_s refers to the apparent temperature of the sun with a value of 6000 K as mentioned by Petela [272]. The following expression gives the global exergy efficiency of the entire system:

$$\eta_{Exergy} = \frac{P_{net}}{Ex_{in}} \quad \textbf{(18)}$$

- **Annual energy**

The annual energy (AE) generated by the Dish Stirling system is simply obtained by integrating the net power over one complete year corresponding to a total of 8760 hours:

$$AE = \int_0^{8760} P_{net}\, dt \quad \textbf{(19)}$$

- **Capacity factor**

The capacity factor (CF) represents the ratio between the cumulative electricity generated for the whole year over the energy obtained by considering a full operation (8760 h) at the rated capacity (P_{rated}).

$$CF = \frac{AE}{P_{rated} * 8760} \quad \textbf{(20)}$$

One should mention that the unit rated power of the investigated system is 25 kW, according to the technical details furnished in **Table 4**.

- **Levelized cost of electricity**

Levelized Cost of Electricity is the most utilised index for analysing solar power generation systems' performance and economic competitiveness. LCOE is the discounted lifecycle cost ratio and the discounted total energy generated by the system. As a financial parameter, nominal $LCOE$ and real $LCOE$ are considered in the present analysis to assess the competitiveness of this technology against other power generation modes. The real LCOE is a constant currency with an adjusted inflation value and is generally used for long-term assessments to analyse the effect of the inflation years over the life of the project. The nominal LCOE considers the present value of the currency and is usually involved in short-term assessments. The $LCOE$ can be expressed as follows:

$$LCOE = \frac{-C_0 - \frac{\sum_{n=1}^{N} C_n}{(1+d_{nomianl})^n}}{\frac{\sum_{n=1}^{N} AE_n}{(1+d_i)^n}} \quad \begin{cases} i = nominal \rightarrow LCOE = LCOE\ (nominal) \\ i = real \rightarrow LCOE = LCOE\ (real) \end{cases} \tag{21}$$

with AE_n is the electricity produced in year n, N describes the project's lifetime in years, C_0 and C_n are the project's equity investment amount and the annual cost, respectively, d_{real} and $d_{nominal}$ are the real discount rate and the nominal discount rate, respectively. **Table 6** reassembles the cost assumptions and financial parameters used in the $LCOE$ calculations.

Table 6: Assumptions and Data ([67], [273])

Assumptions and Data	**Value**
Direct Capital Cost	
Site Improvements ($/m^2)	20
Collector cost ($/m^2)	400
Engine Cost ($/kW)	500
Receiver Cost ($/kW)	200
Operations and Maintenance Cost	
Fixed cost by capacity ($/kW-year)	50
Variable cost by generation ($/MWh)	7
Financial Parameters	
Inflation Rate (%/year)	2.5
Real Discount Rate (%/year)	5
Nominal Discount Rate (%/year)	7.63

- **Mitigated CO2 emissions**

Switching to renewable energy power generation has a positive environmental impact since a great amount of greenhouse gas emissions can be reduced. To quantify the potential of annual emissions reduction properly due to the utilisation of SDS technology, one should evaluate its carbon footprint along with the carbon footprint of the competing method [274]. Here, it is considered that the competing method is the electricity obtained from the current Moroccan energy mix. Two previously published papers dealt with the carbon footprint of the Dish Stirling technology. The first considered a 37.66 gCO_2-eq/kWh for SDS unit of 10 kW [275], and the second estimated a value of 7.3 gCO_2-eq/kWh for a Megawatt-scale SDS plant [276]. In the present analysis, since the SDS plant is of a total capacity of 10 MW, the second reference is retained for the calculations. With respect to the electricity generated from the Moroccan energy mix (based on the year 2019), according to the estimations given in [277], the carbon footprint of electricity from the national grid is given as 592 gCO_2-eq/kWh. Thus, the annual quantity of mitigating CO_2 emissions can be calculated as:

$$AM_{CO_2} = AE\left(cf_{grid} - cf_{SDS}\right) \quad \textbf{(22)}$$

AE is the net annual electricity, cf_{grid} is the carbon footprint of grid electricity and cf_{SDS} is the carbon footprint of SDS technology.

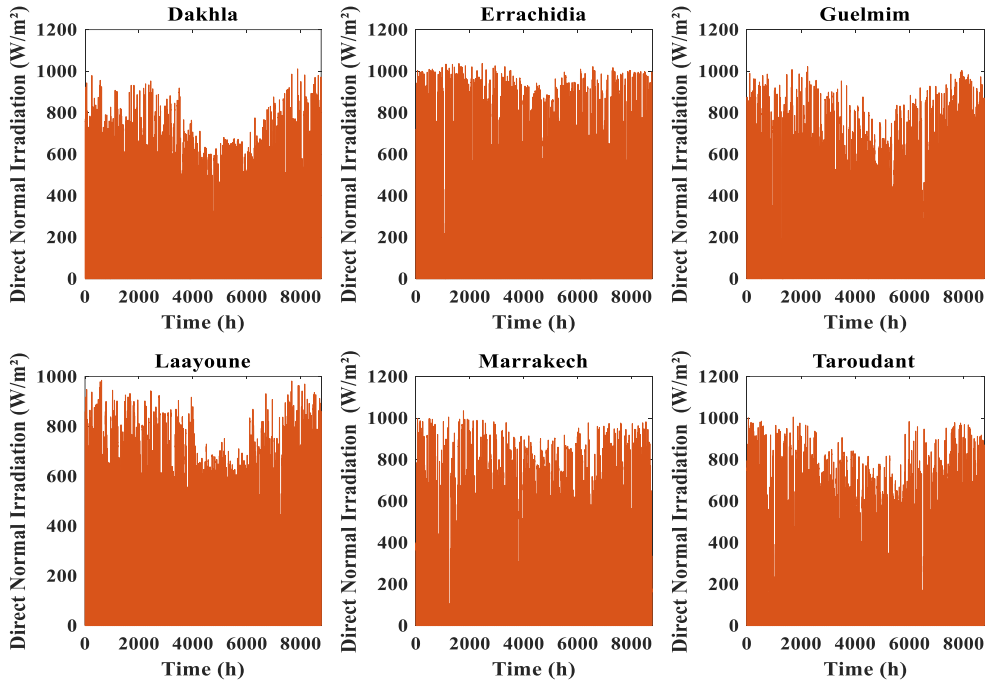
4. Results and discussion

This part of the current chapter includes the evaluation of SDS technology in six cities among the 13 examined sites for readability purposes. Later, an extrapolation to the other cities is undertaken as well be shown in the last subsection.

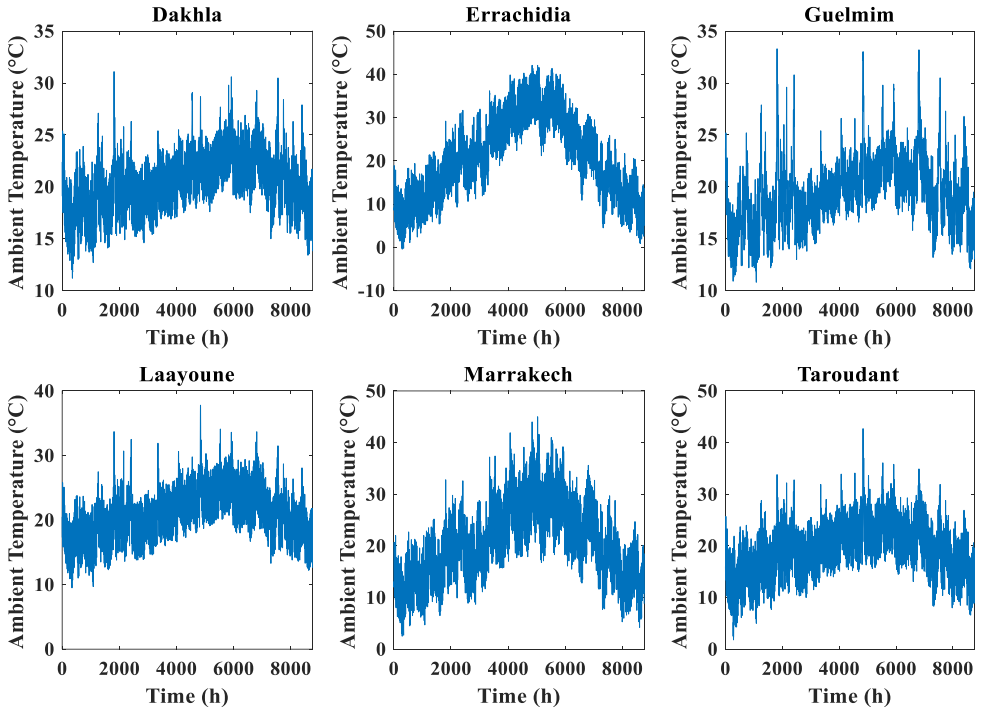
4.1. Weather data

The geographical sites under focus are located in the south of Morocco. These regions enjoy a huge solar energy potential. **Fig. 28** illustrates the hourly variation of the main influential climatic variables for the SDS system. The Direct Normal Irradiation hourly profile for each site is depicted in **Fig. 28 (a)**. It is clearly observed that Errachidia city can receive a maximum value of solar irradiation than can attain a value around 1037 (W/m^2). Since the Sahara is very close, it makes the climate desert (hot and dry). **Fig. 28 (b)** displays the hourly data of the ambient temperature distribution, the only site in which the ambient temperature does not exceed 31.1 °C is Dakhla; the majority of the other cities have ambient temperatures that can surpass 42 °C. The change of the wind speed is caused by air moving from high to low pressure due to the ambient temperature variations. **Fig. 28 (c)** envisions the

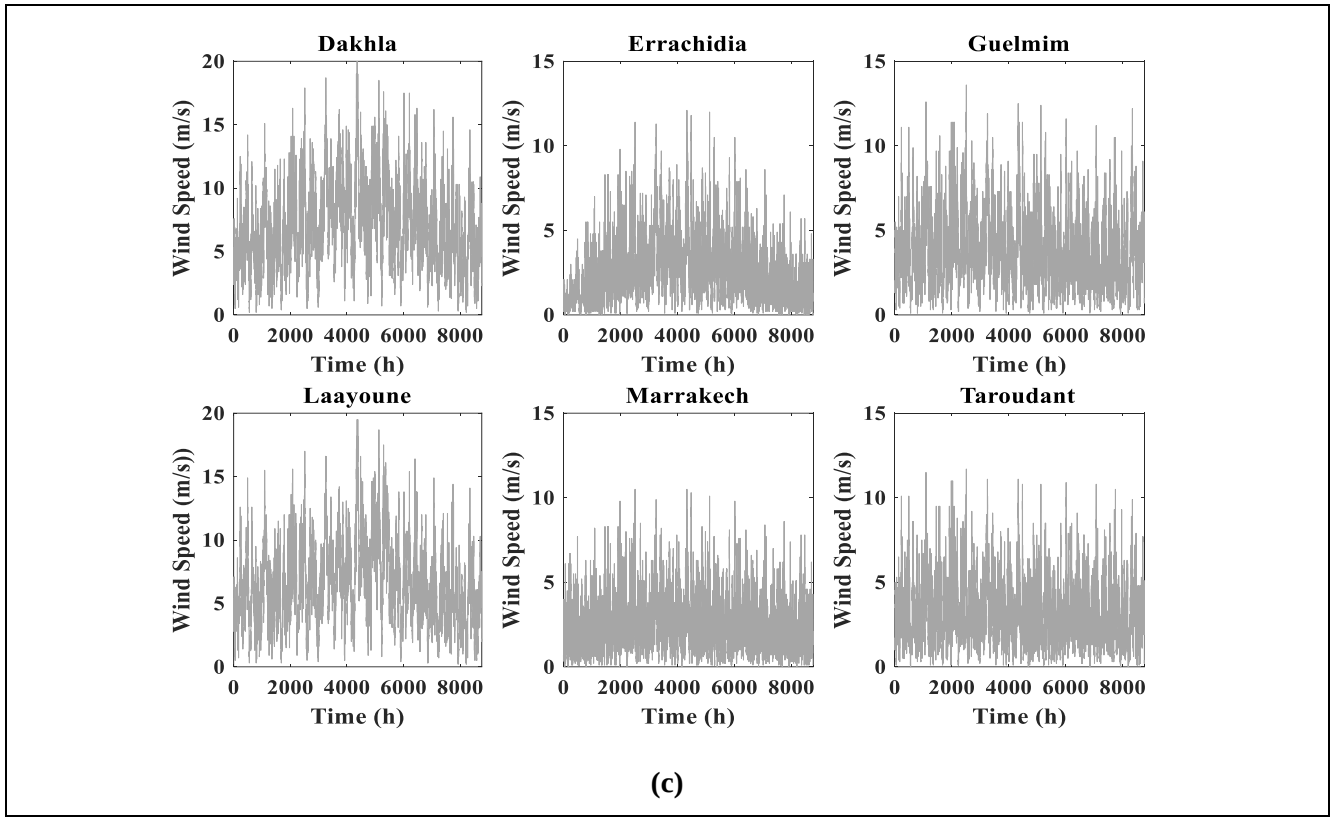
hourly wind speed data of the examined cities; a maximum value can reach over than (20 m/s) in windy areas such as Dakhla and Laayoune.



(a)



(b)



F**igure 28:** Hourly weather data variation during a whole year for the six cities: **(a)**: Beam normal irradiance; **(b)**: Ambient temperature; **(c)**: Wind speed.

4.2. Hourly system energy efficiency

Based on the design parameters given in **Table 4**, simulations were launched to characterise the system efficiencies for special days of the year corresponding to the spring/autumn equinox, and summer/winter solstice). **Fig. 29** displays the energy efficiency during a period of 24 hours for each examined site. The efficiency is influenced by several climatic parameters like ambient temperature and wind speed, but it depends strongly on solar irradiation. It is also affected by the design parameters of the Dish structure and Stirling engine. A general observation is that a 25% energy efficiency can be obtained for most of the sites. Some of the sites seem to be highly influenced by the seasonal variations of climatic data, such as Taroudant and Laayoune. In terms of the energy efficiency dataset for the whole year, it was found that the maximum daily system efficiency was predicted to be about 28% in Errachidia, while the lowest efficiency was anticipated to be about 18% in Dakhla.

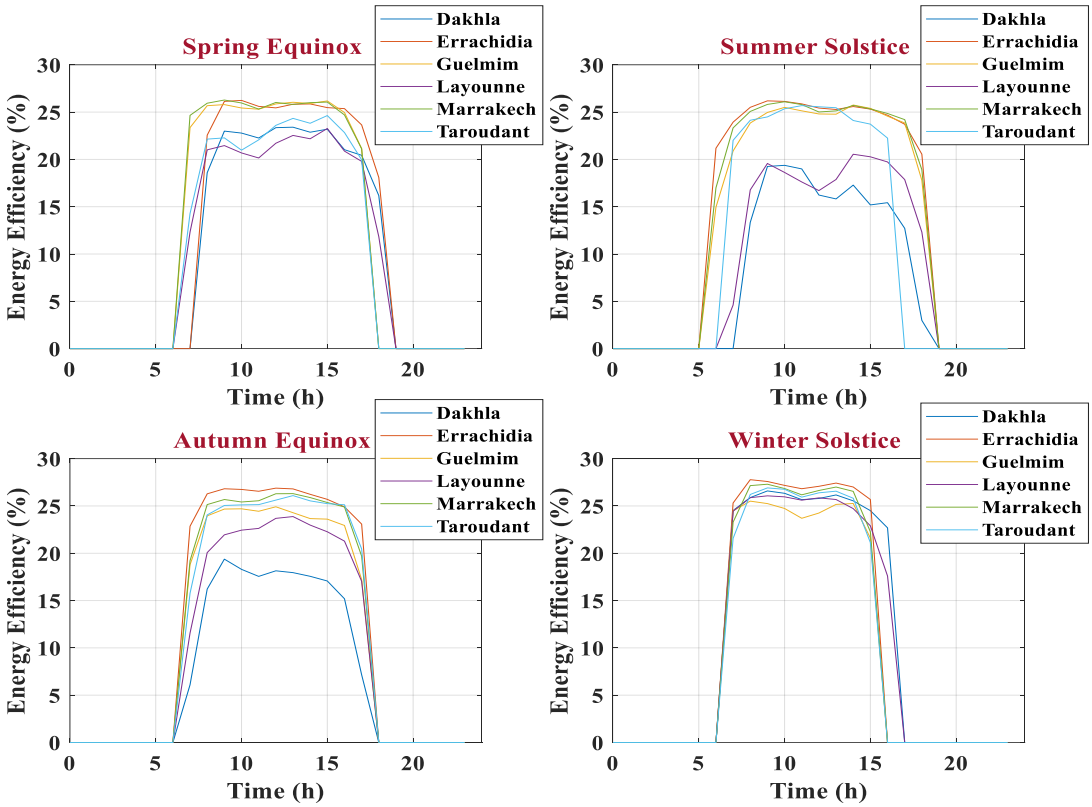


Figure 29: Hourly variation of the energy efficiency of the SDS system corresponding to a specific day in each season.

4.3. Hourly exergy efficiency

For a better analysis of this system, both energy and exergy efficiency must be considered. Based on the same design parameters and using the simulation results and the exergy efficiency equation, **Fig. 30** shows the exergy efficiency corresponding to the same days presented as before. A maximum exergy efficiency value of 26.98% was observed at Marrakech city during the spring equinox day. For the remaining three days, the maximum values were reached by Errachidia. The exergy efficiency in this location attained a value of 28.46% on the winter solstice day. It has been highlighted that the energy efficiency and the exergy efficiency tendency were identical, but a slight increase in the exergy efficiency was detected. These results agree with the findings reported by [241].

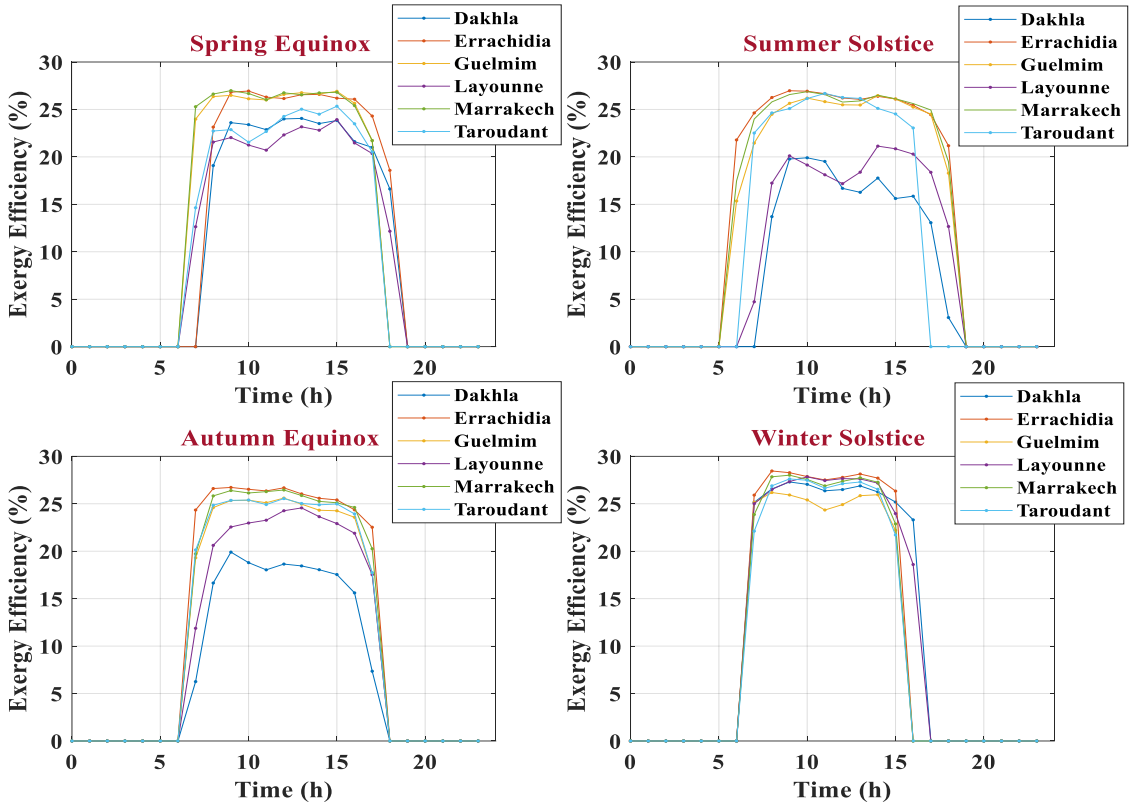


Figure 30 : Hourly variation of the exergy efficiency of the SDS system corresponding to a specific day in each season.

4.4. Parametric analysis and optimisation

The approach to improve the output power and efficiency of the system is optimising the current design for the cooling speed of the pump, aperture diameter, and the insulation thickness of the receiver. The effects of changing these parameters on the annual energy yield are discussed below.

- **Cooling Speed Pump**

First, the analysis is focused on the cooling pump speed. The main role of the cooling system is to lower the temperature inside the compression space and enhance the energy production by ejecting heat losses from the SE [264]. A high cooling pump speed value should be adopted for sites with warmer climates, while a reduced value can be fixed for colder climates. A climate with high ambient temperature increases the parasitic energy consumption of the pump. A parametric study is mandatory to detect the pump's speed, ensuring the maximum annual energy value. The parametric study considers varying this speed from 900 rpm to 2700 rpm and visualising the effect on the annual energy produced for all evaluated sites. According to the **Fig. 31**, an optimum point is detected for each

independent site marking a maximum value of the annual energy generated. A maximum value of the annual energy produced exceeding 61 MWh in the city of Errachidia was reached for a value of 2480 rpm. Dakhla city is presenting the lowest electricity production, increasing the value of the pump speed leads to a maximum energy value, for an optimum speed value of 1980 rpm. Increasing the pump speed generally increases the value of annual energy to a specific limit. This is explained by the fact that the pump has not compensated for the global frictional losses occurring in the cooling fluid loop for low speeds. Once the optimum value of the annual energy is reached, the increase in the speed of the pump will simply generate more energy consumption, consequently resulting in a drop in the net annual energy.

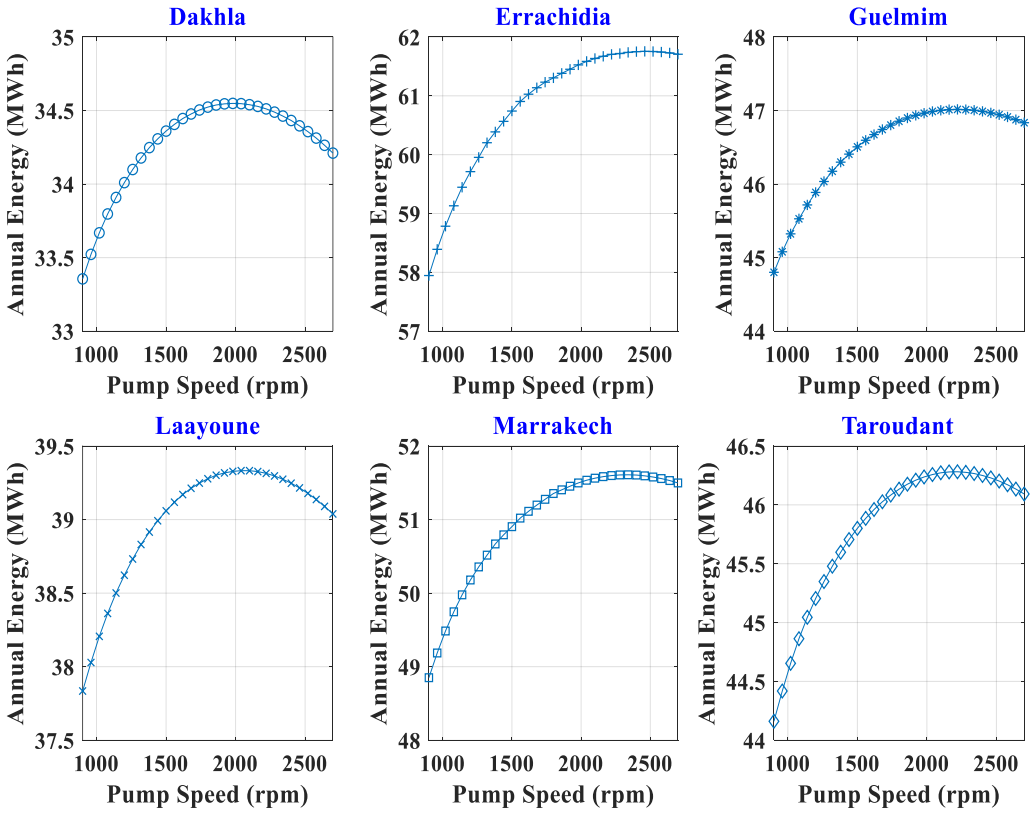


Figure 31: Impact of the variation of the speed of the cooling pump on the annual energy generated.

- **Receiver aperture diameter**

Radiation losses contribute significantly to the global energy losses in the SDS system. These losses can be minimised by balancing the sizing of the opening diameter of the receiver and therefore enhancing the net annual energy of the SDS system. It is also noticed that the design point of aperture diameter depends on the intercepted factor and errors in the collector. In this direction, the value of the receiver aperture diameter was varied from 5 cm to 50 cm.

Fig. 32 shows the impact of this parameter on the energy at the output of the receiver. The diameter would be sizeable enough to intercept the radiation and then transfer it to the absorber. The receiver aperture's diameter is a parameter that appears in the equation of the energy captured by the receiver (See Eq. (1)). If the value of this diameter is increased, the energy entering the receiver will be raised accordingly; however, this value must be carefully tailored and must not exceed limit values in order to avoid the augmentation of the total thermal losses by convection and radiation at the receiver level. An optimum value of the annual energy at the receiver output is reached and found to be 230 MWh, coinciding with a value of about 70 mm of the receiver aperture diameter. Afterwards, this energy will undergo a significant drop per each increment of the diameter value.

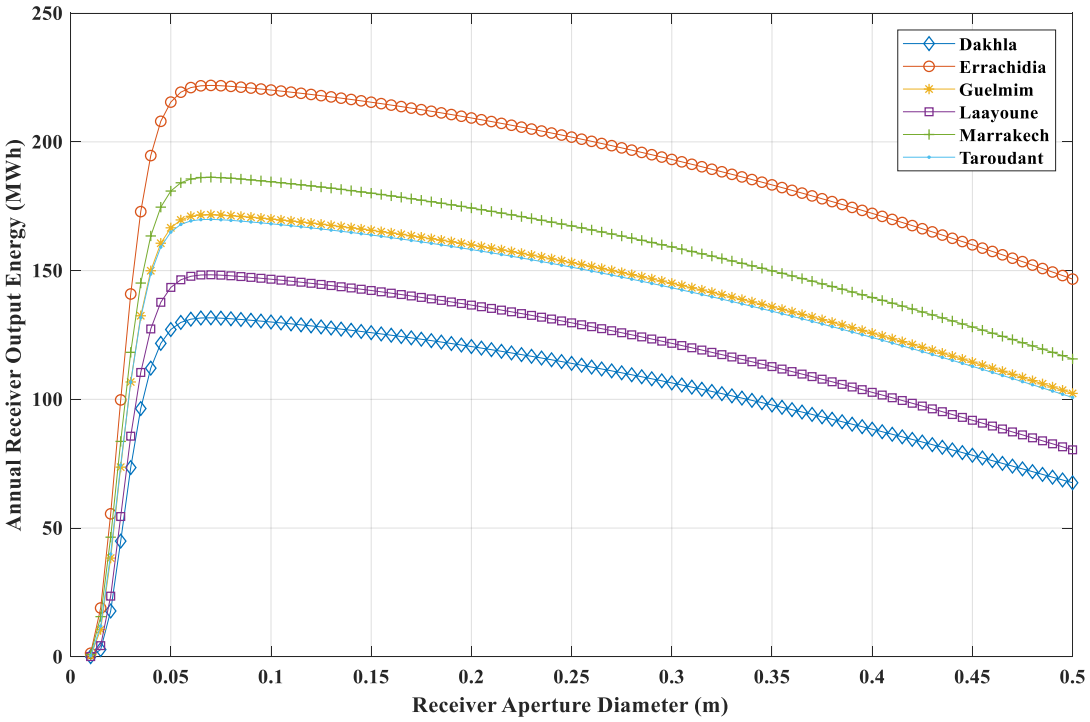


Figure 32: The effect of the change of the receiver aperture diameter on the receiver output energy for the examined sites.

Fig. 33 illustrates the effect of the variation of the receiver aperture diameter on the annual energy generated. The same trend of the previous curves is observed, except that there is a decrease in terms of the energy produced. This implies that the energy at the output of the receiver undergoes several types of losses during the conversion into electrical energy. For both figures, it can be highlighted that when the value of the receiver aperture diameter increases, a maximal value of the annual energy produced of the SDS system is attained,

coinciding with a value of 70 mm. For higher values of the aperture diameter, the annual energy starts to decrease. It appears that 70 mm is recommended as an optimised value of the receiver aperture diameter independent of the examined site.

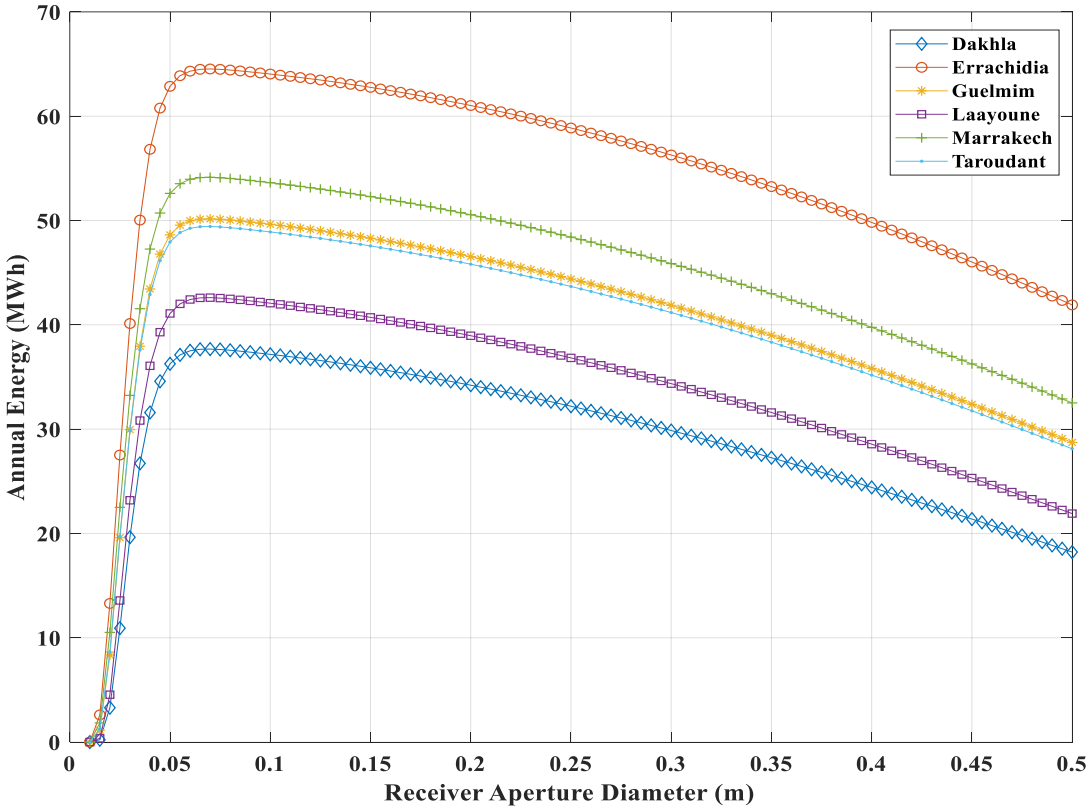


Figure 33: Annual Energy versus the receiver aperture diameter.

Fig. 34 represents the receiver losses with respect to the diameter variation. This figure explains the findings reported in **Figs. 33 and 32**. By increasing the value of the receiver aperture diameter, the captured heat flux will be more significant until an optimum value is reached, corresponding to a minimum of receiver losses. Then, further increase in the diameter will cause an increase of the total thermal losses by convection, and radiation will be observed. As can be seen, the same value (70 mm) concurs with a minimum value of receiver losses which proves the previous patterns of the annual and receiver output energy.

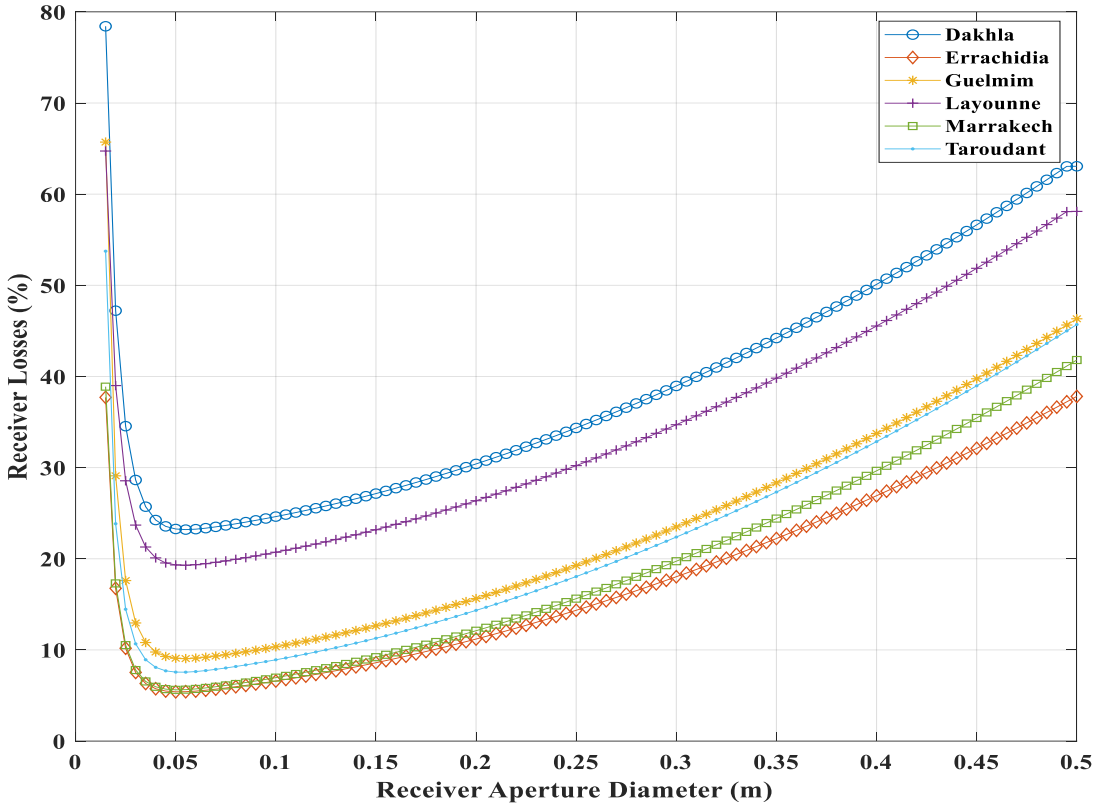


Figure 34: Impact of the variation of the receiver aperture diameter on the receiver losses

- **Receiver insulation thickness**

Convection, radiation, and conduction losses from the receiver are responsible for a considerable quantity of the energy losses in the SDS system. The losses due to conduction can be managed by adjusting the insulation thickness of the receiver. A parametric study has been developed to identify a recommended thickness of the receiver insulation, taking the annual energy generated as the main criterion. From **Fig. 35**, it seems that a thickness of about 30 mm can be recommended as an optimal value to reduce the conduction losses at the receiver level. In fact, for values lower than 30 mm, one can notice a more significant relative enhancement in the annual energy when incrementing the thickness. Beyond this value, the increase in the annual energy seems to be marginal and remains almost constant till the value of 150 mm. For the city Errachidia, which exhibits the most significant energy production, a value of more than 60 MWh per year is obtained for a thickness of 30 mm. The detected optimum value is valid for all the studied cities.

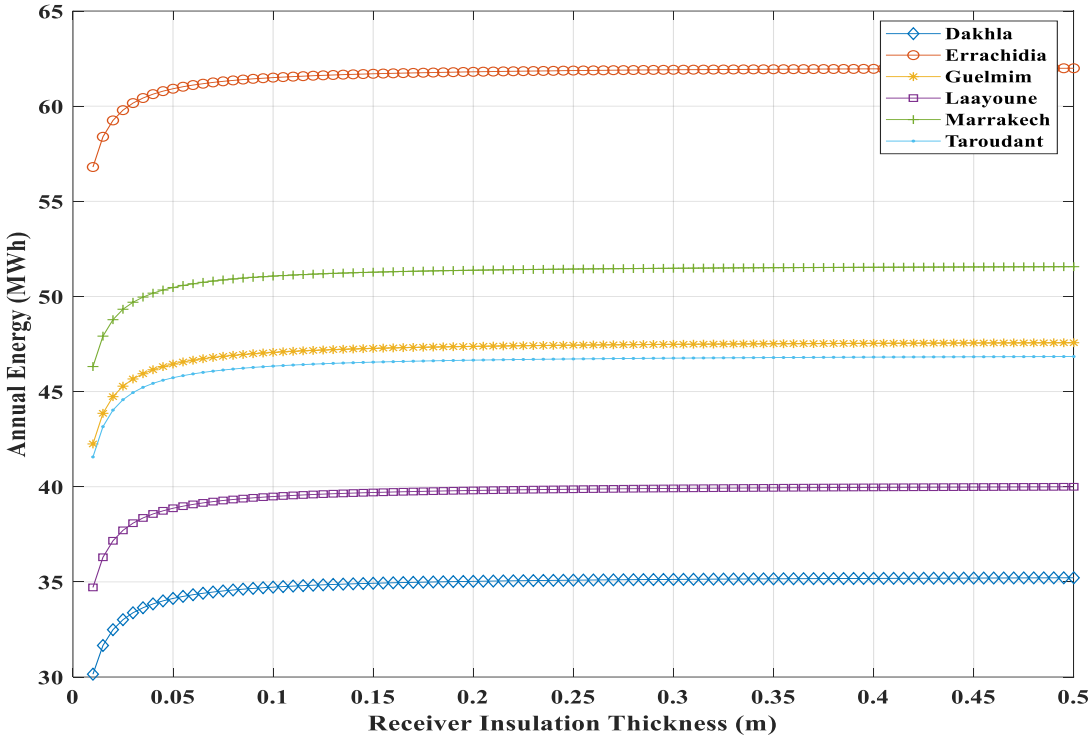
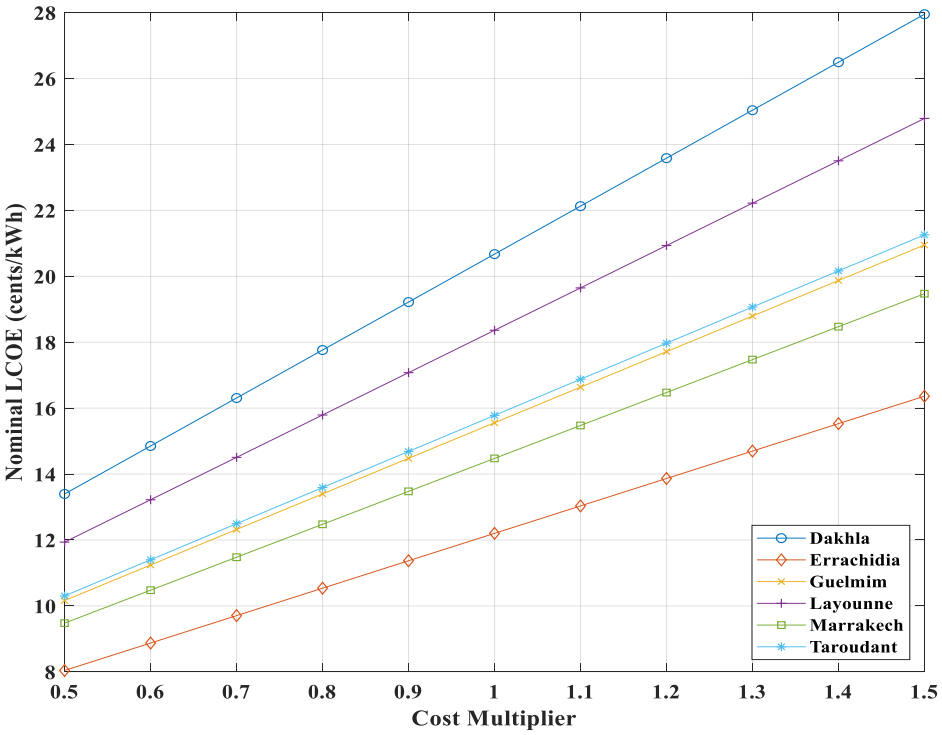


Figure 35: Effect of the change of the receiver insulation thickness on the annual energy.

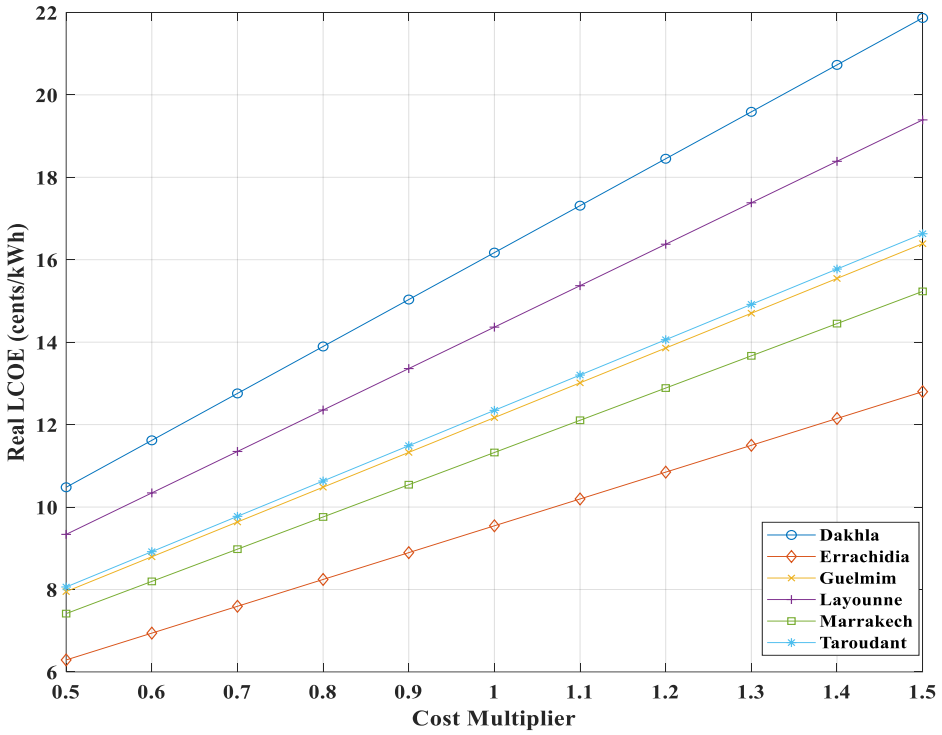
4.5. Economic analysis

The LCOE computations are performed considering a solar power plant with a total capacity of 10 MW. Based on the SDS technology with a rated capacity of 25 kW, the solar field consists of a total of 400 collectors corresponding to a solar field area of 90000 m².

The LCOE analysis is performed using the costs of the SDS system, which cover the direct capital cost involving four expense types (receiver, collector, and engine costs, and site preparation related costs). The objective is to study the sensitivity of the LCOE to capital costs variations. A cost multiplier ranging from 0.5 to 1.5 was applied to the reference capital cost. For direct capital costs multiplied by a 1.5 coefficient, the nominal and real LCOE value reaches 28 c$/kWh (**Fig. 36 (a)**) and 22 c$//kWh (**Fig. 36 (b)**). This corresponds to the city of Dakhla with the lowest annual energy generation. For cities having higher energy yields, the nominal and real LCOE are around 16.5 c$/kWh and 13 c$/kWh, respectively. When direct capital is reduced by 50% of its initial values, the nominal electricity cost for the city with the best annual energy yield (Errachidia) is reduced to 8 c$/kWh (**Fig. 36 (a)**).



(a)



(b)

Figure 36: Levelized Cost of Energy (LCOE) as function of the Cost Multiplier: **(a)** Nominal LCOE; **(b)** Real LCOE.

4.6. Results extrapolation

In this last subsection, the design parameters that maximise the annual energy are considered for each site and according to an extensive parametric analysis for the 13 geographical sites. This includes the optimal value of each of the three parameters: cooling pump speed, receiver aperture diameter, and receiver insulation thickness. The solar plant capacity is taken as 10 MW as already mentioned. **Table 7** illustrates the energetic and economic performances of SDS in the selected sites. The performance indexes are the Annual Energy, Capacity Factor, and Levelized Cost of Energy (LCOE). The most continent city for installing the SDS system is the city which enjoys a high annual energy production with a high-capacity factor and a reduced nominal and real LCOE. It is interesting to highlight that the LCOE values (nominal and real) are delimited within a range corresponding to cost multipliers of 0.5 and 1.5. According to **Table 7**, the best site leading to the highest annual energy production value is the city of Ouarzazate, followed by the city of Errachidia. This also coincides with a maximum value of the capacity factor, which is 27% in Ouarzazate and 26.7% in Errachidia. Followingly, the LCOE is minimal at these sites since the overall costs are similar for the examined sites.

Table 7: Technical and economic performance of the SDS system, including the optimised parameters

	Annual Energy (GWh)	**Yearly energy efficiency (%)**	**Yearly exergy efficiency (%)**	**Capacity Factor (%)**	**Nominal LCOE (c$/kWh)**			**Real LCOE (c$/kWh)**		
					For Initial capital cost	**For 50% cost decrement**	**For 50% cost increment**	**For Initial capital cost**	**For 50% cost decrement**	**For 50% cost increment**
Agadir	16.789	22.85	24.48	19.2	14.97	9.92	20.01	11.71	7.76	15.65
Aousserd	14.879	19.32	20.69	17.0	16.77	11.08	22.47	13.12	8.67	17.57
Dakhla	13.553	18.29	19.58	15.5	18.33	12.08	24.58	14.34	9.45	19.23
Errachidia	23.394	24.33	26.06	26.7	10.99	7.37	14.61	8.60	5.77	11.43
Essemara	17.976	20.70	22.16	20.5	14.04	9.33	18.75	10.98	7.30	14.67
Guelmim	18.156	22.92	24.54	20.7	13.91	9.24	18.57	10.88	7.23	14.53
Laayoune	15.307	19.67	21.06	17.5	16.33	10.80	21.86	12.77	8.45	17.10
Marrakech	19.571	23.82	25.53	22.3	12.97	8.64	17.29	10.14	6.76	13.53
Midelt	21.465	24.42	26.13	24.5	11.90	7.95	15.85	9.31	6.22	12.40
Ouarzazate	23.693	24.26	25.98	27.0	10.87	7.29	14.44	8.50	5.70	11.30
Safi	18.107	23.35	25.02	20.7	13.94	9.26	18.62	10.91	7.25	14.57
Tan-Tan	13.273	19.69	21.15	15.2	18.69	12.31	25.07	14.62	9.63	19.62
Taroudant	17.888	23.15	24.81	20.4	14.10	9.37	18.84	11.03	7.33	14.74

4.7. Environmental impact

From an environmental point of view, producing electricity through the SDS technology in Southern Moroccan regions can reduce a considerable amount of CO_2 emissions. **Fig. 37** shows the annual mitigated CO_2 emissions resulting from using the SDS technology for electricity generation instead of the national grid electricity. The annual mitigation potential of CO_2 emissions for the studied sites ranges between 7.76 ktonne and 13.85 ktonne. Intuitively, the sites having reached high values of the annual energy generated will also avoid significant CO_2 emissions. The maximum value of the annual mitigated CO_2 emissions was observed in Ouarzazate, followed by Errachidia, while minimum values were observed in Tan-Tan and Dakhla.

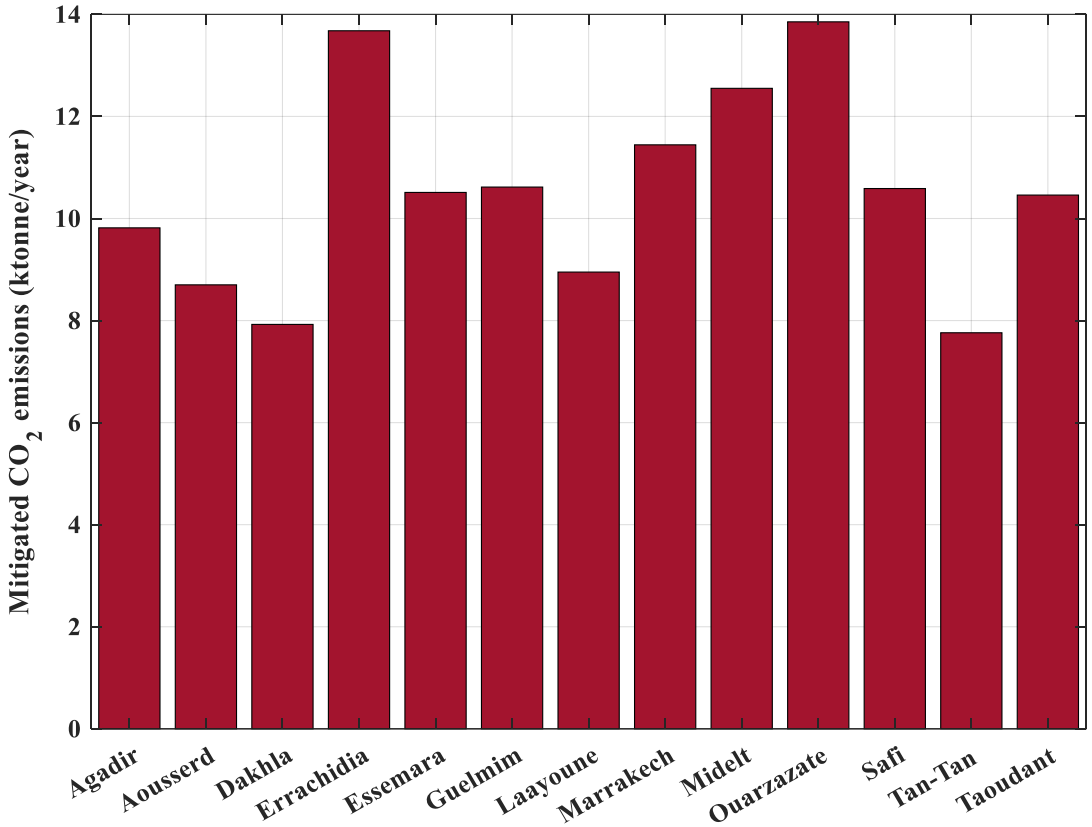


Figure 37: Annual quantity of the mitigated CO_2 emissions per city.

The results obtained by using the optimised parameters of the presented assessment were compared with some latest works in terms of the energetic and economic feasibility. In this case of study, Ouarzazate city has been selected because it enjoys the highest annual direct normal irradiation. **Table 8** presents technical details and main energy and economic outputs for the compared plants. It is observed that Ouarzazate city have a great solar potential regarding the value of the annual bean normal irradiance with a value of 2917 kWh/m²/y. The annual energy generated as well as the overall annual energy efficiency of the

suggested model reported the maximum values of 59.53 MWh and 24.26%, respectively, which are higher than those obtained in Ref ([31], [67], [158], [278], [279]). Regarding the economic viability, it was found that the LCOE for Ouarzazate city is the lowest (about 0.085 $/kWh).

Table 8: Comparison of the current study with other works

Ref	**City, Country**	**Simulation Software**	**Direct Normal Irradiation (kWh/m²/y)**	**Working fluid**	**Rated power**	**Annual energy (MWh)**	**Annual Energy efficiency (%)**	**LCOE ($/kWh)**
Current study	Ouarzazate, Morocco	SAM	2917	Hydrogen	25	59.23	24.26	0.085
Abbas et al. [67]	Tamanrasset, Algeria	SAM	2700	Hydrogen	25	54	24	0.115
Lashari et al. [278]	Jamshoro, Pakistan	SAM	1719.5	Helium	25	38.6	23.39	0.13
Zayed el al. [31]	Tianjin, China	MATLAB	1198.2	Helium	25	28.748	19.55	0.2565
Affandi et al. [158]	George Town, Malaysia	MATLAB	1246	N/A	25	8.385	N/A	0.83
Bataineh and Taamneh [279]	Maan, Jordan	SAM	2700	Hydrogen	9.7	17.53	21	0.115

5. Summary

This chapter presents a techno-economic and environmental assessment and optimisation of the Solar Dish Stirling technology for electricity generation in various sites of the southern Moroccan regions. First, optimum values of the receiver aperture diameter, insulation thickness, and the operational pump speed of the cooling mechanism are determined for each geographical zone. The optimisation results are then used to predict key performance metrics, including the net annual energy, capacity factor, and the Levelized cost of electricity for a 10 MW solar plant. The following conclusions can be made:

- The optimum value of the pump speed varies depending on meteorological parameters for each site, such as the wind speed and the dry bulb temperature. Sites with high ambient temperatures require higher cooling pump speed.

- The SDS's hourly overall energy efficiency was estimated for particular days of the year (i.e., spring/ autumn equinox, and summer/ winter solstice). The maximum reported values range between 17% and 29%.
- The annual energy generated in the various cities fluctuates between 13.273 GWh and 23.693 GWh for a total capacity of 10 MW. These limit values are predicted respectively for Tan-Tan and Ouarzazate.
- An optimum receiver aperture diameter for which the thermal losses are minimal is identified to be 70 mm.
- Increasing the insulation thickness of the receiver leads to an enhancement in the annual energy. The enhancement is marginal for thicknesses larger than 30 mm, which was selected as a recommended value.
- Levelized cost of electricity in the various cities was found to vary in the range of 10.87 c$/kWh and 18.69 c$/kWh, for Ouarzazate and Tan-Tan, respectively. Decreasing the capital cost of used equipment can lead to a remarkable drop in the LCOE values.
- Environmentally, reducing between 7.76 ktonne and 13.85 ktonnes of CO_2 emissions annually is possible.

The current work was conducted for the southern Moroccan regions only; therefore, it will be of interest to extrapolate the present study's findings to other Moroccan regions and other African countries. An experimental platform with a complete weather station is as well needed to validate the obtained results.

CHAPTER IV. Multi- objective optimization of a SDS field layout using Genetic Algorithm and TOPSIS method

1. Introduction

CSP systems have experienced significant growth with great ability to supply clean and eco-friendly electrical power. The existence of many design parameters with mutual influence on both energetic and economic performances of the SDS system leads to a multi-objective problem with high-nonlinearity. The present chapter sheds light into solar dish field layout optimization and characterization of the best trade-off between the Capacity Factor (CF) and the Total Cost of Site Improvement (TCSI) by introducing a novel multi-optimization approach. The case study in this chapter considers a 10 MW Solar Dish Stirling power plant operating under the meteorological data of both Ouarzazate and Madrid cities. The current study involves a combination of numerical tools to achieve optimum field parameters for a given geographical site. The energy evaluation of the solar dish field was conducted using SAM (System Advisor Model) simulation software. Afterwards, surrogate model and optimization process were developed using MATLAB environment. A multi-criteria decision analysis is introduced employing the Technique of Order of Preference by Similarity to Ideal Solution (TOPSIS) which allowed to further select a unique configuration among the solutions given by the Pareto Frontier.

2. Background

Renewables contribute strongly to reduce greenhouse emissions by fulfilling more sustainably and reliably the ever-increasing energy demand [280], [281]. Several leading countries such as China and USA are planning to enhance renewable power generation share to 80% by 2050 [282], [283]. Energy provided by the sun is extensively available and shows a great potential for green energy production [25]. Particularly, special interest has been devoted to Concentrated Solar Power (CSP) technologies which are expected to supply around 7% of the global electricity requirement by 2030 and 25% by 2050 [26].

Environmentally, as **Fig. 38** suggests, these technologies have the potential to mitigate very large amounts of CO2 emissions [284] . In Europe, the overall capacity has been raised from 500 MW to 5000 MW between 2006 and 2015. In USA, it is estimated to reach 118 GW of installed CSP systems by the end of 2030 [15] . Recently, South Africa, China and Morocco have installed a capacity of about 600 MW of CSP technologies [9].

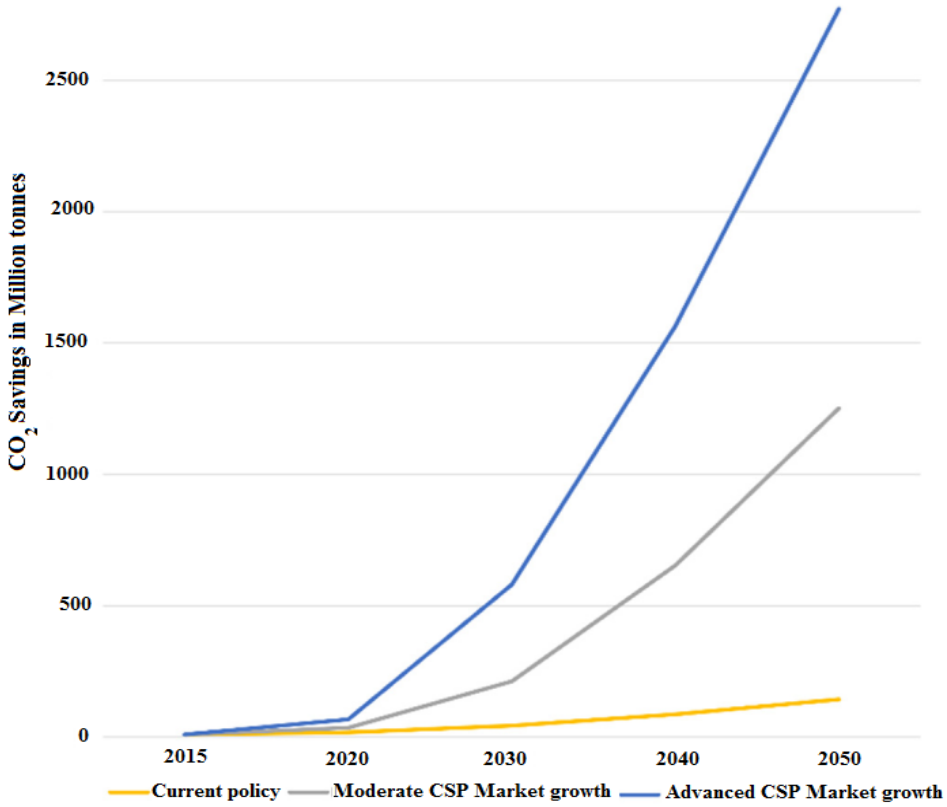


Figure 38: Cumulative amount of CO2 avoided for period between 2015 and 2050 under various scenarios [15].

Several investigators dealt with the technical and economic assessment of CSP technologies operating under various climatic regions. The effect of critical geometrical PTC parameters has been discussed in the work reported by Ehyaei et al. [285] for a site located in Tehran, Iran. Multi-objective optimization has been applied and optimal results ensuring the best trade-off between energy performances and economic feasibility were selected. Zayed et al. [88] performed the opto-geometric parameters of an SDS system under the meteorological conditions of Tianjin, China. The results indicated that the optimization of the different optical and geometrical criteria of the concentrator is mandatory for rational exploitation of this type of technology. Similar attempts were carried out for solar power plants located in USA [286], Spain [287] and Uzbekistan [288].

The sun changes its position throughout the day and efficiencies of CSP systems are greatly dependent on upcoming solar irradiation. As such, for more rational use of this type of technology, it is vital to conduct optimization studies aimed at minimizing the different types of energy losses (end losses, shadings, blockings and cosine effects) by appropriately adjusting the field layout parameters [289]. In this sense, numerous sizing procedures were developed by the research community to solve these problems [77], [290]–[292]. Sharma et al. [293] compared the performance of solar PTC field for different orientations. The North-South orientation enabled the best functioning scenario in terms of the produced energy and the electricity generation cost. Wu et al. [294] proposed a configuration of the PTC field that consisted of 24 loops each comprising 8 collectors in each loop. This configuration avoided the issues caused by the non-uniformity of the heat transfer fluid temperature inside each loop. Several studies on field layout and optical design optimisation for heliostats were carried out and different algorithms have been compared in order to provide the best arrangements, reduce the amount of losses caused by shading and blocking, and get the most out of solar irradiation ([295]–[297]). Atif et al. [298] carried out an analysis to identify an optimal heliostats field layout based on the calculation of all the performance parameters and mainly shading and blocking effects. Wei et al. [299] specified an algorithm which optimized the layout of the field while minimizing the losses of shading and blocking. Four layout modes were studied, and the results revealed that the North-South cornfield layout is the optimum configuration for the investigated 1000 kWe solar tower plant. Crespi et al. [300] analyzed the effect of shading caused by passing clouds on the energy performance for a ST power plant. For a LFR solar field, Sharma et al. [301] studied the variation in shading as a function of the orientation of the solar field. A comparison between several row spacing values was provided. Buck et al. [302] reported a relative gain of about 12% in annual energy generation of a ST plant by optimizing the solar field characteristics.

Only few investigations dealt with the improvement of energy efficiency of SDS systems by adjusting the solar field layout and reducing the shading effects [78]. Using a Bravais lattice disposition and an appropriate choice of the tracking mechanism and dish shape, Dähler et al. [83] reported significant improvements in the performance of large-scale fields. Xu et al. [80] estimated the shading effect of solar dishes during an entire day. The simulation results proved that the spacing in a regular way does not allow for optimum operation. Authors reported several advantages that could be brought by rotating and shifting the solar field rows. Igo et al. [79] developed a concept to minimize power losses in a solar dish field. It was revealed that, to improve the performances at the system output, it is more

useful to adopt an unstaggered and rectangular layout of the field. In India, an analysis was carried out on the optimization of solar dish field by tailoring appropriately different variables such as the spacing between collectors and the amount of shading throughout a year [81]. The final optimal configuration allowed high efficiency while the annual electricity production can reach around 12 GW in Tiruchirappalli city. Cumpston et al. [82] proved that the thermal energy collected by dish fields in a power plant can exceed 49% of annual thermal energy per unit collector surface. This improvement can be obtained by minimizing shading effects while adopting a rectangular arrangement with adjusted spacing oriented north-south.

Few researchers introduced artificial intelligence-based optimization processes for efficient operation and maximum economic competitiveness of the SDS technology [230], [234]. For instance, Khosravi et al. [228] employed two artificial intelligence approaches based on Multi-Layer Perceptron (MLP) Neural Network (ANN) and Adaptive Neuro-Fuzzy Inference System (ANFIS) to select the best operating conditions of a SDS system. It was found that the adoption of ANFIS with the particle swarm optimization (PSO) offers more satisfactory results than other approaches such as MLPNN and GA. Zayed el. [232] carried out a theoretical model based on opto-geometric and thermodynamic assessment of Solar Dish-Stirling System using multi-objective PSO and the final optimal solution was determined using a decision making technique. A maximal power output of about 23.46 kW and a global efficiency of 30.15% were achieved. Rahmati et al. [303] assessed the output work of the Stirling engine using several artificial intelligence techniques such as genetic algorithm (GA), particle swarm optimization (PSO), and imperialist competition algorithm method (ICA). The results from the comparative study proved the effectiveness of the PSO and ICA compared to the GA.

3. Methodology

3.1. System description and problem statement

As it is well-known, the Solar Dish Stirling (SDS) system comprises a set of parabolic mirrors, a tracking mechanism and a metallic support [66]. The working principle of the studied SDS system for power generation was discussed in the previous chapters. **Fig. 39** shows a graphical illustration of a solar Dish Stirling (SDS) power plant with the main devices as well as the different solar field parameters. Technical details and specific design information of the suggested solar power plant are summarized in **Table 9**.

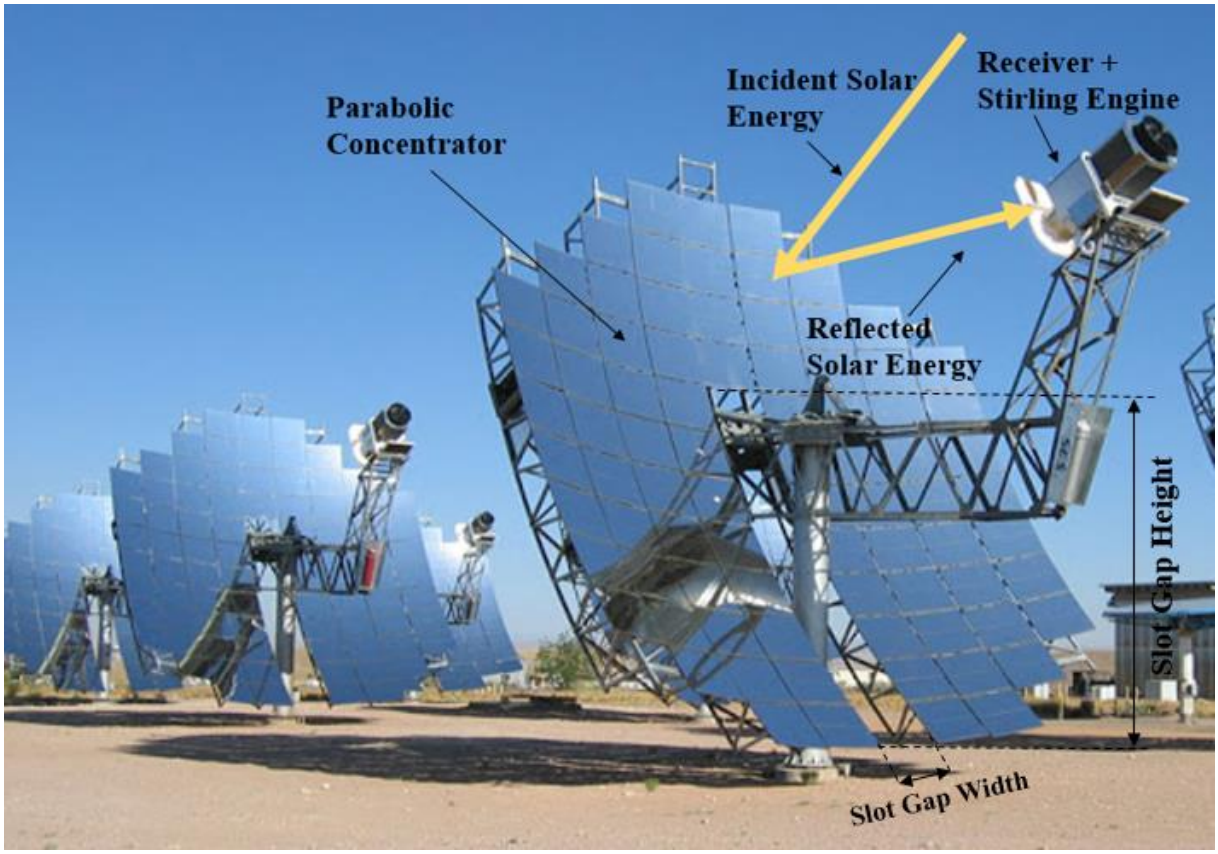


Figure 39: Solar dish Stirling power plant with main field parameters.

It should be noted that the distribution of the collector numbers according to the North-South and East-West orientation has been proved by running several simulations which consider all the possible combinations for a solar field of 400 collectors. Best configuration in terms of number of collectors in North-South and East-West directions are as indicated in **Table 2**.

Table 9: Dimensions, characteristics design and performance parameters of the SDS power plant

Solar Field	
Number of Collectors North-South	10
Number of Collectors East-West	40
Total Number of Collectors	400
System Properties	
Wind Stow Speed (m/s)	16
SDS capacity (kW)	25
Total Capacity (kW)	10000
Collector	
Total area of the mirror (m^2)	91

Reflectance	0.94
Cut-in irradiation (W/m²)	200
Receiver	
Receiver aperture diameter (m)	0.184
Insulation thickness (m)	0.075
Thermal Conductivity (W/m.K)	0.06
Absorptance coefficient of the absorber	0.9
Absorber surface (m²)	0.6
Stirling Engine (SES)	
Single Unit Nominal Capacity (kW)	25
Heater Head Set Temperature (K)	993
Functioning Speed (rpm)	1800
Displaced Volume (m^3)	0.00038
Beale Constant	0.04247
Beale 1st order parameter	1.682e-05
Beale 2nd order parameter	-5.105e-10
Beale 3rd order parameter	7.073e-15
Beale 4th order parameter	-3.586e-20
Pressure constant coefficient	0.658769
Pressure 1st order Coefficient	0.00023496
Parasitics	
Control system (W)	150
Reference cooling pump speed (rpm)	1800
Speed range of the cooling fan (rpm)	400-651

For a given Solar Dish Stirling power plant, several specific design parameters must be carefully adjusted to maximize the energy yield and economic competitiveness. In this work, an optimization process is carried out on the field layout characteristics along with the array shading parameters to maximize the Capacity Factor (CF) as an energy criterion and minimize the Total Cost of Site Improvements (TCSI) as an economic criterion. The geometrical parameters affecting the energy and economic performance of the studied SDS power plant are principally the solar field layout and array shading parameters. A brief description of the examined decision variables is given in what follows:

- The Collector Separation North-South ($d_{CollSep,N-S}$) and East-West ($d_{CollSep,E-W}$) describe the measured distance from center to center of adjacent collectors along the

North-South and East-West lines, respectively. **Fig. 40** illustrates the separation distances between dishes in a solar field.

The array shading criterions that will be discussed are the Ground Slope oriented North-South and East-West as well as the Width and the Height of the Slot Gap. All these parameters are involved in the shading factor estimation.

- Ground slope: describes the rise over run along a North-South direction ($Gr_{s,N-S}$). When the slope is positive, this means that for two dishes aligned, the dish to the south is lower than the dish to the north. With respect to the Ground Slope at the East-West direction ($Gr_{s,E-W}$), the slope is positive, when the dish to the east is lower than the dish to the west.
- Slot Gap Width ($Sl_{g,W}$) is the average width of the aperture in the mirror perpendicular to the vertical support post.
- Slot Gap Height ($Sl_{g,H}$) is the average height of the opening in the mirror parallel to the vertical support post.

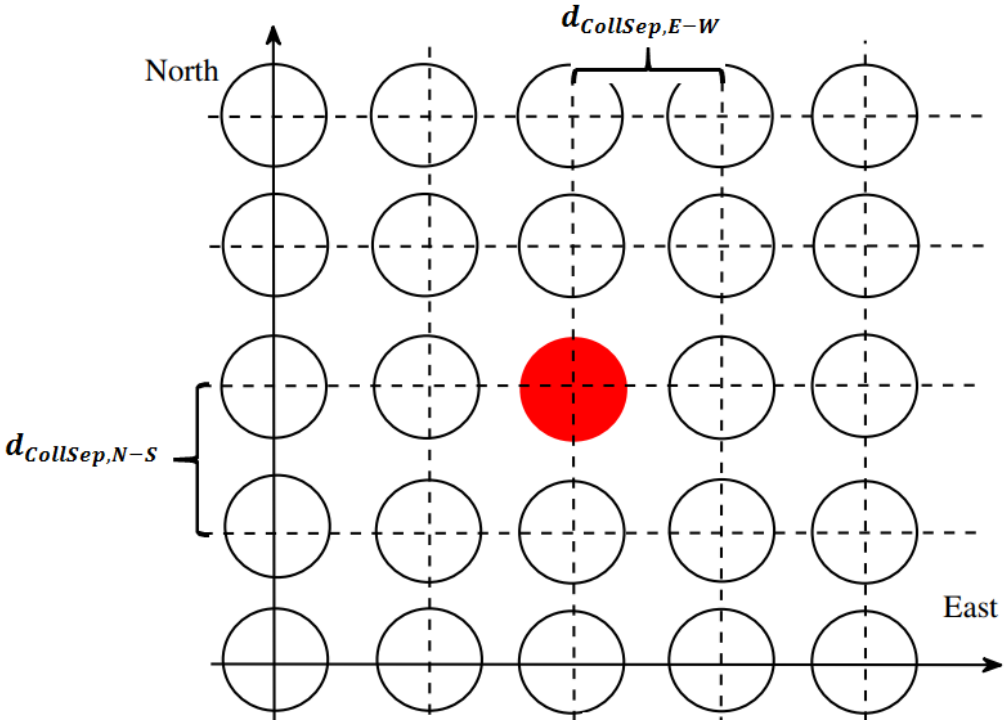


Figure 40: Schematic view of solar SDS field layout power plant [80].

Table 10 reassembles the examined decision variables of the solar field along with reference values before implementing the multi-optimization process.

Table 10: Design parameters of the SDS along with their initial values

Solar field layout	
Collector Separation North-South (m)	15
Collector Separation East-West (m)	15
Array Shading Parameters	
Ground slope, North-South (deg)	0
Ground Slope East-West (deg)	0
Slot gap Width (m)	1
Slot Gap Height (m)	1

3.2. Simulation process and optimization framework

Multi-objective optimization models are suitable to surpass the discontinuity and non-linearity in engineering problems and requires algorithms that are able to provide Pareto set solutions [304]. Genetic algorithm (GA) is a widely utilized technique for this purpose. GA offers considerable potential to handle hard optimization and learning problems and subsequently can be employed for solar and thermal system optimization ([305]–[307]). Using the surrogate model is essential at the beginning of this methodology and allows reducing the intrinsic computational time taking by the Genetic Algorithm [308]. Several approaches were adopted to build surrogate models such as Artificial Neural Networks (ANNs), support vector networks, Gaussian process regression and polynomial. However, there is practically no general opinion proving which approach works better. The selection of the best surrogate model is strongly dependent on the nature of the assessed problem [309].

In the present work, a third-order multiple non-linear regression was adopted to construct the surrogate model. It should be highlighted that System Advisor Model (SAM) was used to assess energetically and economically the investigated SDS power plants by performing hourly simulations for the examined sites. MATLAB solver was used to provide the Pareto Frontiers using *gamultiobj* built-in function that optimizes multiple fitness objectives. A flowchart illustration of the optimization process is depicted in **Fig. 41**.

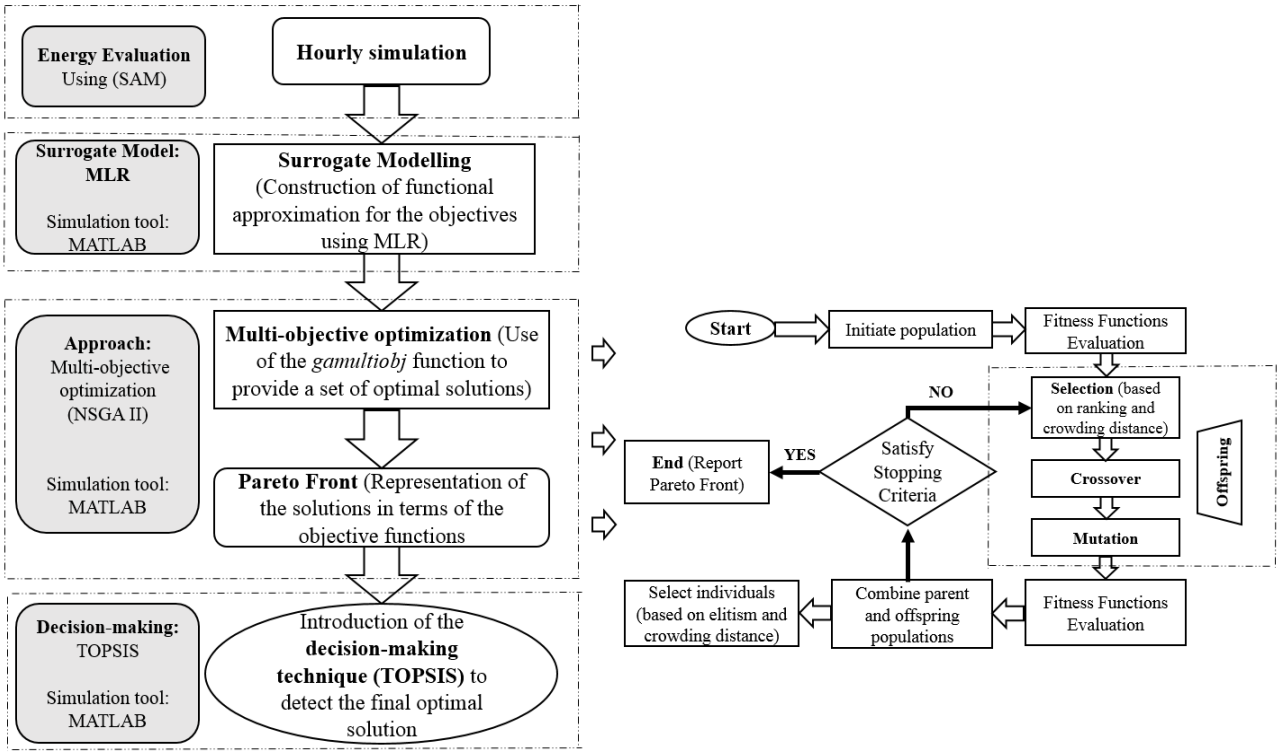


Figure 41: Schematic illustration of the optimization process.

3.2.1. Objective functions

The interest in adopting CSP technologies such as the solar dish Stirling system should necessarily ensure the best compromise between costs and energetic performances. In this study, the adopted approach for solar field optimization consists of two objective functions: annual Capacity Factor (CF) and Total Cost of Site Improvements (TCSI), which are described below:

- **Capacity Factor**

The Capacity Factor (CF) is a parameter which defines the ratio between the cumulative electricity generated for the entire year over the energy that could be generated if the power plant operates continuously for 8760 hours at its rated power (P_{rated}). The rated power of the suggested system is equal to 25 kW according to the technical details appearing in **Table 9**.

$$CF = \frac{AE}{P_{rated} * 8760} \quad \textbf{(23)}$$

where (AE) is the net Annual Electricity generated by the SDS system. It is retrieved by integrating the net power P_{net} over the time:

$$AE = \int_0^{8760} P_{Net}\, dt \quad \textbf{(24)}$$

- **Total Cost of Site Improvements**

The Total Cost of Site Improvements (TCSI) is the product of the total solar field area and the specific Site Improvement Cost (SIC). The SIC considers the global expenditures related to the preparation of the site and other equipment that does not appear in the solar field costs. The same assumptions of the system cost and the main financial characteristics used to assess the performance of the proposed SDS field was selected as reported in **Table 6** (**Chapter III)**.

$$TCSI = A_{SF} \cdot SIC \quad \textbf{(25)}$$

where (A_{SF}) is the total solar field area which is equivalent to the product of the number of collectors and the Collector Separation distances North-South and East-West:

$$A_{SF} = d_{CollSep,N-S} \cdot d_{CollSep,E-W} \cdot N_{Coll} \quad \textbf{(26)}$$

The total collector's number *(N_{Coll})* is expressed in terms of the numbers of the east-west and north-south oriented collectors. It can be defined as follows:

$$N_{Coll} = N_{Coll,N-S} \cdot N_{Coll,E-W} \quad \textbf{(27)}$$

with *($N_{Coll,N-S}$)* and *($N_{Coll,E-W}$)* are the numbers of the collectors in North-South and East-West orientation, respectively.

The total solar field capacity *(P_{SF})* is defined as the product of the total number of collectors (N_{Coll}) and the Stirling engine power *(P_{Engine})* :

$$P_{SF} = P_{Engine} \cdot N_{Coll} \quad \textbf{(28)}$$

3.2.2. Decision variables

The design parameters that may influence the objective functions are the Collector Separation distances East-West ($d_{CollSep,E-W}$) and North-South ($d_{CollSep,N-S}$), the array shading parameters precisely the Ground Slope east-west ($Gr_{s,E-W}$) and north-south ($Gr_{s,N-S}$) as well as the Slot Gap ($Sl_{g,w}$) Width and Height ($Sl_{g,H}$). These six variables were defined as the decision space:

$\vec{x} = (d_{CollSep,N-S}, d_{CollSep,E-W}, Gr_{s,N-S}, Gr_{s,E-W}, Sl_{g,w}, Sl_{g,H})^T$, which varies from a lower x_i^L to an upper value x_i^U. The decision variables limits are presented in **Table 11**.

Table 11: Decision variables and their upper and lower limits

Variables	**Lower value (x_i^L)**	**Upper value (x_i^U)**
Collector Separation distance North-South, $d_{CollSep,N-S}$ (m)	8	20
Collector Separation distance East-West, $d_{CollSep,E-W}$ (m)	8	20
Ground Slope North-South, $Gr_{s,N-S}$ (deg)	0	90
Ground Slope East-West, $Gr_{s,E-W}$ (deg)	0	90
Slot Gap Width, $Sl_{g,W}$ (m)	0.5	3.5
Slot Gap Height, $Sl_{g,H}$ (m)	0.5	3.5

3.2.3. Decision-making process

TOPSIS method was used for the first time by Hwang and Yoon [310]**,** which was introduced to select a single solution among the optimal solutions provided by the Pareto Frontier. TOPSIS selects the final optimum as the closest alternative to the ideal point and farthest from the negative ideal point considering their geometric distance [311]. The positive ideal point is an unrealistic solution which enhances simultaneously all the examined criteria. Whereas, the negative ideal point is a solution that worsens simultaneously all the examined criteria. The best design is marked by its closeness to the ideal point and by its farness to the non-ideal solution at the same time. This approach is carried out based on the following steps [312]:

- Firstly, create an evaluation matrix by putting the evaluation criteria in a vertical form and the design options in a horizontal form $(D_1, D_2, D_3, \dots, D_m)$. The objective functions values are symbolized as $(C_1, C_2, C_3, \dots, C_n)$:

$$\begin{array}{cccccc} & C_1 & C_2 & C_3 & \cdots & C_n \\ D_1 & x_{11} & x_{12} & x_{13} & & x_{1n} \\ D_2 & x_{21} & x_{22} & x_{23} & & x_{2n} \\ \\ \vdots & \cdots & \cdots & \cdots & \cdots & \cdots \\ D_m & x_{m1} & x_{m2} & x_{m3} & \cdots & x_{mn} \end{array} \quad \textbf{(29)}$$

- The second step consists on performing non-dimensionalization of objective functions values. This may be carried out by dividing the design options 'i' and the evaluation criteria 'j' by the norm of the vector. The mathematical expression of the non-dimensionalized objective can be defined as follows:

$$x_{ij}^{n} = \frac{x_{ij}}{\sqrt{\sum_{i=1}^{m}(x_{ij})^{2}}} \quad \textbf{(30)}$$

- The third step consists on multiplying the values of the matrix by the normalized weights considering their relative importance. The weighted normalized values are expressed as follows:

$$x_{ij}^{wn} = w_j x_{ij}^{n} \quad \textbf{(31)}$$

where the relative importance of the criterion 'j' is calculated by the index w_j.

- The following step consists on recognizing the positive and negative ideal points as follows:

$$A+ = \{a_1^+, a_2^+, \dots, a_n^+\} = \{best\ x_{i1}^{wn}, best\ x_{i2}^{wn}, \dots, best\ x_{in}^{wn}\}/i = 1 \dots m \quad \textbf{(32)}$$

$$A- = \{a_1^-, a_2^-, \dots, a_n^-\} = \{worst\ x_{i1}^{wn}, worst\ x_{i2}^{wn}, \dots, worst\ x_{in}^{wn}\}/\ i = 1 \dots m \quad \textbf{(33)}$$

- Then, it is necessary to calculate the Euclidean distance for each design options 'i' from the positive ideal point d+ and the negative ideal point d-:

$$d_i^+ = \sqrt{\sum_{j=1}^{n}\left(x_{ij}^{wn} - a_j^+\right)^2} \qquad i = 1 \dots m \quad \textbf{(34)}$$

$$d_i^- = \sqrt{\sum_{j=1}^{n}\left(x_{ij}^{wn} - a_j^-\right)^2} \qquad i = 1 \dots m \quad \textbf{(35)}$$

- Finally, the relative closeness (RC) for each design must be calculated as given by **Eq. 36** and the optimal solution corresponds to the design with the RC value closest to 1.

$$RC_i = \frac{d_i^-}{d_i^+ + d_i^-} \qquad i = 1 \dots m \quad \textbf{(36)}$$

The optimal solution corresponds to the design with the RC value closest to 1.

3.3. Examined Sites

The optimization approach introduced in the current work was applied for two geographical sites with distinct meteorological variables for comparison purposes. This will allow proving the validity and generalizability of the proposed methodology as well. These sites which are enjoying huge solar potential can host such CSP projects and are briefly discussed below.

- **Ouarzazate**

The average incident solar radiation in Morocco can reach 5.5 kWh/m²/day. The number of hours of sunshine in South regions exceed 3500 hours per year. Ouarzazate is located in the Moroccan Draâ-Tafilalet region. Ouarzazate climate is a hot desert climate, but it is not as hot and dry as the typical climate of the Saharan region. The continental influence makes the climate pre-Saharan. Ouarzazate is among the Moroccan cities which enjoys a very

high annual irradiation. In addition, in this city, a CSP project called "Noor Ouarzazate I" with a total installed capacity of 160 MW is currently operational.

- **Madrid**

Madrid is the capital of Spain. The meteorological data of Madrid shows that the climate is semi-arid Mediterranean. The continental influence appears in its winters, which are moderate, and in its snow, which is relatively occasional. The number of hours of sunshine in Madrid exceeds 2800 hours per year.

Geographical information concerning the two sites is furnished in **Table 12**.

Table 12: Geographic coordinates of each studied city

City	Latitude (°N)	Longitude (°W)	Altitude (m)
Ouarzazate	30° 55′ 23″	6° 54′ 15″	1140
Madrid	40° 26′ 00″	3° 41′ 00″	657

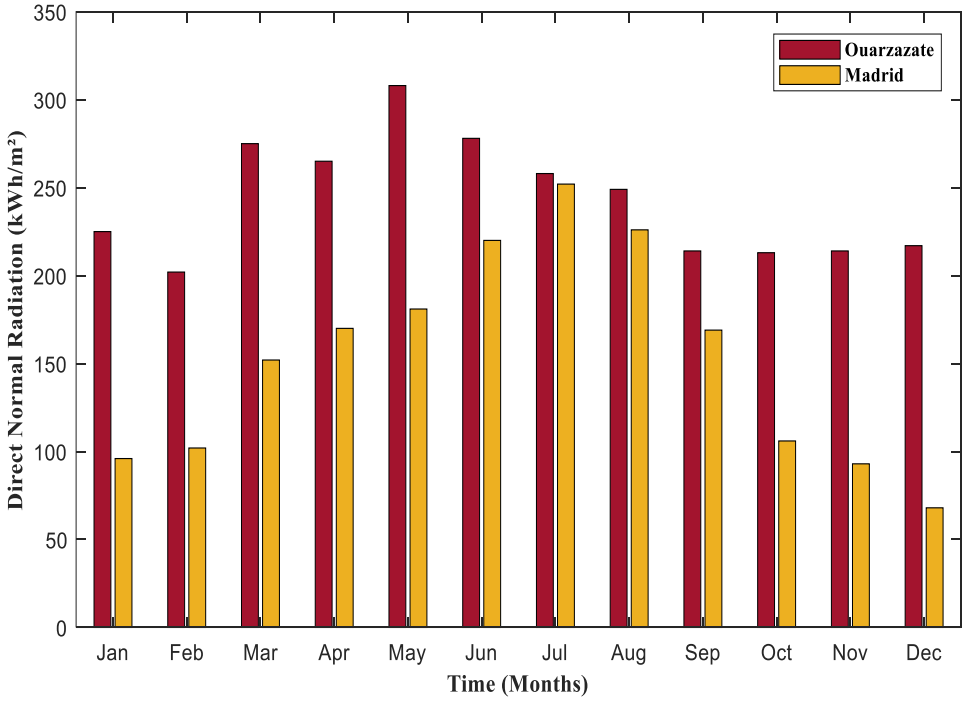
4. Results and discussions

This section of the chapter presents the main findings of the multi-objective optimization process. This section starts with an overview of the main climatic variables affecting the performance of the SDS plant. Then, the validity of the developed surrogate model is discussed. Resulting Pareto Fronts as obtained by the NSGA II are presented. Next, Final optimums based on the introduced decision-making method are identified. Sensitivity to economic variability of the unit improving cost and how it effects the final optimum in both implementation sites is finally elaborated.

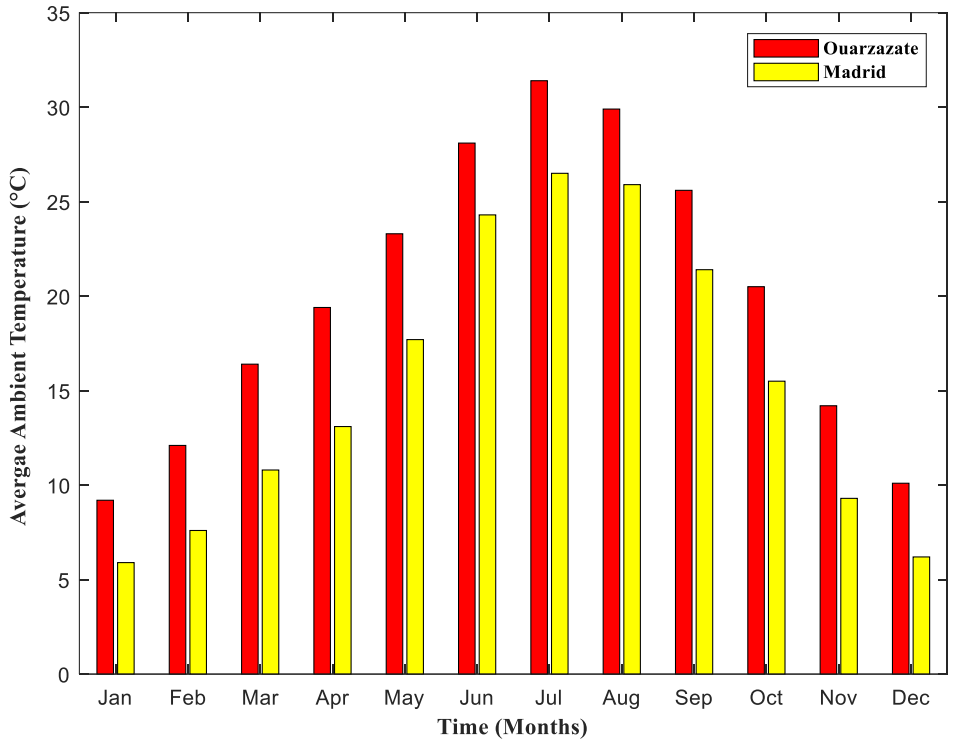
4.1. Weather data

Weather data has strong effect on the energy performance of any CSP power plant. The most influential climatic variables for the SDS technology are the solar direct irradiation, ambient temperature and wind speed. **Fig. 42** illustrates the variation of these parameters on a monthly basis for readability purposes. The adopted simulation process however, uses hourly variation of these parameters. It can be shown that:

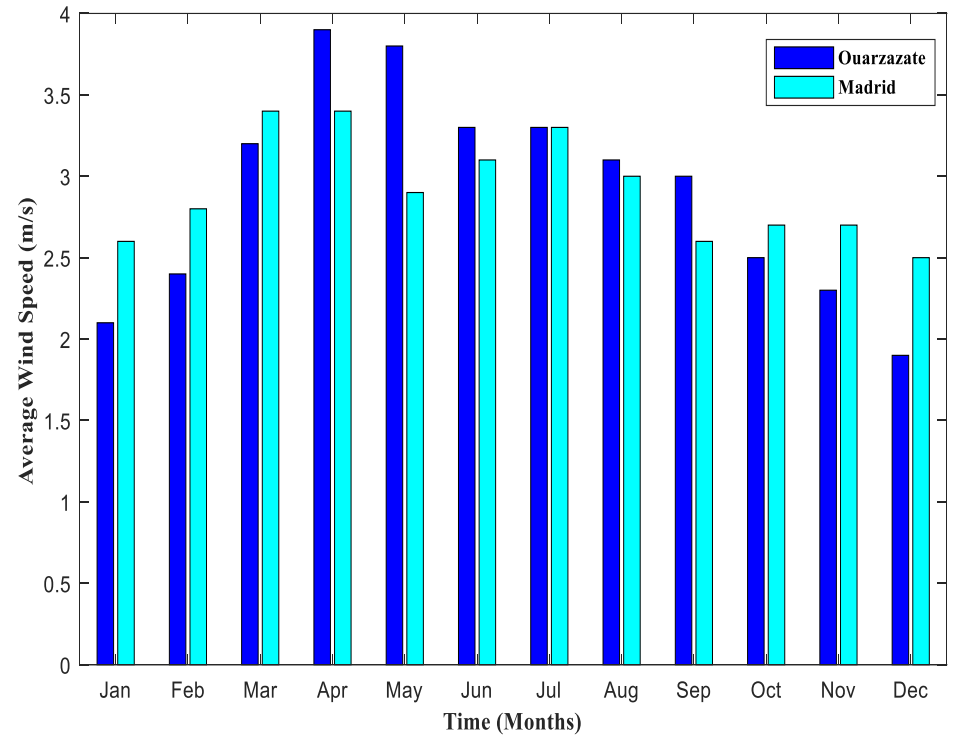
- The monthly average profile of the direct normal irradiation for each site is depicted in **Fig. 42 (a).** It is clearly observed that Ouarzazate city can receive a maximum monthly solar irradiation exceeding 300 kWh/m² for the month of May. However, in Madrid, a maximum value of the monthly direct normal irradiation (around 250 kWh/m^2) is observed for July.
- **Fig. 42 (b)** envisions the monthly average ambient temperatures in Ouarzazate for which the maximum value (about 33°C) is recorded in July. For Madrid, The maximum value average ambient temperature is about 27°C and also observed in July.
- **Fig. 42 (c)** displays the monthly average wind speed for the examined cities. A maximum value can reach over than (3.8 m/s) in Ouarzazate in the month of April and can exceed 3.4 m/s in Madrid during March and April.



(a)



(b)



(c)

Figure 42: Meteorological Data: **(a)** Direct Normal Irradiation; **(b)** Average Ambient Temperature; **(c)** Wind Velocity.

4.2. Surrogate Model and validation

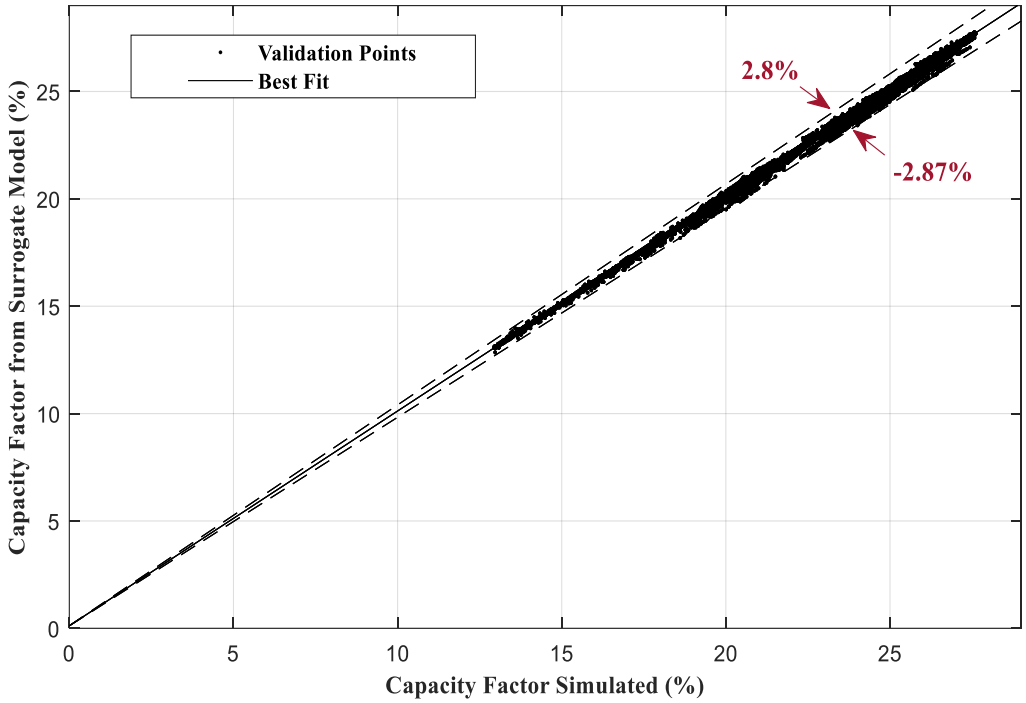
To establish the surrogate model describing the objective functions with sufficient accuracy, a performance map was generated through a parametric study. The decision variables were varied with an equally spaced value while respecting the limitations given in Table 5. The multiple case database was obtained by launching a total of 4096 simulations, considering all possible combinations of the decision-variables. For each design configuration, an estimation of the objective functions was obtained using SAM.

A third-order multiple non-linear regression was developed to determine a mathematical relationship between the involved variables and output. This adopted approximation offers significantly more accurate prediction compared to the extensively used multiple linear regression. The procedure of determining the adequate order of the polynomial equation considered starting with first and the second orders initially and observing the statistical metrics. Very satisfactory results were obtained for the third order model compared to the first and second order models. The coefficients of the third-order multiple non-linear regression were determined using MATLAB software. **Fig. 43** displays the estimated capacity factors using the proposed surrogate model versus the simulated capacity factors. As can be clearly seen, the surrogate model has the capability to approximate with high accuracy the real values of the Capacity Factor within an error range of ± 2.8% for Ouarzazate and not exceeding 4.02% for Madrid. This proves the suitability of the surrogate model to be further explored within the optimization process. Statistical indicators resulting from the comparison are given in **Table 13**. The viability of the surrogate model is illustrated because of R-square values which are equal to 0.995 and 0.9964 for Ouarzazate and Madrid, respectively.

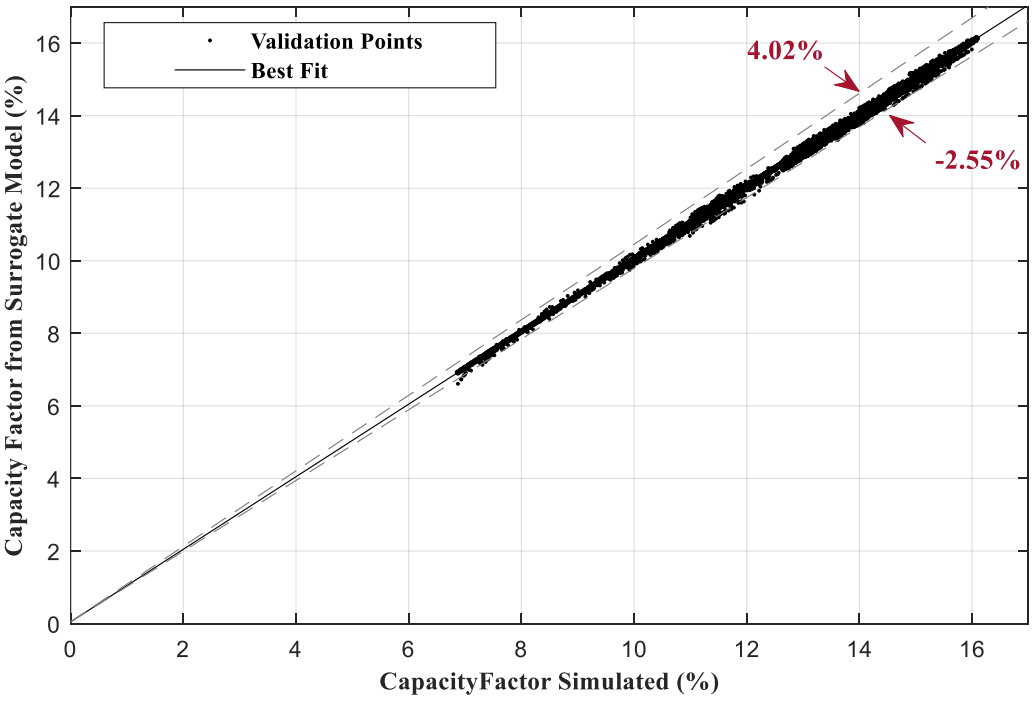
Table 13: Statistical indices resulting from the introduced surrogate model

	Ouarzazate	**Madrid**
R-Square	0.995	0.9964
RMSE	0.2047	0.1114
MAE	0.1652	0.0911

In order to further assert the validity of proposed surrogate model, an additional set of 700 cases randomly selected from a 6-D decision space, was evaluated. This sample of 700 cases were simulated using SAM software and the MATLAB surrogate model to perform the comparisons. The estimated Capacity Factor using the surrogate model and those obtained from SAM were in an excellent agreement.



(a) Ouarzazate



(b) Madrid

Figure 43 : Dispersion illustration of the proposed surrogate model for the SDS power plant.

4.3. Multi-objective optimization results

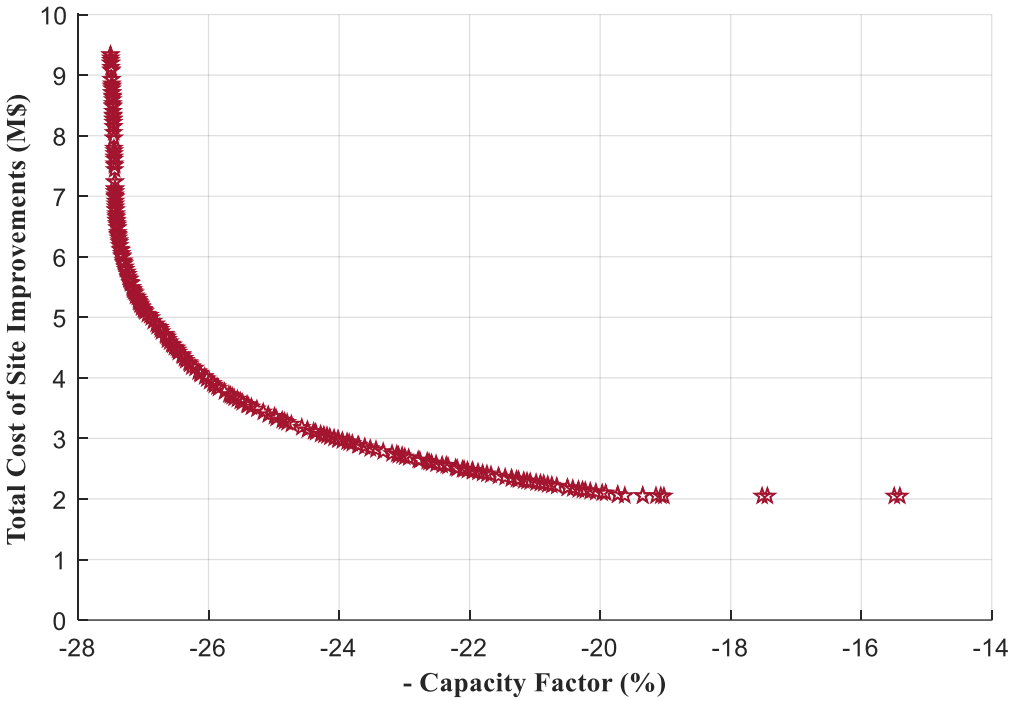
The optimization approach was carried out considering two objective functions: annual Capacity Factor (CF) and the Total Cost of Site Improvements (TCSI). The optimization problem is formulated as follows:

Minimize:
$$\begin{cases} \boldsymbol{F_1}(\overrightarrow{\boldsymbol{x}}) = \boldsymbol{TCSI}(\overrightarrow{\boldsymbol{x}}), \\ \boldsymbol{F_2}(\overrightarrow{\boldsymbol{x}}) = -\boldsymbol{CF}(\overrightarrow{\boldsymbol{x}}), \end{cases}$$

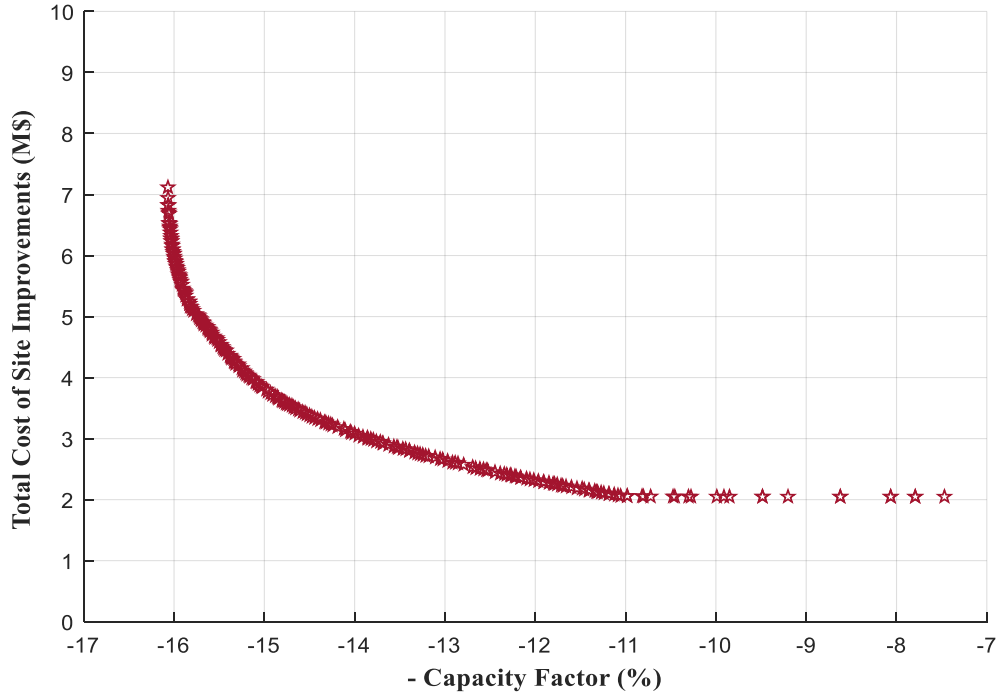
Subject to $x_i^L <= x_i <= x_i^U, \quad i = 1, 2, 3, 4, 5, 6.$

where F_1 and F_2 are the two objective functions and $\vec{x}$ is the vector of the decision variables $\vec{x} = (d_{CollSep,N-S}, d_{CollSep,E-W}, Gr_{s,N-S}, Gr_{s,E-W}, Sl_{g,w}, Sl_{g,H})^T$. It should be stressed that the approach used for the optimization is subjected only to variable constraints illustrated in Table 5, which makes the decision space limited by a lower and an upper values denoted x_i^L and x_i^U, respectively.

Genetic algorithm parametrization and implementation was performed in MATLAB. When the number of decision variables is less than 5, the adequate population size is about 50. Otherwise, it is more appropriate to set the population size at 200 with a value of Pareto fraction of 0.35. Several optimizations have been established for different population sizes and Pareto fractions. The retained population size is 250 with a Pareto fraction equal to 1 since it has the potential to keep the calculation time reasonable with marginal sensitivity of the results. **Fig. 44** depicts the Pareto Frontier obtained for the examined solar dish Stirling power plant in terms of the two objectives functions at the studied locations. It highlights the trade-off between the Capacity Factor (CF) and the Total Cost of Site Improvements (TCSI). The increase in the Capacity Factor results in an increment of the Total Cost of Site Improvements principally because avoiding the shading effects requires additional area in the solar field making its financial contribution higher. In the case of Ouarzazate, the Capacity Factor ranges from around 15.5% to 27.5% while the Total Cost of Site Improvements varies from 2 M$ to 9.5 M$. For Madrid city, the variation ranges of the Capacity Factor and Total Cost of Site Improvements are 7.5% - 16% and 2 M$ - 7.5 M$, respectively. For both sites, one can observe the compromise zones between energy and economic objectives. As such, the Pareto Front is an efficient tool to assist the decision-maker in selecting the best configuration depending on the considered preferences. A single solution could be drawn from among the set of suggested optimal solutions (250 solutions) based on the proposed decision-making method as will be discussed in what follows.



(a) Ouarzazate



(b) Madrid

Figure 44: Two objective Pareto Frontiers for the studied locations.

4.4. Final optimal solution through decision making method

The final optimal solution derived from the decision-making approach is highlighted in **Table 14** and **Table 15** for Ouarzazate and Madrid, respectively. The optimal solution is presented along with the corresponding design variables and the values of each objective function. The design variables should be adjusted as highlighted in Line 99 for Ouarzazate (**Table 14**) and in Line 168 for Madrid (**Table 15**). These lines coincide with the highest values of the relative closeness (RC) introduced as recommended by the TOPSIS method. It should be noted that Capacity Factors for optimum scenarios are 22.99% and 12.91% for Ouarzazate and Madrid, respectively. The corresponding values of the Total Cost of Site Improvements ensuring the best trade-offs between two conflicting criteria are 2.69 M$ and 2.60 M$ for Ouarzazate and Madrid, respectively.

Table 14: Optimal solutions derived using TOPSIS method for Ouarzazate city

	$d_{CollSep,E-W}$ (m)	$d_{CollSep,N-S}$ (m)	$Gr_{s,E-W}$ (deg)	$Gr_{s,N-S}$ (deg)	$Sl_{g,H}$ (m)	$Sl_{g,w}$ (m)	- CF (%)	TCSI (M$)	RC
1	17.5510	8.1850	4.1288	83.4193	3.4651	3.4870	-26.5945	4.5970	0.5069
2	10.2720	8.0440	5.3393	82.4412	3.4564	3.4884	-22.7874	2.6441	0.7514
3	19.9652	9.9374	3.9965	83.4524	3.4669	3.4827	-27.3833	6.3489	0.3749
4	19.9571	9.2929	4.1909	83.1044	3.4868	3.4796	-27.3017	5.9347	0.3916
5	19.9738	9.5816	3.8493	83.0950	3.4642	3.4849	-27.3478	6.1242	0.3831
6	19.9236	14.6428	3.2941	33.7034	3.4291	3.4948	-27.5006	9.3356	0.3751
7	8.5994	8.0362	5.2481	82.3808	3.4596	3.4792	-20.6644	2.2114	0.7208
8	19.9567	9.2172	4.0406	83.1705	3.4709	3.4820	-27.2915	5.8862	0.3942
9	8.0000	8.0000	1.2520	1.3661	3.0002	3.5000	-15.4077	2.0480	0.5947
10	19.9694	9.8055	3.9255	82.7056	3.4695	3.4803	-27.3673	6.2659	0.3776
11	14.3257	8.0625	4.7869	82.9834	3.4618	3.4795	-25.6368	3.6960	0.6382
. . .									

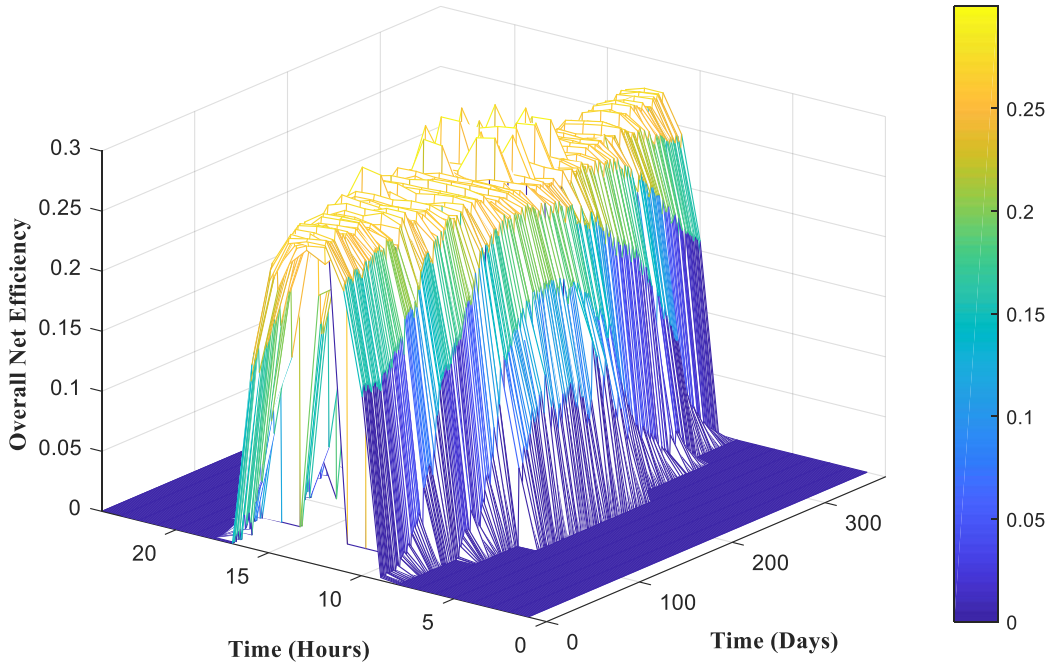
.									
55	19.9563	13.6406	3.2742	46.9781	3.4740	3.4936	-27.4773	8.7109	0.3680
. . .									
98	15.9286	8.0451	4.1586	82.5728	3.4564	3.4913	-26.1584	4.1007	0.5756
99	**10.4738**	**8.0404**	**4.9245**	**82.6971**	**3.4536**	**3.4737**	**-22.9926**	**2.6948**	**0.7514**
100	9.8294	8.0810	4.8693	82.9065	3.4678	3.4945	-22.3308	2.5418	0.7482
. . .									
249	17.4559	8.0691	4.1940	82.9609	3.4626	3.4849	-26.5224	4.5073	0.5183
250	18.6345	8.2025	4.0231	83.2238	3.4727	3.4861	-26.8026	4.8912	0.4725

Table 15: Optimal solutions derived using TOPSIS method for Madrid city

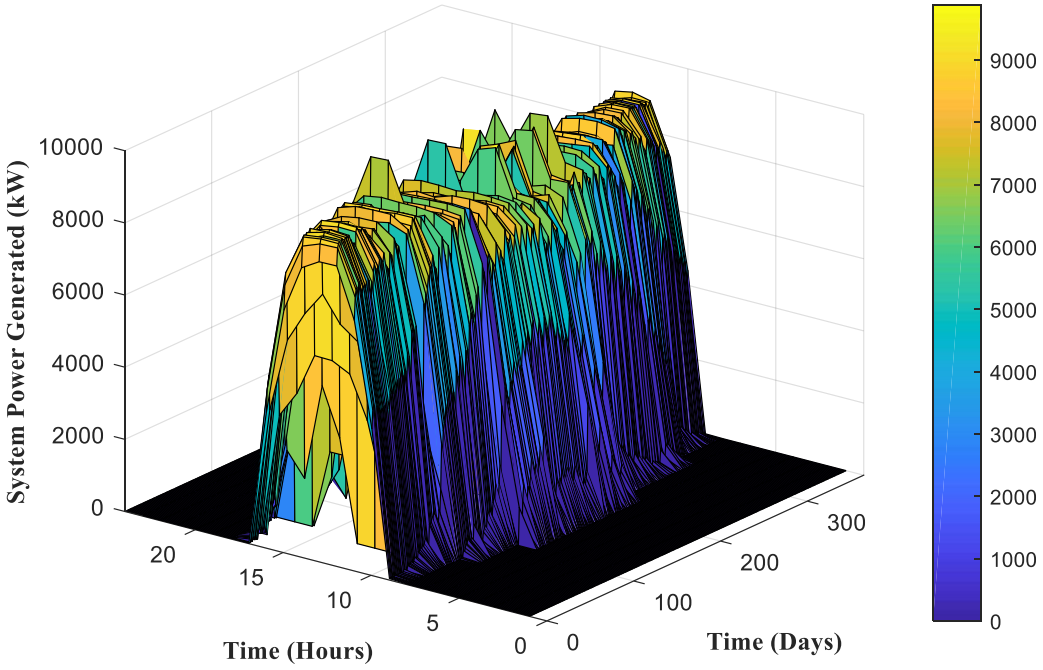
	$d_{CollSep,E-W}$ (m)	$d_{CollSep,N-S}$ (m)	$Gr_{s,E-W}$ (deg)	$Gr_{s,N-S}$ (deg)	$Sl_{g,H}$ (m)	$Sl_{g,w}$ (m)	- CF (%)	TCSI (M$)	RC
1	8.0002	8.0072	10.0380	68.3734	3.0150	2.5807	-10.3035	2.0499	0.6202
2	15.5404	8.0739	3.7087	85.7255	3.4668	3.4766	-15.1658	4.0151	0.5381
3	8.0002	8.0001	5.9566	7.1115	2.3026	2.0190	-7.7925	2.0481	0.5207
4	8.3427	8.0243	20.7271	81.0393	3.4484	3.4203	-11.3418	2.1422	0.6669
5	8.0000	8.0000	0.1875	2.3622	2.6563	1.8438	-7.4690	2.0480	0.5109
6	15.3230	8.1093	3.5400	85.2192	3.4804	3.4702	-15.1259	3.9763	0.5428
7	19.9851	9.0646	3.2925	85.4418	3.4909	3.4792	-15.9654	5.7970	0.4198
8	9.0879	8.0174	10.9885	83.1891	3.4701	3.4850	-12.0591	2.3315	0.6909
9	17.7915	8.1106	4.0372	85.6521	3.4773	3.4883	-15.5196	4.6176	0.4748
10	8.4382	8.0202	13.8556	83.3686	3.4222	3.4760	-11.4579	2.1657	0.6715
11	19.9773	9.5388	2.7947	85.8656	3.4797	3.4859	-16.0163	6.0979	0.4144
. . .									
55	16.1769	8.1444	3.8825	85.0956	3.4767	3.4847	-15.2884	4.2160	0.5135
. . .									

167	12.6276	8.0349	7.4397	85.4368	3.4713	3.4740	-14.2903	3.2468	0.6495
168	**10.1437**	**8.0316**	**9.5704**	**85.6786**	**3.4652**	**3.4609**	**-12.9170**	**2.6071**	**0.7067**
169	14.0689	8.0558	5.1016	85.5011	3.4886	3.4853	-14.8082	3.6268	0.5922
. . .									
249	8.1545	8.0194	19.6158	83.1275	3.4260	3.4462	-11.1826	2.0926	0.6621
250	8.0282	8.0164	12.6874	82.9013	3.4295	3.3486	-10.9825	2.0594	0.6539

Based on the design specifications retained in the framework of the conducted multi-objective optimization, the net power generated of the optimized solar power plant along with the overall net efficiency are illustrated in a 3-D visualization as exhibited in **Fig. 45** and **Fig. 46**. For Ouarzazate city, the overall net efficiency and the annual power generated attain a maximum value of about 28% and 9000 kW, respectively whereas the annual net efficiency reaches a maximum value of about 26% when the annual power generated exceeds slightly 8000 kW in Madrid.

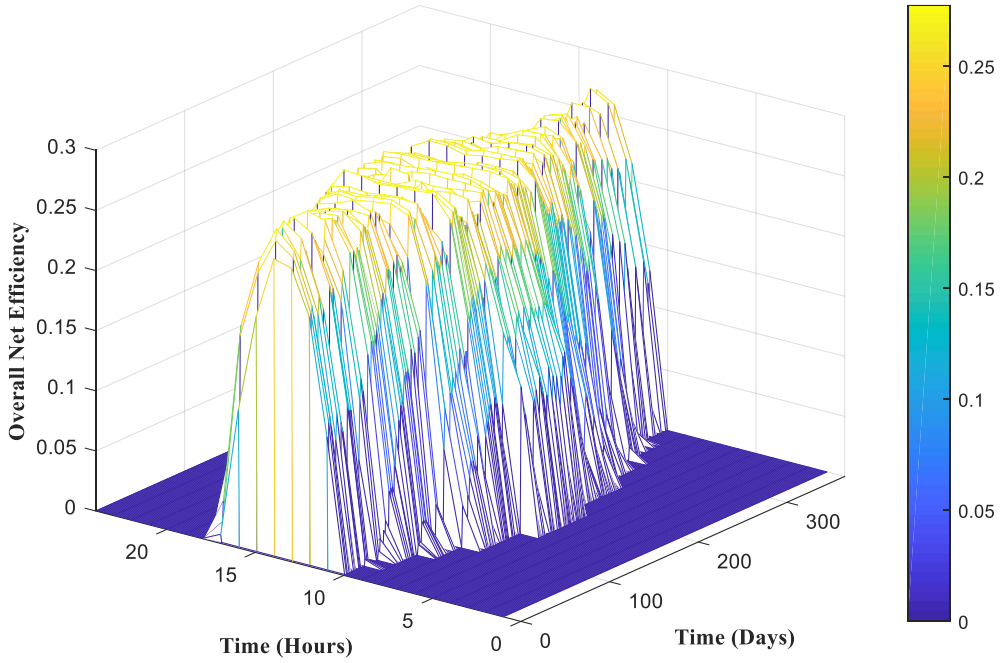


(a) Overall Net Efficiency

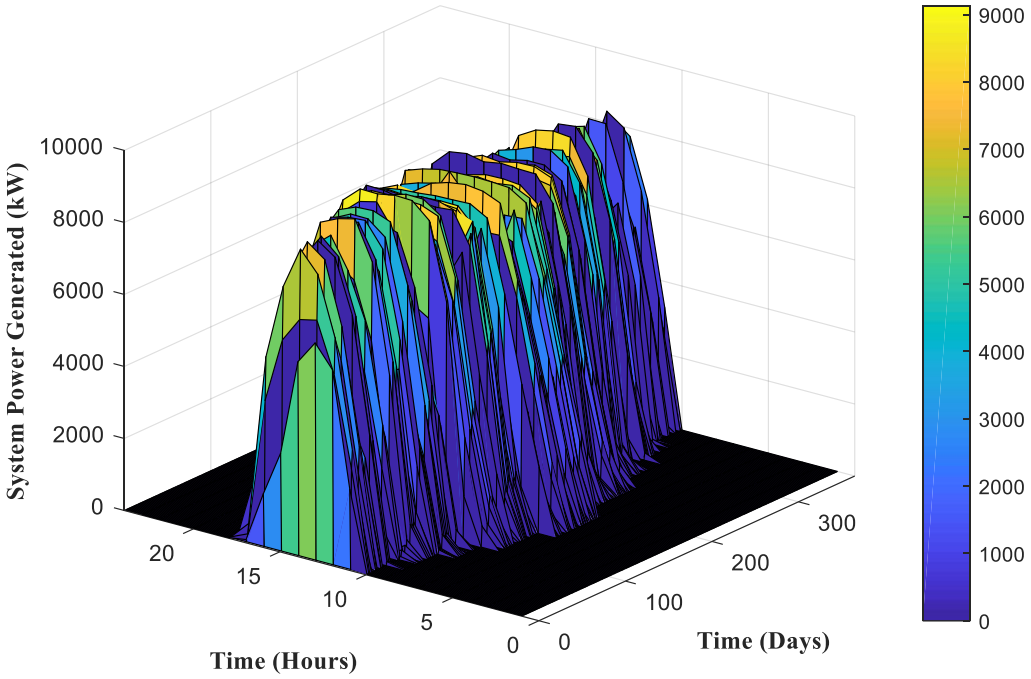


(b) Annual Power Generated

Figure 45: Overall net efficiency and annual power generated using the optimal parameters derived from the optimization approach for Ouarzazate



(a) Overall Net Efficiency



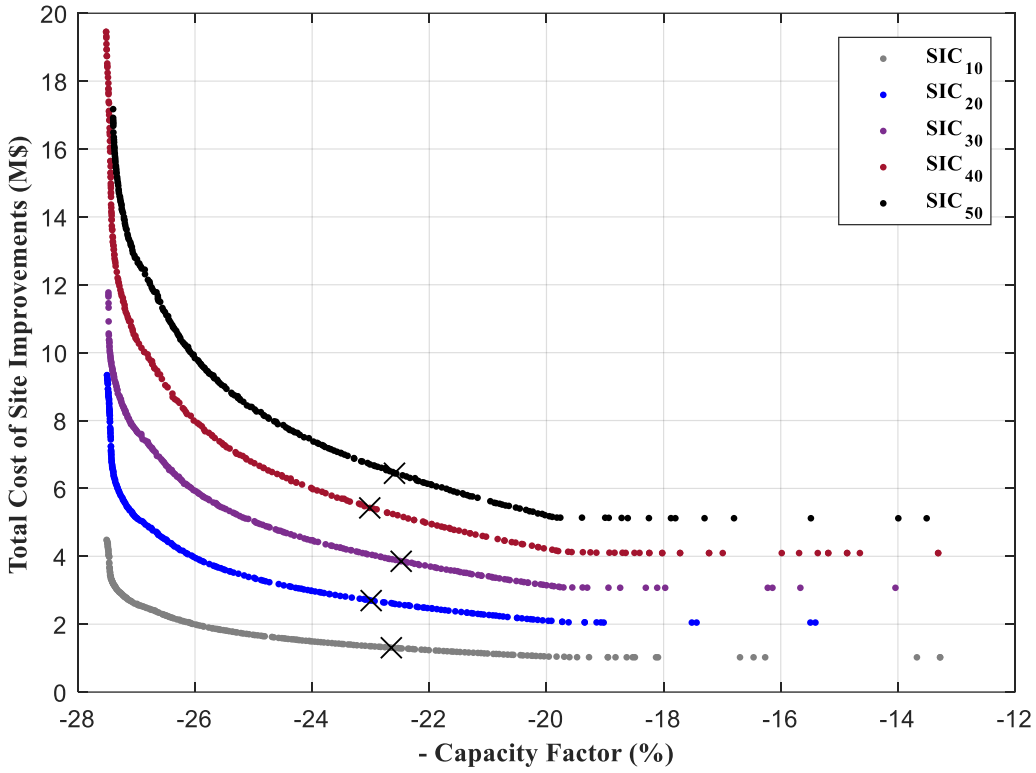
(b) Annual Power Generated

Figure 46: Overall net efficiency and annual power generated using the optimal parameters derived from the optimization approach for Madrid.

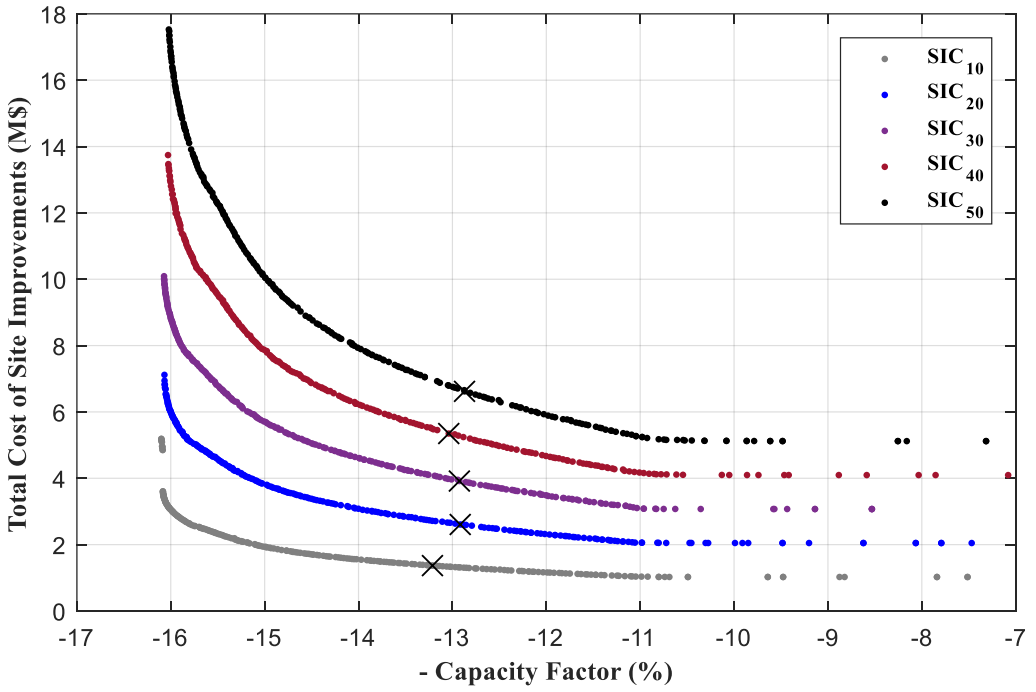
4.5. Sensitivity analyses

Since cost figures are subjected to fluctuations in the future, it is of interest to conduct sensitivity analyses to evidence how specific costs affect the optimum design of the SDS power plant. The investigated sensitivity analyses considers varying the specific Cost (per m^2) of Site Improvements in the range of 10 \$/m² - 50 \$/m².

Pareto Frontiers derived from the objective optimization process considering the variation of the Site Improvement Costs (SIC) for both sites are depicted in **Fig. 47**. These results present the trade-off between the two objective functions for the five costs scenarios. The final optimal solution derived from the decision-making approach is marked for each cost scenario. Detailed results are given in **Table 16** and **Table 17** including the design variables as well as the objective functions for Ouarzazate and Madrid, respectively. The Total Cost of Site Improvements for the final optimum design increases significantly with the augmentation of the specific site cost. However, the Capacity Factor values show only marginal fluctuations at the examined range.



(a) Ouarzazate



(b) Madrid

Figure 47: Two objective Pareto Frontier derived from the optimization process considering the variation of Site Improvement Cost for each site. Final optimal solutions selected by TOPSIS method are marked.

Table 16: Detailed results of the parametrical scenario derived using TOPSIS method showing the optimal decision variables in the case of Ouarzazate city.

	$d_{CollSep,E-W}$ (m)	$d_{CollSep,N-S}$ (m)	$Gr_{s,E-W}$ (deg)	$Gr_{s,N-S}$ (deg)	$Sl_{g,H}$ (m)	$Sl_{g,w}$ (m)	- CF (%)	TCSI (M$)	RC
10	10.1710	8.0268	7.8587	80.8639	3.4777	3.4936	22.6484	1.3063	0.7446
20	10.4738	8.0404	4.9245	82.6971	3.4536	3.4737	22.9926	2.6948	0.7514
30	10.0093	8.0200	6.3042	81.4710	3.4850	3.4907	22.4800	3.8532	0.7252
40	10.5233	8.0565	6.8364	81.9315	3.4088	3.4680	23.0165	5.4260	0.7621
50	10.0519	8.0172	9.2021	84.8151	3.4892	3.4884	22.5942	6.4471	0.7251

Table 17 : Detailed results of the parametrical scenario derived using TOPSIS method showing the optimal decision variables in the case of Madrid city.

	$d_{CollSep,E-W}$ (m)	$d_{CollSep,N-S}$ (m)	$Gr_{s,E-W}$ (deg)	$Gr_{s,N-S}$ (deg)	$Sl_{g,H}$ (m)	$Sl_{g,w}$ (m)	- CF (%)	TCSI (M$)	RC
10	10.6623	8.0185	8.6053	81.1033	3.4891	3.4817	13.2127	1.3679	0.7295
20	10.1437	8.0316	9.5704	85.6786	3.4652	3.4609	12.9170	2.6071	0.7067
30	10.1688	8.0241	6.3837	84.9318	3.4681	3.4850	12.9260	3.9166	0.6907
40	10.4302	8.0131	7.5603	79.7091	3.4778	3.4953	13.0391	5.3490	0.7108
50	10.2626	8.0635	7.6193	76.6057	3.4376	3.4535	12.8711	6.6202	0.7087

5. Summary

Optimizing the design of SDS power plant represents a vital requirement to ensure the highest energy and economic performances. The current paper developed a multi-objective optimization framework for adjusting key geometrical design specifics of a 10 MW SDS power plant located in two different geographical sites, namely Ouarzazate (Morocco) and Madrid (Spain). Two energy and economic conflicting objective functions were considered with the ultimate goal to maximize of the annual Capacity Factor and minimize Total Cost of Site Improvements simultaneously. Pareto Frontiers were determined based on the Genetic Algorithm and final optimum solutions were derived from the TOPSIS method. The following conclusions can be made:

- The viability of the surrogate model in describing the objective functions was demonstrated via the high approximation of the real CF values with errors lower than 4.02% for Madrid and in the range of ± 2.8% for Ouarzazate. In addition, the high R-square values derived from the proposed surrogate model were found to be 0.995 for Ouarzazate and 0.9964 for Madrid.

- The obtained Pareto Frontiers represented the trade-off between the objective functions where the variation range of the Capacity Factor and the Total Cost of Site Improvements were 15.5% - 27.5% and 2 M$ - 9.5 M$, for Ouarzazate, respectively. In the case of Madrid city, the Capacity Factor and Total Cost of Site Improvements ranged from 7.5% to 16% and 2 M$ and 7.5 M$, respectively.
- Final optimal solutions retained using the TOPSIS method coincide with a Capacity Factor values of 22.99% and 12.91% and a Total Cost of Site Improvements of 2.69 M$ and 2.60 M$ for Ouarzazate and Madrid, respectively.
- The design specifications derived from the studied optimization approach allowed for a maximum value of about 28% and 26% in the overall net efficiency along with a value of about 9000 kW and 8000 kW for the power generated for Ouarzazate and Madrid, respectively.
- The sensitivity analysis reveals that the increment of the specific Site Improvement Cost (SIC) significantly increases the Total Cost of Site Improvements but has shown only marginal effect on the optimum capacity factor.

CHAPTER V. Hybrid Renewable Energy System for sustainable residential buildings based Solar Dish Stirling and Wind Turbine with hydrogen production

1. Introduction

Building energy systems are transitioning from a single form of conventional energy to a multi-energy system, typically renewable energy sources. In this chapter, a techno-economic analysis is conducted to determine the viability of a Hybrid Renewable Energy System (HRES) to meet the electric demand in residential buildings belonging to two geographical sites with distinct climatic variables. For the first time, Solar Dish Stirling (SDS) and Wind Turbine (WT) along with the power-to-hydrogen concept are hybridized as dual-power sources in HRES. SDS technology is rarely combined with wind turbines in previous HRES studies despite its promising potential as a sustainable and efficient power generation technique. Furthermore, for more accurate results, a new comprehensive process of sizing HRES adapted to residential applications based on the synergic interaction between dynamic building simulation and HRES optimization is given. In fact, most previous researchers use built-in or synthetic electric loads without showing enough information on building specifics, construction and site-operation that in reality vary significantly depending on the case study and location. Considering Net Present Cost (NPC), Levelized Cost of Energy (LCOE), and Levelized Cost of Hydrogen (LCOH) as performance metrics while investigating the power-to-hydrogen concept within the created HRES is another key element in this work.

2. Background

Recently, the global energy demand is booming proportionally with the remarkable growth of the world population, the rate of urbanization and industrialization, the evolution of transportation devices as well as the improvement in the standard of living [313]. The increase in energy consumption is generally accompanied by the exploitation of conventional energy sources which results in critical environmental issues. Currently, traditional fossil fuels are responsible for about 80% of the primary energy [314]. In 2019, coal and oil are reported as the two largest sources of power production worldwide [315] (**Fig. 48**). In China, the energy generation sector is responsible for practically 90% of the GHG emissions [316]. **Fig. 49** depicts the amount of the emitted GHG caused by fossil combustion according to four

selected economies worldwide. The greenhouse gas emissions derived from fuel combustion attained 10 Gt CO_2-eq and 4.8 Gt CO_2-eq in China and United States, respectively [317].

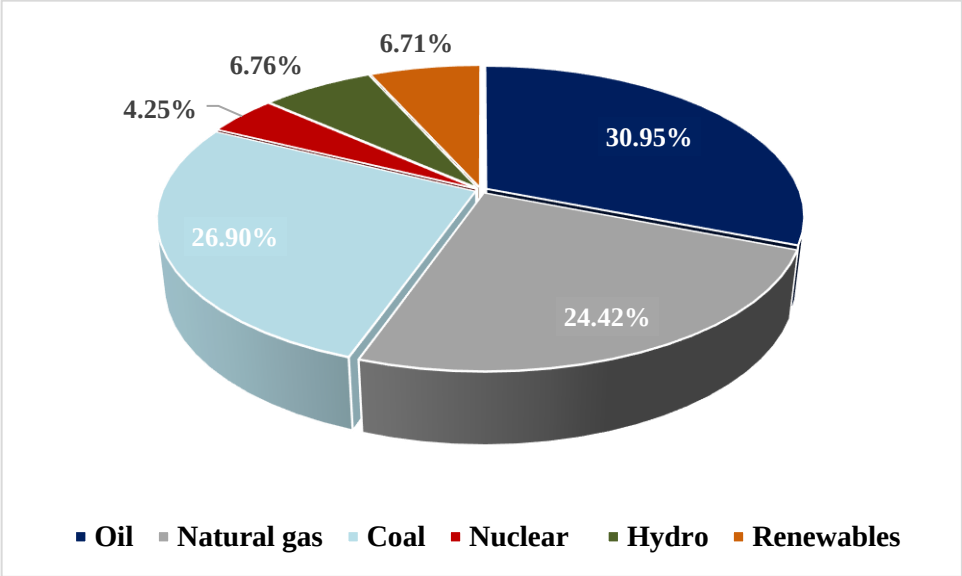


Figure 48: World global primary energy consumption by source in 2021 [318]

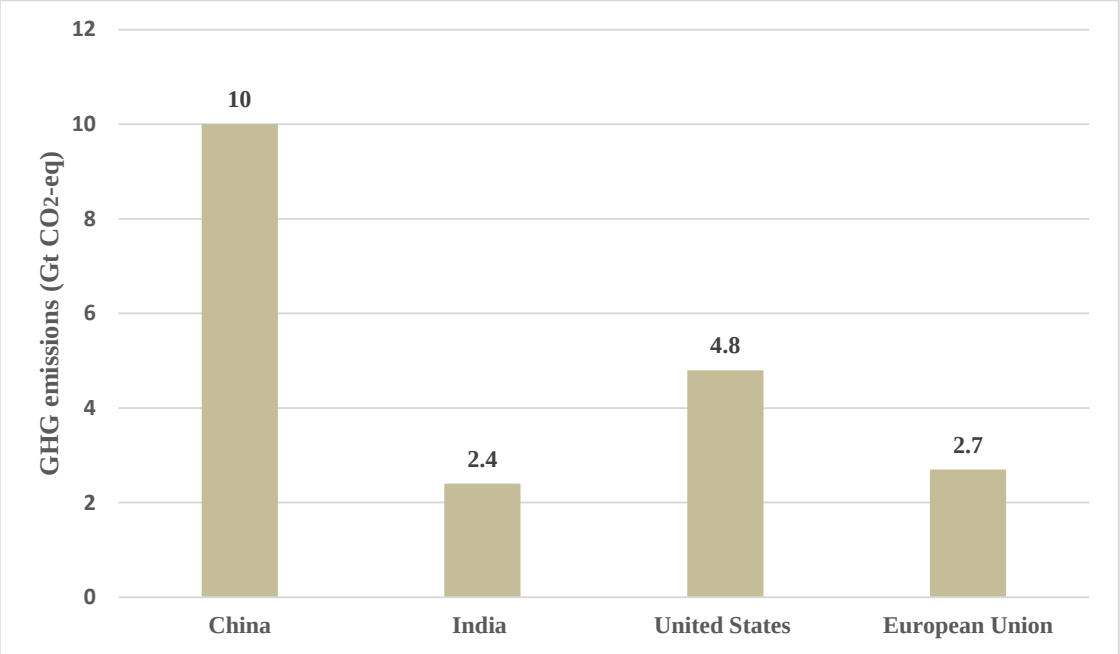


Figure 49: GHG emissions from fuel combustion in selected economies in 2019 [317]

In the current context, the building sector accounts for nearly one-third of the global final energy consumption [319]. It is should be mentioned that this sector is responsible for almost 28% of the energy-related carbon dioxide CO_2 emissions, and about two-thirds of which is associated with emissions from electricity consumption [320]. The energy demand in the building sector could rise by around 50% in 2060 due to the fast increase in global purchasing power [321]. Enhancing the energy efficiency of the building is among the suitable options to

confront climate change issues and reduce the proportions of energy consumption in this sector [322]. In response to the various gaps mentioned before, great interest has been devoted to advancing the concept of Net Zero Energy Building (NZEB) as a promising alternative in managing the building energy demand and stimulating the global prospect of decarbonisation [323]. The NZEB aims can be achieved primarily by incorporating renewables and by applying efficiency measures and approaches to match loads and reduce the overall energy demand of buildings [324]. Several studies reviewed the various development strategies, research applications, recent advances, and progression of NZEB in order to furnish valuable support that can assist stakeholders with its integration in a rational way [325]. Therefore, interest has been devoted to assessing the various renewable energy technologies [326], developed passive designs [327], storage options [328], and their implementations in NZEB considering energetic, exergetic and economic and environmental criteria [329], [330]. Extensive investigations and multi-criteria optimization assessments were carried out to address the promising alternatives leading to net-zero buildings purposes [331]. Accordingly, The application of multi-objective optimization approaches has proven its potential in selecting the optimal key design parameters for NZEB [332], [333].

Renewable energy systems have exhibited great potential in supplying clean and sustainable energy to meet the current demand for electricity in large and small-scale buildings [334].the In UK, renewables-based power generation was able to produce about 30% of the global electricity in the period between April and June 2017 [335]. In 2020, 29% of the global electricity generation has been covered by renewable energy systems. Nevertheless, to attain the objectives of the Net Zero Emissions Scenario, the annual generation based on renewables must increase by an average of about 12% in the period between 2021 and 2030 [336].

The main renewable sources used in electrical power generation, residential buildings and microgrids are solar, wind, biomass, geothermal and hydrogen. However, solar and wind are considered among the most common and promising resources for power generation due to their emission-free and inexhaustibility [177]. Nevertheless, renewables are intermittent, not continuously available and remarkably influenced by meteorological and environmental conditions [337]. Thus, a system based single energy source has constraint to offer energy autonomy throughout the year [338]. For this reason, Hybrid Renewable Energy Systems (HRES) have drawn great attention and were recommended as one of the most promising alternatives in filling the aforementioned gaps. Some constructive studies were established in order to review the existing HRES [339], the related optimization techniques used for

designing and sizing [340]–[342], their integration for off-grid electrification and other multi-end usages [343]–[346] as well as future research directions and perspectives for further implementation [347], [348]. In addition, many works shed light on the optimization of the HRES in order to address the appropriate configuration for various case studies and scenarios. In general, hybrid renewable energy systems based on PV technology and wind turbine were widely recommended to cover the electrical demand for residential buildings. Ma et al. [349] assessed the performances of a hybrid renewable energy system based on PV and wind power technologies designed to meet the heat and power requirements of a residential buildings community in seven Chinese cities. The evaluation was carried out considering technical, economic and environmental aspects. It was concluded that the hybrid proposed system is cost-effective and was able to cover energy requirements and mitigate a great amount of the related CO_2 emissions. Similarly, Krishan and Suhag [350] validated the effectiveness of the hybrid renewable system based on wind power/ PV and battery storage. It was found that the system is cost-effective and can meet the electric demand of a poor community in India. A study of the techno-economic potential of a hybrid renewable energy system (HRES) based microgrid was conducted to deal with a real case of a large scale residential community in Beijing [351]. The HRES system can cover more than 90% of the required electricity by exploiting a rate of renewable sources ranging between 47 and 100%. The overall eco-environmental benefits could be significantly improved if the main energy source adopted in the HRES is wind power combined with an appropriate size and capacity of PV and batteries. Liu et al. [352] conducted a multi-criteria optimization to assess the techno-economic potential of a hybrid renewable energy system for residential buildings in Hong Kong. Several case studies were performed and findings highlighted that 81.29% of the annual load can be met with the optimum configuration encompassing PV/WT and battery at a LCOE of around 0.2230 $/kWh. Das et al. [353] studied the technical and economic feasibility of a stand-alone HRES designed to meet the thermal and electricity demand of a remote community in Broome. It is expected that the electricity demand will be satisfied by the HRES; which mainly consists of PV modules, wind turbine and battery. Then, the excess energy will be exploited via a thermal load controller to meet the thermal energy demand. Various case scenarios were analyzed and compared to select the optimal configuration considering energetic, economic and environmental indicators. The energy excess from the optimized configuration PV/ WT/ battery and thermal load controller can cover 31% of the overall thermal load at the lowest COE of 0.255 $/kWh. Moreover, attention has been also paid to hybridization with other types of power generation resources. Li et al.[354] established a

comparative assessment of various HRESs that can be implemented in residential net-zero energy buildings. Twelve combination systems were evaluated based on energetic and economic indicators to select the suitable hybrid system for residential net-zero energy building. Findings point out that the system combination of 8.4 m² PV and heat insulation solar glass can ensure a high primary energy saving ratio with a reduced LCOE of about 5920 $/ year. It was also deduced that the optimized hybrid system consisting of solar thermal, PV and insulation solar glass is highly recommended to attain net-zero energy aims. Ashrafi Goudarzi et al. [355] carried out a performance assessment of a HRES designed to meet the energy requirements of a residential building in Iran via solar and wind systems. The evaluation involved the comparison of the suggested hybrid system with the diesel system considering technical and economic indicators. Results confirm that the hybrid system is cost effective and show great potential in mitigating GHG emissions. Ghenai et al. [356] conducted an optimization study of an off grid hybrid renewable energy system by combining PV and Fuel Cell technology. Technical and economic metrics were considered to unveil the potential of such configuration in meeting the electric load of 150 houses located in the desert region. The total power generated from PV and fuel cell were found at 52% and 48%, respectively. Overall, it is deduced that the proposed system is eco-friendly and can offer a high renewable fraction of 40.2%. at a LCOE of 145 $/MWh. Kumar et al. [357] performed the technical and economical performances of a grid independent based hybrid renewable energy microgrid for a remote community in India. The analysis assessed the hybridization of PV technology, Wind Turbine (WT), Diesel Generator (DG) and a storage battery. It was found that the combination set of PV, WT and battery energy storage system can guarantee high energetic and economic performances can extremely contribute to attain sustainable development targets scenario. Singh et al. [358] carried out an optimization assessment using HOMER software and applied a decision making approach to identify the appropriate hybrid renewable system based microgrid for supplying electricity in rural Indian areas. Results proved that the configuration composed of PV/Diesel generator/Battery/Fuel Cell/WT and converter offers the best scenario for electrification. Shboul et al. [171] revealed the competitivity of the hybrid system composed of SD/WT and battery bank against the conventional hybrid systems which usually encompass the PV/WT and battery. Accordingly, technical and economic analysis has been performed at the level of each component to select the optimal operational configuration in Madaba and Mafraq, Jordan. The peak power produced by the studied hybrid system attained 1500 kWe in summer periods for both

locations. The range of the LCOE is observed 0.1307 $/kWh - 0.1361 $/kWh and 0.1307 $/kWh – 0.1483 $/kWh for Madaba and Mafraq, respectively.

Furthermore, many works shed light on hybridization based renewable energy sources for multi-generation. In particular, HRES will generate both electricity and hydrogen either for meeting the required electric and hydrogen loads or exploiting the excess of the generated electricity to produce hydrogen which can be stored or directly used. Nowadays, hydrogen is among the most abundant chemical elements in the universe. When produced by renewable sources, hydrogen can serve as green electricity using fuel cells. Duman and Güler [359] assessed the feasibility of a hybrid system based on PV technology combined with fuel cells and wind technology to cover the energy demand of off-grid vacation homes. The hybrid system was analyzed from technical and economic aspects and performed under meteorological conditions of Izmir for both seasonal and regular occupancy scenarios. Findings highlighted that the resulting LCOE was found to be superior to that provided by grid electricity. Storage options based on battery and hydrogen were economically compared and priority was dedicated to storage with battery. Kalinci et al. [360] established a techno-economic evaluation of an off-grid HRES which uses hydrogen as a storage option. It has been deduced that the optimum configuration of the hybrid system encompassing WT (E33*2) combined with a PV array system of 300 kW, fuel cell with a capacity of 100 kW, 150 kW converter, 200 kW electrolyzer and Hydrogen tank of 400 kg, was able to meet a primary load of 1875 kWh/day at a competitive COE of 0.83 $/kWh. Al-Sharafi et al. [361] carried out the technical and economical performances of a stand-alone HRES powered by solar and wind resources for power and hydrogen production at various sites in Saudi Arabia. It turned out that the minimum LCOE of 0.609 $/kW was achieved at the Yanbu location with the optimum configuration encompassing a 2 kW PV array, 3 wind turbines, 2 kW converter and 7 batteries storage bank. In Abha, the optimum configuration based on PV/Wind and Fuel Cell leads to a LCOE and LCOH of 1.208 $/kWh and 43.1 $/kg, respectively. Mohammadi et al. [362] integrated solar dish collector technology to provide thermal and electrical energy for hydrogen production via a solid oxide electrolyzer cell. Results show that the resulting LCOH was found 9.1203 $/kg.

Besides, many studies have focused on modelling and performing hydrogen fuelling station powered by HRES as a sustainable solution limiting the use of fossil sources. Gökçek and Kale [363] conducted a techno-economical assessment of a HRES for supplying hydrogen via Wind and PV systems to a refuelling station in Turkey, which is expected to power 25 fuel cell electric vehicles every day. Optimization results using HOMER software

pointed out that the Levelized Cost of Hydrogen (LCOH) considering various configurations was ranging between 7.526 $/kg and 7.866 $/kg. Ayodele et al. [364] assessed the techno-economic feasibility of a hydrogen refuelling station powered by wind energy resource in seven South African sites. Competitive LCOH were achieved and were found to range between 6.34 $/kg and 8.97 $/kg.

3. Methodology

To investigate the optimal design of a grid-connected HRES for residential usage, the present work adopted the following guidelines: (1) Determining the hourly electric load of the designed building by running BEopt simulation. The BEopt simulation considers the common construction practices for the Moroccan context as well as the climatic conditions of the examined sites. (2) Since the proposed design of the HRES model includes the integration of the SDS technology, System Advisor Model (SAM) was employed to estimate the net electric production of a single 25 kW-SDS system on an hourly basis. (3) The last step concerns the identification of the optimal configuration of the HRES using Homer Pro software based on energy and financial metrics. Homer Pro is commonly used to determine the feasible sizes of major HRES components. **Fig. 50** summarizes the details of the established steps to find out the optimal model of the HRES for residential building usage in Morocco.

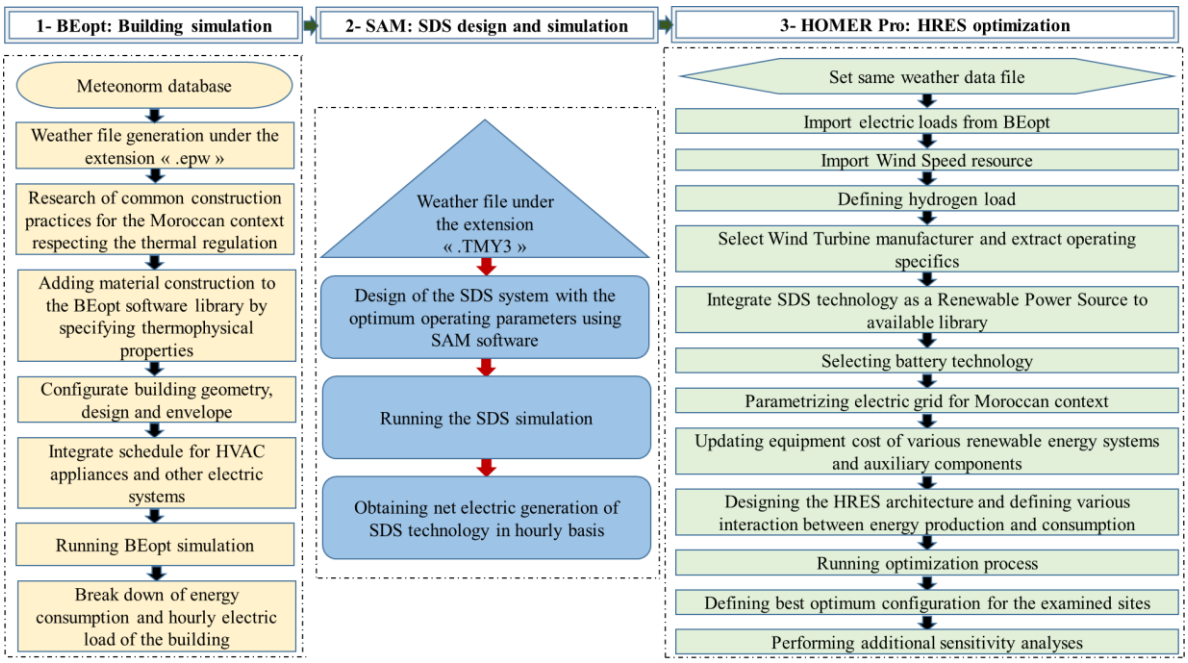


Figure 50: Outline of the adopted steps employed for the multi-family building design and HRES assessment

3.1. Buildings simulation

In the present work, a residential community consisting of 4 multi-family buildings located in the Southern Moroccan region is presented. Each multi-family building is oriented south with a total area of 3520 m² and is composed of 4 floor. Each floor contains 10 apartments with a total apartment area of about 88 m² and encompasses 3 beds and 2 baths. Each building has a total window area of around 227 m². A 3-D sketch of the multi-family building is envisioned in **Fig. 51**. Moreover, the residential building is equipped with an air Source Heat Pump (SHP) with a COP of 3.05 for air conditioning purposes. The cooling and heating set temperature are set to 24.5 °C and 21.5°C, respectively. All the appliance in the building such as TV, water heater, and cooker are electrically powered. The rated energy factor and the input electric of the water heating system are 0.95 and 5.5 kW, respectively. The electric water heater system contains a tank with a volume of about 190 L. By employing these data, BEopt software is used to simulate the building energy performance and provide the hourly electric consumption based on meteorological data of the investigated site. BEopt is a computer tool used to detect cost-effective building design according to the Net-Zero Energy scenario [365]. The software calls the EnergyPlus processing tool to simulate the energy consumption of the designed building based on discrete building options.

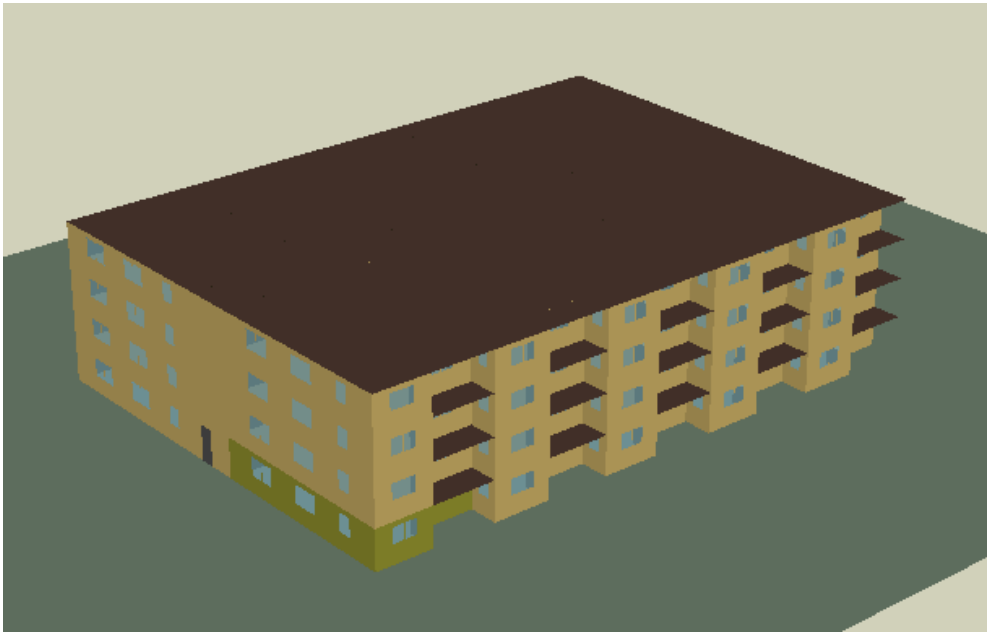


Figure 51: Architecture of the simulated building using BEopt software

For this study, a weather meteorological data of each investigated site has been communicated to BEopt software to provide real climatic data for simulation. Additionally, some adjustments are made to the default databases of the software with the aim of describing the common construction practices for the Moroccan context. **Table 18** lists the technical

features of the envelope materials employed in the building simulation. Other characteristics of the building such as the design specifications of lighting, fixtures, appliances, miscellaneous, and their related schedules are predetermined based on the program default values. Based on the predefined inputs, BEopt runs the simulation of the designed building and delivers the electric load on hourly basis. Simulation findings based on BEopt software quantifies the temporary variation of the electricity consumption and illustrates various energy uses in the building.

Table 18: Main specification details of the envelope materials [366]:

Building constituents	**Layers material**	**Thickness (mm)**	**Thermal conductivity (W/m.K)**	**Density (kg/m^3)**	**Specific heat (J/kg.K)**
Walls	Mortar	20	1.1533	2000	840
	Hallow brick	100	0.1958	938	741
	Polystyrene	50	0.0391	25	1380
	Hallow brick	200	0.2083	664	740
	Cement plaster	20	1.1533	1700	1000

3.1. Examined sites

- **Dakhla**

Dakhla is a Moroccan city located on the Southern Atlantic coast. The city has a temperate and windy climate where the sky is practically clear throughout the year. The average air temperature and wind speed are about 20°C and 8.8 m/s, respectively, with an average relative humidity of about 73%. For its relative high wind speed, Dakhla is considered among the most promising site for WTs employment [367].

- **Ouarzazate**

Ouarzazate is a Moroccan city located in the Draa-Tafilalet region. Ouarzazate has a subtropical desert climate, well known for its hot and sunny summers with relatively mild winters. However, a relatively high solar potential that exceeds a daily average solar irradiation intensity of about 6 kWh/m²/day has been reported in literature [368].

Table 19 illustrates the geographic coordinates of the studied locations. It should be mentioned that the choice of the two studied cities is based on the fact that:

- Ouarzazate is one of the best cities in Morocco which enjoys a high solar potential and which is currently integrating several CSP projects such as Noor 1 and Noor 2.
- Dakhla has certain merits with regard to natural and renewable resources, this allows it to be located in several areas related to sustainable development. Thus,

Dakhla is among the cities where the wind speed reaches the highest values worldwide. Moreover, it turned out that the integration of wind turbines allows solving several problems according to the accessibility to electricity in such Saharan regions and where Moroccan policy has encouraging visions to turn them into an economic hub and a platform for trade and attraction for international investment and tourism.

Table 19: Geographic coordinates of each examined site

Site	Latitude (°N)	Longitude (°W)
Dakhla	23° 43’ 00”	15° 57’ 00”
Ouarzazate	30° 55’ 23”	6° 54’ 15”

3.2. HRES structure

The main purpose of the current study is to propose a Hybrid Renewable Energy System (HRES) that can fulfill electrical demand in multi-family residential buildings and convert excess electricity into hydrogen that can be used for industrial or transportation applications. For this purpose, Homer Pro software is the tool employed to investigate the HRES design and optimization [364]. The suggested model includes the following elements: (1) Renewable electricity production system, namely the SDS system and WT, (2) Electric and hydrogen loads, (3) a converter, a hydrogen tank, a battery bank, and (4) an electrolyzer. It must be noted that the system is grid-connected, and therefore, the required loads of the buildings could be met via the electric network in case that the renewable system is not able to do so. The different capital costs and additional expenditures of the system devices and other relevant technical details are provided in **Table 20**.

Table 20: Cost assumptions and additional technical details

Component	Capital Cost	Replacement	Operations & Maintenance Cost (€/year)	Life Cycle (Year)	Capacity	Ref
Electrolyzer	1620 €/kW	1620	50	15	0-300 kW	[369], [370]
Converter	400 €/kW	400 €/kW	5	15	Homer Optimizer	[365]
Hydrogen Tank	600 €/kg	600 €/kg	3	25	0-350 kg	[363]
Battery	300 €/unit	300 €/unit	10	15	Homer Optimizer	[365]
Wind Turbine	20000 €/unit	20000 €/unit	140	20	Homer Optimizer	[371]

SDS	54455 €/unit	54455 €/unit	1250	25	Homer Optimizer	[67]

The electric and hydrogen production driven by the energy conversion technologies evaluated in this work as well as the electric connection between the HRES and the imposed loads are presented in **Fig. 52**.

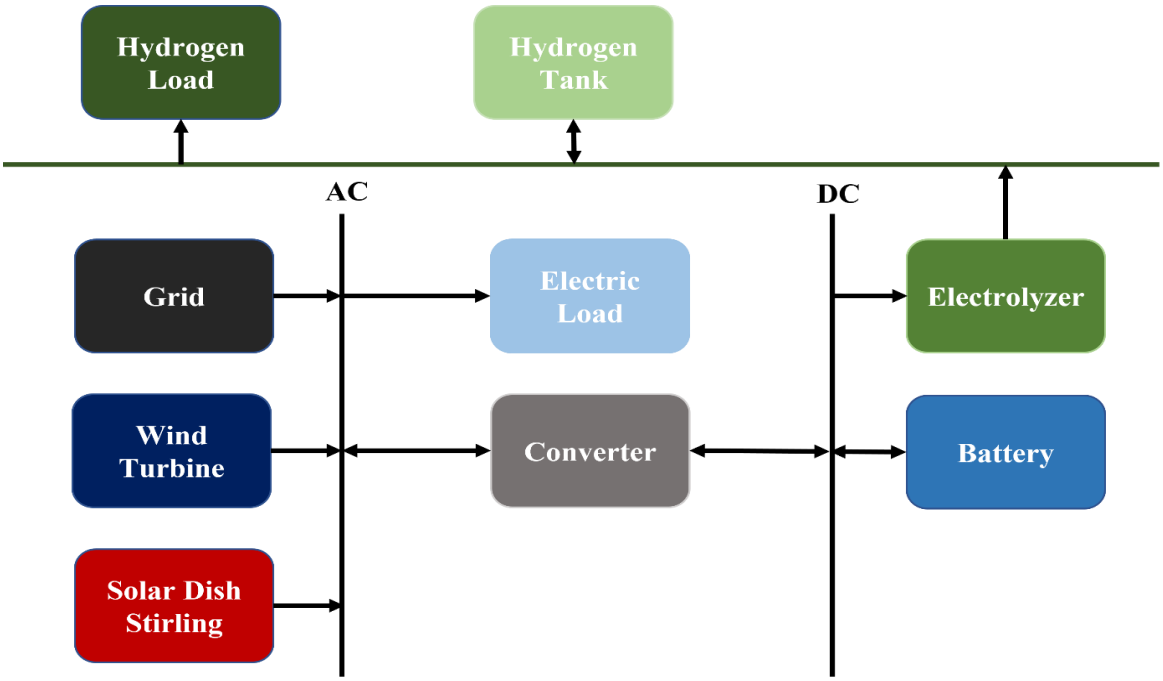


Figure 52: Schematic illustration of the examined HRES

Several parameters should be defined to run the simulation in Homer Pro namely: economic metrics such as the project lifetime, discount and inflation rates and the set optimization constraints. Homer pro has the capability to rank the system configuration for which the global system can assure any specific energy demand under the user-defined constraints according to the lowest Net Present Cost (NPC). Climatic conditions, load profiles and the technical and economic specifications of the overall components are the necessary inputs to perform the optimization analysis. It is interesting to note that an hourly dynamic simulation is performed under SAM software to forecast the electric output of the SDS technology which was imported to Homer Pro. Then, Homer Pro run the simulation for several SDS and WT sizes until the imposed loads are satisfied. The software adopts an energy balance process between the generated and consumed energy in an hourly basis to evaluate the feasible architectures over the project lifetime [364]. Homer Optimizer tool selects the optimal size and capacity of the examined system components based on the lowest

NPC and provides a ranking of most suitable configurations. A simplified flowchart of the optimization process adopted by Homer Pro is depicted in **Fig. 53**.

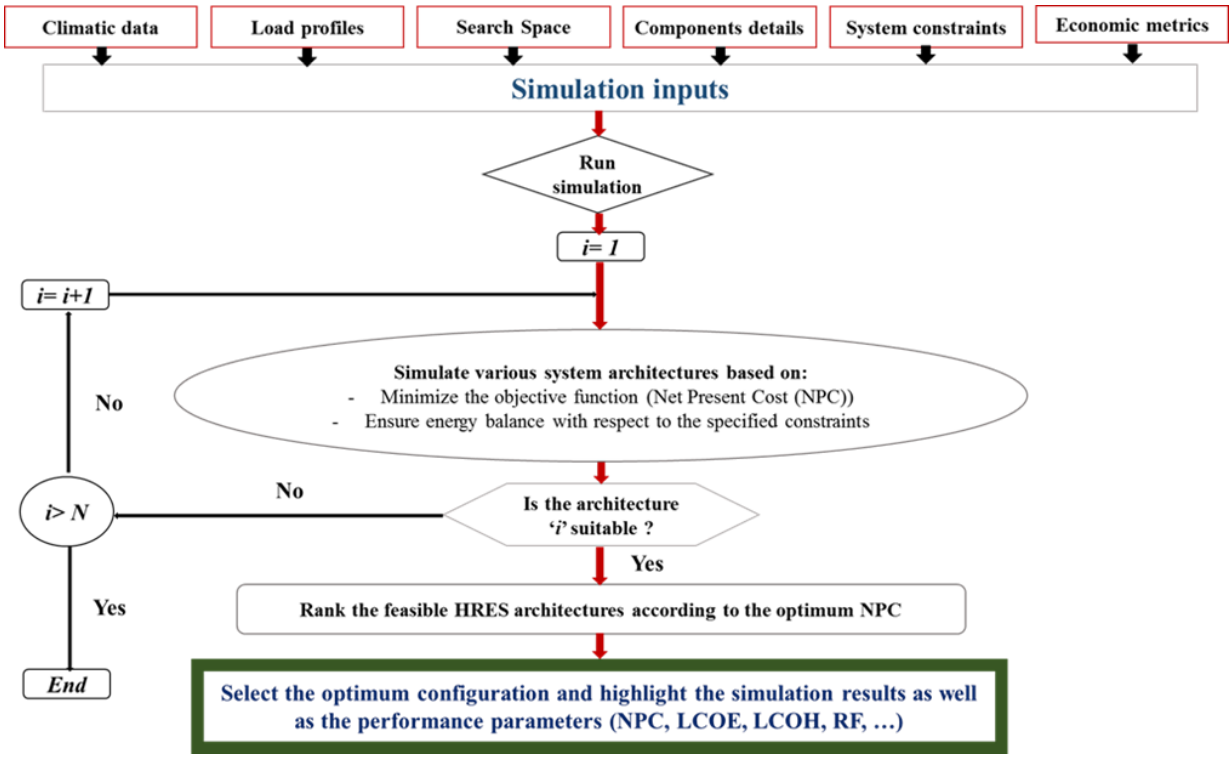


Figure 53 : Flow chart diagram illustrating the main steps of the optimization process adopted by Homer Pro software

3.2.1. Solar Dish Stirling

For the technical analysis of the single Solar Dish Stirling system, System Advisor Model (SAM) simulation software is employed. SAM is a simulation tool that can address both technical and economical assessment of various types of renewable power systems [372]. In the first step, METEONORM software is introduced to generate the Meteorological dataset under the TMY3 (Typical Meteorological Year) format required by SAM. Then, SAM software performs dynamic simulation of the energy performances, generating a set of 8760 hourly values of the SDS electricity production over an entire year [263]. The specifications of Solar Dish Stirling Technology used in the established model are listed in **Table 21**.

Table 21:Optimal design specifications of the Solar Dish Stirling system based on Ref. [110]

Solar Field	
Wind Stow Speed (m/s)	16
SDS Capacity (kW)	25

Collector	
Total area of the mirror (m^2)	91
Reflectance	0.94
Cut-in irradiation (W/m^2)	200
Receiver	
Receiver aperture diameter (m)	0.07
Insulation thickness (m)	0.03
Thermal Conductivity (W/m.K)	0.06
Absorptance coefficient of the absorber	0.9
Absorber surface (m^2)	0.6
Stirling Engine (SE)	
Single Unit Nominal Capacity (kW)	25
Heater Head Set Temperature (K)	993
Functioning Speed (rpm)	1800
Displaced Volume (m3)	0.00038
Beale Constant	0.04247
Beale 1st order parameter	1.682×10^{-5}
Beale 2nd order parameter	-5.105×10^{-10}
Beale 3rd order parameter	7.073×10^{-15}
Beale 4th order parameter	-3.586×10^{-20}
Pressure constant coefficient	0.658769
Pressure 1st order Coefficient	0.00023496
Parasitics	
Control system (W)	150
Cooling System Pump Speed (rpm)	1980-2480
Speed range of the cooling fan (rpm)	400-650

3.2.1. Wind Turbine

The power generated by the WT technology is computed based on several steps. First, the wind speed at the hub height U_{hub} is determined using the inputs data derived from the weather file given by METEONORM database. Homer pro employs the power law to compute this parameter based on the expression below:

$$U_{hub} = U_{anem} \cdot \left(\frac{z_{hub}}{z_{anem}}\right)^{\alpha} \quad \textbf{(37)}$$

where U_{anem} characterizes the wind speed measured at the height of the anemometer in (m/s), z_{hub} and z_{anem} are the terms describing the hub height of the selected WT (in (m)) and the anemometer height (in (m)), respectively, and α defines the power law exponent.

Secondly, the WT power output is calculated at standard operating conditions based on the WT's power curve (See **Fig. 61**). Finally, the WT power output is obtained by applying the density correlation in order to regulate the actual conditions accordingly with the standard conditions [373]. The WT power output P_{WT} can be expressed as function of WT power output under standard temperature and pressure conditions $P_{WT,STC}$ in kW based on the power curve given in **Fig. 61**, and the air density ratio which is expressed in terms of the actual air density ρ and the air density at the standard temperature and pressure conditions ρ_0 in (kg/m^3), respectively. The following equation represent the power output P_{WT} provided by the studied WT:

$$P_{WT} = \left(\frac{\rho}{\rho_0}\right) \cdot P_{WT,STC} \quad \textbf{(38)}$$

In this study, a horizontal axis small WT, called Bergey Excel 10 (XL 10), is selected to provide as the second renewable energy system. The characteristics of the Bergey WT are presented in **Table 22**.

Table 22: Technical features of the used Bergey Excel (XL10) wind turbine [374].

Specifications	Value
Type	Upwind, Horizontal axis, 3 blade
Rated power (kW)	10
Rotor diameter (m)	7
Hub Height (m)	30
Cut-in wind speed (m/s)	2.5
Cut-out wind speed	None
Furling wind speed (m/s)	14~20
Max. design wind speed (m/s)	60

3.2.2. Battery and converter

In HRES, batteries are necessary for energy storage to offset the erratic nature of the power production by the renewable resources. The battery that is employed for the energy storage in this study is a Generic 1 kWh Li-Ion (1 kWh LI). The battery is selected due to its high roundtrip efficiency which is approximately 90% and has a nominal voltage of 6V. Also, a converter a nominal efficiency of 95% is utilized between AC and DC buses. It is worth of mention that the existing converter in Homer Pro integrates both rectifier and inverter modes.

The optimizer tool found within the HOMER Pro software is adopted to identify the suitable sizes of both the battery and the converter.

3.2.3. Electrolyzer

The main purpose of electrolyzer is to produce hydrogen through the electrolysis process that uses electricity to extract hydrogen from water. The electrolyzer depends on two main parameters, namely the efficiency and the minimum load ratio. Based on a constant value of the efficiency, it is supposed that the electricity will be certainly transformed to a quantity of hydrogen. In Homer Pro, the hydrogen is normally produced only by the excess of electricity. In this case, a generic electrolyzer with an efficiency of 85% is employed and a hydrogen load is imposed to the system, so the electrolyzer necessarily requires electricity to supply the requested amount of hydrogen. A value ranging from 0 to 300 kW of the electrolyzer capacity size with an increment step of 50 kW has been applied as a research domain. During the optimization process, Homer Pro determines the optimum value of the electrolyzer capacity size.

3.2.4. Hydrogen tank

The amount of the produced hydrogen has useful uses and may be used in many sectors mainly to refuel hydrogen cars or to produce electricity through fuel cell technology. Here, the applications making use of producing system are not modelled. The hydrogen that is created by the electrolyzer is stored in a hydrogen tank when there is no hydrogen demand or when there is an excess of electricity. In this study, a generic hydrogen tank is employed where the initial tank level is fixed as 50 percent of the tank size. The capacity size of the hydrogen tank was assessed in a given interval (from 0 to 350 kg with an increment step of 50 kg). The performance of the hydrogen tank as well as the overall cost assumptions are given in **Table 20.**

3.3. Assessments metrics and economic model

3.3.1. Total Net Present Cost (TNPC)

Several possible configurations of the HRES are assessed to select the optimum feasible one by obtaining the size of each HRES components. The optimization framework is performed based on power balance and technical constraints and by considering the net present cost NPC as a principal objective function. All suitable arrangements are ranked from the lowest to highest NPC with the optimum design corresponding to the lowest NPC. The NPC of the proposed HRES is the result of the difference between the present values of all

expenses that HRES incurs throughout the system lifetime period (capital, replacement, and operating & maintenance costs) and the present value of all income earned in this duration. The total net present cost C_{TNPC} is expressed in terms of the total annualized cost C_{TAC} (€/year) and the capital recovery factor CRF [375]

$$C_{TNPC} = \frac{C_{TAC}}{CRF} \quad \textbf{(39)}$$

The *CRF* is employed to determine the present value of a sequence of identical annual cash flow values. The Capital Recovery Factor (CRF) is expressed as function of the annual real discount rate (i) (real interest rate) and the lifetime of the project (N). The CRF equation can be defined as follows [363]:

$$CRF = \frac{i(1+i)^N}{(1+i)^N - 1} \quad \textbf{(40)}$$

The annual real interest rate allows conversion between one-time costs and the annualized costs. The expression of the annual real discount rate (i) is formulated in terms of the nominal discount rate (i') and the expected inflation rate (f) [363]. In the current analysis, the values of the nominal discount rate and inflation rate were taken 5% and 2%, respectively. The techno-economic analysis was performed by considering a project lifetime of 25 years:

$$i = \frac{i' - f}{1+f} \quad \textbf{(41)}$$

3.3.2. Levelized Cost of Energy (LCOE)

The Levelized Cost of Energy *LCOE* is defined as the average cost per kWh of the useful energy gain generated by the proposed system [363]. It is expressed as the ratio between the total annualized cost C_{TAC} of generating electricity and the entire electric load served E_{served}. The total annualized cost C_{TAC} refers to the summation of the annualized cost of each individual HRES component. The total electric load served E_{served} represents the total amount of energy required to meet the sum of the imposed electric load and the energy sold to the grid in kWh/year. The LCOE equation is written as follows [363]:

$$LCOE = \frac{C_{TAC}}{E_{served}} \quad \textbf{(42)}$$

3.3.3. Levelized Cost of Hydrogen (LCOH)

The levelized cost of hydrogen $LCOH$ is computed as a function of the difference between the total annualized cost C_{TAC} of the simulated system and the revenue from the total annualized electricity served divided by the total amount of hydrogen production $M_{Hydrogen}$. In this study, the analysis carried out the assessment of the gross levelized cost of hydrogen which did not include the total revenue of electricity produced by the proposed HRES. In this case, the $LCOH$ value is computed considering that the proposed system is intended to meet the hydrogen requirement only and neglects other loads. The gross value of the Levelized Cost of Hydrogen can be expressed as follows:

$$LCOH = \frac{C_{TAC}}{M_{Hydrogen}} \quad \textbf{(41)}$$

3.3.4. Renewable Fraction (RF)

To evaluate the model of the proposed HRES from a sustainability aspect, the fraction of renewable energy is considered. Renewable fraction *RF* designates the fraction of the energy supplied to meet the loads and which is derived from renewable sources. This energy output is described in terms of the electricity generated from nonrenewable sources E_{nonren}, thermal energy derived from nonrenewable sources H_{nonren}, the total electrical E_{served} and thermal loads H_{served} served. In the present work, no thermal load is considered. The nonrenewable electrical production is equal to the electricity provided by the nonrenewable modules in the energy system. In the studied system, this energy corresponds mainly to the load delivered by the grid. The *RF* formula is given as follows [376]:

$$RF = 1 - \frac{E_{nonren} + H_{nonren}}{E_{served} + H_{served}} \quad \textbf{(42)}$$

4. Results and discussion

In this section, the results simulation based on BEopt and Homer Pro software were analyzed to appropriately model a multi-family building as well as the Hybrid Renewable Energy System to meet the electric and hydrogen loads for the designed residential buildings located in Dakhla and Ouarzazate.

4.1. Meteorological data

Meteorological variables have a remarkable influence on the overall performances of any renewable energy system. Direct Normal Irradiation *DNI*, Ambient Temperature *AT* and Wind Speed *WS* are the most important variables that strongly affect the outputs of the present HRES. In the current work, two geographical sites located in the southern Moroccan

region are considered. These sites present discrepancies regarding solar and wind potentials. In **Fig. 54** and **55**, it is clearly visible that Ouarzazate attain relatively high *DNI* and *AT* values compared to Dakhla implying substantial solar potential at Ouarzazate. *DNI* and *AT* in this city can exceed the values of 1040 W/m² and 40 °C, respectively. On the other hand, Dakhla is among the windiest city in Morocco, as shown in **Fig. 56** that depicts the hourly variation of the *WS* in Dakhla and Ouarzazate. It is clearly observed that higher values of the *WS* are detected in Dakhla where values of about 20 m/s is reached.

According to the displayed figures, the selection of the sites is justified. It can be deduced that the city of Ouarzazate promotes the integration of the different types of CSP technology due to the higher detected value of *DNI*. However, it turned out that wind power resource can exhibit satisfactory yields in Dakhla city comparatively.

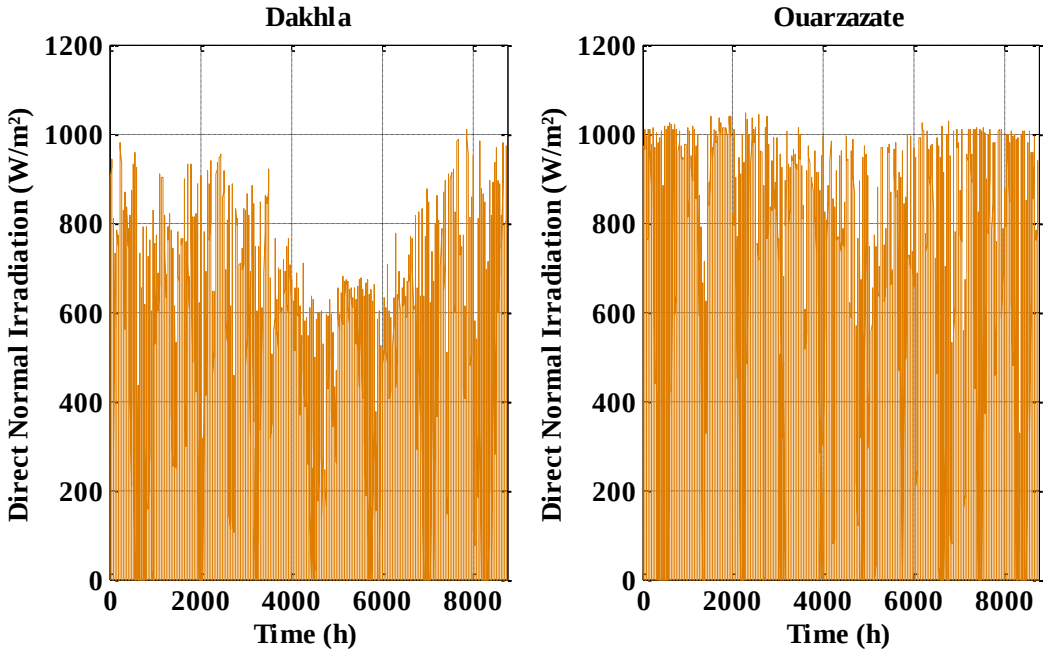


Figure 54: Hourly profile of the Direct Normal Irradiation during a whole year for Dakhla and Ouarzazate

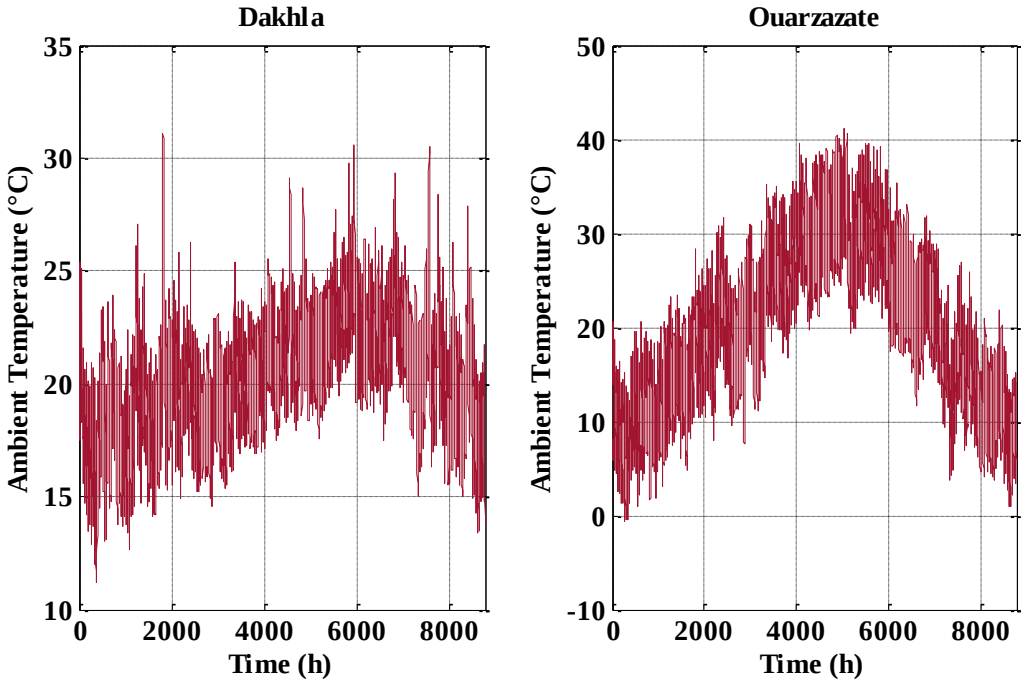


Figure 55: Hourly profile of the Ambient Temperature during a complete year for Dakhla and Ouarzazate

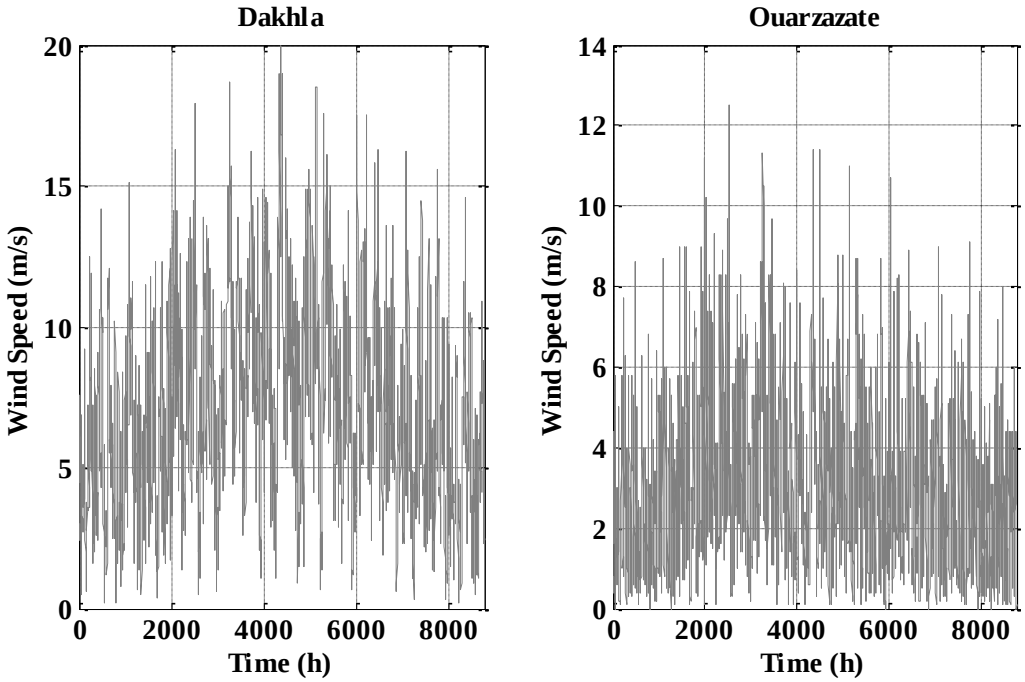


Figure 56: Hourly profile of the Wind Speed during a whole year for Dakhla and Ouarzazate

4.2. BEopt simulation results

The main objective of this subsection is to discern the temporary change of the electricity load of a residential community made up of 4 identical multi-family buildings. Breakdown of various energy usages including the electric consumption of the air conditioning systems, lighting, plug loads (Miscellaneous) and the larges appliances

(refrigerators, cooking, dishwashers, clothes dryer and washer, etc.) is illustrated as well for both Dakhla and Ouarzazate.

4.3. Electric load Dakhla city

The electric consumption of the buildings is highly affected by the climatic conditions of the studied sites. In Dakhla, the total annual electric load for the simulated buildings is found 1271.42 MWh/year. From **Fig. 57**, one can notice that the total load is mainly dominated by the Large Appliances utilization, followed by lights, plug loads and air cooling consumption. Since Dakhla city does not experience significant temperature drops throughout the year (See **Fig. 55**), no need for heating was identified. Thus, a maximum value of the electric load is detected 385.19 kW and the scaled annual average electric load is about 3483.32 kWh/day.

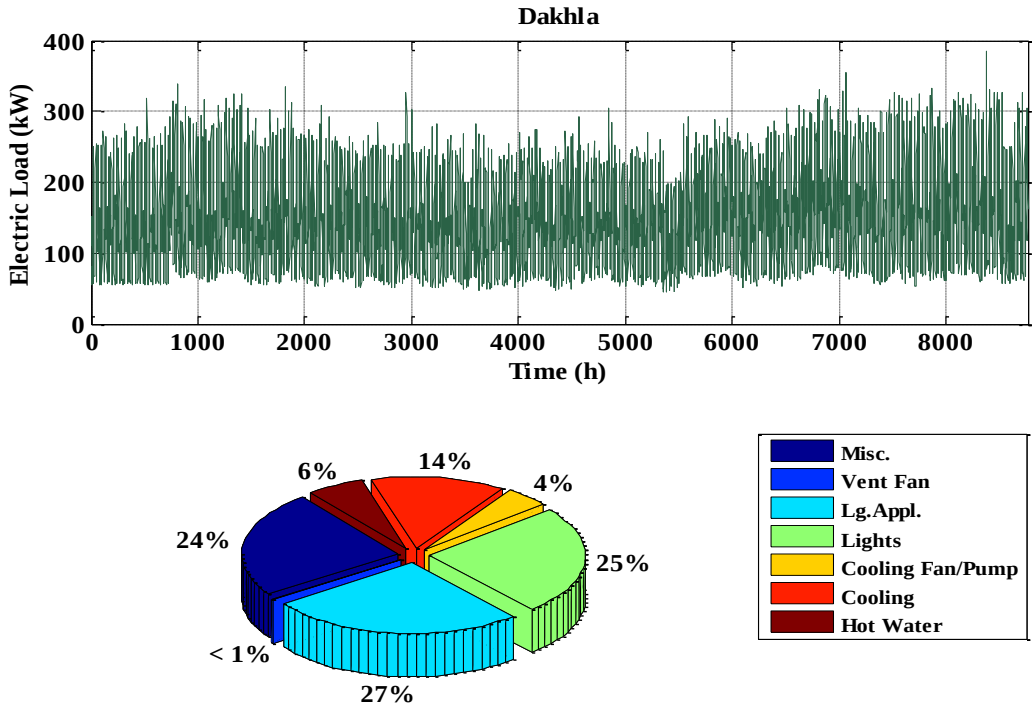


Figure 57: Hourly variation of the total electric load and break down of the multi-uses consumption of the residential buildings for Dakhla city.

4.4. Electric load Ouarzazate city

Fig. 58 depicts the hourly electric load profile as well as the breakdown of the energy usage for the investigated residential buildings. The total electric load in Ouarzazate buildings is estimated to be about 1301.300 MWh/year which is superior to that of Dakhla city. Particularly, the electric consumption attributed to Large Appliances, Lights and

Miscellaneous represent 26%, 24% and 23%, respectively. Cooling and heating of water consume 15% and 6% of the total electric consumption, respectively. The required energy for heating is relatively low and is found to be about 2497.08 kWh which represents less than 1% of the total electric load. The peak of the electric consumption as well as the scaled annual average electric load of the investigated residential buildings at Ouarzazate site are found to be about 367.67 kW and 3565.21 kWh/ day, respectively.

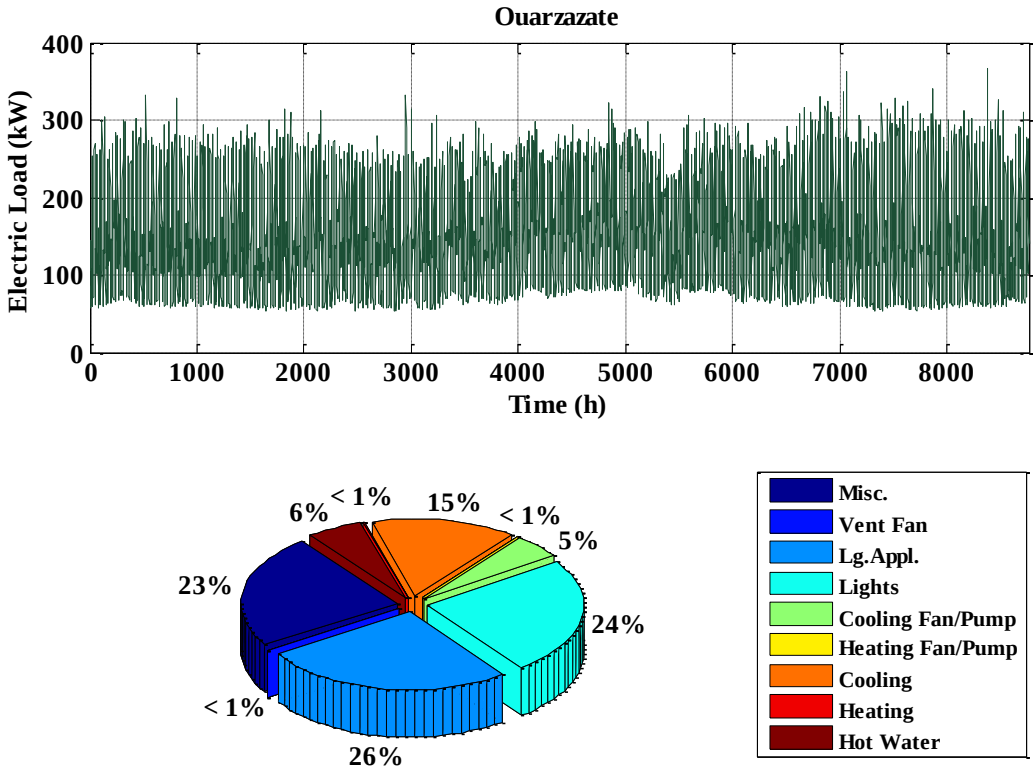


Figure 58: Hourly profile of the total electric consumption and break down of the application uses of the residential buildings for Ouarzazate city.

4.5. Hydrogen load

This study investigates the potential of sustainable hydrogen generation by exploring the electricity generated by the grid connected HRES according to the imposed hydrogen load. Of course, priority is given to electric loads and in the presence of excess power, the HRES convert it into hydrogen. For both investigated sites, the same hydrogen load is considered. A predetermined model of hydrogen consumption to provide a time-varying hydrogen load with a scaled annual average of about 22.52 kg/day is considered. The hydrogen load variation with respect to time is shown in **Fig. 59**. The peak of the load is

around 2.8 kg/h. The cumulative yearly hydrogen production that is needed to be produced by the electrolyzer is close to 8213 kg/year.

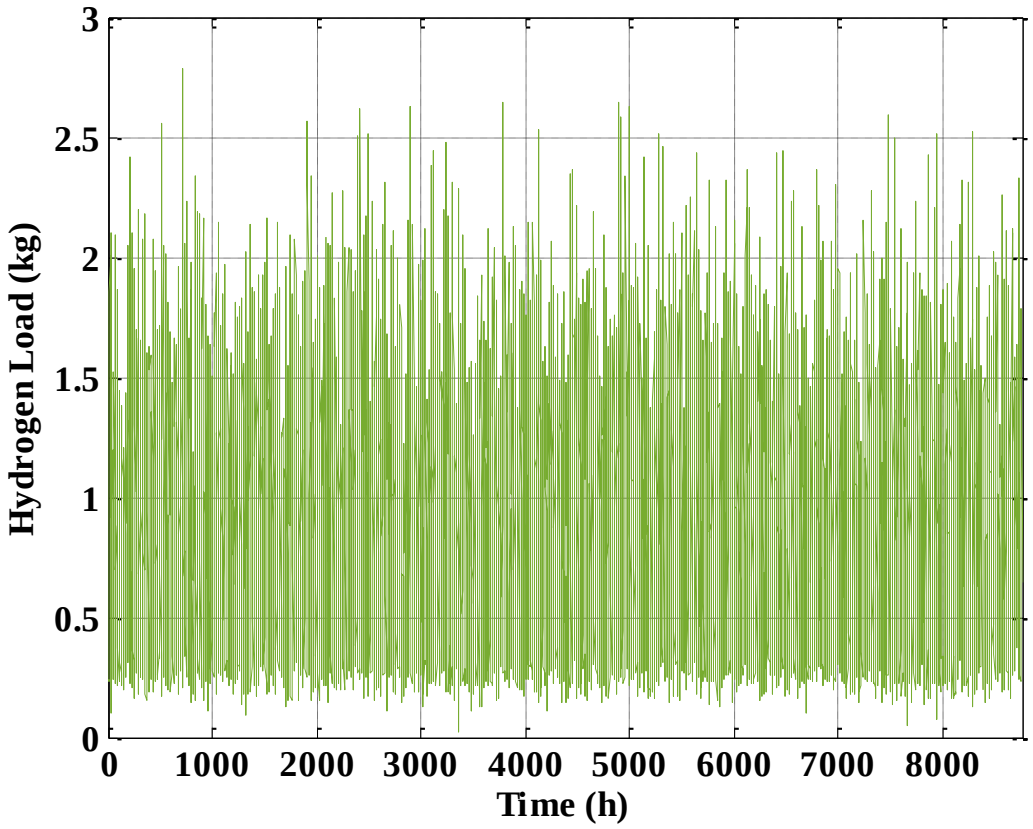


Figure 59: Hourly variation of the imposed hydrogen load throughout the year for the examined sites

4.6. Solar Dish Stirling results from System Advisor Model (SAM)

In this section, the hourly power generated by the SDS in both Dakhla and Ouarzazate are presented. Design and simulation of the SDS system is performed using System Advisor Model software (SAM) based on weather data for both sites. **Fig. 60** envisions the hourly variation of the SDS power generated throughout the year for Dakhla and Ouarzazate. The simulation integrated the optimum design specifications of the SDS system as given in **Table 21** to achieve the best energy performances. It has been mentioned before that the *DNI* in Ouarzazate reaches higher values over the year compared to Dakhla (See **Fig. 54**). Therefore, the power generated by the SDS in Ouarzazate seems to be higher compared to Dakhla. The annual energy generated by the SDS system at Ouarzazate reaches approximately 67.372 MWh while it is in the range of 38.075 MWh at Dakhla.

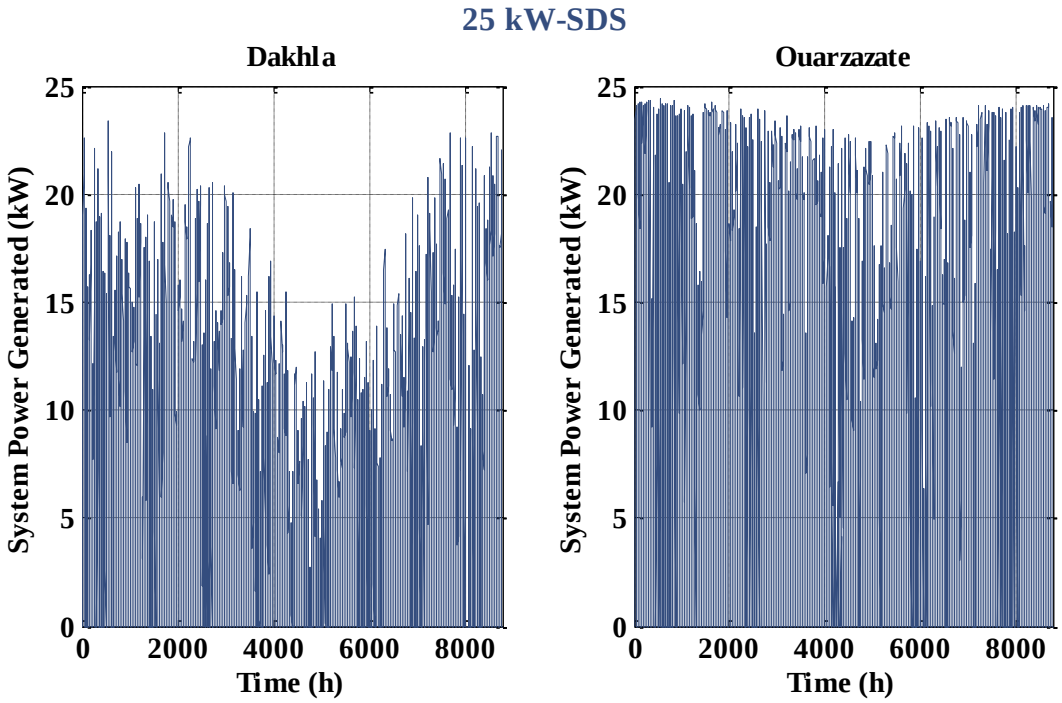


Figure 60: System Power generated of the SDS system using SAM for Dakhla and Ouarzazate

4.7. Wind Turbine power output from Homer Pro

Wind turbines are used to partially supply energy requirements of the investigated residential buildings and thus will contribute to increase the renewable energy fraction of the proposed HRES. The selected WT is Bergey Excel 10 (XL 10) with a power capacity of 10 kW. The power curve of the Bergey excel WT is displayed in **Fig. 61.** Based on WS profiles of both sites, hourly variations of power generated in Dakhla and Ouarzazate are obtained as highlighted in two lower captions of **Fig. 61**. The windy nature of Dakhla region allows functioning of the WT at its rated power for longer durations as compared to Ouarzazate which is instead have limited wind potential. The annual energy generated by the 10 kW- WT is about 41.402 MWh in Dakhla while it is merely 5.53 MWh in Ouarzazate.

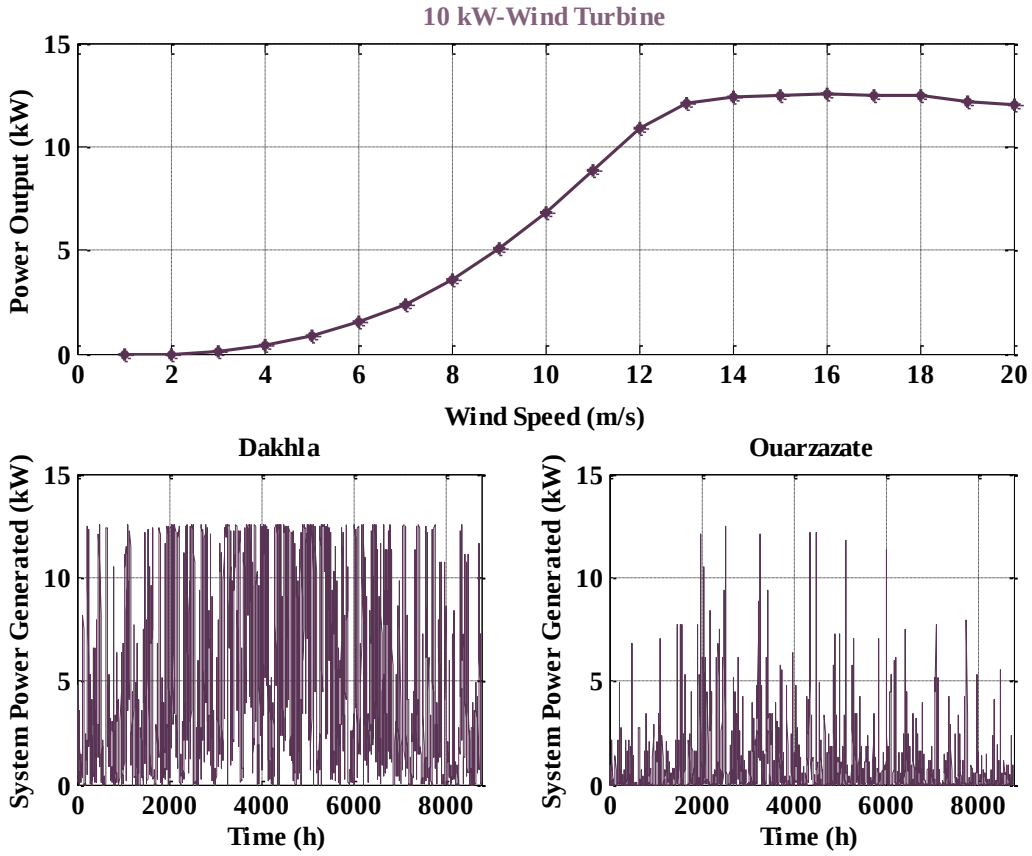


Figure 61: Power curve of the Bergey Excel XL 10 Wind Turbine and its related produced power in Dakhla and Ouarzazate

4.8. Optimum configuration at Dakhla city

The optimization results of the proposed HRES in Dakhla and Ouarzazate are displayed in this section considering the previous technical and financial inputs. The objective of the optimization process is to identify the optimum HRES configuration that corresponds to lower net present cost (NPC). Six attractive HRES configurations ranked from the lowest to the highest NPC are given for Dakhla and Ouarzazate in **Table 23** and **24**, respectively. For each configuration, it is possible to highlight renewable energy installed capacities, storage capacity, grid connection possibility (yes for a value of 1 and no for a blank value), converter, electrolyzer capacity as well as hydrogen tank size. Also, main financial outputs such as NPC, LCOE and LCOH are visualized in the **Table 23 and 24** along with the corresponding renewable fraction. Comparing the best proposed configurations (design 1) in both regions, it is possible to see that Dakhla has a reduced NPC and a higher renewable fraction compared to Ouarzazate. The share of wind capacity is remarkably higher at Dakhla due to the excellent wind condition which renders its overall viability competitive. Also, one can see that installing WTs in Ouarzazate is not recommended. Instead, installing SDS technology is more

appealing at Ouarzazate and the optimum installed capacity is about 435.625 kW (which corresponds to a range of 17 unit of 25 kW SDS). The best configurations in Dakhla and Ouarzazate allowed for LCOE of 0.0697 €/kWh and 0.126 €/kWh, respectively, LCOH of 21.4 €/kg and 23.6 €/kg, respectively and renewable fractions of about 86.04% and 50.38%, respectively. At this stage, it is worth of mention that if the LCOH calculations considers the electricity revenues of the HRES, the optimum configuration allows producing the required amount of hydrogen freely in Dakhla and at a cost of merely about 4.88 €/kg at Ouarzazate.

Table 23: Optimized HRES design with specific details of all components in Dakhla city

Architecture N°	WT (kW)	SDS (kW)	Battery	Grid	Electrolyzer (kW)	Hydrogen Tank (kg)	Converter (kW)	NPC (M€)	LCOE (€/kWh)	LCOH (€/kg)	Renewable Fraction (%)
1	610	13.43		1	150	300	152.01	3.053	0.0697	21.4	86.04
2	630			1	150	300	165.33	3.074	0.0685	21.5	86.37
3	580	31.25	23	1	150	350	153.53	3.078	0.0732	21.5	85.43
4	520		21	1	200	350	200.93	3.088	0.0822	21.6	81.87
5	1090	578.125	5879		100	250	505.75	9.129	0.4099	63.6	100
6	1950		12912		100	300	541.35	14.057	0.6312	98.4	100

4.9. Optimum Configuration at Ouarzazate city

Table 24: Optimized HRES design with specific details of all components in Ouarzazate city

Architecture N°	WT (kW)	SDS (kW)	Battery	Grid	Electrolyzer (kW)	Hydrogen Tank (kg)	Converter (kW)	NPC (M€)	LCOE (€/kWh)	LCOH (€/kg)	Renewable Fraction (%)
1		435.625		1	150	200	151	3.391	0.1260	23.6	50.38
2	10	445.05		1	150	150	150.56	3.407	0.1246	23.6	51.41
3		450	20	1	150	150	151.58	3.409	0.1242	23.5	51.48
4	10	435.525	12	1	150	200	150.93	3.420	0.1269	23.8	50.61
5	890	750	10585		300	350	621	12.850	0.5638	91	100
6	4800			1	300	350	301.51	15.255	0.2970	108	77.20

For design 1 (optimum configuration), the breakdown of energy production and energy utilization can be seen in the case of Dakhla in **Fig. 62**. It should be highlighted that the annual generation in this case is about 2894 MWh/year. The high installed capacity of

WTs leads to a high energy production (87% of the total energy generated). The grid contributed about 12% of the total energy while the SDS contributed less than 1% at Dakhla. Plus, about 44% of the available electricity is consumed by the residential buildings, 14% is consumed by the electrolyzer to generate hydrogen while 42% can be injected into the national grid. Also, the hydrogen load (8213 kg/year) is almost totally satisfied with the proposed configuration in Dakhla with a rate garter than 99.3%.

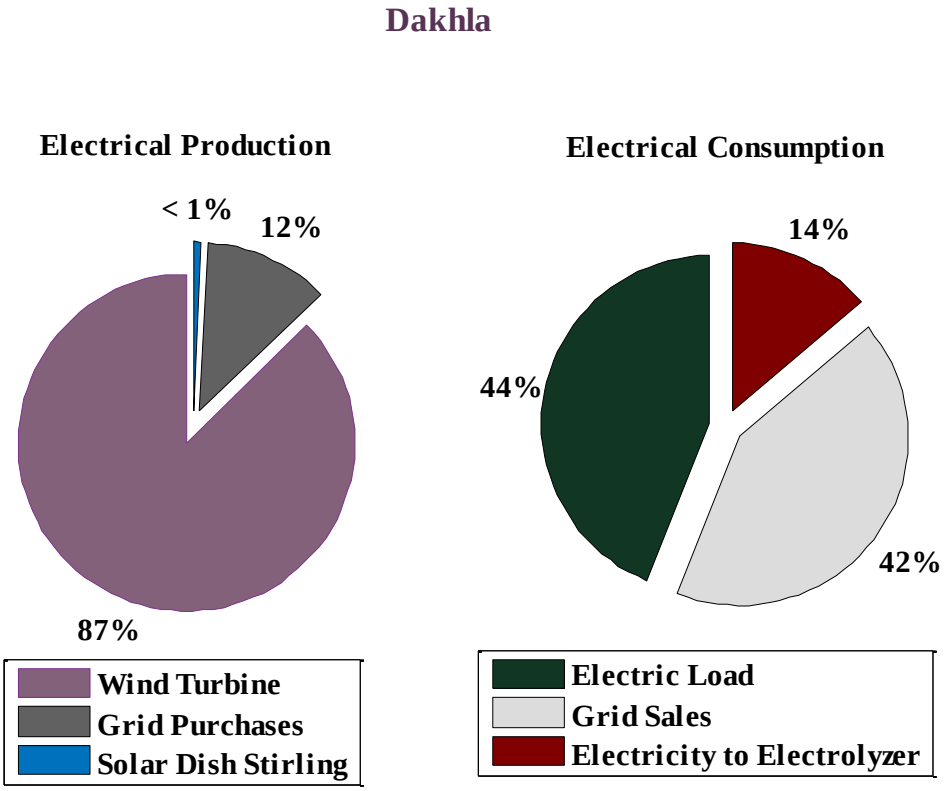


Figure 62: Break down of the total electric generation and total electric consumption for Dakhla according to the optimal configuration

Similarly, the repartition of electricity production and utilization for the best HRES configuration operating in Ouarzazate are illustrated in **Fig. 63**. As the optimum HRES does not utilize wind energy systems, the energy generation in Ouarzazate is mostly fulfilled by the SDS with a share of 61% and the electric grid with a share of 39%. In Ouarzazate, the total annual energy generation, which is about 1935 MWh/year, is consumed as follows: 67% to satisfy electricity requirements of the residential buildings, 21% to produce hydrogen and 12% is to be injected in the grid. This HRES configuration meets almost entirely the needed hydrogen load in Ouarzazate with a share of about 99.9%

Ouarzazate

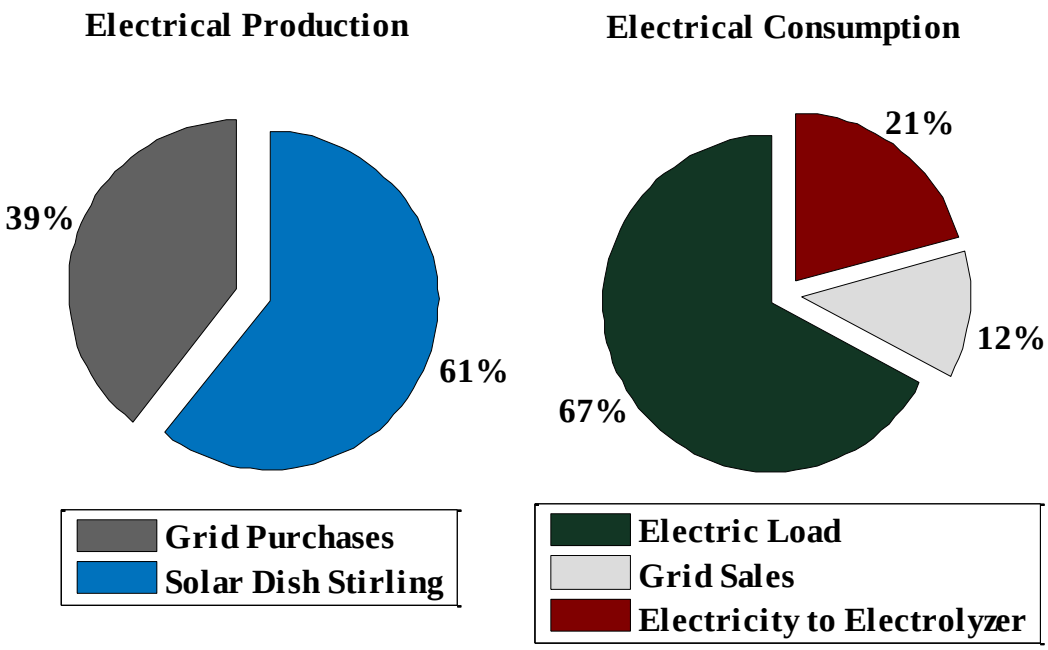


Figure 63: Break down illustration of the total energy production and energy utilization for Ouarzazate according to the optimal configuration

4.10. Sensitivity analysis

The last set of results corresponds to sensitivity analyses that were performed on the basis of a financial input which is the cost reduction of the SDS technology and the wind resource availability by considering the annual average wind speed.

The first sensitivity analysis considered the HRES operating in Dakhla. As was pointed out earlier, the SDS contribution was very weak in Dakhla. Applying cost reductions to the SDS system is expected to have a significant effect on the optimized configuration and its overall viability. The NPC is reduced from 3.05 to 2.72 M€ when cost multipliers from 1 to 0.6 are applied (See **Fig. 64**). However, for a cost reduction of 40% (cost multiplier of 0.6), the LCOE seems to increase compared to the baseline configuration (cost multiplier of 1). For the maximum cost reduction (cost multiplier of 0.6), the SDS installed capacity is about 352.5 kW compared to 13.425 kW in the baseline configuration while WT capacity was decreased from 610 kW in the baseline configuration to 230 kW in the maximum cost reduction configuration (See **Table 25**).

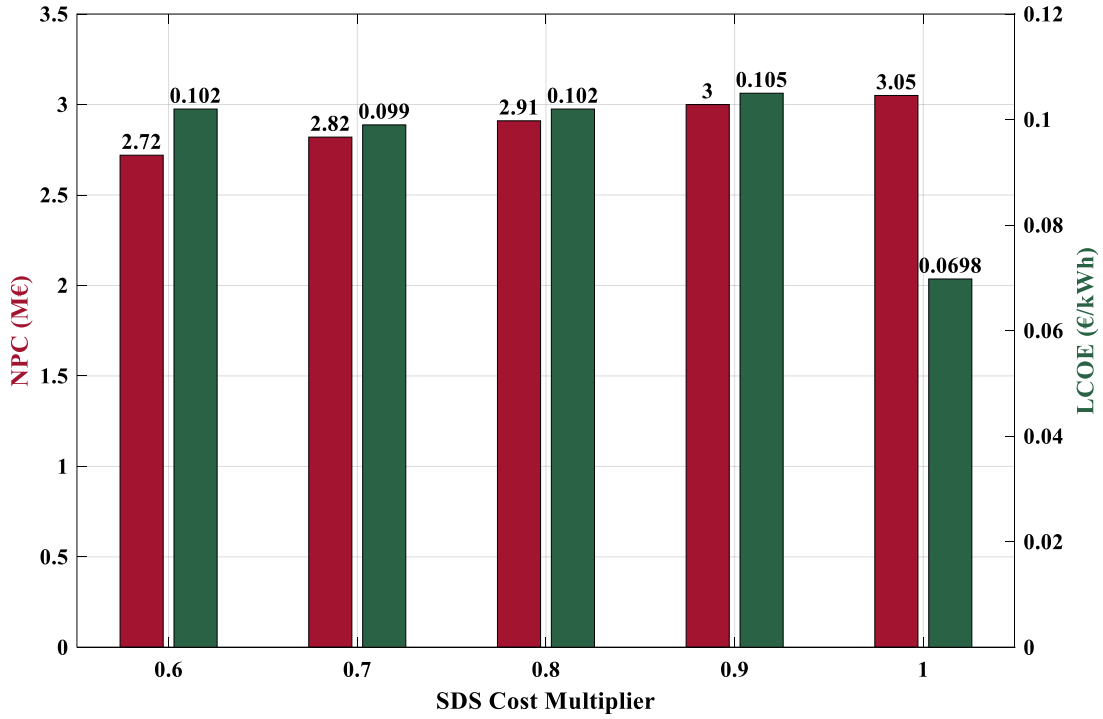


Figure 64: Sensitivity analysis considering the SDS Cost reduction from 1 to 0.6 in Dakhla

Table 25: Sensitivity analysis based on SDS Cost Multiplier reduction in Dakhla city

Sensitivity	Architecture							Economic metrics			Environmental criteria
SDS Cost Multiplier	WT (kW)	SDS (kW)	Battery	Grid	Electrolyzer (kW)	Hydrogen Tank (kg)	Converter (kW)	NPC (M€)	LCOE (€/kWh)	LCOH (€/kg)	Renewable Fraction (%)
1	610	13.425		1	150	300	152	3.05	0.0698	21.4	86
0.9	280	297.5		1	150	200	148	3	0.105	21	74.8
0.8	280	297.5		1	150	200	148	2.91	0.102	20.3	74.8
0.7	280	297.5		1	150	200	148	2.82	0.099	19.7	74.8
0.6	230	352.5		1	150	150	157	2.72	0.102	19	71.2

As highlighted earlier, optimization results indicated that the poor wind potential in Ouarzazate caused that WTs are not recommended in the optimum HRES. So, a variation of the average annual *WS* from 2 m/s and 8 m/s was applied considering the same SDS generation system. From **Fig. 65**, it can be highlighted that the increase of WS tends to make the HRES more economically viable with noticeable reduction in the NPC and LCOE. At the maximum average WS of 8 m/s, the NPC is only 2.71 M€ compared to 3.39 M€ in the baseline configuration. The LCOE is also reduced from 0.126 €/kWh in the baseline configuration (annual average WS in the baseline configuration is equal to 2.9 m/s) to 0.0963 €/kWh. From the **Table 26**, it can be seen that increasing *WS* values tend to increase the share of WTs in the optimum configurations. For instance, the installed WT capacity increased

from 0 kW in the baseline configuration to 240 kW when considering a yearly average *WS* of 8 m/s.

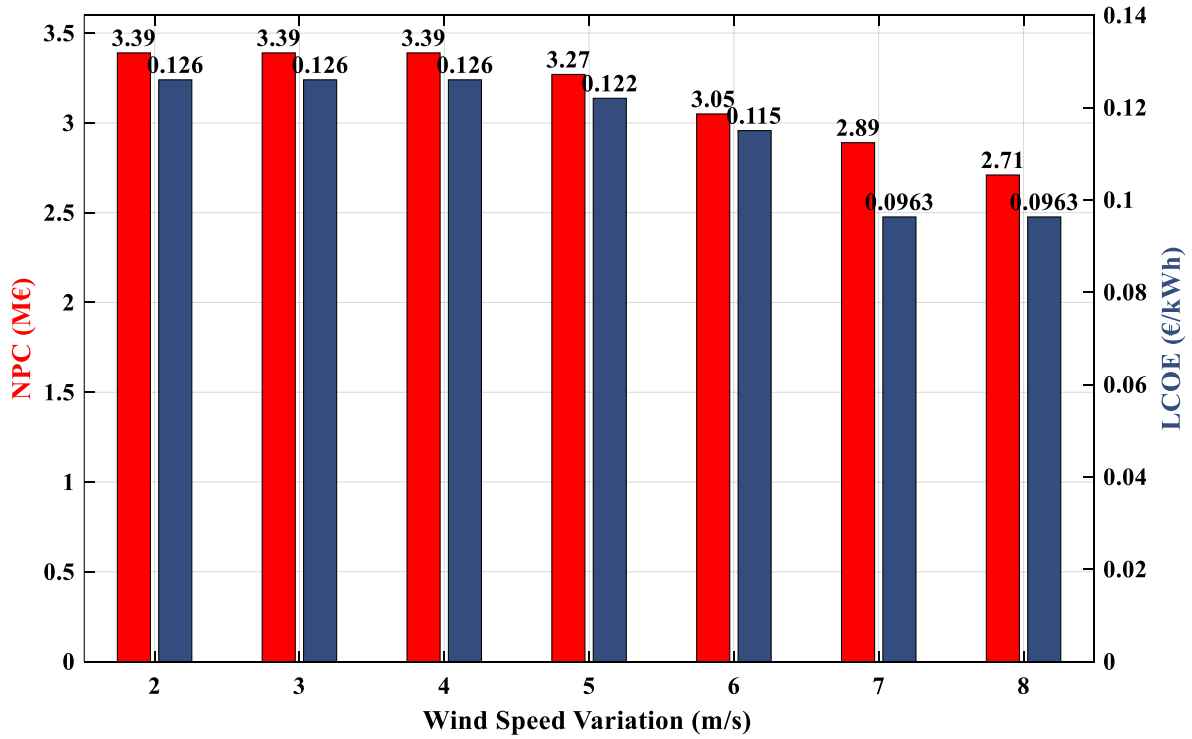


Figure 65: Sensitivity analysis considering the variation of the annual average wind speed in Ouarzazate

Table 26: Sensitivity analysis based on scaled average wind speed variation in Ouarzazate city

Sensitivity	Architecture							Economic metrics			Environmental criteria
Scaled Annual Wind Speed (m/s)	WT (kW)	SDS (kW)	Battery	Grid	Electrolyzer (kW)	Hydrogen Tank (kg)	Converter (kW)	NPC (M€)	LCOE (€/kWh)	LCOH (€/kg)	Renewable Fraction (%)
2		435.625		1	150	200	151	3.39	0.126	23.6	50.4
3		435.625		1	150	200	151	3.39	0.126	23.6	50.4
4		435.625		1	150	200	151	3.39	0.126	23.6	50.4
5	200	322.5		1	150	150	154	3.27	0.122	22.9	60.2
6	190	285		1	150	150	150	3.05	0.115	21.4	63.1
7	290	209.25		1	150	100	161	2.89	0.0963	20.2	72.7
8	240	197.75		1	150	100	150	2.71	0.0963	18.9	71.2

5. Summary

In this chapter, the design, dimensions, and cost of a novel integrated hybrid solar and wind power generation system for residential buildings have been assessed. The Hybrid

Renewable Energy System (HRES) consists of a SDS technology, a WT, an electrolyzer, a hydrogen storage tank, as well as a battery bank that may store electricity for residential supply applications in two Moroccan regions. The simulation of the residential buildings is established, the energy performance of the SDS technology is performed and the optimization of the HRES is carried out. The findings of the techno-economic optimization indicate that:

- The energy consumption of the building in Ouarzazate is equivalent to $1.9x10^6$ kWh/y and more than $2.8x10^6$ kWh/year in Dakhla region. The hydrogen load is estimated to 8214 kg/year for both Dakhla and Ouarzazate.
- The annual energy generated by the SDS based on the optimum design specification reaches 67.372 MWh and 38.075 MWh at Ouarzazate and Dakhla, respectively.
- The optimization results revealed that the optimum configuration of the proposed HRES at Dakhla strongly promote the integration of WT technology while at Ouarzazate, the proposed HRES based primarily on SDS technology is highly recommended.
- The optimum configuration highlighted that the total electric and hydrogen loads could be covered at an NPC/ LCOE of about 3.053 M€/0.0697 €/kWh and 3.391 M€/ 0.126 €/kWh at Dakhla and Ouarzazate, respectively.
- The gross value of LCOH according to the optimum configuration are found 21.4 €/kg and 23.6 €/kg at Dakhla and Ouarzazate, respectively.
- Sensitivity analyses turned out that decreasing the total SDS cost in the case of Dakhla tends to make its integration with WT technology cost effective. However, sensitivity results based on the evaluation of the *WS* at Ouarzazate unveiled that the use of WTs is relatively dependent on the annual average *WS* values and the augmentation of this criteria makes its implementation more economically viable.

The current work involved only electric and hydrogen production based on the proposed HRES, therefore, it will be of interest to establish a HRES that integrate fuel cell technology and propose an improved architectures with multigenerational integrated systems coupling buildings, transport, and industrial sector where hydrogen is a critical energy carrier.

GENERAL CONCLUSION AND PERSPECTIVES

The use of solar dish as a renewable system constitutes a promising alternative in reducing fossil fuel consumption and their related harmful gas emissions. However, insufficient experimental data regarding the operating parameters of this technology limits its characterization, modelling, design, optimization, and as such its further utilization. In this thesis, light was shed into the SDS technology as a clean power generation technology. The followings aspects were dealt with:

- First, the objective was to position solar dish technology with respect to the existing CSP technologies and show how it was technologically progressed over the past years. Specifically: **CHAPTER I** provided a clear illustration of the different Concentrating Solar Power technologies and described the contribution of each technology in the current solar market. Then, it presented a comprehensive review of state of the art on research and development of the solar dish technology, while revealing the confirmed approaches and pathways used to improve the performances of each system components. Further, the progress of this technology worldwide was discussed based on the available assessment studies figuring in the literature.
- The second objective focused on the selection of the optimum configurations and combinations that can help attaining the highest energy performances of the SDS technology and make its integration cost-effective. **CHAPTER II** introduced the general concepts required for the study of the SDS technology, involving the novel designs and applications and presenting the more recent advances, the global prospect and outlooks and the different optimization approaches and methods that can contribute in the development and progress of this technology.
- The third objective was of a local interest and treated the topic of integrating Solar Dish Stirling system for electrification in rural Moroccan zones. Accordingly, a comprehensive 4-E analysis was carried out for thirteen Southern Moroccan sites as reported in **CHAPTER III**. The potential benefits of SDS implementation especially in location enjoying high solar irradiation was highlighted via a multi-criteria analysis. Then, a parametric analysis was performed to select appropriately specific design parameters such as the receiver aperture diameter, cooling pump speed and receiver insulation thickness leading to maximal energy and financial performances. It should

be stressed that system simulation was conducted on an hourly basis with the help of System Advisor Model software (SAM). Additionally, specific energetic and exergetic criteria, economic and environmental indicators were addressed to perform the overall performances of the SDS power plant. Top three potential sites for implementing the Solar Dish Stirling technology were identified as Ouarzazate, Errachidia, and Midelt, assisting Moroccan policymakers in developing strategies to promote and plan future projects.

- Through **Chapter IV**, a multi-objective optimization is carried out at the level of the solar field layout to configure an optimal SDS power plant. Meteorological hourly data from two distinct locations have been considered to simulate the technical and economical performances of 10 MW SDS power plant. It was put in evidence that optimal solar field layout arrangement must satisfy simultaneously a high energy performance with an affordable cost. Two main energy and economic conflicting objective functions were considered and the main goal was to address the trade-off between the annual Capacity Factor and the Total Cost of Site Improvements. Multi-objective optimization approach using Elitist Non-Dominated Sorting Genetic Algorithm (NSGA-II) has been performed to extract the optimum combination that ensures the best compromise between the two objective functions. Pareto Frontier was identified accordingly and final optimal solution was determined using a decision-making method (TOPSIS). Thereafter, a sensitivity analysis considering various economical scenarios was conducted to reveal how specific costs can influence the optimum design of the SDS power plant. It was recommended that for more rational exploitation of such CSP technology to conduct more investigation based on multi-criteria objective optimization.
- The last objective was to exhibit the potential of Hybrid Renewable Energy System based on SDS integration to meet the energy demand in residential sector. In this sense, a techno-economic assessment was conducted to evaluate the viability of a HRES powered by a hybrid renewable power generation system to meet the electric and hydrogen loads of a multi-family design buildings located in two distinct geographical sites in Morocco as detailed in **Chapter V.** The residential building is designed under BEopt software and an annual hourly data of the electrical consumption of the modelled building is presented. The hybrid system includes a Solar Dish Stirling (SDS) combined with a Wind Turbine (WT) for power generation, an electrolyzer, a hydrogen storage tank, as well as a battery bank. The novelty

reported in this chapter resides in the replacement of conventional hybrid systems, such as a photovoltaic (PV)/wind assembly, with a SDS/WT system that has the potential to reach greater efficiencies and economic competitiveness. Advanced modelling in the HOMER Pro environment was used to build a simulation that integrates the various energy components of the hybrid system in an effective manner. All the units have were assessed from a technic and economic aspects to minimize the respective design limits and establish the optimal operational parameters. It has been deduced that the implementation of Wind Turbines is more economically viable in Dakhla city due to the great wind energy resource. Alternatively, the integration of SDS seems to be more favourable in Ouarzazate. In addition, the high cost of SDS technology remarkably affect its contribution especially in areas which did not enjoy high solar potential.

Even though this thesis contributed to the assessment and optimization of this promising technology. However, there are many future prospects and challenges that require further investigation to be a good guideline for the solar dish-technology enthusiast:

- There is a growing need for accurate mathematical models to govern cavity design (mainly for material properties and geometry optimization). The developed models are also expected to be experimentally validated.
- Efficient solar dishes need to be of a moderate weight, firmness to wind load, lower costs, and constructed from durable material withstanding external effects (temperature, moisture etc.). This is why a thermo-mechanic analysis and optimization should be carried out to develop low-cost and efficient solar dishes.
- The need for investigations at high-temperature applications for solar dishes can serve other end-use applications. Alternative working fluids such as supercritical CO_2 and nanofluids. Therefore, there is a need for conducting investigations regarding the cost, performance when adopting new alternative working fluids.
- Hybridization of solar dish systems with conventional and renewable sources can offer significant advantages, i.e., biogas and PV-CSP. Modelling and optimizing systems and subsystems are needed to optimize the overall processes, performance, and grid connection, ensuring a low energy cost.
- Furthermore, energy poverty and water scarcity in diverse regions unveil the necessity for seawater desalination. Solar dish desalination techniques could remedy this situation to some extent. Hence, further real experimental studies are needed to

approve the potential in the arid areas. Therefore, hybrid technology will pose a long-term issue for technology providers and researchers.

- Also, using sun light could promote the formation of hydrogen fuel such as H_2 which has enormous potential yet another renewable and sustainable energy source. As such solar dish technology utilizes concentrated solar radiation to obtain hydrogen with no environmentally harmful by-products. Numerical and experimental investigations are thus necessary to study the potential of solar energy to hydrogen via SDS systems.
- Additionally, the integration of thermal storage also has its merits resulting in energy-efficient dish-Stirling systems and reducing the cost per unit of energy. In this context, identification, characterization, compatibility, and cost assessment of various thermal storage options (sensible and latent) should be investigated in future works.
- Finally, more experimental studies would serve to better understanding and improving the SDS operation and undoubtedly lead to generating heat and power at reasonable costs, which would eventually stimulate solar dish technology.

REFERENCES

[1] L. Aljerf, “Reduction of gas emission resulting from thermal ceramic manufacturing processes through development of industrial conditions,” *Sci. J. King Faisal Univ.*, vol. 17, no. 1, pp. 1–10, 2016.

[2] J. Byrne, K. Hughes, W. Rickerson, and L. Kurdgelashvili, “American policy conflict in the greenhouse: Divergent trends in federal, regional, state, and local green energy and climate change policy,” *Energy Policy*, vol. 35, no. 9, pp. 4555–4573, 2007.

[3] L. C. Lau, K. T. Lee, and A. R. Mohamed, “Global warming mitigation and renewable energy policy development from the Kyoto Protocol to the Copenhagen Accord—A comment,” *Renew. Sustain. Energy Rev.*, vol. 16, no. 7, pp. 5280–5284, Sep. 2012, doi: 10.1016/J.RSER.2012.04.006.

[4] S. Kumar, B. Bhattacharyya, and V. K. Gupta, “Present and future energy scenario in India,” *J. Inst. Eng. Ser. B*, vol. 95, no. 3, pp. 247–254, 2014.

[5] M. Shahbaz, B. A. Topcu, S. S. Sarıgül, and X. V. Vo, “The effect of financial development on renewable energy demand: The case of developing countries,” *Renew. Energy*, vol. 178, pp. 1370–1380, 2021.

[6] J. G. J. Olivier, G. Janssens-Maenhout, M. Muntean, and J. Peters, “Trends in global co2 emissions 2016 Report, PBL Netherlands Environmental Assessment Agency, The Hague,” *PBL Publ.*, vol. 2315, 2016.

[7] K. Alkhathlan and M. Javid, “Carbon emissions and oil consumption in Saudi Arabia,” *Renew. Sustain. Energy Rev.*, vol. 48, pp. 105–111, 2015.

[8] F. Adusah-Poku, “Carbon dioxide emissions, urbanization and population: empirical evidence from Sub-Sahran Africa,” *Energy Econ. Lett.*, vol. 3, no. 1, pp. 1–16, 2016.

[9] “IEA – International Energy Agency.” .

[10] R. Duarte, A. Mainar, and J. Sánchez-Chóliz, “The impact of household consumption patterns on emissions in Spain,” *Energy Econ.*, vol. 32, no. 1, pp. 176–185, 2010.

[11] O. Edenhofer, *Climate change 2014: mitigation of climate change*, vol. 3. Cambridge

University Press, 2015.

[12] L. Hernández-Callejo, S. Gallardo-Saavedra, and V. Alonso-Gómez, “A review of photovoltaic systems: Design, operation and maintenance,” *Sol. Energy*, vol. 188, pp. 426–440, 2019.

[13] T. Delise *et al.*, “Technical and economic analysis of a CSP plant presenting a low freezing ternary mixture as storage and transfer fluid,” *Appl. Energy*, vol. 265, p. 114676, 2020, doi: https://doi.org/10.1016/j.apenergy.2020.114676.

[14] D. Azofra, E. Martínez, E. Jiménez, J. Blanco, and J. C. Saenz-Díez, “Comparison of the influence of biomass, solar–thermal and small hydraulic power on the Spanish electricity prices by means of artificial intelligence techniques,” *Appl. Energy*, vol. 121, pp. 28–37, 2014.

[15] E. Greenpeace, “SolarPACES, Solar thermal electricity global outlook 2016,” *Exec. Summ.*, 2016.

[16] M. T. Islam, N. Huda, A. B. Abdullah, and R. Saidur, “A comprehensive review of state-of-the-art concentrating solar power (CSP) technologies: Current status and research trends,” *Renew. Sustain. Energy Rev.*, vol. 91, pp. 987–1018, 2018.

[17] O. Achkari and A. El Fadar, “Latest developments on TES and CSP technologies–Energy and environmental issues, applications and research trends,” *Appl. Therm. Eng.*, vol. 167, p. 114806, 2020.

[18] A. Kassem, K. Al-Haddad, and D. Komljenovic, “Concentrated solar thermal power in Saudi Arabia: Definition and simulation of alternative scenarios,” *Renew. Sustain. Energy Rev.*, vol. 80, pp. 75–91, 2017.

[19] S. A. Kalogirou, “Chapter 10 - Solar Thermal Power Systems,” S. A. B. T.-S. E. E. (Second E. Kalogirou, Ed. Boston: Academic Press, 2014, pp. 541–581.

[20] S. Mihoub, “Design, economic, and environmental assessments of linear Fresnel solar power plants,” *Environ. Prog. Sustain. Energy*, vol. 39, no. 3, p. e13350, 2020.

[21] “Concentrating Solar Power Projects | NREL.” https://solarpaces.nrel.gov/ (accessed Dec. 24, 2021).

[22] E. L. P. da S. Santos, “Dimensionamento e simulação de um sistema de energia solar com concentrador parabólico e motor stirling.”

[23] “Stirling Solar Array - Tooele Army… | American Galvanizers Association.” https://galvanizeit.org/project-gallery/stirling-solar-array-tooele-army-depot (accessed Apr. 03, 2022).

[24] M. T. Islam, S. A. Shahir, T. M. I. Uddin, and A. Z. A. Saifullah, “Current energy scenario and future prospect of renewable energy in Bangladesh,” *Renew. Sustain. Energy Rev.*, vol. 39, pp. 1074–1088, 2014.

[25] Y. Kadri and H. H. Abdallah, “Performance evaluation of a stand-alone solar dish Stirling system for power generation suitable for off-grid rural electrification,” *Energy Convers. Manag.*, vol. 129, pp. 140–156, 2016.

[26] J. Sun, Q. Liu, and H. Hong, “Numerical study of parabolic-trough direct steam generation loop in recirculation mode: characteristics, performance and general operation strategy,” *Energy Convers. Manag.*, vol. 96, pp. 287–302, 2015.

[27] M. A. Qaisrani, J. Wei, and L. A. Khan, “Potential and transition of concentrated solar power: A case study of China,” *Sustain. Energy Technol. Assessments*, vol. 44, p. 101052, 2021.

[28] W. van Sark and B. Corona, “Concentrating solar power,” in *Technological Learning in the Transition to a Low-Carbon Energy System*, Elsevier, 2020, pp. 221–231.

[29] W. B. Stine and R. B. Diver, “A compendium of solar dish/Stirling technology,” 1994.

[30] C. Monné, Y. Bravo, F. Moreno, and M. Munoz, “Analysis of a solar dish–Stirling system with hybridization and thermal storage,” *Int. J. Energy Environ. Eng.*, vol. 5, no. 2, pp. 1–5, 2014.

[31] M. E. Zayed *et al.*, “Performance prediction and techno-economic analysis of solar dish/stirling system for electricity generation,” *Appl. Therm. Eng.*, vol. 164, p. 114427, 2020, doi: https://doi.org/10.1016/j.applthermaleng.2019.114427.

[32] A. Ummadisingu and M. S. Soni, “Concentrating solar power–technology, potential and policy in India,” *Renew. Sustain. energy Rev.*, vol. 15, no. 9, pp. 5169–5175, 2011.

[33] S. Ziuku, L. Seyitini, B. Mapurisa, D. Chikodzi, and K. van Kuijk, “Potential of concentrated solar power (CSP) in Zimbabwe,” *Energy Sustain. Dev.*, vol. 23, pp. 220–227, 2014.

[34] I. Purohit and P. Purohit, “Technical and economic potential of concentrating solar thermal power generation in India,” *Renew. Sustain. Energy Rev.*, vol. 78, pp. 648–667, 2017.

[35] W. H. Stein and R. Buck, “Advanced power cycles for concentrated solar power,” *Sol. Energy*, vol. 152, pp. 91–105, 2017.

[36] B. Belgasim, Y. Aldali, M. J. R. Abdunnabi, G. Hashem, and K. Hossin, “The potential of concentrating solar power (CSP) for electricity generation in Libya,” *Renew. Sustain. energy Rev.*, vol. 90, pp. 1–15, 2018.

[37] G. K. Manikandan, S. Iniyan, and R. Goic, “Enhancing the optical and thermal efficiency of a parabolic trough collector – A review,” *Appl. Energy*, vol. 235, pp. 1524–1540, 2019, doi: https://doi.org/10.1016/j.apenergy.2018.11.048.

[38] A. Mohamad, J. Orfi, and H. Alansary, “Heat losses from parabolic trough solar collectors,” *Int. J. energy Res.*, vol. 38, no. 1, pp. 20–28, 2014.

[39] F. Cavallaro, “Multi-criteria decision aid to assess concentrated solar thermal technologies,” *Renew. Energy*, vol. 34, no. 7, pp. 1678–1685, 2009.

[40] R. Siva Subramanian, G. Kumaresan, R. Palanivel, P. Nishanth kalathil, and B. Nirmal, “Comparative performance analysis of parabolic trough solar collector by varying absorber surface,” *Mater. Today Proc.*, 2020, doi: https://doi.org/10.1016/j.matpr.2020.04.248.

[41] M. Yang, M. A. Moghimi, Y. Zhu, R. Qiao, Y. Wang, and R. A. Taylor, “Optical and thermal performance analysis of a micro parabolic trough collector for building integration,” *Appl. Energy*, vol. 260, p. 114234, 2020, doi: https://doi.org/10.1016/j.apenergy.2019.114234.

[42] A. Colmenar-Santos, E. Palomo-Torrejón, F. Mur-Pérez, and E. Rosales-Asensio, “Thermal desalination potential with parabolic trough collectors and geothermal energy

in the Spanish southeast," *Appl. Energy*, vol. 262, p. 114433, 2020, doi: https://doi.org/10.1016/j.apenergy.2019.114433.

[43] L. S. Mendoza Castellanos, A. L. Galindo Noguera, E. I. Gutiérrez Velásquez, G. E. C. Caballero, E. E. Silva Lora, and V. R. Melian Cobas, "Mathematical modeling of a system composed of parabolic trough solar collectors integrated with a hydraulic energy storage system," *Energy*, vol. 208, p. 118255, 2020, doi: https://doi.org/10.1016/j.energy.2020.118255.

[44] Z.-D. Cheng, Y.-L. He, B.-C. Du, K. Wang, and Q. Liang, "Geometric optimization on optical performance of parabolic trough solar collector systems using particle swarm optimization algorithm," *Appl. Energy*, vol. 148, pp. 282–293, 2015, doi: https://doi.org/10.1016/j.apenergy.2015.03.079.

[45] R. Bader, A. Pedretti, M. Barbato, and A. Steinfeld, "An air-based corrugated cavity-receiver for solar parabolic trough concentrators," *Appl. Energy*, vol. 138, pp. 337–345, 2015, doi: https://doi.org/10.1016/j.apenergy.2014.10.050.

[46] L. Salgado Conrado, A. Rodriguez-Pulido, and G. Calderón, "Thermal performance of parabolic trough solar collectors," *Renew. Sustain. Energy Rev.*, vol. 67, pp. 1345–1359, 2017, doi: https://doi.org/10.1016/j.rser.2016.09.071.

[47] S. A. Makkeh, A. Ahmadi, F. Esmaeilion, and M. A. Ehyaei, "Energy, exergy and exergoeconomic optimization of a cogeneration system integrated with parabolic trough collector-wind turbine with desalination," *J. Clean. Prod.*, vol. 273, p. 123122, 2020, doi: https://doi.org/10.1016/j.jclepro.2020.123122.

[48] M. Babaelahi, E. Mofidipour, and E. Rafat, "Combined Energy-Exergy-Control (CEEC) analysis and multi-objective optimization of parabolic trough solar collector powered steam power plant," *Energy*, vol. 201, p. 117641, 2020, doi: https://doi.org/10.1016/j.energy.2020.117641.

[49] Z. Zhang, J. Sun, L. Wang, and J. J. Wei, "Multiphysics-coupled study of wind load effects on optical performance of parabolic trough collector," *Sol. Energy*, vol. 207, pp. 1078–1087, 2020, doi: https://doi.org/10.1016/j.solener.2020.06.107.

[50] X. Li, H. Chang, C. Duan, Y. Zheng, and S. Shu, "Thermal performance analysis of a

novel linear cavity receiver for parabolic trough solar collectors," *Appl. Energy*, vol. 237, pp. 431–439, 2019, doi: https://doi.org/10.1016/j.apenergy.2019.01.014.

[51] H. Liang, C. Zhu, M. Fan, S. You, H. Zhang, and J. Xia, "Study on the thermal performance of a novel cavity receiver for parabolic trough solar collectors," *Appl. Energy*, vol. 222, pp. 790–798, 2018, doi: https://doi.org/10.1016/j.apenergy.2018.04.030.

[52] E. Bellos and C. Tzivanidis, "Solar concentrating systems and applications in Greece – A critical review," *J. Clean. Prod.*, vol. 272, p. 122855, 2020, doi: https://doi.org/10.1016/j.jclepro.2020.122855.

[53] M. Binotti, M. Astolfi, S. Campanari, G. Manzolini, and P. Silva, "Preliminary assessment of sCO2 cycles for power generation in CSP solar tower plants," *Appl. Energy*, vol. 204, pp. 1007–1017, 2017, doi: https://doi.org/10.1016/j.apenergy.2017.05.121.

[54] T. E. Boukelia, A. Bouraoui, A. Laouafi, S. Djimli, and Y. Kabar, "3E (Energy-Exergy-Economic) comparative study of integrating wet and dry cooling systems in solar tower power plants," *Energy*, vol. 200, p. 117567, 2020, doi: https://doi.org/10.1016/j.energy.2020.117567.

[55] M. A. Abaza, W. M. El-Maghlany, M. Hassab, and F. Abulfotuh, "10 MW Concentrated Solar Power (CSP) plant operated by 100% solar energy: Sizing and techno-economic optimization," *Alexandria Eng. J.*, vol. 59, no. 1, pp. 39–47, 2020, doi: https://doi.org/10.1016/j.aej.2019.12.005.

[56] Y. Filali Baba, H. Ajdad, A. Al Mers, A. Bouatem, B. Bououlid Idrissi, and S. El Alj, "Preliminary cost-effectiveness assessment of a Linear Fresnel Concentrator: Case studies," *Case Stud. Therm. Eng.*, vol. 22, p. 100730, 2020, doi: https://doi.org/10.1016/j.csite.2020.100730.

[57] E. Bellos, "Progress in the design and the applications of linear Fresnel reflectors – A critical review," *Therm. Sci. Eng. Prog.*, vol. 10, pp. 112–137, 2019, doi: https://doi.org/10.1016/j.tsep.2019.01.014.

[58] C. Bayón-Cueli, A. Barbón, L. Bayón, and N. Barbón, "A cost-energy based

methodology for small-scale linear Fresnel reflectors on flat roofs of urban buildings," *Renew. Energy*, vol. 146, pp. 944–959, 2020, doi: https://doi.org/10.1016/j.renene.2019.07.005.

[59] J. D. Nixon and P. A. Davies, "Cost-exergy optimisation of linear Fresnel reflectors," *Sol. Energy*, vol. 86, no. 1, pp. 147–156, 2012, doi: https://doi.org/10.1016/j.solener.2011.09.024.

[60] M. Babu, P. Sekhar Babu, S. S. Raj, and S. Saravanan, "Theoretical design, material study and material selection for compact linear Fresnel reflector concentrating system," *Mater. Today Proc.*, 2020, doi: https://doi.org/10.1016/j.matpr.2020.08.559.

[61] E. M. A. Mokheimer, Y. N. Dabwan, and M. A. Habib, "Optimal integration of solar energy with fossil fuel gas turbine cogeneration plants using three different CSP technologies in Saudi Arabia," *Appl. Energy*, vol. 185, pp. 1268–1280, 2017, doi: https://doi.org/10.1016/j.apenergy.2015.12.029.

[62] M. A. Moghimi, K. J. Craig, and J. P. Meyer, "Optimization of a trapezoidal cavity absorber for the Linear Fresnel Reflector," *Sol. Energy*, vol. 119, pp. 343–361, 2015, doi: https://doi.org/10.1016/j.solener.2015.07.009.

[63] H. H. Sait, J. M. Martinez-Val, R. Abbas, and J. Munoz-Anton, "Fresnel-based modular solar fields for performance/cost optimization in solar thermal power plants: A comparison with parabolic trough collectors," *Appl. Energy*, vol. 141, pp. 175–189, 2015, doi: https://doi.org/10.1016/j.apenergy.2014.11.074.

[64] O. Ogunmodimu and E. C. Okoroigwe, "Concentrating solar power technologies for solar thermal grid electricity in Nigeria: A review," *Renew. Sustain. Energy Rev.*, vol. 90, pp. 104–119, 2018.

[65] U. R. Singh and A. Kumar, "Review on solar Stirling engine: Development and performance," *Therm. Sci. Eng. Prog.*, vol. 8, pp. 244–256, 2018, doi: https://doi.org/10.1016/j.tsep.2018.08.016.

[66] M. E. Zayed *et al.*, "Performance augmentation of flat plate solar water collector using phase change materials and nanocomposite phase change materials: A review," *Process Saf. Environ. Prot.*, vol. 128, pp. 135–157, 2019, doi:

https://doi.org/10.1016/j.psep.2019.06.002.

[67] M. Abbas, B. Boumeddane, N. Said, and A. Chikouche, “Dish Stirling technology: A 100 MW solar power plant using hydrogen for Algeria,” *Int. J. Hydrogen Energy*, vol. 36, no. 7, pp. 4305–4314, 2011, doi: https://doi.org/10.1016/j.ijhydene.2010.12.114.

[68] L. Geok Pheng, R. Affandi, M. R. Ab Ghani, C. K. Gan, and J. Zanariah, “Stirling Engine Technology for Parabolic Dish-Stirling System based on Concentrating Solar Power (CSP),” in *Applied Mechanics and Materials*, 2015, vol. 785, pp. 576–580.

[69] A. B. Awan, M. Zubair, Z. A. Memon, N. Ghalleb, and I. Tlili, “Comparative analysis of dish Stirling engine and photovoltaic technologies: Energy and economic perspective,” *Sustain. Energy Technol. Assessments*, vol. 44, p. 101028, 2021.

[70] J. Khan and M. H. Arsalan, “Solar power technologies for sustainable electricity generation–A review,” *Renew. Sustain. Energy Rev.*, vol. 55, pp. 414–425, 2016.

[71] U. Desideri, F. Zepparelli, V. Morettini, and E. Garroni, “Comparative analysis of concentrating solar power and photovoltaic technologies: technical and environmental evaluations,” *Appl. Energy*, vol. 102, pp. 765–784, 2013.

[72] R. Affandi, M. R. Ab Ghani, C. K. Ghan, and L. G. Pheng, “The impact of the solar irradiation, collector and the receiver to the receiver losses in parabolic dish system,” *Procedia-Social Behav. Sci.*, vol. 195, pp. 2382–2390, 2015.

[73] A. C. Ferreira, J. Silva, S. Teixeira, J. C. Teixeira, and S. A. Nebra, “Assessment of the Stirling engine performance comparing two renewable energy sources: Solar energy and biomass,” *Renew. Energy*, 2020.

[74] R. Vasu and F. B. Ismail, “Design and implementation of solar powered stirling engines,” in *AIP Conference Proceedings*, 2018, vol. 2035, no. 1, p. 40002.

[75] A. Z. Hafez, A. Soliman, K. A. El-Metwally, and I. M. Ismail, “Design analysis factors and specifications of solar dish technologies for different systems and applications,” *Renew. Sustain. Energy Rev.*, vol. 67, pp. 1019–1036, 2017, doi: https://doi.org/10.1016/j.rser.2016.09.077.

[76] J. Coventry and C. Andraka, “Dish systems for CSP,” *Sol. Energy*, vol. 152, pp. 140–

170, 2017, doi: https://doi.org/10.1016/j.solener.2017.02.056.

[77] M. E. Zayed, J. Zhao, A. H. Elsheikh, W. Li, S. Sadek, and M. M. Aboelmaaref, "A comprehensive review on Dish/Stirling concentrated solar power systems: Design, optical and geometrical analyses, thermal performance assessment, and applications," *J. Clean. Prod.*, p. 124664, 2020.

[78] G. Xiao, T. Yang, D. Ni, K. Cen, and M. Ni, "A model-based approach for optical performance assessment and optimization of a solar dish," *Renew. Energy*, vol. 100, pp. 103–113, 2017.

[79] J. Igo and C. E. Andraka, "Solar dish field system model for spacing optimization," in *Energy Sustainability*, 2007, vol. 47977, pp. 981–987.

[80] J. Xu *et al.*, "Dish layouts analysis method for concentrative solar power plant," *Springerplus*, vol. 5, no. 1, p. 1850, 2016.

[81] K. S. Reddy and G. Veershetty, "Viability analysis of solar parabolic dish stand-alone power plant for Indian conditions," *Appl. Energy*, vol. 102, pp. 908–922, 2013.

[82] J. Cumpston and J. D. Pye, "Optimisation of paraboloidal dish fields for direct-steam generation," in *Energy Sustainability*, 2015, vol. 56840, p. V001T05A024.

[83] F. Dähler, G. Ambrosetti, and A. Steinfeld, "Optimal solar dish field layouts for maximum collection and shading efficiencies," *Sol. Energy*, vol. 144, pp. 286–294, 2017.

[84] P. D. Malali, S. K. Chaturvedi, and R. Agarwala, "Effects of circumsolar radiation on the optimal performance of a Stirling heat engine coupled with a parabolic dish solar collector," *Appl. Therm. Eng.*, vol. 159, p. 113961, 2019, doi: https://doi.org/10.1016/j.applthermaleng.2019.113961.

[85] J. Yan, Z. Cheng, and Y. Peng, "Effect of tracking error of double-axis tracking device on the optical performance of solar dish concentrator," *Int. J. Photoenergy*, vol. 2018, 2018.

[86] A. Buscemi, V. Lo Brano, C. Chiaruzzi, G. Ciulla, and C. Kalogeri, "A validated energy model of a solar dish-Stirling system considering the cleanliness of mirrors,"

Appl. Energy, vol. 260, p. 114378, 2020, doi: https://doi.org/10.1016/j.apenergy.2019.114378.

[87] L. S. Mendoza Castellanos, G. E. Carrillo Caballero, V. R. Melian Cobas, E. E. Silva Lora, and A. M. Martinez Reyes, "Mathematical modeling of the geometrical sizing and thermal performance of a Dish/Stirling system for power generation," *Renew. Energy*, vol. 107, pp. 23–35, 2017, doi: https://doi.org/10.1016/j.renene.2017.01.020.

[88] M. E. Zayed, J. Zhao, A. H. Elsheikh, Z. Zhao, S. Zhong, and A. E. Kabeel, "Comprehensive parametric analysis, design and performance assessment of a solar dish/Stirling system," *Process Saf. Environ. Prot.*, 2020, doi: https://doi.org/10.1016/j.psep.2020.09.007.

[89] A. Z. Hafez, A. Soliman, K. A. El-Metwally, and I. M. Ismail, "Solar parabolic dish Stirling engine system design, simulation, and thermal analysis," *Energy Convers. Manag.*, vol. 126, pp. 60–75, 2016, doi: https://doi.org/10.1016/j.enconman.2016.07.067.

[90] F. Cavallaro, E. K. Zavadskas, D. Streimikiene, and A. Mardani, "Assessment of concentrated solar power (CSP) technologies based on a modified intuitionistic fuzzy topsis and trigonometric entropy weights," *Technol. Forecast. Soc. Change*, vol. 140, pp. 258–270, 2019.

[91] N. Bushra and T. Hartmann, "A review of state-of-the-art reflective two-stage solar concentrators: Technology categorization and research trends," *Renew. Sustain. Energy Rev.*, vol. 114, p. 109307, 2019.

[92] H. Hijazi, O. Mokhiamar, and O. Elsamni, "Mechanical design of a low cost parabolic solar dish concentrator," *Alexandria Eng. J.*, vol. 55, no. 1, pp. 1–11, 2016.

[93] A. C. Ferreira, S. Teixeira, J. C. Teixeira, and L. B. Martins, "Design optimization of a solar dish collector for its application with stirling engines," in *ASME international mechanical engineering congress and exposition*, 2015, vol. 57434, p. V06AT07A033.

[94] M. Schmitz, G. Ambrosetti, T. Cooper, and A. Steinfeld, "On-sun optical characterization of a solar dish concentrator based on elliptical vacuum membrane facets," *Sol. Energy*, vol. 153, pp. 732–743, 2017.

[95] A. Buscemi, S. Guarino, G. Ciulla, and V. Lo Brano, “A methodology for optimisation of solar dish-Stirling systems size, based on the local frequency distribution of direct normal irradiance,” *Appl. Energy*, vol. 303, p. 117681, 2021.

[96] A. Basem, M. Moawed, M. H. Abbood, and W. M. El-Maghlany, “The Energy and Exergy Analysis of a Combined Parabolic Solar Dish - Steam Power Plant,” *Renew. Energy Focus*, 2022, doi: 10.1016/j.ref.2022.01.003.

[97] F. Liu, K. Wu, Z. Rao, and Y. Peng, “Spatial layouts and absorbing surface design of heater tube arrays of direct-illumination receiver used in high power dish/stirling system,” *Energy*, vol. 188, p. 116026, 2019, doi: https://doi.org/10.1016/j.energy.2019.116026.

[98] A. Mohammadnia, B. M. Ziapour, F. Sedaghati, L. Rosendahl, and A. Rezania, “Utilizing thermoelectric generator as cavity temperature controller for temperature management in dish-Stirling engine,” *Appl. Therm. Eng.*, vol. 165, p. 114568, 2020, doi: https://doi.org/10.1016/j.applthermaleng.2019.114568.

[99] S. Pavlovic, R. Loni, E. Bellos, D. Vasiljević, G. Najafi, and A. Kasaeian, “Comparative study of spiral and conical cavity receivers for a solar dish collector,” *Energy Convers. Manag.*, vol. 178, pp. 111–122, 2018, doi: https://doi.org/10.1016/j.enconman.2018.10.030.

[100] M. Tharun, S. R. Navin, K. Arjun Singh, A. Sampathkumar, and S. K. Natarajan, “Numerical Comparison of Elliptical and Conical Cavity Receiver of Solar Parabolic Dish Collector System,” in *Advances in Mechanical and Materials Technology*, Springer, 2022, pp. 607–618.

[101] J. Garrido, L. Aichmayer, A. Abou-Taouk, and B. Laumert, “Experimental and numerical performance analyses of Dish-Stirling cavity receivers: Radiative property study and design,” *Energy*, vol. 169, pp. 478–488, 2019, doi: https://doi.org/10.1016/j.energy.2018.12.033.

[102] A. M. Daabo, S. Mahmoud, and R. K. Al-Dadah, “The effect of receiver geometry on the optical performance of a small-scale solar cavity receiver for parabolic dish applications,” *Energy*, vol. 114, pp. 513–525, 2016.

[103] T. Hussain, M. D. Islam, I. Kubo, and T. Watanabe, “Study of heat transfer through a cavity receiver for a solar powered advanced Stirling engine generator,” *Appl. Therm. Eng.*, vol. 104, pp. 751–757, 2016.

[104] S. Yang, J. Wang, P. D. Lund, S. Wang, and C. Jiang, “Reducing convective heat losses in solar dish cavity receivers through a modified air-curtain system,” *Sol. Energy*, vol. 166, pp. 50–58, 2018.

[105] J. Yan, Z. Cheng, and Y. Peng, “Effects of geometrical parameters of a dish concentrator on the optical performance of a cavity receiver in a solar dish-Stirling system,” *Int. J. Energy Res.*, vol. 42, no. 6, pp. 2152–2168, 2018.

[106] J. Garrido, L. Aichmayer, A. Abou-Taouk, and B. Laumert, “Experimental and numerical performance analyses of a Dish-Stirling cavity receiver: Geometry and operating temperature studies,” *Sol. Energy*, vol. 170, pp. 913–923, 2018, doi: https://doi.org/10.1016/j.solener.2018.06.031.

[107] J.-Q. Li, J.-T. Kwon, and S.-J. Jang, “The Power and Efficiency Analyses of the Cylindrical Cavity Receiver on the Solar Stirling Engine,” *Energies*, vol. 13, no. 21, p. 5798, 2020.

[108] R. Gil, C. Monné, N. Bernal, M. Muñoz, and F. Moreno, “Thermal model of a dish stirling cavity-receiver,” *Energies*, vol. 8, no. 2, pp. 1042–1057, 2015.

[109] C. Zou, Y. Zhang, Q. Falcoz, P. Neveu, J. Li, and C. Zhang, “Thermal modeling of a pressurized air cavity receiver for solar dish Stirling system,” in *AIP Conference Proceedings*, 2017, vol. 1850, no. 1, p. 30053.

[110] H. Allouhi, A. Allouhi, A. Bentamy, S. Zafar, and A. Jamil, “Solar Dish Stirling technology for sustainable power generation in Southern Morocco: 4-E analysis,” *Sustain. Energy Technol. Assessments*, vol. 52, p. 102065, 2022.

[111] M. Chandrashekara and A. Yadav, “An experimental study of the effect of exfoliated graphite solar coating with a sensible heat storage and Scheffler dish for desalination,” *Appl. Therm. Eng.*, vol. 123, pp. 111–122, 2017.

[112] R. Loni *et al.*, “Research and review study of solar dish concentrators with different

nanofluids and different shapes of cavity receiver: Experimental tests," *Renew. Energy*, vol. 145, pp. 783–804, 2020.

[113] V. Kumar and A. Yadav, "Experimental investigation of parabolic dish concentrator with various sizes of receiver," *Mater. Today Proc.*, vol. 44, pp. 4966–4971, 2021.

[114] R. al Loni, E. A. Asli-Ardeh, B. Ghobadian, A. B. Kasaeian, and S. Gorjian, "Thermodynamic analysis of a solar dish receiver using different nanofluids," *Energy*, vol. 133, pp. 749–760, 2017.

[115] S. Pavlovic, E. Bellos, and R. Loni, "Exergetic investigation of a solar dish collector with smooth and corrugated spiral absorber operating with various nanofluids," *J. Clean. Prod.*, vol. 174, pp. 1147–1160, 2018.

[116] R. Loni, S. Pavlovic, E. Bellos, C. Tzivanidis, and E. A. Asli-Ardeh, "Thermal and exergy performance of a nanofluid-based solar dish collector with spiral cavity receiver," *Appl. Therm. Eng.*, vol. 135, pp. 206–217, 2018.

[117] R. Loni, E. A. Asli-Ardeh, B. Ghobadian, and A. Kasaeian, "Experimental study of carbon nano tube/oil nanofluid in dish concentrator using a cylindrical cavity receiver: Outdoor tests," *Energy Convers. Manag.*, vol. 165, pp. 593–601, 2018.

[118] D. R. Rajendran, E. G. Sundaram, and P. Jawahar, "Experimental studies on the effect of enhanced thermal conductivity of SiC+ water nanofluid in the performance of small scale solar parabolic dish receiver," *Int. J. Nanosci.*, vol. 17, no. 01n02, p. 1760025, 2018.

[119] J. N. Pakhare, H. Pandey, M. Selvam, and C. P. Jawahar, "Experimental performance evaluation of a parabolic solar dish collector with nanofluid," in *Concentrated Solar Thermal Energy Technologies*, Springer, 2018, pp. 115–123.

[120] J. Buongiorno and D. Venerus, "The international nanofluid property benchmark exercise," *Int. J. Heat Fluid Flow*, vol. 31, no. 2, pp. 246–247, 2010.

[121] J. Buongiorno *et al.*, "A benchmark study on the thermal conductivity of nanofluids," *J. Appl. Phys.*, vol. 106, no. 9, p. 94312, 2009.

[122] D. C. Venerus *et al.*, "Viscosity measurements on colloidal dispersions (nanofluids) for

heat transfer applications," *Appl. Rheol.*, vol. 20, no. 4, 2010.

[123] A. Kasaeian, A. Kouravand, M. A. V. Rad, S. Maniee, and F. Pourfayaz, "Cavity receivers in solar dish collectors: A geometric overview," *Renew. Energy*, vol. 169, pp. 53–79, 2021.

[124] F. Ahmed, H. Hulin, and A. M. Khan, "Numerical modeling and optimization of beta-type Stirling engine," *Appl. Therm. Eng.*, vol. 149, pp. 385–400, 2019.

[125] G. Ding, W. Chen, T. Zheng, Y. Li, and Y. Ji, "Volume ratio optimization of Stirling engine by using an enhanced model," *Appl. Therm. Eng.*, vol. 140, pp. 615–621, 2018.

[126] D. Dai, F. Yuan, R. Long, Z. Liu, and W. Liu, "Performance analysis and multi-objective optimization of a Stirling engine based on MOPSOCD," *Int. J. Therm. Sci.*, vol. 124, pp. 399–406, 2018.

[127] G. Xiao *et al.*, "An approach to combine the second-order and third-order analysis methods for optimization of a Stirling engine," *Energy Convers. Manag.*, vol. 165, pp. 447–458, 2018.

[128] R. V Rao, K. C. More, L. S. Coelho, and V. C. Mariani, "Multi-objective optimization of the Stirling heat engine through self-adaptive Jaya algorithm," *J. Renew. Sustain. Energy*, vol. 9, no. 3, p. 33703, 2017.

[129] A. Rahmati, S. M. Varedi-Koulaei, M. H. Ahmadi, and H. Ahmadi, "Dynamic synthesis of the alpha-type stirling engine based on reducing the output velocity fluctuations using Metaheuristic algorithms," *Energy*, vol. 238, p. 121686, 2022.

[130] H. Jiang, Z. Xi, A. A. Rahman, and X. Zhang, "Prediction of output power with artificial neural network using extended datasets for Stirling engines," *Appl. Energy*, vol. 271, p. 115123, 2020.

[131] A. Abuelyamen and R. Ben-Mansour, "Energy efficiency comparison of Stirling engine types (α, β, and γ) using detailed CFD modeling," *Int. J. Therm. Sci.*, vol. 132, pp. 411–423, 2018.

[132] K. M. Bataineh, "Optimization analysis of solar-powered average temperature Stirling heat engine," *J. Energy South. Africa*, vol. 26, no. 1, pp. 55–66, 2015.

[133] D. J. Shendage, S. B. Kedare, and S. L. Bapat, “Numerical investigations on the Dish–Stirling engine system,” *Int. J. Ambient Energy*, vol. 40, no. 3, pp. 274–284, 2019.

[134] T. Kumaravelu and S. Saadon, “Heat transfer enhancement of a Stirling engine by using fins attachment in an energy recovery system,” *Energy*, vol. 239, p. 121881, 2022.

[135] K. M. Bataineh and M. F. Maqableh, “A new numerical thermodynamic model for a beta-type Stirling engine with a rhombic drive,” *Therm. Sci. Eng. Prog.*, vol. 28, p. 101071, 2022.

[136] C.-H. Cheng, H.-S. Yang, and Y.-H. Tan, “Theoretical model of a α-type four-cylinder double-acting stirling engine based on energy method,” *Energy*, vol. 238, p. 121730, 2022.

[137] S. Zhu *et al.*, “A free-piston Stirling generator integrated with a parabolic trough collector for thermal-to-electric conversion of solar energy,” *Appl. Energy*, vol. 242, pp. 1248–1258, 2019, doi: https://doi.org/10.1016/j.apenergy.2019.03.169.

[138] F. Aksoy and H. Karabulut, “Performance testing of a Fresnel/Stirling micro solar energy conversion system,” *Energy Convers. Manag.*, vol. 75, pp. 629–634, 2013, doi: https://doi.org/10.1016/j.enconman.2013.08.001.

[139] S. Acharya and S. Bhattacharjee, “Stirling engine based solar-thermal power plant with a thermo-chemical storage system,” *Energy Convers. Manag.*, vol. 86, pp. 901–915, 2014, doi: https://doi.org/10.1016/j.enconman.2014.06.030.

[140] M. Majidniya, T. Boileau, B. Rémy, and M. Zandi, “Performance simulation by a nonlinear thermodynamic model for a Free Piston Stirling Engine with a linear generator,” *Appl. Therm. Eng.*, vol. 184, p. 116128, 2021.

[141] X. Lai, M. Yu, R. Long, Z. Liu, and W. Liu, “Dynamic performance analysis and optimization of dish solar Stirling engine based on a modified theoretical model,” *Energy*, vol. 183, pp. 573–583, 2019, doi: https://doi.org/10.1016/j.energy.2019.06.131.

[142] A. S. Nielsen, B. T. York, and B. D. MacDonald, “Stirling engine regenerators: How to

attain over 95% regenerator effectiveness with sub-regenerators and thermal mass ratios," *Appl. Energy*, vol. 253, p. 113557, 2019.

[143] D. D. Dai, F. Yuan, R. Long, Z. C. Liu, and W. Liu, "Imperfect regeneration analysis of Stirling engine caused by temperature differences in regenerator," *Energy Convers. Manag.*, vol. 158, pp. 60–69, 2018.

[144] W. Ye, Z. Yang, and Y. Liu, "Exergy loss analysis of the regenerator in a solar Stirling engine," *Therm. Sci.*, vol. 22, no. Suppl. 2, pp. 729–737, 2018.

[145] M. Chahartaghi and M. Sheykhi, "Energy and exergy analyses of beta-type Stirling engine at different working conditions," *Energy Convers. Manag.*, vol. 169, pp. 279–290, 2018.

[146] T. R. Lessandro, C. P. Bruno, and A. A. Elaine, "Localization study for the implementation of a solar power plant in Brazil using Dish-Stirling systems," *J. Renew. Sustain. Energy*, vol. 12, no. 3, p. 33702, 2020.

[147] O. F. Farsakoglu and A. Alahmad, "Comprehensive Design of Stirling Engine Based Solar Dish Power Plant with Solar Tracking System," *J Electr Electron Syst*, vol. 7, no. 248, pp. 796–2332, 2018.

[148] M. H. Babikir *et al.*, "Simplified Modeling and Simulation of Electricity Production from a Dish/Stirling System," *Int. J. Photoenergy*, vol. 2020, 2020.

[149] Ö. F. Farsakoğlu, N. Aksoy, H. Y. Hasirci, and A. Alahmad, "Design and application of solar dish-gamma type stirling system," in *2018 5th International Conference on Electrical and Electronic Engineering (ICEEE)*, 2018, pp. 242–246.

[150] L. S. Mendoza Castellanos *et al.*, "Experimental analysis and numerical validation of the solar Dish/Stirling system connected to the electric grid," *Renew. Energy*, vol. 135, pp. 259–265, 2019, doi: https://doi.org/10.1016/j.renene.2018.11.095.

[151] K. Mansiri, S. Sukchai, and C. Sirisamphanwong, "Investigations to Conduct a Study about Possibilities to Use Small Scale Solar Dish Stirling Engine System in Thailand," *Energy Procedia*, vol. 56, pp. 367–377, 2014, doi: https://doi.org/10.1016/j.egypro.2014.07.169.

[152] R. S. Moghadam, H. Sayyaadi, and H. Hosseinzade, “Sizing a solar dish Stirling micro-CHP system for residential application in diverse climatic conditions based on 3E analysis,” *Energy Convers. Manag.*, vol. 75, pp. 348–365, 2013, doi: https://doi.org/10.1016/j.enconman.2013.06.008.

[153] M. Vahidi Bidhendi and Y. Abbassi, “Exploring dynamic operation of a solar dish-stirling engine: Validation and implementation of a novel TRNSYS type,” *Sustain. Energy Technol. Assessments*, vol. 40, p. 100765, 2020, doi: https://doi.org/10.1016/j.seta.2020.100765.

[154] D. Barbosa *et al.*, “BIOSTIRLING-4SKA: A cost effective and efficient approach for a new generation of solar dish-Stirling plants based on storage and hybridization; An Energy demo project for Large Scale Infrastructures,” *arXiv Prepr. arXiv1712.03029*, 2017.

[155] K. Sookramoon, P. Bunyawanichakul, and B. Kongtragool, “Experimental Study of a 2-stage Parabolic Dish-Stirling Engine in Thailand,” *Walailak J. Sci. Technol.*, vol. 13, no. 8, pp. 579–594, 2016.

[156] J. Yan, Y. D. Peng, Z. R. Cheng, F. M. Liu, and X. H. Tang, “Design and implementation of a 38 kW dish-Stirling concentrated solar power system,” in *IOP Conf Ser: Earth Environ Sci*, 2017, vol. 93, p. 12052.

[157] E. Gholamalizadeh and J. D. Chung, “Thermal Analysis of the Receiver of a Standalone Pilot Solar Dish–Stirling System,” *Entropy*, vol. 20, no. 6, p. 429, 2018.

[158] R. Affandi, Z. Omar, and M. R. Ab Ghani, “Feasibility of 25kw Parabolic Dish-Stirling Engine Based Concentrating Solar Power under Malaysia Environment,” *Int. J. Eng. Technol.*, vol. 7, no. 4, pp. 3874–3878, 2018.

[159] M. Shahabuddin, M. A. Alim, T. Alam, M. Mofijur, S. F. Ahmed, and G. Perkins, “A critical review on the development and challenges of concentrated solar power technologies,” *Sustain. Energy Technol. Assessments*, vol. 47, p. 101434, 2021.

[160] M. M. Aboelmaaref *et al.*, “Hybrid solar desalination systems driven by parabolic trough and parabolic dish CSP technologies: Technology categorization, thermodynamic performance and economical assessment,” *Energy Convers. Manag.*,

vol. 220, p. 113103, 2020, doi: https://doi.org/10.1016/j.enconman.2020.113103.

[161] D. Kumar and M. Agrawal, “A Review on Development and Applications of Solar Dish Stirling System,” in *Advancement in Materials, Manufacturing and Energy Engineering, Vol. II*, Springer, 2022, pp. 57–70.

[162] A. M. A. Al-Dafaie, M.-E. Dahdolan, and M. A. Al-Nimr, “Utilizing the heat rejected from a solar dish Stirling engine in potable water production,” *Sol. Energy*, vol. 136, pp. 317–326, 2016, doi: https://doi.org/10.1016/j.solener.2016.07.007.

[163] F. Jabari, M. Nazari-heris, B. Mohammadi-ivatloo, S. Asadi, and M. Abapour, “A solar dish Stirling engine combined humidification-dehumidification desalination cycle for cleaner production of cool, pure water, and power in hot and humid regions,” *Sustain. Energy Technol. Assessments*, vol. 37, p. 100642, 2020, doi: https://doi.org/10.1016/j.seta.2020.100642.

[164] M. A. Al-Nimr and W. A. Al-Ammari, “A novel hybrid and interactive solar system consists of Stirling engine/vacuum evaporator/thermoelectric cooler for electricity generation and water distillation,” *Renew. Energy*, vol. 153, pp. 1053–1066, 2020, doi: https://doi.org/10.1016/j.renene.2020.02.072.

[165] E. Açıkkalp, S. Y. Kandemir, and M. H. Ahmadi, “Solar driven stirling engine-chemical heat pump-absorption refrigerator hybrid system as environmental friendly energy system,” *J. Environ. Manage.*, vol. 232, pp. 455–461, 2019.

[166] D. Dai, Z. Liu, F. Yuan, R. Long, and W. Liu, “Finite time thermodynamic analysis of a solar duplex Stirling refrigerator,” *Appl. Therm. Eng.*, vol. 156, pp. 597–605, 2019.

[167] M. I. Al-Amayreh and A. Alahmer, “On improving the efficiency of hybrid solar lighting and thermal system using dual-axis solar tracking system,” *Energy Reports*, vol. 8, pp. 841–847, 2022.

[168] S. Guarino, A. Buscemi, G. Ciulla, M. Bonomolo, and V. Lo Brano, “A dish-stirling solar concentrator coupled to a seasonal thermal energy storage system in the southern mediterranean basin: A cogenerative layout hypothesis,” *Energy Convers. Manag.*, vol. 222, p. 113228, 2020, doi: https://doi.org/10.1016/j.enconman.2020.113228.

[169] O. R. Sandoval, B. C. Caetano, M. U. Borges, J. J. García, and R. M. Valle, "Modelling, simulation and thermal analysis of a solar dish/Stirling system: A case study in Natal, Brazil," *Energy Convers. Manag.*, vol. 181, pp. 189–201, 2019, doi: https://doi.org/10.1016/j.enconman.2018.12.005.

[170] Y. Kadri and H. H. Abdallah, "New grid connected hybrid generation system using wind turbine and solar Dish/Stirling engine," in *2017 International Conference on Green Energy Conversion Systems (GECS)*, 2017, pp. 1–7.

[171] B. Shboul *et al.*, "Design and Techno-economic assessment of a new hybrid system of a solar dish Stirling engine instegrated with a horizontal axis wind turbine for microgrid power generation," *Energy Convers. Manag.*, vol. 245, p. 114587, 2021.

[172] A. Rahman, L. C. Saikia, and N. Sinha, "Automatic generation control of an interconnected two-area hybrid thermal system considering dish-stirling solar thermal and wind turbine system," *Renew. Energy*, vol. 105, pp. 41–54, 2017, doi: https://doi.org/10.1016/j.renene.2016.12.048.

[173] X. Lai, M. Yu, R. Long, Z. Liu, and W. Liu, "Clean and stable utilization of solar energy by integrating dish solar Stirling engine and salinity gradient technology," *Energy*, vol. 182, pp. 802–813, 2019, doi: https://doi.org/10.1016/j.energy.2019.06.082.

[174] A. Yerbury, A. Coote, V. Garaniya, and H. Yu, "Design of a solar Stirling engine for marine and offshore applications," *Int. J. Renew. Energy Technol.*, vol. 7, no. 1, pp. 1–45, 2016.

[175] F. Jabari, S. Nojavan, B. Mohammadi-ivatloo, H. Ghaebi, and H. Mehrjerdi, "Risk-constrained scheduling of solar Stirling engine based industrial continuous heat treatment furnace," *Appl. Therm. Eng.*, vol. 128, pp. 940–955, 2018, doi: https://doi.org/10.1016/j.applthermaleng.2017.09.042.

[176] A. R. Tavakolpour-Saleh and H. Jokar, "Neural network-based control of an intelligent solar Stirling pump," *Energy*, vol. 94, pp. 508–523, 2016.

[177] F. Jabari, M. Nazari-Heris, B. Mohammadi-Ivatloo, S. Asadi, and M. Abapour, "Toward energy-efficient microgrids under summer peak electrical demand integrating

solar dish Stirling heat engine and diesel unit," *J. Energy Manag. Technol.*, vol. 4, no. 3, pp. 23–29, 2020.

[178] R. Beltrán-Chacon, D. Leal-Chavez, D. Sauceda, M. Pellegrini-Cervantes, and M. Borunda, "Design and analysis of a dead volume control for a solar Stirling engine with induction generator," *Energy*, vol. 93, pp. 2593–2603, 2015.

[179] L. Aichmayer, J. Spelling, and B. Laumert, "Preliminary design and analysis of a novel solar receiver for a micro gas-turbine based solar dish system," *Sol. energy*, vol. 114, pp. 378–396, 2015.

[180] G. Gavagnin, D. Sánchez, J. M. Rodríguez, A. Muñoz, and G. S. Martínez, "Economic-Competitiveness of Dish-mGT Solar Power Generators," in *Turbo Expo: Power for Land, Sea, and Air*, 2017, vol. 50831, p. V003T06A024.

[181] L. Aichmayer, J. Spelling, and B. Laumert, "Thermoeconomic analysis of a solar dish micro gas-turbine combined-cycle power plant," *Energy procedia*, vol. 69, pp. 1089–1099, 2015.

[182] W. Wang, G. Ragnolo, L. Aichmayer, T. Strand, and B. Laumert, "Integrated design of a hybrid gas turbine-receiver unit for a solar dish system," *Energy Procedia*, vol. 69, pp. 583–592, 2015.

[183] S. Semprini, D. Sanchez, and A. De Pascale, "Performance analysis of a micro gas turbine and solar dish integrated system under different solar-only and hybrid operating conditions," *Sol. Energy*, vol. 132, pp. 279–293, 2016.

[184] A. Mohammadi and M. Mehrpooya, "Exergy analysis and optimization of an integrated micro gas turbine, compressed air energy storage and solar dish collector process," *J. Clean. Prod.*, vol. 139, pp. 372–383, 2016.

[185] D. Sánchez, M. Rollán, L. García-Rodríguez, and G. S. Martínez, "Solar Desalination Based on Micro Gas Turbines Driven by Parabolic Dish Collectors," *J. Eng. Gas Turbines Power*, vol. 142, no. 3, 2020.

[186] W. Wang, H. Xu, B. Laumert, and T. Strand, "An inverse design method for a cavity receiver used in solar dish Brayton system," *Sol. energy*, vol. 110, pp. 745–755, 2014.

[187] W. G. Le Roux and A. Sciacovelli, “Recuperated solar-dish Brayton cycle using turbocharger and short-term thermal storage,” *Sol. Energy*, vol. 194, pp. 569–580, 2019.

[188] Y. Li, G. Liu, X. Liu, and S. Liao, “Thermodynamic multi-objective optimization of a solar-dish Brayton system based on maximum power output, thermal efficiency and ecological performance,” *Renew. Energy*, vol. 95, pp. 465–473, 2016.

[189] M. S. Khan, M. Abid, H. M. Ali, K. P. Amber, M. A. Bashir, and S. Javed, “Comparative performance assessment of solar dish assisted s-CO2 Brayton cycle using nanofluids,” *Appl. Therm. Eng.*, vol. 148, pp. 295–306, 2019, doi: https://doi.org/10.1016/j.applthermaleng.2018.11.021.

[190] Y. Li, S. Liao, and G. Liu, “Thermo-economic multi-objective optimization for a solar-dish Brayton system using NSGA-II and decision making,” *Int. J. Electr. Power Energy Syst.*, vol. 64, pp. 167–175, 2015.

[191] R. Figaj, M. Szubel, E. Przenzak, and M. Filipowicz, “Feasibility of a small-scale hybrid dish/flat-plate solar collector system as a heat source for an absorption cooling unit,” *Appl. Therm. Eng.*, vol. 163, p. 114399, 2019.

[192] K.-K. Chong, T.-K. Yew, C.-W. Wong, M.-H. Tan, W.-C. Tan, and B.-H. Lim, “Dense-array concentrator photovoltaic prototype using non-imaging dish concentrator and an array of cross compound parabolic concentrators,” *Appl. Energy*, vol. 204, pp. 898–911, 2017.

[193] R. P. Angel, B. M. Coughenour, T. E. Stalcup, and B. Love, “Solar generator with large reflector dishes and concentrator photovoltaic cells in flat arrays.” Google Patents, Aug. 14, 2018.

[194] X. Ju, C. Xu, Y. Hu, X. Han, G. Wei, and X. Du, “A review on the development of photovoltaic/concentrated solar power (PV-CSP) hybrid systems,” *Sol. Energy Mater. Sol. Cells*, vol. 161, pp. 305–327, 2017.

[195] H. Lv *et al.*, “The prototype construction and performance evaluation of dish-type concentrator photovoltaic system,” *Int. J. Low-Carbon Technol.*, vol. 14, no. 2, pp. 294–301, 2019.

[196] S. Shanmugam, M. Eswaramoorthy, and A. R. Veerappan, “Modeling and analysis of a solar parabolic dish thermoelectric generator,” *Energy Sources, Part A Recover. Util. Environ. Eff.*, vol. 36, no. 14, pp. 1531–1539, 2014.

[197] M. Eswaramoorthy and S. Shanmugam, “Solar parabolic dish thermoelectric generator: a technical study,” *Energy Sources, Part A Recover. Util. Environ. Eff.*, vol. 35, no. 5, pp. 487–494, 2013.

[198] V. Verma, K. B. Rana, and S. S. Sharma, “Experimental study and comparative analysis of modified solar paraboloidal dish–thermoelectric generator systems,” *Environ. Sci. Pollut. Res.*, pp. 1–11, 2020.

[199] H. Fan, R. Singh, and A. Akbarzadeh, “Electric power generation from thermoelectric cells using a solar dish concentrator,” *J. Electron. Mater.*, vol. 40, no. 5, pp. 1311–1320, 2011.

[200] S. Shanmugam, A. R. Veerappan, and M. Eswaramoorthy, “An experimental evaluation of energy and exergy efficiency of a solar parabolic dish thermoelectric power generator,” *Energy Sources, Part A Recover. Util. Environ. Eff.*, vol. 36, no. 17, pp. 1865–1870, 2014.

[201] M. Eswararmoorthy and S. Shanmugam, “Thermodynamic analysis of solar parabolic dish thermoelectric generator,” *Int. J. Renew. energy Technol.*, vol. 1, no. 3, pp. 348–360, 2010.

[202] P. Bamroongkhan, C. Lertsatitthanakorn, and S. Soponronnarit, “Experimental performance study of a solar parabolic dish photovoltaic-thermoelectric generator,” *Energy Procedia*, vol. 158, pp. 528–533, 2019.

[203] I. L. Mohammed, “Design and development of a parabolic dish solar water heater,” *Int. J. Eng. Res. Appl.*, vol. 2, no. 1, pp. 822–830, 2012.

[204] A. Bianchini, A. Guzzini, M. Pellegrini, and C. Saccani, “Performance assessment of a solar parabolic dish for domestic use based on experimental measurements,” *Renew. Energy*, vol. 133, pp. 382–392, 2019.

[205] G. Prinsloo, R. Dobson, and A. Mammoli, “Model based design of a novel Stirling

solar micro-cogeneration system with performance and fuel transition analysis for rural African village locations," *Sol. Energy*, vol. 133, pp. 315–330, 2016, doi: https://doi.org/10.1016/j.solener.2016.04.014.

[206] L. A. Andrade, M. A. S. Barrozo, and L. G. M. Vieira, "A study on dynamic heating in solar dish concentrators," *Renew. Energy*, vol. 87, pp. 501–508, 2016.

[207] G. Gavagnin, D. Sánchez, G. S. Martínez, J. M. Rodríguez, and A. Muñoz, "Cost analysis of solar thermal power generators based on parabolic dish and micro gas turbine: Manufacturing, transportation and installation," *Appl. Energy*, vol. 194, pp. 108–122, 2017.

[208] M. Schmitz *et al.*, "A 6-focus high-concentration photovoltaic-thermal dish system," *Sol. Energy*, vol. 155, pp. 445–463, 2017.

[209] L. Gu *et al.*, "Research on a new type of solar dish Stirling cogeneration system based on adjustable receiver and control strategy," *Energy Convers. Manag.*, vol. 249, p. 114836, 2021.

[210] M. Moradi and M. Mehrpooya, "Optimal design and economic analysis of a hybrid solid oxide fuel cell and parabolic solar dish collector, combined cooling, heating and power (CCHP) system used for a large commercial tower," *Energy*, vol. 130, pp. 530–543, 2017.

[211] F. Piadehrouhi, B. Ghorbani, M. Miansari, and M. Mehrpooya, "Development of a new integrated structure for simultaneous generation of power and liquid carbon dioxide using solar dish collectors," *Energy*, vol. 179, pp. 938–959, 2019.

[212] Q. Chen, H. Ai, Y. Zhang, and J. Hou, "Marketization and water resource utilization efficiency in China," *Sustain. Comput. Informatics Syst.*, vol. 22, pp. 32–43, 2019.

[213] G. O. Prado, L. G. M. Vieira, and J. J. R. Damasceno, "Solar dish concentrator for desalting water," *Sol. Energy*, vol. 136, pp. 659–667, 2016.

[214] M. Javidmehr, F. Joda, and A. Mohammadi, "Thermodynamic and economic analyses and optimization of a multi-generation system composed by a compressed air storage, solar dish collector, micro gas turbine, organic Rankine cycle, and desalination

system," *Energy Convers. Manag.*, vol. 168, pp. 467–481, 2018.

[215] K. Srithar, T. Rajaseenivasan, N. Karthik, M. Periyannan, and M. Gowtham, "Stand alone triple basin solar desalination system with cover cooling and parabolic dish concentrator," *Renew. energy*, vol. 90, pp. 157–165, 2016.

[216] A. Rafiei, A. S. Alsagri, S. Mahadzir, R. Loni, G. Najafi, and A. Kasaeian, "Thermal analysis of a hybrid solar desalination system using various shapes of cavity receiver: cubical, cylindrical, and hemispherical," *Energy Convers. Manag.*, vol. 198, p. 111861, 2019.

[217] M. Bahrami, V. M. Avargani, and M. Bonyadi, "Comprehensive experimental and theoretical study of a novel still coupled to a solar dish concentrator," *Appl. Therm. Eng.*, vol. 151, pp. 77–89, 2019.

[218] A. E. Kabeel, M. M. K. Dawood, K. Ramzy, T. Nabil, and B. Elnaghi, "Enhancement of single solar still integrated with solar dishes: An experimental approach," *Energy Convers. Manag.*, vol. 196, pp. 165–174, 2019.

[219] A. O. Nayak, M. Gowtham, R. Vinod, and G. Ramkumar, "Analysis of PCM material in thermal energy storage system," *Int. J. Environ. Sci. Dev.*, vol. 2, no. 6, p. 437, 2011.

[220] M. Mehrpooya, B. Ghorbani, and M. Sadeghzadeh, "Hybrid solar parabolic dish power plant and high-temperature phase change material energy storage system," *Int. J. Energy Res.*, vol. 43, no. 10, pp. 5405–5420, 2019.

[221] G. Muthu, S. Thulasi, V. Dhinakaran, and T. Mothilal, "Performance of solar parabolic dish thermoelectric generator with PCM," *Mater. Today Proc.*, 2020, doi: https://doi.org/10.1016/j.matpr.2020.06.123.

[222] C. E. Andraka, A. M. Kruizenga, B. A. Hernandez-Sanchez, and E. N. Coker, "Metallic Phase Change Material Thermal Storage for Dish Stirling," *Energy Procedia*, vol. 69, pp. 726–736, 2015, doi: https://doi.org/10.1016/j.egypro.2015.03.083.

[223] C. E. Andraka, "Dish Stirling Advanced Latent Storage Feasibility," *Energy Procedia*, vol. 49, pp. 684–693, 2014, doi: https://doi.org/10.1016/j.egypro.2014.03.074.

[224] B. Saleh *et al.*, "Investigating the performance of dish solar distiller with phase change

material mixed with Al2O3 nanoparticles under different water depths," *Environ. Sci. Pollut. Res.*, pp. 1–12, 2022.

[225] A. C. Ferreira, M. L. Nunes, J. C. F. Teixeira, L. A. S. B. Martins, S. F. C. F. Teixeira, and S. A. Nebra, "Design of a solar dish Stirling cogeneration system: Application of a multi-objective optimization approach," *Appl. Therm. Eng.*, vol. 123, pp. 646–657, 2017, doi: https://doi.org/10.1016/j.applthermaleng.2017.05.127.

[226] M. H. Ahmadi, A. H. Mohammadi, S. Dehghani, and M. A. Barranco-Jiménez, "Multi-objective thermodynamic-based optimization of output power of Solar Dish-Stirling engine by implementing an evolutionary algorithm," *Energy Convers. Manag.*, vol. 75, pp. 438–445, 2013, doi: https://doi.org/10.1016/j.enconman.2013.06.030.

[227] G. E. Carrillo Caballero *et al.*, "Optimization of a Dish Stirling system working with DIR-type receiver using multi-objective techniques," *Appl. Energy*, vol. 204, pp. 271–286, 2017, doi: https://doi.org/10.1016/j.apenergy.2017.07.053.

[228] A. Khosravi, S. Syri, J. J. G. Pabon, O. R. Sandoval, B. C. Caetano, and M. H. Barrientos, "Energy modeling of a solar dish/Stirling by artificial intelligence approach," *Energy Convers. Manag.*, vol. 199, p. 112021, 2019, doi: https://doi.org/10.1016/j.enconman.2019.112021.

[229] M. H. Ahmadi, H. Sayyaadi, A. H. Mohammadi, and M. A. Barranco-Jimenez, "Thermo-economic multi-objective optimization of solar dish-Stirling engine by implementing evolutionary algorithm," *Energy Convers. Manag.*, vol. 73, pp. 370–380, 2013, doi: https://doi.org/10.1016/j.enconman.2013.05.031.

[230] R. V. Rao, H. S. Keesari, P. Oclon, and J. Taler, "Improved multi-objective Jaya optimization algorithm for a solar dish Stirling engine," *J. Renew. Sustain. Energy*, vol. 11, no. 2, p. 25903, 2019.

[231] M. R. Nazemzadegan, A. Kasaeian, S. Toghyani, M. H. Ahmadi, R. Saidur, and T. Ming, "Multi-objective optimization in a finite time thermodynamic method for dish-Stirling by branch and bound method and MOPSO algorithm," *Front. Energy*, pp. 1–17, 2018.

[232] M. E. Zayed, J. Zhao, A. H. Elsheikh, W. Li, and M. Abd Elaziz, "Optimal design

parameters and performance optimization of thermodynamically balanced dish/Stirling concentrated solar power system using multi-objective particle swarm optimization," *Appl. Therm. Eng.*, vol. 178, p. 115539, 2020.

[233] A. C. Ferreira, M. L. Nunes, J. C. F. Teixeira, L. A. S. B. Martins, and S. F. C. F. Teixeira, "Thermodynamic and economic optimization of a solar-powered Stirling engine for micro-cogeneration purposes," *Energy*, vol. 111, pp. 1–17, 2016.

[234] M. Sameti, M. A. Jokar, and F. R. Astaraei, "Prediction of solar Stirling power generation in smart grid by GA-ANN model," *Int. J. Comput. Appl. Technol.*, vol. 55, no. 2, pp. 147–157, 2017.

[235] S. D. Nazemi and M. Boroushaki, "Design, Analysis and Optimization of a Solar Dish/Stirling System.," *Int. J. Renew. Energy Dev.*, vol. 5, no. 1, 2016.

[236] M. E. Zayed *et al.*, "Predicting the performance of solar dish Stirling power plant using a hybrid random vector functional link/chimp optimization model," *Sol. Energy*, vol. 222, pp. 1–17, 2021.

[237] I. Hussain, D. C. Das, and N. Sinha, "Reactive power performance analysis of dish–Stirling solar thermal–diesel hybrid energy system," *IET Renew. Power Gener.*, vol. 11, no. 6, pp. 750–762, 2017.

[238] S. Ranjan, D. C. Das, N. Sinha, A. Latif, S. M. S. Hussain, and T. S. Ustun, "Voltage stability assessment of isolated hybrid dish-stirling solar thermal-diesel microgrid with STATCOM using mine blast algorithm," *Electr. Power Syst. Res.*, vol. 196, p. 107239, 2021.

[239] R. Kumar and N. Sinha, "Modeling and control of dish-stirling solar thermal integrated with PMDC generator optimized by meta-heuristic approach," *IEEE Access*, vol. 8, pp. 26343–26355, 2020.

[240] Y. Li, B. Xiong, Y. Su, J. Tang, and Z. Leng, "Particle swarm optimization-based power and temperature control scheme for grid-connected DFIG-based dish-Stirling solar-thermal system," *Energies*, vol. 12, no. 7, p. 1300, 2019.

[241] E. Gholamalizadeh and J. D. Chung, "Exergy analysis of a pilot parabolic solar dish-

Stirling system," *Entropy*, vol. 19, no. 10, p. 509, 2017.

[242] R. V Rao, K. C. More, J. Taler, and P. Ocłoń, "Optimal design of Stirling heat engine using an advanced optimization algorithm," *Sādhanā*, vol. 41, no. 11, pp. 1321–1331, 2016.

[243] M. Hooshang, R. A. Moghadam, S. A. Nia, and M. T. Masouleh, "Optimization of Stirling engine design parameters using neural networks," *Renew. Energy*, vol. 74, pp. 855–866, 2015.

[244] V. Patel, V. Savsani, and A. Mudgal, "Many-objective thermodynamic optimization of Stirling heat engine," *Energy*, vol. 125, pp. 629–642, 2017.

[245] S. Toghyani, M. H. Ahmadi, A. Kasaeian, and A. H. Mohammadi, "Artificial neural network, ANN-PSO and ANN-ICA for modelling the Stirling engine," *Int. J. Ambient Energy*, vol. 37, no. 5, pp. 456–468, 2016.

[246] H. Allouhi, A. Allouhi, and A. Jamil, "Multi-objective optimization of a CSP-based dish Stirling field layout using Genetic Algorithm and TOPSIS method: Case studies in Ouarzazate and Madrid," *Energy Convers. Manag.*, vol. 254, p. 115220, 2022.

[247] Y. Cui, Z. Geng, Q. Zhu, and Y. Han, "Multi-objective optimization methods and application in energy saving," *Energy*, vol. 125, pp. 681–704, 2017.

[248] G. Liu *et al.*, "Effects of different sizes and dispatch strategies of thermal energy storage on solar energy usage ability of solar thermal power plant," *Appl. Therm. Eng.*, vol. 156, pp. 14–22, 2019.

[249] N. Kincaid, G. Mungas, N. Kramer, M. Wagner, and G. Zhu, "An optical performance comparison of three concentrating solar power collector designs in linear Fresnel, parabolic trough, and central receiver," *Appl. Energy*, vol. 231, pp. 1109–1121, 2018, doi: https://doi.org/10.1016/j.apenergy.2018.09.153.

[250] A. E. Elmohlawy, V. F. Ochkov, and B. I. Kazandzhan, "Thermal performance analysis of a concentrated solar power system (CSP) integrated with natural gas combined cycle (NGCC) power plant," *Case Stud. Therm. Eng.*, vol. 14, p. 100458, 2019, doi: https://doi.org/10.1016/j.csite.2019.100458.

[251] M. E. Zayed, J. Zhao, A. H. Elsheikh, W. Li, S. Sadek, and M. M. Aboelmaaref, “A comprehensive review on Dish/Stirling concentrated solar power systems: Design, optical and geometrical analyses, thermal performance assessment, and applications,” *J. Clean. Prod.*, vol. 283, p. 124664, 2021.

[252] S. Pavlovic, E. Bellos, and Z. Said, “Cogeneration system driven by solar dish concentrators,” *Environ. Prog. Sustain. Energy*, p. e13644, 2021.

[253] A. Aldabesh, M. Hussain, N. Khan, A. Riahi, S. U. Khan, and I. Tlili, “Thermal variable conductivity features in Buongiorno nanofluid model between parallel stretching disks: Improving energy system efficiency,” *Case Stud. Therm. Eng.*, vol. 23, p. 100820, 2021.

[254] S. U. Khan, K. Al-Khaled, A. Aldabesh, M. Awais, and I. Tlili, “Bioconvection flow in accelerated couple stress nanoparticles with activation energy: bio-fuel applications,” *Sci. Rep.*, vol. 11, no. 1, pp. 1–15, 2021.

[255] L. Mastropasqua, I. Pecenati, A. Giostri, and S. Campanari, “Solar hydrogen production: Techno-economic analysis of a parabolic dish-supported high-temperature electrolysis system,” *Appl. Energy*, vol. 261, p. 114392, 2020, doi: https://doi.org/10.1016/j.apenergy.2019.114392.

[256] E. Jiaqiang *et al.*, “Harmonic response analysis of a large dish solar thermal power generation system with wind-induced vibration,” *Sol. Energy*, vol. 181, pp. 116–129, 2019.

[257] H. Zuo *et al.*, “Catastrophic analysis on the stability of a large dish solar thermal power generation system with wind-induced vibration,” *Sol. Energy*, vol. 183, pp. 40–49, 2019.

[258] V. Siva Reddy, S. C. Kaushik, and S. K. Tyagi, “Exergetic analysis and performance evaluation of parabolic dish Stirling engine solar power plant,” *Int. J. Energy Res.*, vol. 37, no. 11, pp. 1287–1301, 2013.

[259] S. Abdelhady, “Performance and cost evaluation of solar dish power plant: Sensitivity analysis of levelized cost of electricity (LCOE) and net present value (NPV),” *Renew. Energy*, vol. 168, pp. 332–342, 2021.

[260] W. Reinalter *et al.*, “Detailed performance analysis of a 10kW dish/stirling system,” *J. Sol. Energy Eng.*, vol. 130, no. 1, 2008.

[261] T. Mancini *et al.*, “Dish-Stirling systems: An overview of development and status,” *J. Sol. Energy Eng.*, vol. 125, no. 2, pp. 135–151, 2003.

[262] E. Sproul, K. Chavez, and J. Yellowhair, “The development of the heliostat focusing and canting enhancement technique: an optical heliostat alignment tool for the national solar thermal test facility,” in *Energy Sustainability*, 2011, vol. 54686, pp. 611–619.

[263] N. Blair *et al.*, “System advisor model, sam 2014.1. 14: General description,” *NREL Rep. No. TP-6A20-61019, Natl. Renew. Energy Lab. Golden, CO*, no. February, p. 13, 2014, doi: 10.2172/1126294.

[264] P. R. Fraser, *Stirling dish system performance prediction model*. Madison, 2008.

[265] D. B. Osborn, “Generalized shading analysis for paraboloidal collector fields,” in *American Society of Mechanical Engineers, Energy Technology Conference and Exhibition*, 1980.

[266] W. B. Stine, “Cavity receiver convection heat loss,” in *Proc. of the International Solar Energy Society. Solar World Congress*, 1989, vol. 1318.

[267] R. Y. Ma, “Wind effects on convective heat loss from a cavity receiver for a parabolic concentrating solar collector,” Sandia National Labs., Albuquerque, NM (United States); California State …, 1993.

[268] J. A. Duffie and W. A. Beckman, *Solar engineering of thermal processes*. Wiley New York, 1980.

[269] A. McMahan, S. A. Klein, and D. T. Reindl, “A finite-time thermodynamic framework for optimizing solar-thermal power plants,” 2007.

[270] F. M. White, “Fluid Mechanics, fifth editionMcGraw Hill.” Boston, 2003.

[271] R. V. Padilla, A. Fontalvo, G. Demirkaya, A. Martinez, and A. G. Quiroga, “Exergy analysis of parabolic trough solar receiver,” *Appl. Therm. Eng.*, vol. 67, no. 1–2, pp. 579–586, 2014.

[272] R. Petela, “Exergy of undiluted thermal radiation,” *Sol. energy*, vol. 74, no. 6, pp. 469–488, 2003.

[273] A. Allouhi, R. Saadani, T. Kousksou, R. Saidur, A. Jamil, and M. Rahmoune, “Grid-connected PV systems installed on institutional buildings: Technology comparison, energy analysis and economic performance,” *Energy Build.*, vol. 130, pp. 188–201, 2016.

[274] A. Allouhi, R. Saadani, M. S. Buker, T. Kousksou, A. Jamil, and M. Rahmoune, “Energetic, economic and environmental (3E) analyses and LCOE estimation of three technologies of PV grid-connected systems under different climates,” *Sol. Energy*, vol. 178, pp. 25–36, 2019.

[275] Y. Bravo *et al.*, “Environmental evaluation of dish-Stirling technology for power generation,” *Sol. Energy*, vol. 86, no. 9, pp. 2811–2825, 2012, doi: https://doi.org/10.1016/j.solener.2012.06.019.

[276] F. Cavallaro and L. Ciraolo, “A life cycle assessment (LCA) of a paraboloidal-dish solar thermal power generation system,” in *2006 First International Symposium on Environment Identities and Mediterranean Area*, 2006, pp. 260–265.

[277] A. Allouhi, “Solar PV integration in commercial buildings for self-consumption based on life-cycle economic/environmental multi-objective optimization,” *J. Clean. Prod.*, p. 122375, 2020.

[278] A. A. Lashari, P. H. Shaikh, Z. H. Leghari, M. I. Soomro, Z. A. Memon, and M. A. Uqaili, “The performance prediction and techno-economic analyses of a stand-alone parabolic solar dish/stirling system, for Jamshoro, Pakistan,” *Clean. Eng. Technol.*, vol. 2, p. 100064, 2021.

[279] K. Bataineh and Y. Taamneh, “Performance analysis of stand-alone solar dish Stirling system for electricity generation,” *Int. J. Heat Technol.*, vol. 35, no. 3, pp. 498–508, 2017.

[280] M. Caccia *et al.*, “Ceramic–metal composites for heat exchangers in concentrated solar power plants,” *Nature*, vol. 562, no. 7727, pp. 406–409, 2018.

[281] L. Huaxu *et al.*, “Experimental investigation of cost-effective ZnO nanofluid based spectral splitting CPV/T system,” *Energy*, vol. 194, p. 116913, 2020.

[282] E. R. I. China, “2050 High Renewable Energy Penetration Scenario and Roadmap Study,” *Energy Res. Inst. Beijing, China*, 2015.

[283] M. M. Hand *et al.*, “Renewable electricity futures study. Volume 1. Exploration of high-penetration renewable electricity futures,” National Renewable Energy Lab.(NREL), Golden, CO (United States), 2012.

[284] S. Guillén-Lambea and M. Carvalho, “A critical review of the greenhouse gas emissions associated with parabolic trough concentrating solar power plants,” *J. Clean. Prod.*, p. 125774, 2021.

[285] M. A. Ehyaei, A. Ahmadi, M. E. H. Assad, and T. Salameh, “Optimization of parabolic through collector (PTC) with multi objective swarm optimization (MOPSO) and energy, exergy and economic analyses,” *J. Clean. Prod.*, vol. 234, pp. 285–296, 2019.

[286] A. Boretti, “A realistic expectation of electricity production from current design concentrated solar power solar tower with thermal energy storage,” *Energy Storage*, vol. 1, no. 3, p. e57, 2019.

[287] C. Marugán-Cruz, S. Sánchez-Delgado, J. Gómez-Hernández, and D. Santana, “Towards zero water consumption in solar tower power plants,” *Appl. Therm. Eng.*, vol. 178, p. 115505, 2020, doi: https://doi.org/10.1016/j.applthermaleng.2020.115505.

[288] K. Alikulov, T. D. Xuan, O. Higashi, N. Nakagoshi, and Z. Aminov, “Analysis of environmental effect of hybrid solar-assisted desalination cycle in Sirdarya Thermal Power Plant, Uzbekistan,” *Appl. Therm. Eng.*, vol. 111, pp. 894–902, 2017.

[289] V. Sharma, J. K. Nayak, and S. B. Kedare, “Effects of shading and blocking in linear Fresnel reflector field,” *Sol. Energy*, vol. 113, pp. 114–138, 2015.

[290] L. S. M. Castellanos, G. E. C. Caballero, V. R. M. Cobas, E. E. S. Lora, and A. M. M. Reyes, “Mathematical modeling of the geometrical sizing and thermal performance of a Dish/Stirling system for power generation,” *Renew. Energy*, vol. 107, pp. 23–35, 2017.

[291] Z. Li, D. Tang, J. Du, and T. Li, “Study on the radiation flux and temperature distributions of the concentrator–receiver system in a solar dish/Stirling power facility,” *Appl. Therm. Eng.*, vol. 31, no. 10, pp. 1780–1789, 2011.

[292] D. Yu, A. G. Ebadi, K. Jermsittiparsert, N. H. Jabarullah, M. V. Vasiljeva, and S. Nojavan, “Risk-constrained stochastic optimization of a concentrating solar power plant,” *IEEE Trans. Sustain. Energy*, vol. 11, no. 3, pp. 1464–1472, 2019.

[293] V. M. Sharma, J. K. Nayak, and S. B. Kedare, “Shading and available energy in a parabolic trough concentrator field,” *Sol. energy*, vol. 90, pp. 144–153, 2013.

[294] J. Wu, Y. Han, H. Hou, and Y. Sun, “Optimization of solar field layout and flow velocity in a solar-aided power generation system,” *Energy*, vol. 208, p. 118344, 2020.

[295] J. G. Barberena, A. M. Larrayoz, M. Sánchez, and A. Bernardos, “State-of-the-art of heliostat field layout algorithms and their comparison,” *Energy Procedia*, vol. 93, pp. 31–38, 2016.

[296] M. J. Wagner and T. Wendelin, “SolarPILOT: A power tower solar field layout and characterization tool,” *Sol. Energy*, vol. 171, pp. 185–196, 2018.

[297] F. Eddhibi, M. Ben Amara, M. Balghouthi, and A. Guizani, “Design and analysis of a heliostat field layout with reduced shading effect in southern Tunisia,” *Int. J. Hydrogen Energy*, vol. 42, no. 48, pp. 28973–28996, 2017.

[298] M. Atif and F. A. Al-Sulaiman, “Optimization of heliostat field layout in solar central receiver systems on annual basis using differential evolution algorithm,” *Energy Convers. Manag.*, vol. 95, pp. 1–9, 2015.

[299] X. Wei, Z. Lu, Z. Lin, H. Zhang, and Z. Ni, “Optimization procedure for design of heliostat field layout of a 1MWe solar tower thermal power plant,” in *Solid State Lighting and Solar Energy Technologies*, 2008, vol. 6841, p. 684119.

[300] F. Crespi, A. Toscani, P. Zani, D. Sánchez, and G. Manzolini, “Effect of passing clouds on the dynamic performance of a CSP tower receiver with molten salt heat storage,” *Appl. Energy*, vol. 229, pp. 224–235, 2018, doi: https://doi.org/10.1016/j.apenergy.2018.07.094.

[301] V. Sharma, “Hourly and monthly variation in shading and blocking of aperture area in a linear Fresnel reflector field,” *Energy Procedia*, vol. 48, pp. 233–241, 2014.

[302] R. Buck, A. Pfahl, and T. H. Roos, “Target aligned heliostat field layout for non-flat terrrain,” 2012.

[303] A. Rahmati, S. M. Varedi-Koulaei, M. H. Ahmadi, and H. Ahmadi, “Dimensional synthesis of the Stirling engine based on optimizing the output work by evolutionary algorithms,” *Energy Reports*, vol. 6, pp. 1468–1486, 2020.

[304] Y. Collette and P. Siarry, *Multiobjective optimization: principles and case studies*. Springer Science & Business Media, 2004.

[305] M. M. Keshtkar, “Energy, exergy analysis and optimization by a genetic algorithm of a system based on a solar absorption chiller with a cylindrical PCM and nano-fluid, Int,” *J. Heat Technol.*, vol. 35, no. 2, pp. 416–420, 2017.

[306] M. S. Javed and T. Ma, “Techno-economic assessment of a hybrid solar-wind-battery system with genetic algorithm,” *Energy Procedia*, vol. 158, pp. 6384–6392, 2019.

[307] J. A. Wright, H. A. Loosemore, and R. Farmani, “Optimization of building thermal design and control by multi-criterion genetic algorithm,” *Energy Build.*, vol. 34, no. 9, pp. 959–972, 2002.

[308] L. Magnier and F. Haghighat, “Multiobjective optimization of building design using TRNSYS simulations, genetic algorithm, and Artificial Neural Network,” *Build. Environ.*, vol. 45, no. 3, pp. 739–746, 2010.

[309] Y. Jin, “A comprehensive survey of fitness approximation in evolutionary computation,” *Soft Comput.*, vol. 9, no. 1, pp. 3–12, 2005.

[310] K. Yoon and C. L. Hwang, “TOPSIS (technique for order preference by similarity to ideal solution)–a multiple attribute decision making, w: Multiple attribute decision making–methods and applications, a state-of-the-at survey,” *Berlin: Springer Verlag*, 1981.

[311] E. Roszkowska, “Multi-criteria decision making models by applying the TOPSIS method to crisp and interval data,” *Mult. Criteria Decis. Making/University Econ.*

Katowice, vol. 6, no. 1, pp. 200–230, 2011.

[312] N. Mao, M. Song, and S. Deng, "Application of TOPSIS method in evaluating the effects of supply vane angle of a task/ambient air conditioning system on energy utilization and thermal comfort," *Appl. Energy*, vol. 180, pp. 536–545, 2016.

[313] M. T. Alam *et al.*, "Co-gasification of treated solid recovered fuel residue by using minerals bed and biomass waste blends," *Energies*, vol. 13, no. 8, p. 2081, 2020.

[314] M. Shahabuddin and S. Bhattacharya, "Effect of reactant types (steam, CO2 and steam+ CO2) on the gasification performance of coal using entrained flow gasifier," *Int. J. Energy Res.*, vol. 45, no. 6, pp. 9492–9501, 2021.

[315] https://www.iea.org/reports/key-world-energy-statistics-2021/supply (accessed Apr. 22, 2022).

[316] "China has a clear pathway to build a more sustainable, secure and inclusive energy future - News - IEA." https://www.iea.org/news/china-has-a-clear-pathway-to-build-a-more-sustainable-secure-and-inclusive-energy-future (accessed Apr. 24, 2022).

[317] "Global GHG emissions – Greenhouse Gas Emissions from Energy: Overview – Analysis - IEA." https://www.iea.org/reports/greenhouse-gas-emissions-from-energy-overview/global-ghg-emissions (accessed Apr. 22, 2022).

[318] https://www.bp.com/en/global/corporate/energy-economics/statistical-review-of-world-energy/primary-energy.html (accessed Sep. 02, 2022).

[319] https://www.iea.org/topics/buildings (accessed Apr. 22, 2022).

[320] "Perspectives for the Clean Energy Transition – Analysis - IEA." https://www.iea.org/reports/the-critical-role-of-buildings (accessed Apr. 22, 2022).

[321] M. Ma, X. Ma, W. Cai, and W. Cai, "Low carbon roadmap of residential building sector in China: Historical mitigation and prospective peak," *Appl. Energy*, vol. 273, p. 115247, 2020.

[322] W. Feng *et al.*, "A review of net zero energy buildings in hot and humid climates: Experience learned from 34 case study buildings," *Renew. Sustain. Energy Rev.*, vol.

114, p. 109303, 2019.

[323] A. Ahmed, T. Ge, J. Peng, W.-C. Yan, B. T. Tee, and S. You, “Assessment of the renewable energy generation towards net-zero energy buildings: A review,” *Energy Build.*, vol. 256, p. 111755, 2022.

[324] G. Tumminia *et al.*, “Grid interaction and environmental impact of a net zero energy building,” *Energy Convers. Manag.*, vol. 203, p. 112228, 2020.

[325] W. Wu and H. M. Skye, “Residential net-zero energy buildings: Review and perspective,” *Renew. Sustain. Energy Rev.*, vol. 142, p. 110859, 2021.

[326] A. Naveen Chakkaravarthy, M. S. P. Subathra, P. Jerin Pradeep, and N. Manoj Kumar, “Solar irradiance forecasting and energy optimization for achieving nearly net zero energy building,” *J. Renew. Sustain. Energy*, vol. 10, no. 3, p. 35103, 2018.

[327] A. Alajmi, S. Rodríguez, and D. Sailor, “Transforming a passive house into a net-zero energy house: a case study in the Pacific Northwest of the US,” *Energy Convers. Manag.*, vol. 172, pp. 39–49, 2018.

[328] Q. A. Phan, T. Scully, M. Breen, and M. D. Murphy, “Determination of optimal battery utilization to minimize operating costs for a grid-connected building with renewable energy sources,” *Energy Convers. Manag.*, vol. 174, pp. 157–174, 2018.

[329] M. M. Ahmadi *et al.*, “Net-zero exergoeconomic and exergoenvironmental building as new concepts for developing sustainable built environments,” *Energy Convers. Manag.*, vol. 244, p. 114418, 2021.

[330] S. Arif, J. Taweekun, H. M. Ali, D. A. I. Yanjun, and A. Ahmed, “Feasibility study and economic analysis of grid connected solar powered net zero energy building (NZEB) of shopping mall for two different climates of Pakistan and Thailand,” *Case Stud. Therm. Eng.*, vol. 26, p. 101049, 2021.

[331] A. Arabkoohsar, A. Behzadi, and A. S. Alsagri, “Techno-economic analysis and multi-objective optimization of a novel solar-based building energy system; An effort to reach the true meaning of zero-energy buildings,” *Energy Convers. Manag.*, vol. 232, p. 113858, 2021.

[332] F. Ascione, N. Bianco, G. M. Mauro, and D. F. Napolitano, “Building envelope design: Multi-objective optimization to minimize energy consumption, global cost and thermal discomfort. Application to different Italian climatic zones,” *Energy*, vol. 174, pp. 359–374, 2019.

[333] N. Abdou, Y. E. L. Mghouchi, S. Hamdaoui, N. E. L. Asri, and M. Mouqallid, “Multi-objective optimization of passive energy efficiency measures for net-zero energy building in Morocco,” *Build. Environ.*, vol. 204, p. 108141, 2021.

[334] R. Hemmati, “Technical and economic analysis of home energy management system incorporating small-scale wind turbine and battery energy storage system,” *J. Clean. Prod.*, vol. 159, pp. 106–118, 2017.

[335] D. Greenwood, S. Walker, N. Wade, S. Munoz-Vaca, A. Crossland, and C. Patsios, “Integration of High Penetrations of Intermittent Renewable Generation in Future Electricity Networks Using Storage,” in *Future Energy*, Elsevier, 2020, pp. 649–668.

[336] “Renewable Power – Analysis - IEA.” https://www.iea.org/reports/renewable-power (accessed Apr. 25, 2022).

[337] S. Ambec and C. Crampes, “Decarbonizing electricity generation with intermittent sources of energy,” *J. Assoc. Environ. Resour. Econ.*, vol. 6, no. 6, pp. 1105–1134, 2019.

[338] S. Sanaye and A. Sarrafi, “Cleaner production of combined cooling, heating, power and water for isolated buildings with an innovative hybrid (solar, wind and LPG fuel) system,” *J. Clean. Prod.*, vol. 279, p. 123222, 2021.

[339] Y. Sawle, S. C. Gupta, and A. K. Bohre, “Review of hybrid renewable energy systems with comparative analysis of off-grid hybrid system,” *Renew. Sustain. Energy Rev.*, vol. 81, pp. 2217–2235, 2018.

[340] C. Ammari, D. Belatrache, B. Touhami, and S. Makhloufi, “Sizing, optimization, control and energy management of hybrid renewable energy system—A review,” *Energy Built Environ.*, 2021.

[341] S. A. Memon and R. N. Patel, “An overview of optimization techniques used for sizing

of hybrid renewable energy systems," *Renew. Energy Focus*, vol. 39, pp. 1–26, 2021.

[342] J. Lian, Y. Zhang, C. Ma, Y. Yang, and E. Chaima, "A review on recent sizing methodologies of hybrid renewable energy systems," *Energy Convers. Manag.*, vol. 199, p. 112027, 2019.

[343] E. I. C. Zebra, H. J. van der Windt, G. Nhumaio, and A. P. C. Faaij, "A review of hybrid renewable energy systems in mini-grids for off-grid electrification in developing countries," *Renew. Sustain. Energy Rev.*, vol. 144, p. 111036, 2021.

[344] A. Z. Arsad *et al.*, "Hydrogen energy storage integrated hybrid renewable energy systems: A review analysis for future research directions," *Int. J. Hydrogen Energy*, 2022.

[345] M. A. M. Khan, S. Rehman, and F. A. Al-Sulaiman, "A hybrid renewable energy system as a potential energy source for water desalination using reverse osmosis: A review," *Renew. Sustain. Energy Rev.*, vol. 97, pp. 456–477, 2018.

[346] W. Ma, X. Xue, and G. Liu, "Techno-economic evaluation for hybrid renewable energy system: Application and merits," *Energy*, vol. 159, pp. 385–409, 2018.

[347] L. Li and X. Wang, "Design and operation of hybrid renewable energy systems: current status and future perspectives," *Curr. Opin. Chem. Eng.*, vol. 31, p. 100669, 2021.

[348] D.-A. Ciupageanu, L. Barelli, and G. Lazaroiu, "Real-time stochastic power management strategies in hybrid renewable energy systems: A review of key applications and perspectives," *Electr. Power Syst. Res.*, vol. 187, p. 106497, 2020.

[349] W. Ma, X. Xue, G. Liu, and R. Zhou, "Techno-economic evaluation of a community-based hybrid renewable energy system considering site-specific nature," *Energy Convers. Manag.*, vol. 171, pp. 1737–1748, 2018.

[350] O. Krishan and S. Suhag, "Techno-economic analysis of a hybrid renewable energy system for an energy poor rural community," *J. Energy Storage*, vol. 23, pp. 305–319, 2019.

[351] L. He, S. Zhang, Y. Chen, L. Ren, and J. Li, "Techno-economic potential of a renewable energy-based microgrid system for a sustainable large-scale residential

community in Beijing, China," *Renew. Sustain. Energy Rev.*, vol. 93, pp. 631–641, 2018.

[352] J. Liu, M. Wang, J. Peng, X. Chen, S. Cao, and H. Yang, "Techno-economic design optimization of hybrid renewable energy applications for high-rise residential buildings," *Energy Convers. Manag.*, vol. 213, p. 112868, 2020.

[353] B. K. Das, M. S. H. K. Tushar, and R. Hassan, "Techno-economic optimisation of stand-alone hybrid renewable energy systems for concurrently meeting electric and heating demand," *Sustain. Cities Soc.*, vol. 68, p. 102763, 2021.

[354] X. Li, A. Lin, C.-H. Young, Y. Dai, and C.-H. Wang, "Energetic and economic evaluation of hybrid solar energy systems in a residential net-zero energy building," *Appl. Energy*, vol. 254, p. 113709, 2019.

[355] S. Ashrafi Goudarzi, F. Fazelpour, G. B. Gharehpetian, and M. A. Rosen, "Techno-economic assessment of hybrid renewable resources for a residential building in tehran," *Environ. Prog. Sustain. Energy*, vol. 38, no. 5, p. 13209, 2019.

[356] C. Ghenai, T. Salameh, and A. Merabet, "Technico-economic analysis of off grid solar PV/Fuel cell energy system for residential community in desert region," *Int. J. Hydrogen Energy*, vol. 45, no. 20, pp. 11460–11470, 2020.

[357] N. M. Kumar, S. S. Chopra, A. A. Chand, R. M. Elavarasan, and G. M. Shafiullah, "Hybrid renewable energy microgrid for a residential community: A techno-economic and environmental perspective in the context of the SDG7," *Sustainability*, vol. 12, no. 10, p. 3944, 2020.

[358] S. Singh, N. Kanwar, D. Zindani, and V. K. Jadoun, "Decision making approach for assessing the suitable hybrid renewable energy based microgrid system for rural electrification in India," *Mater. Today Proc.*, vol. 51, pp. 21–25, 2022.

[359] A. C. Duman and Ö. Güler, "Techno-economic analysis of off-grid PV/wind/fuel cell hybrid system combinations with a comparison of regularly and seasonally occupied households," *Sustain. Cities Soc.*, vol. 42, pp. 107–126, 2018.

[360] Y. Kalinci, A. Hepbasli, and I. Dincer, "Techno-economic analysis of a stand-alone

hybrid renewable energy system with hydrogen production and storage options," *Int. J. Hydrogen Energy*, vol. 40, no. 24, pp. 7652–7664, 2015.

[361] A. Al-Sharafi, A. Z. Sahin, T. Ayar, and B. S. Yilbas, "Techno-economic analysis and optimization of solar and wind energy systems for power generation and hydrogen production in Saudi Arabia," *Renew. Sustain. Energy Rev.*, vol. 69, pp. 33–49, 2017.

[362] A. Mohammadi and M. Mehrpooya, "Techno-economic analysis of hydrogen production by solid oxide electrolyzer coupled with dish collector," *Energy Convers. Manag.*, vol. 173, pp. 167–178, 2018.

[363] M. Gökçek and C. Kale, "Techno-economical evaluation of a hydrogen refuelling station powered by Wind-PV hybrid power system: A case study for İzmir-Çeşme," *Int. J. Hydrogen Energy*, vol. 43, no. 23, pp. 10615–10625, 2018.

[364] T. R. Ayodele, T. C. Mosetlhe, A. A. Yusuff, and M. Ntombela, "Optimal design of wind-powered hydrogen refuelling station for some selected cities of South Africa," *Int. J. Hydrogen Energy*, vol. 46, no. 49, pp. 24919–24930, 2021.

[365] A. Allouhi, S. Rehman, and M. Krarti, "Role of energy efficiency measures and hybrid PV/biomass power generation in designing 100% electric rural houses: A case study in Morocco," *Energy Build.*, vol. 236, p. 110770, 2021.

[366] S. Hamdaoui, M. Mahdaoui, A. Allouhi, R. El Alaiji, T. Kousksou, and A. El Bouardi, "Energy demand and environmental impact of various construction scenarios of an office building in Morocco," *J. Clean. Prod.*, vol. 188, pp. 113–124, 2018.

[367] A. Allouhi, "Energetic, exergetic, economic and environmental (4 E) assessment process of wind power generation," *J. Clean. Prod.*, vol. 235, pp. 274–289, 2019.

[368] Y. El Mghouchi, T. Ajzoul, and A. El Bouardi, "Prediction of daily solar radiation intensity by day of the year in twenty-four cities of Morocco," *Renew. Sustain. Energy Rev.*, vol. 53, pp. 823–831, 2016.

[369] A. Allouhi, "Management of photovoltaic excess electricity generation via the power to hydrogen concept: A year-round dynamic assessment using Artificial Neural Networks," *Int. J. Hydrogen Energy*, vol. 45, no. 41, pp. 21024–21039, 2020.

[370] https://www2.deloitte.com/global/en/industries/energy-resources-industrials.html (accessed May 17, 2022).

[371] “Wind Turbine Cost: Worth The Million-Dollar Price In 2022?” https://weatherguardwind.com/how-much-does-wind-turbine-cost-worth-it/ (accessed May 17, 2022).

[372] A. Dobos, T. Neises, and M. Wagner, “Advances in CSP simulation technology in the System Advisor Model,” *Energy Procedia*, vol. 49, pp. 2482–2489, 2014.

[373]https://www.homerenergy.com/products/pro/docs/latest/how_homer_calculates_wind_turbine_power_output.html (accessed Jun. 16, 2022).

[374] M. O. Atallah, M. A. Farahat, M. E. Lotfy, and T. Senjyu, “Operation of conventional and unconventional energy sources to drive a reverse osmosis desalination plant in Sinai Peninsula, Egypt,” *Renew. Energy*, vol. 145, pp. 141–152, 2020.

[375] https://www.homerenergy.com/products/pro/docs/latest/total_net_present_cost.html (accessed Jun. 21, 2022).

[376] https://www.homerenergy.com/products/pro/docs/latest/_renewable_fraction.html (accessed Jun. 22, 2022).